uOttawa

L'Université canadienne
Canada's university

FACULTÉ DES ÉTUDES SUPÉRIEURES ET POSTOCTORALES

uOttawa

L'Université canadienne
Canada's university

FACULTY OF GRADUATE AND POSDOCTORAL STUDIES

Jamil Andrei Sader
AUTEUR DE LA THÈSE / AUTHOR OF THESIS

Ph.D. (Earth Sciences)
GRADE / DEGREE

Department of Earth Sciences
FACULTÉ, ÉCOLE, DÉPARTEMENT / FACULTY, SCHOOL, DEPARTMENT

Geochemical Responses of Buried Kimberlites in Shallow Groundwater in the Attawapiskat Kimberlite Field, James Bay Lowlands, Canada

TITRE DE LA THÈSE / TITLE OF THESIS

Keiko Hattori
DIRECTEUR (DIRECTRICE) DE LA THÈSE / THESIS SUPERVISOR

CO-DIRECTEUR (CO-DIRECTRICE) DE LA THÈSE / THESIS CO-SUPERVISOR

Ian Clark

Frederick Michel

Michel Robin

Kurt Kyser
Queen's University

Gary W. Slater
Le Doyen de la Faculté des études supérieures et postdoctorales / Dean of the Faculty of Graduate and Postdoctoral Studies

GEOCHEMICAL RESPONSES OF BURIED KIMBERLITES IN SHALLOW GROUNDWATER IN THE ATTAWAPISKAT KIMBERLITE FIELD, JAMES BAY LOWLANDS, CANADA

By

Jamil Andrei Sader, B.Sc., M.Sc.

A thesis submitted to the

Faculty of Graduate & Postdoctoral Studies

in partial fulfillment of the requirement for the

Doctor of Philosophy Degree, in Earth Sciences

Ottawa-Carleton Geoscience Centre and

University of Ottawa

Department of Earth Sciences

Your file Votre référence
ISBN: 978-0-494-74231-0
Our file Notre référence
ISBN: 978-0-494-74231-0

Abstract

Shallow groundwaters were examined in the Attawapiskat kimberlite region, James Bay Lowlands, Ontario, Canada in order to assess buried kimberlite impacts on shallow groundwater geochemistry. Peat groundwaters were collected along transects over and outside of Yankee, Zulu, and Golf kimberlites, at select locations at kimberlites Bravo-1 and Alpha-1, and at a Control site (where no known kimberlite is present). Deeper groundwaters were collected from Tyrell Sea sediment (TSS), and from exploration boreholes within kimberlite and limestone. Sites of upwelling minerotrophic groundwaters were identified using hydrogeological and geochemical measurements. Elevated pH, electrical conductivity (EC), and Ca concentrations, and low Eh relative to ombrotrophic peat groundwaters indicate groundwaters that have moved upwards from below the peat zone, and which are minerotrophic. Kimberlite pathfinder metals consisting of light rare earth elements (LREEs), Ni, Cr, Ti, Ba, Rb, Cs, and the ratio of Mg/Ca are commonly elevated in peat groundwaters along sampling transects as far as 200 m outside of kimberlite margins. The principal mechanism in transporting these metals upwards from kimberlites, through up to 21 m of TSS and up to 4 m of peat, is upward movement of deep groundwater. This mechanism is inferred based on hydrogeology and geochemistry of groundwaters in the TSS and peat. Fractures along the boundaries between kimberlites and limestone are suggested to provide pathways for upward groundwater movement.

Chromium, Ni, Ti, LREEs are typically elevated in peat groundwaters at or near kimberlite margins, where there are lower contributions of inferred upwelling groundwaters to the peat (based on pH, Eh, and EC). At sites of strongly minerotrophic groundwater

contributions (i e high EC, pH, etc), Cr, Ni, Ti, LREEs are lower than local baseline concentrations for ombrotrophic peat groundwaters. Conversely, alkali and alkaline earth pathfinder metals such as K, Rb, Cs, Ba, and Mg/Ca are commonly displaced from Cr, Ni, Ti, and LREEs and are usually found at sites of strong upwelling. The unusual spatial distribution among pathfinder metals (transition metals are lower than baseline values at sites with high contributions from minerotrophic waters) likely relates to differences in metal solubility due to variable metal complexation with dissolved organic matter (DOM). Metal – DOM speciation calculations using Visual MINTEQ 3.0 and the NICA-Donnan database were conducted for Nd, Ni, Ba, and K. These pathfinder metals were used, as they are analogs for trivalent and divalent transition metals, alkaline earth metals, and alkali metals, respectively. The model predicts almost 100% of soluble Nd, Ni, and Ba form complexes with DOM at sampling sites with little to no contribution from upwelling (minerotrophic) groundwater (i.e., dissolved organic carbon (DOC) concentrations = 40 to 132 mg/L, pH = 3.9 to 5.5, and log ionic strength = < -3). Comparatively, as little as 10% of Nd and Ni, and 0% K and Ba are predicted to complex with DOM under conditions with large contributions from upwelling groundwaters (i.e., DOC concentrations = < 40 mg/L, pH = 5.5 to 6.5, and log ionic strength = -3 to -2). Based on modeling calculations, competitive availability of DOM binding sites where ionic strength is elevated (upward migration of groundwater) is the dominant control on metal-DOM complexation. MINTEQ modeling calculations indicate soluble Ni and Nd are likely scavenged from solution under strong upwelling conditions (i.e. high ionic strength). Metal scavenging is likely due to increased adsorption onto precipitating ferrihydrite (based on $\log SI_{ferr}$ close to or greater than 0) coupled with decreases in metal fractions complexed with DOM. Total Ni and Nd concentrations are

typically 5 times lower than waters with little to no upwelling and ferrihydrite saturation indices ($logSI_{ferr}$) strongly indicate precipitation (up to 5). Comparatively, the concentrations of dissolved Ni and Nd in peat groundwaters are elevated where they are predicted to dominantly complex with DOM, and ferrihydrite is highly under saturated ($logSI_{ferr}$ -18 to -5). Metal complexation with DOM may effectively inhibits metal scavenging from solution.

In TSS groundwaters overlying kimberlites, methane concentrations and $\Delta^{13}C_{DIC\text{-}CH4}$ (isotope separation) values of 72‰ ±1‰ indicate methane production via biological DIC reduction. They also display a trend of increasing methane concentrations and $\delta^{13}C_{CH4}$ values that plot along a Rayleigh fractionation trend of biological DIC reduction. In contrast, groundwaters from TSS over limestone, from boreholes in limestone, and kimberlites have lower CH_4 concentrations and variable $\Delta^{13}C_{DIC\text{-}CH4}$ values (55 to 70‰) consistent with biological methane oxidation. All but one CH_4 sample in TSS groundwater over kimberlite indicates *in situ* formation. Less negative $\delta^{2}H_{H2O}$ values (greater than the local meteoric water line) are typically those samples from TSS over kimberlites and suggest the production of CH_4, as biological DIC reduction requires H^+ ions from H_2O to form CH_4. The ratio of CH_4 to the concentrations of Fe^{3+}, SO_4^{2-}, and $O_{2(aq)}$ are greatest in the majority of TSS groundwater samples collected over kimberlites, and suggests kimberlites may indirectly influence the CO_2-CH_4 system by consuming oxidized ions in the overlying TSS.

The results of this study suggest that buried kimberlites can be identified through the detection of high Ni, Cr, Ti, LREEs, K, Rb, Ba concentrations, and the ratio of Mg/Ca in peat groundwaters over or near the kimberlite margin. However, geochemical processes such as metal – DOM complexation, adsorption, and incorporation of metals into precipitated minerals are important considerations when identifying the spatial distribution of pathfinder

metals along transects Variations in CH_4 emissions occur in soils and groundwaters overlying kimberlites could be due to the release of reduced ions during serpentinization reactions. Methane gas coupled with C isotopic variations in CH_4 and DIC may represent a possible pathfinder geochemical tool to use in conjunction with pathfinder metals.

Acknowledgements

There are a number of people involved in this project I wish to thank. First and foremost, I would like to thank my advisor, Dr. Keiko Hattori. Although we have sometimes disagreed on the thesis subject matter, she has always been willing to engage in constructive discussions with me, which have ultimately improved the quality of the thesis. Keiko's quick responses to emails and eagerness to help, whether she is in the department or on the other side of the globe, have been instrumental in me being able to finish this thesis efficiently. I would also like to thank her for offering this project to me. The assistance of Stewart Hamilton (Ontario Geological Survey) in the bush, providing thousands of dollars worth of field equipment for fieldwork, and providing me with comments on written work is very much appreciated. I would also like to thank Stew for the many times he has picked up the tab at Shawarma King. Kerstin Brauneder has put in many hours of her time helping in the field and has been kind enough to allow me usage of her unpublished data from the Attawapiskat region. Her helpfulness and strong work ethic in the field went beyond what most would expect of a field assistant. Sean Fulcher, field assistant at Ville Marie, QC, is thanked for taking time out of his schedule to assist me in collecting water samples.

Financial support was provided by a NSERC Collaborative Research grant to Keiko Hattori. DeBeers Canada (Julie Kong, Brad Wood, and Ed Francisco) are thanked for financial and logistical support for the project. Graduate study support in the form of an Ontario Graduate Scholarship and a student research grant from the Society of Economic Geologists supported me. The Brian Rust Memorial Scholarship and the G.G. Hatch Student Bursary are also acknowledged. Travel grants to conferences from the Faculty of Graduate Studies and the Graduates Students Association helped off-set travel costs.

Research at the Ville Marie, QC site was made possible by Northern Superior Resources' Dr. Tom Morris and Matt Sooley who took us to their claim sites, and provided maps and geological information of the area. Harry Anderson of Gore Associates is thanked for providing geochemical samplers and hydrocarbon analyses of the samplers. G.G. Hatch Laboratory personnel (Paul Middlestead, Wendy Abdi, and Patricia Wickham) are thanked for their assistance, time, and patience showing me how to use the analytical equipment. Marcus Burnham and Merilla Clement (Geoscience Laboratories, Ontario Geological Survey) are thanked for their quick responses to my enquiries regarding analytical work conducted by them.

Jan Peter, M. Beth McClenaghan, and Matthew Leybourne are thanked for help proof reading my work and for reminding me that there really is a light at the end of the thesis tunnel. I would like to thank my in-laws, Brian and Elva Heney for the many, many times they drove to Ottawa from Pembroke to take our girls, Portia and Gwendolyn, for sometimes as long as a week, so that I could get uninterrupted work done on my thesis. My father, Solly Sader, is thanked for support and much needed financial top-ups here and there. A special thank-you is reserved for my wife, Erin, who many times has done the lion's share of house work and child-rearing so that I could work. Without her love, support, and encouragement, this thesis would not have been possible

Lastly, this thesis is dedicated to our two girls Portia, and Gwendolyn.

Table of Contents

List of Figures

List of Tables

Introduction

The Attawapiskat kimberlite field in the James Bay Lowlands, Ontario is one of the largest continuous peat bogs on Earth, and represents the only diamond producing region in Ontario in 2010. In addition to the Attawapiskat kimberlite field, the only other known kimberlites in the region are in the Kyle Lake kimberlite field approximately 120 km northwest. The potential exists for more kimberlite discoveries within these known fields or the discovery of new fields. Kimberlites in this region are emplaced into Silurian and Ordovician carbonate rocks, which are overlain by < 1 m of glacial till, 2.1 to 21 m of fine marine sediment (Tyrell Sea sediment) and 3 to 4 m of sphagnum peat.

The use of geophysical methods for exploration of buried kimberlites is common in a host of geological and surficial settings. However, geophysical methods may fail to identify kimberlites that are not magnetic or may indicate false positives (intrusive dikes, etc.). Due to this uncertainty, surficial geochemical methods are implemented to gain more information as to whether a geophysical target is kimberlite prior to proceeding with drilling or further exploration activities. In most northern boreal and tundra glaciated settings geochemical methods utilize tills and soils (Mann *et al.*, 1998; Cameron *et al.*, 2004b; McClenaghan *et al.*, 2006; Hattori *et al.*, 2009; Sader *et al.*, 2009) and recently peat (Hattori and Hamilton, 2008) at or just below the ground surface to identify geochemical indicators of buried ore. However, soil and till geochemical methods are impractical in the James Bay Lowlands, due to water saturated sphagnum peat and fine Tyrell Sea sediment, which overlies kimberlites and the host Palaeozoic rocks. In response to the lack of mineral soil and saturated conditions at the James Bay Lowlands, the impact of buried kimberlite on peat groundwater geochemistry and it's utility as an effective medium for surficial geochemical exploration is

investigated. Researchers have shown that surface and shallow subsurface waters in wetlands have been effective in providing information relating to buried rock types (Hattori and Cameron, 2004; Syrovetnik *et al.*, 2004). Additionally, water geochemistry has been shown to effectively vector to mineral deposits in a variety of settings (Leybourne and Cameron, 2010).

In this thesis I present the results of my research into the geochemical responses in shallow groundwaters over buried kimberlites in the Attawapiskat kimberlite field. The goals of this study are to: 1) Identify dissolved metals that are indicative of water-kimberlite reactions such as low-temperature serpentinization (Sader *et al.*, 2007a), but that are not expected to be elevated in waters from other sources (i.e. limestone, Tyrell Sea sediment, or ombrotrophic peat groundwater); 2) Investigate the most likely mechanism responsible for the upward migration of metals from kimberlites to peat groundwaters. A number of mechanisms have been suggested in the literature to explain metal transport from ore deposits to near surface environments including upward ionic diffusion, advection, gas transport, electro-chemical transport, and seismic pumping (Cameron *et al.*, 2004b). Hydrogeological measurements and groundwater geochemistry are used to determine the most likely metal transport mechanism; 3) This research assesses the geochemical controls on kimberlite pathfinder metals in peat groundwater. In organic rich peat groundwaters there are 4 predominant controls on metal solubility. These consist of metal complexation with dissolved organic material (DOM), adsorption to insoluble humic substances, adsorption to Fe-oxyhydroxides, and secondary mineral precipitation. Identification of these processes and their impact on pathfinder metal concentrations will be used to assist in the determination of spatial variability between locations of individual pathfinder metals along sampling

transects; and 4) Because water-kimberlite interactions can result in more reducing groundwater geochemistry, this thesis will addresses the possible effects that buried kimberlite may have on the $CO_2 - CH_4$ system in the Tyrell Sea sediment. The addition or removal of oxidized ions such as SO_4^{2-}, Fe^{3+}, and $O_{2(aq)}$ commonly impacts the consumption or production of methane in soil and peat bogs (Whiticar and Faber, 1986; Segers, 1988; Miura *et al.*, 1992; Kumaraswamy *et al.*, 2001; Yu *et al.*, 2007).

OUTLINE

This thesis is written as 3 chapters, which are in the form of stand-alone articles, and a fourth *Summary and Implication* chapter. These chapters represent important aspects of this project addressing how and why buried kimberlites influence shallow groundwater geochemistry in a sphagnum peat bog environment.

Chapter 1: This chapter focuses on the connection between LREE, Ni, Cr, Ba, Rb, Cs, and Mg/Ca ratios in peat groundwaters and hydrogeological influences. The suite of pathfinder metals are commonly elevated in both minerals and waters associated with kimberlite, but low in waters and whole-rock geochemistry from the host limestone. Results suggest that the primary mechanism responsible for transporting kimberlite pathfinder metals to the surface is the upwelling of groundwater. This chapter also suggests possible geochemical processes that could impact metal solubility in peat groundwaters.

Chapter 2: This chapter addresses why kimberlite pathfinder metals, transported to the surface in upwelling groundwater, are not elevated at the same locations. Pathfinder metal complexation with dissolved organic material and adsorption to ferrihydrite are modeled using Visual MINTEQ 3.0 (Gustafsson, 2010) and the calculations are compared to analytical peat groundwater metal data. Combined, analytical and model calculations

indicate transition pathfinder metal concentrations are elevated where high dissolved organic carbon exists. The high solubility of these metals is due to the formation of metal – DOM complexes. Conversely, at sites of strong upwelling where metal – DOM complexes are less likely to form, a greater fraction of dissolved metals are predicted as free ions. Elevated concentrations of free ions (particularly transition metals) are likely scavenged from solution through adsorption to ferrihydrite or insoluble organics.

Chapter 3: This chapter focuses on variations in the CO_2 – CH_4 system in TSS groundwaters overlying kimberlites and limestone. The results of this study, based on DIC and methane concentrations, and their respective isotopes indicate methane formation via biological DIC reduction is the most common pathway in TSS over kimberlites. Methane formation may be due to the consumption of oxidized ions in the TSS by the more reducing conditions originating within buried kimberlites, thus making conditions favourable for bacterial CO_2 reduction. In comparison, methane concentration and isotopic evidence suggest that methane is undergoing anaerobic oxidation in most groundwaters from TSS over limestone, and in kimberlite and limestone.

Chapter 4: This chapter represents a summary and geochemical exploration implications for kimberlites based on the findings of this study.

STATEMENT OF ORIGINAL CONTRIBUTION

All fieldwork conducted in the Attawapiskat kimberlite region in the summer and fall of 2007 pertaining to groundwater and gas sampling was conducted by a team consisting of Keiko Hattori, Stewart Hamilton (Ontario Geological Survey), Kerstin Brauneder, and me. This work included the planning, organization, and implementation of sampling programs. During these fieldwork events, groundwater samples were collected from peat, Tyrell Sea

sediment, and exploration boreholes within kimberlite and limestone. Gas samples were collected from groundwaters within Tyrell Sea sediment and exploration boreholes. Keiko Hattori, Kerstin Brauneder, and I also conducted fieldwork in fall 2007, spring 2008 and fall 2008 in the Ville Marie region of Quebec. This work consisted of the collection of soil, groundwater and Gore Sorbers^{TM} (soil hydrocarbon samplers). My research relating to buried kimberlites near Ville Marie was additional to the main thesis research on groundwater and methane in the Attawapiskat region. Results of the Ville Marie research were presented as a conference poster. The extended abstract from the conference proceedings is located in the *Appendix* section of my thesis.

All water and gas samples analyzed for isotopes, DIC, DOC, and gas concentrations were conducted by me at the G.G. Hatch Laboratory, University of Ottawa. This included water and gas sample preparation and operation of analytical equipment (gas chromatograph and mass spectrometers). Major and trace cations and anions in waters were measured at a commercial laboratory (Geoscience Laboratories of the Ministry of Northern Development of Mines, Sudbury, Ontario, Canada).

Calculations, modeling, and interpretation of all geochemical data (metals, gas, and isotopes) discussed in this thesis are based on my ideas. The 2006 peat groundwater data from Golf kimberlite was from Kerstin Brauneder's B.Sc. thesis (Brauneder, 2007) prior to my involvement in the project and was used to supplement my data collected from the Attawapiskat kimberlite field in 2007. The addition of these data was due to accessibility constraints that prevented sample collection at Attawapiskat in years following 2007. I have indicated in the text where 2006 data (Brauneder, 2007) were used.

This research represents the first published work on shallow peat groundwaters as a medium for surficial geochemical exploration of kimberlites. It also represents that first time that water geochemical data relating to kimberlites in the James Bay Lowlands have been presented as manuscripts for publication. This research provides results that suggest a transport mechanism responsible for movement of metals from the kimberlite to overlying peat groundwaters (groundwater upwelling), not considered before in diamond exploration. It also highlights the importance of metal solubility, complexation with DOM, and adsorption processes on the spatial distribution of metals in near surface environments.

My thesis presents results, for the first time, that combine isotopes and the concentrations of DIC and methane to suggest buried lithology may influence the $CO_2 - CH_4$ system in surficial media. Buried kimberlite may indirectly impact the $CO_2 - CH_4$ system in a northern boreal wetland setting and is likely a result of greater concentrations of reduced ions due to water-kimberlite interactions. A study by Rejmankova and Post (1996) addressed the influence of buried lithology on the $CO_2 - CH_4$ system, however, their study area was conducted at an equatorial wetland with different dynamics from northern boreal peat bogs. Additionally a study by Reeve *et al.* (1996), conducted in the James Bay lowlands 170 km south of the Attawapiskat kimberlites, suggested sulfate from buried lithology may inhibit methane production. However, their study was based solely on methane and sulfate concentrations.

The work in the Ville Marie region represents the first time that variations in soil hydrocarbons from Gore Sorbers^{TM} have been contrasted with soil partial leach and peat groundwater geochemistry. It also represents the first time that Gore Sorbers^{TM} data utilized in diamond exploration applications has been reported.

CONTRIBUTIONS OF COLLABORATORS

Co-authors on manuscripts (thesis chapters) contributed the following: 1) Keiko Hattori, my thesis advisor, contributed guidance, suggestions, comments on manuscripts, and assistance with fieldwork. She was also instrumental in obtaining financial support for the project through a NSERC-CRD program.; 2) Stewart Hamilton provided the field equipment, assisted with fieldwork, and offered suggestions on thesis subject matter. He also facilitated the analysis of metals in groundwaters at the Ministry of Northern Development and Mines in Sudbury, Ontario, and; 3) Julie Kong (DeBeers Canada) facilitated fieldwork support; and 4) Kerstin Brauneder provided fieldwork assistance and allowed me to use some of her unpublished data.

Chapter 1

GEOCHEMICAL RESPONSES IN PEAT GROUNDWATER OVER ATTAWAPISKAT KIMBERLITES, JAMES BAY LOWLANDS, CANADA AND THEIR APPLICATION TO DIAMOND EXPLORATION

Jamil A. Sader[1*], Keiko H. Hattori[1], Julie M. Kong[2], Stewart M. Hamilton[3], Kerstin Brauneder[1]

[1]University of Ottawa, Earth Sciences Department, Ottawa, Ontario, K1N 6N5, Canada
[2]DeBeers Canada Inc., 65 Overlea Blvd., Toronto, Ontario, K4H 1P1, Canada
[3]Sedimentary Geoscience Division, Ontario Geological Survey, Sudbury, Ontario, P3E 2G9, Canada
*Corresponding author (e-mail: jamilsader@yahoo.com)

Manuscript accepted for publication in Geochemistry: Exploration Environment Analysis

1.1 ABSTRACT

Peat groundwater compositions at depths of 0.4 and 1.1 m below the surface in the Attawapiskat region of the James Bay Lowlands are evaluated for diamond exploration applications. Samples were collected along transects that typically extend at least 200 m beyond the margins of Yankee, Zulu, and Golf kimberlites. Locations of upwelling groundwater usually occur at or near kimberlite margins based on hydrogeological measurements and variations in peat groundwater geochemical parameters (pH and EC are high, and the Eh is low relative to ombrotrophic peat groundwaters). Concentrations of the kimberlite pathfinder metals Ni, Cr, light rare earth elements (LREEs), Ba, Mg/Ca, and alkalis are commonly elevated at sample sites at or near kimberlite margins and where groundwaters are upwelling. The presence of elevated kimberlite pathfinders at these sites suggest that fractures along the boundaries between kimberlites and limestone formed during kimberlite emplacement provide pathways for upward movement of groundwater with elevated kimberlite pathfinder metals. Typically, Ni, Cr, LREE, and Ba behave similarly and thus high concentrations of these metals are found at similar locations along transects. Conversely, locations of elevated alkalis and Mg/Ca vary. The spatial variations among pathfinder metals in peat groundwaters are possibly due to geochemical processes in the peat, such as metal binding to dissolved organic material, adsorption to insoluble organics or Fe-oxyhydroxides, and incorporation into secondary mineral precipitates, which can act to increase or decrease metal solubility. The findings of this study are readily applicable in diamond exploration in wetlands elsewhere.

1.2 INTRODUCTION

The James Bay Lowlands in northern Ontario, Canada represents one of the largest continuous peat bogs on Earth with an area of *c.* 300,000 km^2 (Sjors, 1963). In addition to the Attawapiskat kimberlite field, there are several kimberlites that make up the Kyle Lake kimberlite field in the James Bay Lowlands. It is likely that there are additional kimberlites that have not been discovered at these two fields. On a global scale, there have been numerous kimberlite discoveries in other northern regions such as Russia and Finland (Janse and Sheahan, 1995; O'Brien and Tyni, 1999; Lehtonen *et al.*, 2005) where peat bog terrain is common (Frenzel, 1983). Due to the lack of mineral soil at surface, the most common exploration methods used in the James Bay region are geophysical. However, kimberlites are not always magnetic, and magnetic geophysical anomalies are not necessarily kimberlite. To gain further information as to whether a geophysical response concealed by sediment cover may be kimberlite, surficial geochemical exploration in glaciated terrains commonly utilize tills and soils (Mann *et al.*, 1998; Cameron *et al.*, 2004b; McClenaghan *et al.*, 2006; Hattori *et al.*, 2009; Sader *et al.*, 2009) and recently peat (Hattori and Hamilton, 2008).

In wetlands, conventional mineral soil sampling is not feasible in geochemical exploration due to the dominance of sphagnum peat at surface. As the James Bay Lowland region is dominantly composed of water-saturated peat, peat groundwaters may be useful as a medium for surficial geochemical exploration. Groundwater geochemistry has been shown to provide information related to underlying rock types in wetlands (Syrovetnik *et al.*, 2004) and has also been used to effectively vector to mineral deposits in a variety of settings (Leybourne and Cameron, 2010). Anomalous geochemical responses in near-surface media

are typically the result of water - ore interactions due to weathering processes at depth (Leybourne and Cameron, 2006; Sader *et al.*, 2007a).

This study was conducted to examine whether shallow peat groundwater may be used to identify buried kimberlites in wetlands. The results present evidence to suggest that peat groundwaters have metal anomalies due to underlying kimberlites. Kimberlites easily undergo low temperature serpentinization (Sader *et al.*, 2007a; Sader *et al.*, 2007b), which results in an unusual groundwater geochemistry relative to waters flowing through a host of other rock types (Leybourne and Cameron, 2010). The geochemical contrast with waters whose origin is limestone or Tyrell Sea sediment may be used for diamond exploration in wetlands. Geochemical results, coupled with hydrogeological parameters, are used to discuss metal transport mechanisms in wetlands.

1.3 LOCATION, GEOLOGICAL SETTING AND MINERALOGY

The kimberlites in this study are located in the James Bay Lowlands *c.* 90 km west of the community of Attawapiskat and within 15 km of the DeBeers Victor diamond mine (Fig. 1-1a & b). These mid Jurassic (*c.* 170 Ma) kimberlites are emplaced into Ordovician and Silurian limestone, dolostone, clastic sedimentary rocks, and Archean basement igneous and metamorphic rocks (Norris, 1993; Webb *et al.*, 2004); (Fig. 1-2). Host rock to kimberlites at the bedrock surface is the Upper Attawapiskat Formation limestone (Fig. 1-2), which also locally outcrops in the form of bioherms up to 2 m above the surrounding ground surface. Bioherms are reef cores composed of coral and skeletal remains of marine organisms (Cowell, 1983). They generally represent locations of groundwater recharge, as bioherms contain abundant void spaces and karstic textures.

A thin till layer (< 1 m in thickness) was deposited on the glacially eroded bedrock surface during the Quaternary. Tyrell Sea sediment (TSS) (2.1 to 21 m in thickness) is composed of varying fractions of grey silt and clay. Small 10 to 20 cm thick sand lenses and small pebbles are occasionally observed. This sediment was deposited between 10 and 5 Ka following the end of the last glaciation when the shoreline of James Bay (referred to as the Tyrell Sea during that period) extended inland approximately 300 km west and southwest of its present location. Isostatic rebound resulted in ground surface elevation increases of 100 to 300 m since the retreat of the Laurentide ice sheet in the Attawapiskat region (Shilts, 1986). Peat (2.5 to *c.* 4.0 m in thickness) is located at the surface and has been accumulating since the retreat of the Tyrell Sea approximately 5000 years BP. The peat is dominantly composed of sphagnum and becomes progressively more decomposed with depth. All kimberlites are buried by Quaternary sediment, with the exception of the Zulu kimberlite, which outcrops at one location at the south margin.

The Yankee kimberlite is located in a shallow bowl-shaped depression and bioherms are located southwest and northeast of the kimberlite (Fig. 1-3a). The Zulu kimberlite is located on the east part of a lobate raised bog and there is a small bioherm beside the south margin of the kimberlite (Fig. 1-3b). Ground surface at the Golf kimberlite is similar to that of Zulu, as they both slope gently from west to east. However, no bioherm was noted in the areas adjacent to Golf (Fig. 1-3c). The ground surface at the Control site grades gently towards the Attawapiskat River *c.* 600 m to the north (Fig. 1-3d). Geophysical data (DeBeers unpublished) suggest that there is no kimberlite in the vicinity of the Control site.

1.3.1 Attawapiskat kimberlite mineralogy and geochemistry

Detailed mineralogical descriptions of each kimberlite were made by Sage (2000a). To summarize his work:

Yankee kimberlite is hypabyssal with mantle and crustal xenoliths. It contains macrocrysts of garnet, ilmenite, phlogopite, clinopyroxene, and olivine in no particular order of abundance. Diamond has not been found in this kimberlite. Zulu kimberlite is diamondiferous and is composed of hypabyssal and brecciated facies with limestone, basement, and mantle xenoliths. It contains macrocrysts of olivine, phlogopite, ilmenite, and chrome diopside with minor garnet, chromite, and clinopyroxene. Golf kimberlite is hypabyssal with xenocrysts composed of mantle olivine, pyroxene, and xenoliths of limestone. It also contains, ilmenite, and clinopyroxene, minor garnet and, minor chromite. It is unknown whether the kimberlite is diamondiferous or barren. The Alpha-1 and Alpha-1 North kimberlites are hypabyssal with limestone, basement, and mantle xenoliths. Olivine, pyroxene, phlogopite, ilmenite, minor chromite and minor chrome diopside have been identified. It is unknown whether the kimberlite is diamondiferous or barren. The X-Ray kimberlite consists of hypabyssal facies and contains limestone and other crustal xenoliths. The mineralogy includes olivine, ilmenite, chrome diopside, and garnet, and the kimberlite is diamondiferous. The Bravo-1 kimberlite consists of hypabyssal facies with fresh and altered olivine, clinopyroxene, ilmenite, chromite, and rarely garnet. This kimberlite is diamondiferous. Carbonate, spinel, phlogopite, apatite, and perovskite are common groundmass minerals in Attawapiskat kimberlites (Kong *et al.*, 1999; Armstrong *et al.*, 2004).

The whole rock metal compositions of Attawapiskat kimberlites (DeBeers unpublished data) are comparable to other Jurassic kimberlites along the Timiskaming fault such as those from Kirkland Lake and New Liskeard (Sage, 2000b), and other kimberlites worldwide (Mitchell, 1986).

1.4 METHODS

1.4.1 Field procedures

1.4.1.1 Water sampling

Water samples were collected in the summer (August 14-23) and fall (October 14-18) of 2007, and in the summer (early August) and fall (late September) of 2006. Samples collected in 2006 and 2007 are denoted by the prefixes *06* and *07*, respectively, and samples collected in fall are denoted by the suffix *F*. Samples along Yankee, Zulu, and Golf transects are denoted by the prefixes of *Y*, *Z*, and *G*, respectively. All water samples from 2006 were reported by Brauneder (2007). Compositions of water samples collected in 2007 are presented in Table 1-1.

Peat groundwaters were collected using piezometers with an internal diameter of 19 mm, and which are made of 1.5 m long white (environmental grade) polyvinyl chloride (PVC) or grey PVC. Piezometers function as a method to collect groundwater from a desired depth with minimal influence of waters from shallower zones within an aquifer. In this study they were installed 1.1 m below ground surface (mbgs) into the peat at the Zulu, Yankee, and Control locations in 2007, and to 0.4 mbgs along the transect at Golf and Control in 2006. Piezometers were pushed into the peat with a loosely fitting plastic champagne cork at the end to prevent peat from entering the pipe while it was being installed. The pipe was then

pulled up *c* 0.1 m so that the cork did not impede water from flowing into the piezometer. Piezometers were installed approximately every 25 to 50 m along each transect and at least 200 m beyond the kimberlite margins (where conditions permitted).

Monitoring wells were installed below the peat/TSS interface at each kimberlite location (two over the kimberlite and one outside the kimberlite margin) to collect deeper groundwater. Monitoring wells 07-MW-Y-10 and 11.5 at Yankee (Fig. 1-3a), 07-MW-Z-15 and 17 at Zulu (Fig. 1-3b), 06-MW-G-10 and 11 at Golf (Fig. 1-3c), 07-A-MW-11 and 12 at Alpha-1, and 07-B-MW-01 and 03 at Bravo-1 were installed over the kimberlites. Wells 07-MW-Y-01 at Yankee, 07-MW-Z-05 at Zulu, 06-MW-G-01 at Golf, 07-A-MW-01 at Alpha-1, and 07-B-MW-02 at Bravo-1 were installed outside kimberlite margins. One well (07-MW-C-01) was installed at the Control site (Fig. 1-3d). Each monitoring well was installed within 30 cm of the piezometer with the same identification (i.e. 07-MW-Z-17 and 07-Z-17) with the exception of 07-MW-Y-11.5. Wells were installed 70 cm below the peat/TSS interface except for 07-MW-Z-15, which could only be advanced 13 cm below the peat.

Groundwater samples were collected at a depth of *c.* 14 mbgs from five exploration boreholes, All boreholes are cased through Quaternary units. They are located south of center at the Zulu kimberlite (07-Z-07-12C) (Fig. 1-3b), *c.* 10 m outside and up-gradient of the Yankee kimberlite margin (07-Y-07-7H) (Fig. 1-3a), and near the centers of Alpha-1 (06-A-BH-06), X-ray (07-X-07-014C) and Bravo-1 (07-B1-07-08C) kimberlites. In addition, a spring discharging from limestone near the Attawapiskat River and the Control Site was sampled (Fig. 1-3d).

1.4.1.2 Field measurements

The water levels were recorded for all piezometers and monitoring wells from Yankee and Zulu. The top of piezometers and monitoring well casings were surveyed using a theodolite and a surveying rod to determine the water table elevation, the general direction of horizontal groundwater flow, and sites of upwelling groundwater.

The pH, oxidation-reduction potential (ORP), electrical conductivity (EC), dissolved oxygen content (DO), and temperature were measured on-site with a Hanna HI-9828 multi probe. The pH, DO, and EC probes were calibrated daily. Oxidation-reduction potential values have been corrected to the standard hydrogen electrode (SHE) for waters at 10 °C by adding 207 mV to the ORP values, and are reported as Eh. Water samples were filtered through 0.45-μm Sterivex-HV filters (Millipore Corporation) into Nalgene high-density polyethylene bottles for cation and anion analysis, and into 40-mL brown tinted borosilicate bottles with a silicone- polytetrafluoroethylene septum cap for dissolved inorganic carbon (DIC). A polytetrafluoroethylene-rubber septaum manufactured by Chromatographic Specialties Inc. was inserted underneath the septa cap to prevent DIC loss, as silicone is gas-permeable. Samples were not treated with $HgCl_2$ to kill bacteria, as all water samples were kept cool in ice-packed coolers or refrigerated and were analysed shortly after returning from the field.

1.4.2 Laboratory procedures

The elemental composition data of groundwaters were measured at the Geoscience Laboratories of the Ministry of Northern Development of Mines, Sudbury, Ontario, Canada. Waters were analysed for Ca, K, Mg, Na, and S using a Spectro inductively coupled plasma

emission spectrometer (ICP-ES) Analysis of certified references FP83MI1 and FP83TE1 before, during, and after the run indicate a precision, calculated in terms of relative standard deviation (RSD), of better than 5% for all metals except K (14%). The concentrations of Fe, Mn, Cr, Ni, Rb, Cs, Ba, and LREEs were determined using an inductively-coupled plasma mass spectrometer (ICP-MS). Analysis of certified reference SLRS-4 from the National Research Council of Canada before, during, and after the run indicate a precision of better than 5% RSD for all metals except Mn (7%) and Cs (7%). Prior to analysis, water samples for cation analysis were acidified to 1% concentration using Baseline-grade HNO_3 from Seastar Chemicals. Anions (Cl^- and SO_4^{2-}) were determined using a Dionex ion chromatograph. The RSDs for internal references, which were included during the runs are less than 5% for both Cl^- and SO_4^{2-}. Waters were analysed for DIC concentrations at the University of Ottawa G.G. Hatch Stable Isotope Laboratory using a Finnigan-Mat Delta Plus mass spectrometer. The 2 σ analytical precision is $\pm$ 0.002 ppm.

1.5 RESULTS

1.5.1 Hydrogeology and groundwater movement

The lateral velocity (v) of peat groundwater movement down-gradient was calculated using Darcy's Law:

$$v=(-Ki)/n$$

where K is the hydraulic conductivity of the peat, i is the gradient, and n is peat porosity. The calculation used a hydraulic conductivity value of 0.001 cm/s based on measurements from northern sphagnum bogs and spring fens (Chason and Siegel, 1986). This K value is in the

upper range for the catotelum (peat zone deeper than 0.3-0.5 mbgs), as K typically ranges from 10^{-2} to 10^{-6} cm/s (Ingram, 1983; Hoag and Price, 1995; Price, 2003) in this zone. An active peat porosity (n) value of 0.3 was used based on measurements of the catotelum from sphagnum peat bogs (Hoag and Price, 1995; 1997).

Peat groundwaters along the Yankee transect flow from approximately southwest to northeast with a gradient (i) of -1.66×10^{-3}. The water table is virtually horizontal between 07-Y-5.5 and 10 ($i = -1.46 \times 10^{-5}$), and between 07-Y-12 and 15 ($i = -4.67 \times 10^{-5}$) (Fig. 1-4a). The calculated velocity of peat groundwater is 5.53×10^{-6} cm/s for the entire length of the Yankee transect. However, the velocity is significantly lower for the segment between 07-Y-5.5 and 10 (4.82×10^{-8} cm/s), and for the segment between 07-Y-12 and 15 (1.56×10^{-7} cm/s) along the transect. Upwelling of deep minerotrophic groundwater was detected at sites 07-Y-01, 04, 08, 09 and 12 where the saturated zone is close to or above the ground surface. Additionally, the potentiometric surface of monitoring wells suggests upwelling in the vicinity of 07-MW-Y-01 and 07-MW-Y-11.5 (Fig. 1-4a). At Zulu, peat groundwater flows from west to east with a horizontal gradient of -1.95×10^{-3} and is generally parallel to the ground surface (Fig. 1-4b). The velocity of peat groundwater along the length of the Zulu transect is 6.50×10^{-6} cm/s. Upwelling deep groundwater is noted at 07-MW-Z-17 based on the potentiometric surface in the monitoring well and likely extends to the end of the transect.

At Golf, geochemical data are used to evaluate sites of upwelling groundwater, as hydrogeological surveying was not conducted at this location. Elevated relative values of pH and low Eh (Fig. 1-5c), and elevated Ca and EC (Fig. 1-6c) indicates upwelling deep groundwater along the transect between sites 06-G-08 (near the western margin of the

kimberlite) to the eastern end of the transect Elevated values of Ca, EC, and pH, and low values of Eh are commonly used to identify contrasts between upwelling minerotrophic and ombrotrophic groundwaters in wetlands (Ingram, 1983; Hill and Siegel, 1991; Hoag and Price, 1995). Regional drainage patterns of the area surrounding Golf observed in aerial photography suggest that regional groundwater movement is from west to east.

1.5.2 Geochemistry of Groundwaters from Kimberlite, Limestone and Tyrell Sea Sediment

The pH values in water samples collected from exploration boreholes within Attawapiskat kimberlites vary from 7.5 to 8.5 and the Eh varies from 23 to 272 mV. Concentrations of pathfinder metals such as LREE, Ni, Cr, Ba, Mg, Rb, and Cs in kimberlite groundwaters are typically greater than those in groundwaters collected from limestone (Table 1-1). On average, the majority of pathfinder metals are also elevated in kimberlite borehole groundwaters relative to waters in TSS that are directly above kimberlites. However, in TSS waters over kimberlites Ni and Cr have average concentrations of 26.5 and 4.5 μg/l, respectively, which is twice the concentration average in kimberlite borehole groundwaters (Table 1-1).

The pH values of groundwater in TSS vary between 6.5 and 8.5; however, at 06-G-MW-11F and 07-Y-MW-10 the pH values are as high as 9.25 and 9.05, respectively. The Eh values in TSS groundwaters (average = 217 mV) are typically more elevated compared with Eh values in kimberlite groundwaters (average = 90 mV). Concentrations of LREEs, Ni, Cr, Ba, Mg, and Rb in TSS groundwaters are an average of 1.8, 1.7, 3.9, 2.8, 2.3, and 1.2 times greater, respectively, over kimberlites compared to samples collected outside their margins (Table 1-1). Additionally, the Mg/Ca weight ratios in TSS groundwaters are an average of

3 9 times greater over compared to outside kimberlites However, Cs concentrations in TSS waters over kimberlites are only 0.8 times the concentration of TSS waters outside kimberlite margins.

1.5.3 Peat groundwater geochemistry

In peat groundwater samples, the pH values vary from 3.8 to 7.1 and Eh values range from 125 to 512 mV (Fig. 1-5a, b, c). The highest pH and lowest Eh values are assumed to be associated with sites of upwelling minerotrophic groundwater along each transect. Of Yankee, Zulu, and Golf peat groundwaters, samples from Golf have the lowest pH and highest Eh values. This may be explained by the shallower collection depth of water at Golf (0.4 mbgs).

Ombrotrophic peat groundwaters are indicated by low EC (< 100 μS/cm) and Ca concentrations (< 8 mg/l) (Ingram, 1983; Hill and Siegel, 1991; Hoag and Price, 1995). Conversely, high EC values (> 100 μS/cm) and Ca concentrations (up to 70 mg/l) suggest high contributions of minerotrophic groundwaters, which are observed at sites of groundwater upwelling along the transects (Fig. 1-6a, b, c). High EC and Ca are accompanied by elevated DIC (Table 1-1). Dissolved organic carbon (DOC) concentrations vary between 3.30 and 158 mg/l, have a broad negative correlation (r = -0.61) with EC, and are typically low at sites where hydrogeological and geochemical measurements indicate upwelling.

Baseline values are derived for metals (Ni, Cr, LREE, Ca, Mg, Mg/Ca, Ba, Rb, and Cs) and for pH, Eh, and EC from peat groundwaters that were collected at 1.1 mbgs greater than 200 m from kimberlite margins and from Control Site. As Golf peat groundwaters were collected from a more shallow depth of 0.4 mbgs, baseline values are those of waters

collected 200 m beyond the Golf, Yankee, Alpha-1 kimberlite margins and Control Site during 2006 sampling events (Brauneder, 2007). All waters used to obtain baseline values are ombrotrophic with EC values of < 100 uS/cm.

Transition metals consisting of Ni, Cr, and LREE (La-Sm) are consistently elevated along transects at sites near kimberlite margins. Although the Yankee transect shows four sites of upwelling (07-Y-01, 04, 08-09, and 12), only site 07-Y-08 (west kimberlite margin) has significantly elevated Ni and Cr (Fig. 1-7a), and LREE (Fig. 1-8a) concentrations. These metals are between 1.5 and 2.5 orders of magnitude greater than the baseline concentrations and are similar to concentrations observed in groundwaters from exploration boreholes in kimberlites (Table 1-1). Nickel, Cr and LREE are low at 07-Y-12 (near the east kimberlite margin) (Figs. 1-7a, 1-8a). Elevated Ni, Cr, and LREE concentrations in peat groundwaters from Zulu and Golf are typically 2-3 times greater than mean baseline values. At Zulu, Ni is elevated near the east kimberlite margin (07-Z-13 to 19); however, Cr is only elevated at sites 07-Z-13, and to a lesser extent, at 07-Z-15 (Fig. 1-7b). Light REEs are significantly greater than baseline concentrations at the east kimberlite margin (07-Z-15 and 17; Fig. 1-8b). The location of Ni, Cr and LREEs concentration profiles along the transect at Golf are similar to those of Zulu except that the highest concentrations of these metals are located at the west margin of Golf kimberlite (between 06-G-04 and 08) (Figs. 1-7c, 1-8c). However, elevated concentrations of Ni occur at 06-G-11 and at the east kimberlite margin from 06-G-15 to 17 (Fig. 1-7c). At both Zulu and Golf, the highest transition metal concentrations usually coincide with a small contribution of upwelling minerotrophic groundwater. Nickel, Cr, and LREE concentrations are typically lower than baseline values at sites down-gradient at both Zulu and Golf, and at 07-Y-12 (Yankee) where minerotrophic waters are more

dominant. Collectively, Ni, Cr, and LREEs are referred to as 'Group 1 metals' due to the similarity of their spatial distribution along the transects in this study.

Peat groundwaters along the Yankee transect show elevated Mg concentrations at 07-Y-08 and 11 (Fig. 1-9a). The Mg/Ca ratios are high at 07-Y-08 and between 07-Y-13 and 15, but are low at 07-Y-11 (Fig. 1-9a). Elevated concentrations of Ca (Figs. 1-6b & c), and Mg (Figs. 1-9b & c) observed along Zulu and Golf transects are consistent with upwelling minerotrophic groundwaters inferred from the geochemistry. However, the Mg/Ca ratios are highest at sites of inferred upwelling near kimberlite margins (Figs. 1-9b & c). High Mg/Ca ratios are also noted at some sites where groundwater is not inferred upwelling such as 07-Z-13 and 15 at Zulu and 07-G-02 to 05 at Golf.

Concentrations of Ba in peat groundwaters are 1 to 1.5 orders of magnitude higher relative to the baseline concentrations at or near Yankee and Zulu kimberlite margins. The Ba profile along the Yankee transect (Fig. 1-10a) is consistent with other alkaline earth metals. The profile is almost identical to that of Mg (Fig. 1-9a), with elevated concentrations at 07-Y-08, 11 and 12. However, Ba is low at 07-Y-04 even though Ca is high. The Ba concentration profiles along at Zulu and Golf sampling transects are not consistent with other alkaline earth metals, but are more similar to the profiles of Group 1 metals. Barium is highest along the Zulu transect near the eastern margin of the kimberlite between sites 07-Z-17 and 21 (Fig. 1-10b). Along the Golf transect, Ba is elevated at the up-gradient margin of the kimberlite (between 06-G-06 and 09; Fig. 1-10c). Note that the Ba concentrations at Golf are 2 orders of magnitude greater than Yankee or Zulu. All waters collected from this sampling event (summer 2006) have high Ba values. Because of these high concentrations, we have revised the baseline data for Ba to reflect only waters collected during summer 2006

for consistency. Although the reason is not clear, we have ruled out the possibility of contamination, or analytical artifact. Laboratory QA and QC results indicated an relative standard deviation (RSD) of < 5% for Ba and analytical runs for Ba using ICP-MS and runs using ICP-AES had almost identical concentrations. Furthermore, Ba concentrations in peat groundwaters from 2006, which were collected at 0.4 mbgs along the Yankee transect, had similar profile shape compared with the Yankee profile in this study.

Concentration profiles of alkali metals (Rb and Cs) in peat groundwaters differ from those of Group 1 and alkaline earth metals along transects and are typically displaced 50 to 100 m from sites of elevated Group 1 metals and Ba. The highest alkali metal concentrations at Yankee are at 07-Y-02, 08, and 09 (Fig. 1-11a). Along the Zulu transect, alkalis are elevated at sites of inferred upwelling from 07-Z-19 to 29, but sharply decrease farther east along the transect even though upwelling appears to continue (Fig. 1-11b). At Golf, the highest alkali concentrations are observed at 06-G-05, in waters considered ombrotrophic (Fig. 1-11c). At Golf and Yankee alkali concentrations are only slightly higher than baseline values.

Sulfate concentrations are low at all sites (mean = 0.35, median = 0.3, max = 3.97 mg/l) (Table 1-1) and total sulfur concentrations in waters are also low (mean = 0.4, max = 0.9, min = < 0.3 mg/l) (Table 1-1). Chloride concentrations are low and range from 0.12 to 25.43 mg/l with mean and median concentrations of 3.6 and 2.0 mg/l, respectively (Table 1-1).

1.6 DISCUSSION

1.6.1 Metal sources in peat groundwaters

There are only three possible sources of metals in the study area that could contribute to elevated pathfinder metals in peat groundwaters: 1) host rock (dominantly Attawapiskat Formation limestone); 2) TSS; or 3) kimberlite. A limestone source for the elevated metals can be discounted because the concentrations of Group 1, Ba, Mg/Ca and alkali metals in peat, TSS, and kimberlite groundwaters are greater than concentrations in limestone groundwater (sometimes by more than one order of magnitude). Additionally, the Upper Attawapiskat Formation limestone is typically much lower in minerals that host high concentrations of Group 1, Ba, or alkali metals (Norris, 1993), especially compared to the mineral composition of kimberlites (Mitchell, 1986). Plots of kimberlite and limestone groundwaters from this study, together with groundwaters from Kirkland Lake kimberlites (Sader *et al.*, 2007a) (Fig. 1-12) highlight the differences in pathfinder metal concentrations between kimberlite and limestone sources. The elevated pathfinder metals observed in Attawapiskat and Kirkland Lake kimberlite groundwaters in slightly alkaline conditions (pH = 7 to 8.5) are due to the chemical weathering of olivine, pyroxene, and phlogopite in kimberlites (Sader *et al.*, 2007a). High Mg/Ca ratios are due to the serpentinization of olivine, which often results in an Mg-HCO_3^- water (Barnes and O'Neil, 1969; Palandri and Reed, 2004). In kimberlite waters that have circum-neutral pH (7-9) and bicarbonate alkalinity Mg/Ca ratios are typically 0.5 to 0.8 (Sader *et al.*, 2007a) and are comparable to kimberlite waters in this study (Fig. 1-12).

Elevated metal concentrations at or near the kimberlite margins are most likely due to geochemical influences from kimberlite rather than TSS. Of the TSS groundwaters,

concentrations of Group 1, Ba, and alkalis are 1.2 to 4 times greater (with the exception of Cs) for those waters collected over kimberlites versus those collected outside the margins. The Mg/Ca ratios in TSS groundwaters over kimberlites support a kimberlite origin as they are approximately 4 times greater than TSS groundwaters collected outside kimberlites and 10 times greater than ratios in groundwaters from limestone. Although there is a dolomite unit within the host Palaeozoic rock, it is 200 m below the Upper Attawapiskat Formation and is likely of little influence on groundwater geochemistry in this study.

1.6.2 Spatial distribution of kimberlite pathfinder metals in peat groundwaters

1.6.2.1 Hydrogeological controls on vertical metal movement

The most likely pathway for the upward migration of pathfinder metals from kimberlites is along kimberlite-limestone margins. Group 1, Ba, Mg/Ca, and alkalis are commonly found at peat groundwater sample sites that have evidence of upwelling and that are also within 200 m of kimberlite margins. Conversely, upwelling at other sites such as near bioherms (07-Y-04 at Yankee), or sites that are greater than 200 m from kimberlites did not usually indicate elevated pathfinder metals.

The location of upwelling deep groundwaters to peat near the margins of kimberlites is likely due to elevated hydraulic conductivity in the fractured rocks along the boundary between kimberlite and the host rock. During kimberlite emplacement in various geological settings, the margins of kimberlite pipes and adjacent host rocks are commonly fractured due to the explosive release of volatiles (Mitchell, 1986; Wilson and Head, 2007). These fractures likely represent preferential pathways for upward groundwater movement from kimberlite. In the Attawapiskat kimberlite field, the highly fractured zone surrounding the

Victor kimberlite forms a ring up to 150 m wide and has a hydraulic conductivity of 5.79 x 10^{-3} cm/s (Hydrologic Consultants, 2004). In contrast, non-fractured host Attawapiskat Formation limestone had a moderately lower lateral hydraulic conductivity (1.16 x 10^{-3} cm/s), and a much lower vertical hydraulic conductivity (1.16 x 10^{-5} cm/s), (Hydrologic Consultants, 2004). Additionally, the less common occurrence of elevated pathfinder metal concentrations directly over kimberlites in this study could be explained by their low relative hydraulic conductivities. The K values in several brecciated kimberlites such as Diavik in Canada (Kuchling *et al.*, 2000), and Letlhakane, The Oaks and Venetia in South Africa (Morton and Mueller, 2003) are 4 x 10^{-5}, 1.97 x 10^{-6}, 1.62 x 10^{-7}, and 5.8 x 10^{-8} cm/s respectively.

1.6.2.2 Hydrogeological controls on lateral peat groundwater movement

Profiles of geochemical parameters (i.e. EC, pH, Eh) along transects do not have a characteristic dispersion plume pattern down-gradient, such as those observed in streams (Leybourne *et al.*, 2003), or aquifers (Freeze and Cherry, 1979). This suggests limited lateral movement of metals within peat groundwaters and is consistent with low hydraulic conductivity of peat within the catotelum (Ingram, 1983; Chason and Siegel, 1986; Fraser *et al.*, 2001; Price, 2003). The profiles likely indicate the presence of mixing as peat groundwaters grade from dominantly ombrotrophic to minerotrophic. The portion of water from deep sources increases relative to ombrotrophic peat groundwater at sites along transects at Zulu (07-Z-17 to 29) and Golf (06-G-08 to 15).

The combination of the hydraulic conductivity of peat and the small water table gradients suggest that at the depth of sample collection (1.1 mbgs), peat groundwater will migrate laterally between 0.2 and 200 cm/year. It could also be less if the peat freezes to sample

depth during winter There is a greater potential for metals to migrate laterally at Golf, as samples were only collected at 0.4 m, and may be in a zone of higher hydraulic conductivity (i.e. the acrotelm); however, a dispersion-plume profile of geochemical parameters was not observed.

1.6.2.3 Peat geochemical controls

It is possible that geochemical processes within the peat exert considerable controls on kimberlite pathfinder metals in peat groundwaters and may explain the spatial variability between metals and/or groups of metals along transects. Although it is assumed the suite of pathfinder metals originates from buried kimberlite, their displacement relative to each other and relative to sites of upwelling suggests adsorption, binding and mineral precipitation may play a role in controlling their solubility in peat groundwaters.

Variable DOC concentrations may influence metal concentrations in ombrotrophic and minerotrophic peat groundwaters. Where DOC concentrations are elevated (low contributions from upwelling groundwaters), pathfinder metals such as Group 1 may preferentially bind to dissolved organic matter (DOM) and result in enhanced metal solubility. Metals bound to DOM are typically inhibited from adsorption or precipitation processes (Cornell and Schwertmann, 2003). Conversely, where waters are strongly minerotrophic and DOC concentrations are low, Group 1 metals may be less likely to form complexes with DOM. Decreases in metal-DOM complexes typically result in greater concentrations of free ions, which could easily be scavenged from solution by adsorption or secondary mineral precipitation (Tang and Johannesson, 2005; Syrovetnik *et al.*, 2008). In this study, Group 1 metals are usually lower than baseline values at sites of strong upwelling such as 07-Y-12, at Yankee, 07-Z-21 to 35 at Zulu, and 07-G-10 to 17 at Golf. At these sites,

Group 1 metals may adsorb to Fe-oxyhydroxides or be incorporated into their structure. Fe contents in Attawapiskat peat along Yankee and Golf transects determined by Hattori and Hamilton (2008), increase with increasing upwelling groundwater contributions observed in this study.

In comparison to Group 1 metals, alkaline earth and alkalis have lower affinities to bind to dissolved organics, or to adsorb to insoluble organics (Stevenson, 1994), and they have almost no affinity to adsorb onto Fe-oxyhydroxides at pH values in this study (Kinniburgh *et al.*, 1976). Elevated Mg/Ca ratios are typically observed at sites of other elevated pathfinder metals such as Group 1, Ba, and alkalis. Because both Mg and Ca behave similarly in peat groundwaters with respect to adsorption or binding to organic substances and because Mg/Ca is a ratio and not an absolute metal concentration, Mg/Ca ratios may be less susceptible to variable geochemical processes in peat.

1.6.3 Contrasts between peat and peat groundwater geochemistry

The peat groundwater hydrogeological and geochemical data suggest that metal anomalies in peat at Yankee and Golf (Hattori and Hamilton, 2008) are the result of upward movement of deep groundwater from kimberlites. Peat samples of Hattori and Hamilton (2008) were collected at the same sites as peat groundwater samples of this study, but at 0.6 mbgs. Good correlations were observed between the results of ammonia acetate leach at pH 5 ('AA5') of peat (Hattori & Hamilton 2008) and alkaline earth metals in peat groundwaters. As AA5 typically leaches metals weakly adsorbed and metals that co-precipitate with carbonates, Mg/Ca ratios in peat and peat groundwaters are positively correlated ($r = 0.76$).

Elevated LREEs, Ni, and Rb in peat (by AA5) and peat groundwater correlated well at Yankee sites 07-Y-08 and 09. Light REEs are also elevated at similar locations in both

peat (AA5) and peat groundwaters at the Golf kimberlite. However, the elevated LREE and Ni concentrations in peat at 07-Y-11 at Yankee and Ni at Golf are coupled with groundwater concentrations that are the same as or less than baseline values. The elevated metals in peat groundwaters are instead observed at locations where peat (AA5) concentrations are low. There are a number of possibilities as to why discrepancies between the locations of elevated LREE, Ni, and Rb concentrations in peat (AA5) and peat groundwaters exist at some sites. It is possible that spatial discrepancies are related to the affinity of these metals to remain in solution, or to be removed from solution via precipitation or adsorption. It is also possible that AA5 is not the optimum leach for some metals. The recovery of Ni, LREEs, and Rb in AA5 compared to total peat concentration was only 30, 4, and 17%, respectively (Hattori and Hamilton, 2008), as AA5 is not favoured to leach metals strongly adsorbed to insoluble humic substances or Fe-oxyhydroxides. Differences in the spatial distribution of elevated Ni, LREEs, and Rb in peat (AA5) and peat groundwaters may also be related to different sampling depths of media. Peat groundwaters were collected at 1.1 mbgs at Yankee and 0.4 mbgs at Golf. Redox conditions, metal concentrations, concentrations of dissolved organic material, and the degree of peat humification vary significantly with small changes in depth (Clymo, 1983; Syrovetnik *et al.*, 2004; Beer and Blodau, 2007).

1.7 PEAT GROUNDWATERS IN GEOCHEMICAL EXPLORATION

1.7.1 Application to exploration

Groundwaters from peat and other geological units are excellent media for geochemical surveys (Leybourne *et al.*, 2003; Sader *et al.*, 2007a; Leybourne and Cameron, 2010). This study suggests that kimberlite pathfinder metals in peat groundwaters are likely reliant on the presence of upwelling groundwater from kimberlites. Pathfinder metals in these

groundwaters contrast with dilute ombrotrophic peat groundwaters and groundwaters that have upwelled from limestone or TSS. The limestone host rock in this study does not contain minerals that host high concentrations of kimberlite pathfinder metals. Furthermore, at locations where the kimberlite host rock is igneous or metamorphic crystalline such as the Superior, the Slave, and the Churchill cratons in Canada, kimberlite pathfinder metals are typically released to groundwater more readily from kimberlites due to the relatively rapid weathering of ultramafic minerals such as olivine and pyroxene (Sader *et al.* 2007). Therefore, groundwaters influenced by kimberlite-water interactions are likely distinguishable from upwelling groundwaters that passed through different rock types.

Large cratonic regions in the northern hemisphere have high potential for the existence of undiscovered diamondiferous kimberlite occurrences (Janse and Sheahan, 1995). As these regions commonly have vast wetlands, shallow groundwater has the potential to be utilized as a geochemical exploration tool to mitigate the greater challenges involved in implementing more established exploration methods such as geophysics. Other intrusive bodies such as syenite and mafic dykes may show geophysical features similar to kimberlites. Surficial water geochemical methods can assist by providing evidence as to whether a geophysical anomaly is a kimberlite before the commencement of drilling.

1.7.2 Survey design

This study suggests that sampling of groundwaters should be combined with a hydrogeological survey of the areas near a potential buried kimberlite body. A hydrogeological survey provides information on the flow direction of groundwaters and sites of upwelling deep waters. Installation of monitoring wells is useful to confirm upwelling and they are typically more precise at locating sites of upwelling in peat groundwaters compared

with the detection of variations in geochemical parameters such as EC, Eh, and pH For example, the 07-Z-MW-17 (Zulu) monitoring well hydrogeological data indicate upwelling; however, there are only low to moderate geochemical upwelling indicators in peat groundwaters at that site relative to sites farther east along the transect. The disadvantage of monitoring wells is that installation is physically demanding and time-consuming. As it is not feasible to install monitoring wells at each site that a piezometer is installed at, it is important to rely on variations in geochemical parameters in conjunction with hydrogeology to detect groundwater upwelling. One alternative to the installation of many monitoring wells would be to install piezometer nests that are only within the peat zone. Hydrogeological data from piezometers beside each other at various depths in the peat would permit the construction of flow nets and better indications of peat groundwater movement.

The collection of peat groundwater samples should be carried out along transects parallel to groundwater flow because of possible displacement of pathfinder metals. Transects positioned perpendicular may risk failure in intersecting upwelling groundwater. Peat groundwater samples should be collected at least 200 m beyond the suspected kimberlite margins where possible, as fractured host rock may extend as far as 150 m from the margin. If upwelling of deep groundwater is present, a transect may be extended longer than 200 m to gauge possible differences in peat groundwater geochemistry from different sources. Additionally, the data from samples > 200 m from the suspected kimberlite body provide local baseline values. Peat and soil sampling well beyond the margin of kimberlites was also suggested in exploration surveys for kimberlites in wetlands (Hattori and Hamilton, 2008). Depending on site conditions, it is likely that grid sampling would provide an

enhanced portrait of peat groundwater geochemistry associated with a potential buried kimberlite.

1.8 ACKNOWLEDGEMENTS

We thank DeBeers Canada for providing financial and logistic support for the project. Ed Francisco, and Brad Wood were particularly helpful. The financial support was also provided by a NSERC Collaborative Research grant to Keiko Hattori. Fieldwork was assisted by and Katherine Mellor. Jamil Sader acknowledges an Ontario Graduate Scholarship and a student research grant from the Society of Economic Geologists. Journal reviewers Mats Astrom and Agnete Steenfelt, and Editor Gwendy Hall provided thorough and insightful reviews that greatly benefited this paper.

1.9 FIGURES

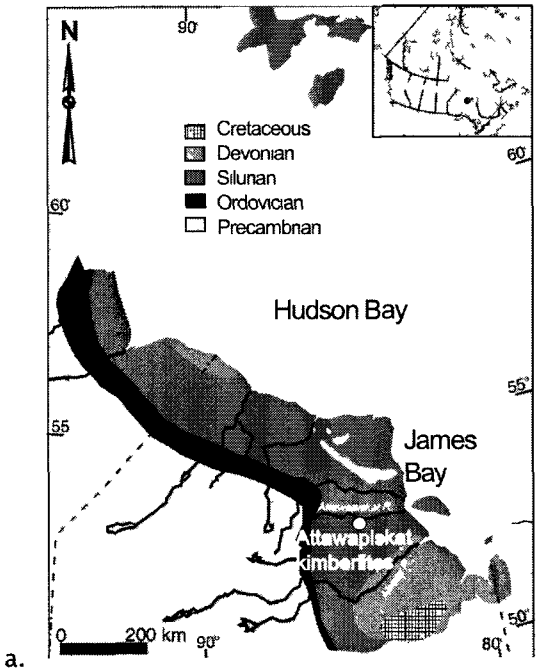

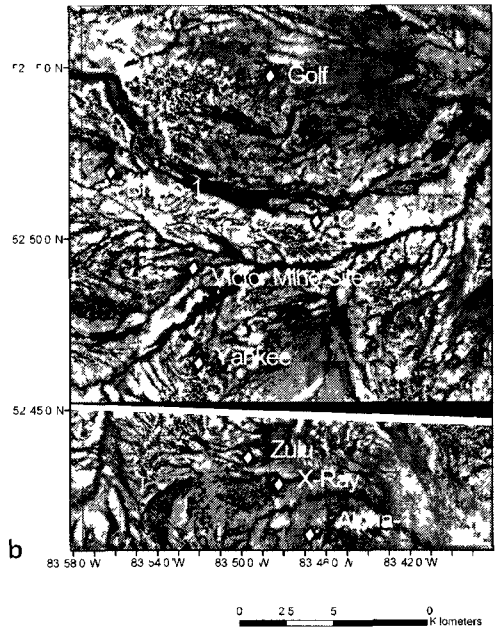

Figure 1-1. (a) Regional geology of the James Bay Lowlands, from Bellefleur *et al* (2005), and (b) the locations of Attawapiskat kimberlites and the Control site in this study

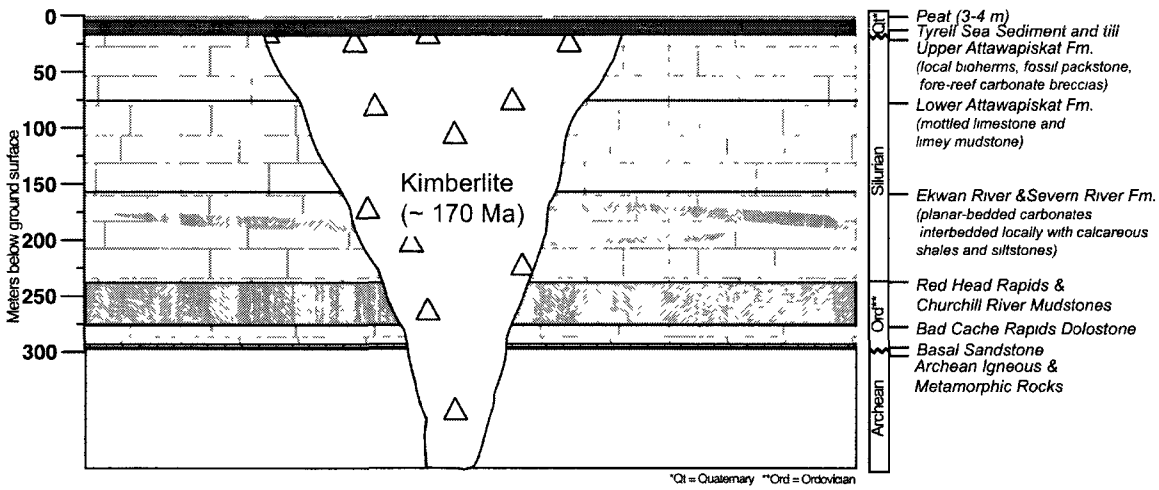

Figure 1-2. A schematic vertical section of rocks and sediment into which Attawapiskat kimberlites are emplaced. The kimberlite and host rocks are overlain by a thin basal till layer (not shown), Quaternary Tyrell Sea sediment (10 to 5 Ka), and peat (5 Ka to present). Figure modified from Webb *et al.* (2004); geology from Norris (1993).

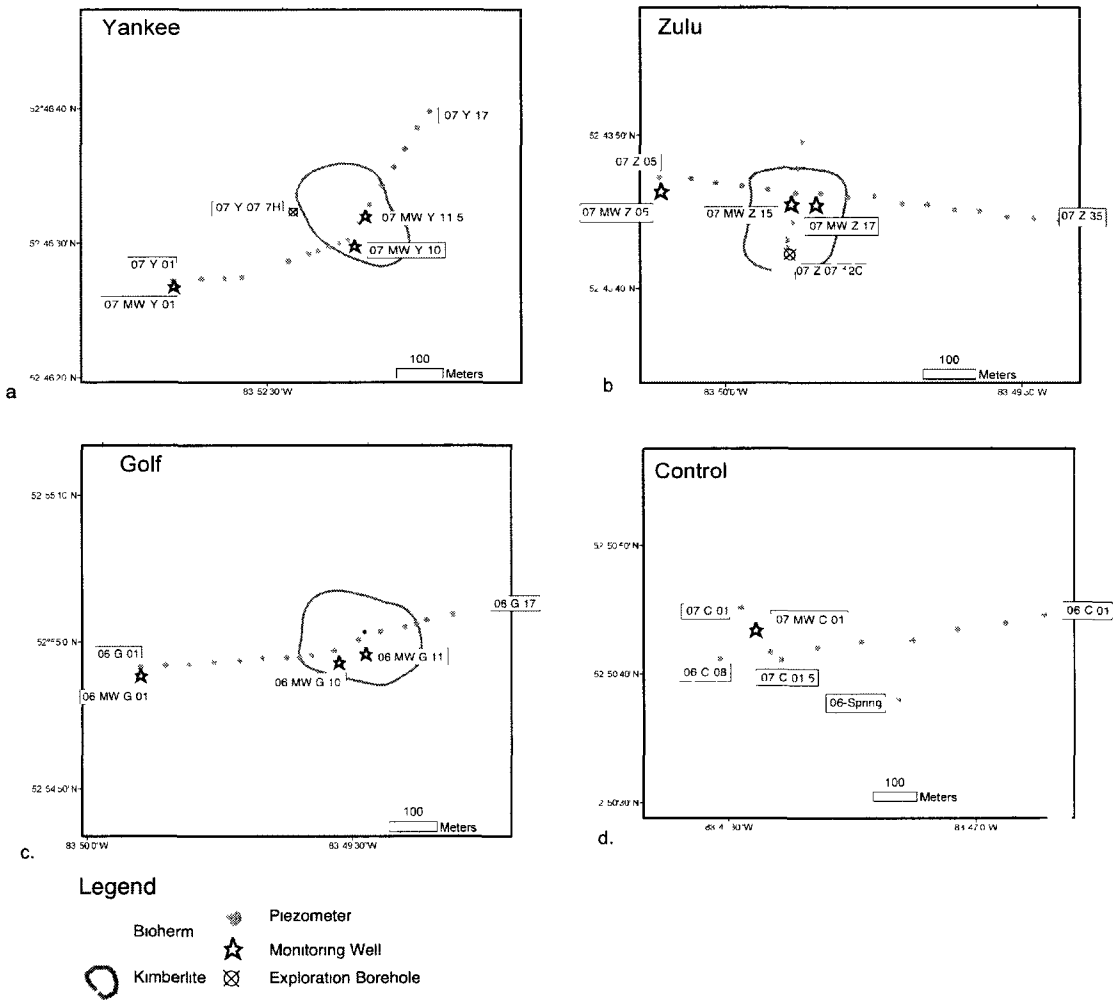

Figure 1-3. Locations of piezometer transects, monitoring wells, and boreholes at (a) Yankee, (b) Zulu, (c) Golf, and (d) Control Site. Locations of bioherms have been drawn to make them more identifiable on the aerial photos. Outlines of kimberlites were determined by geophysics and drilling by DeBeers Canada.

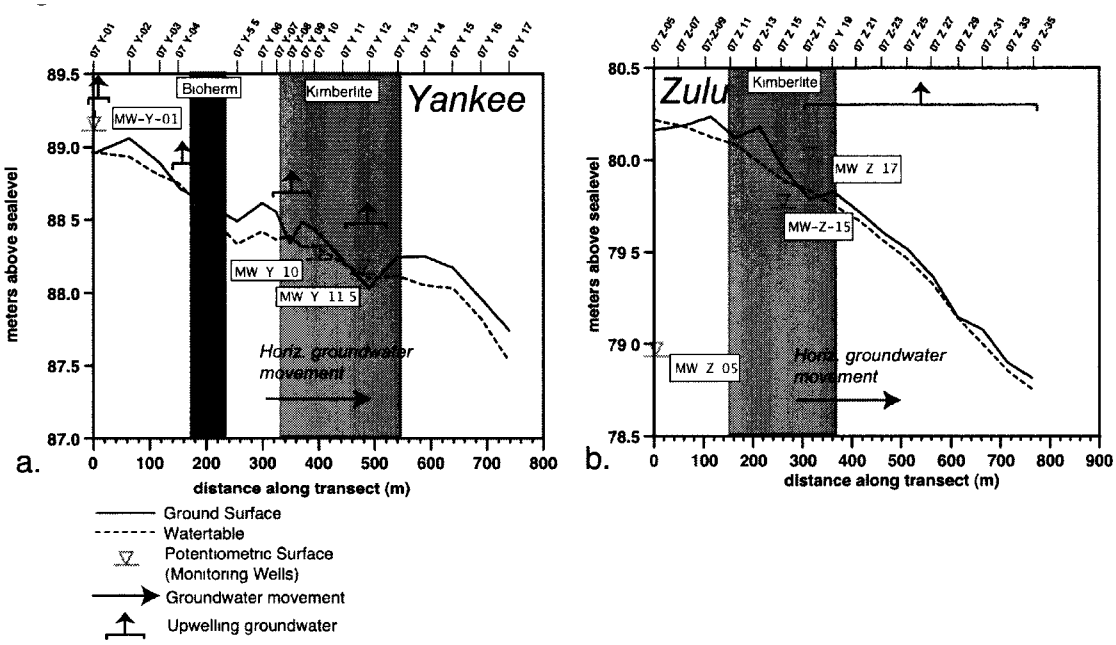

Figure 1-4. Profiles of the ground surface, the water table, and potentiometric surfaces along the transects at (a) Yankee and (b) Zulu kimberlites Sites with potentiometric surfaces greater than the water table indicate upwelling groundwater

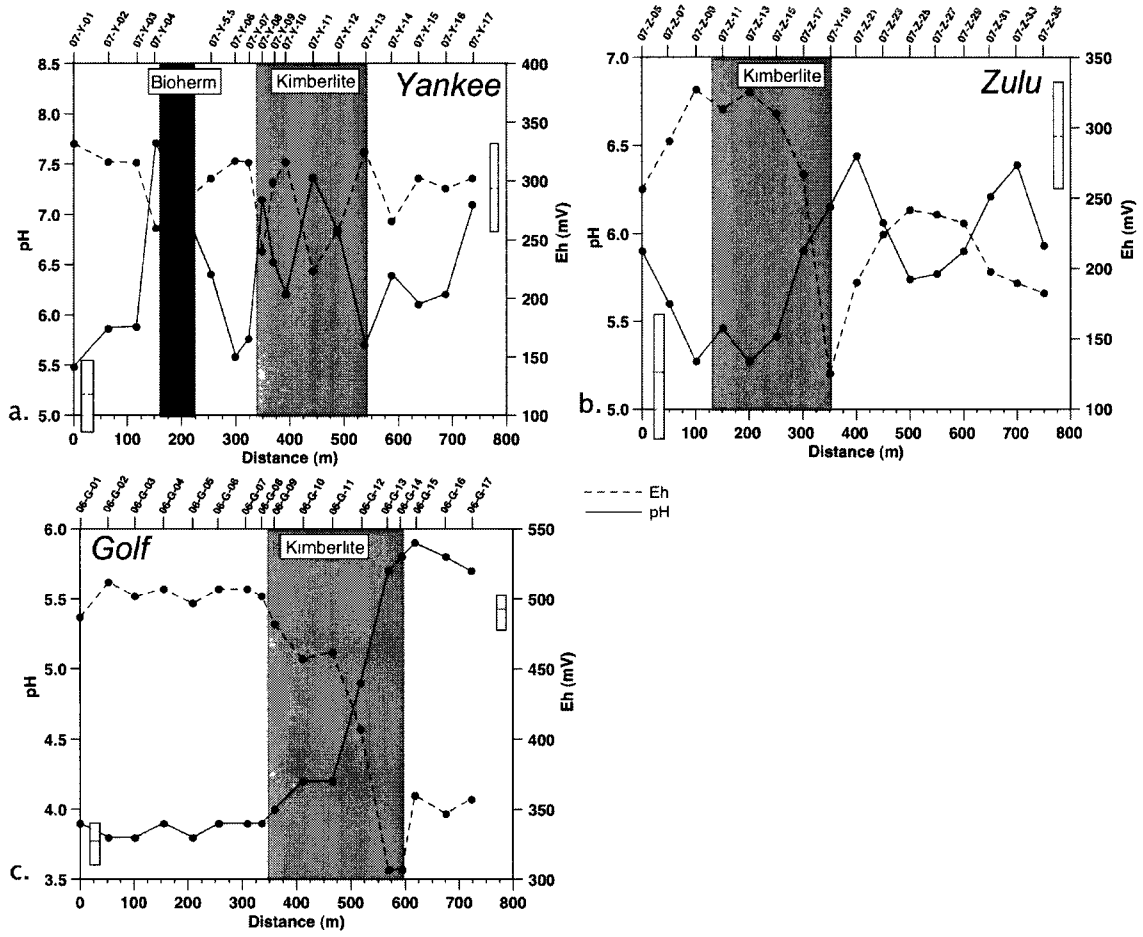

Figure 1-5. Profiles of pH and Eh along transects over: (a) Yankee, (b) Zulu, and (c) Golf kimberlites. Typically, pH and Eh indicate sites of upwelling groundwater and a shift from ombrotrophic to minerotrophic peat groundwater conditions. Box plots represent the mean, first and third quartile values for baseline ombrotrophic peat groundwaters.

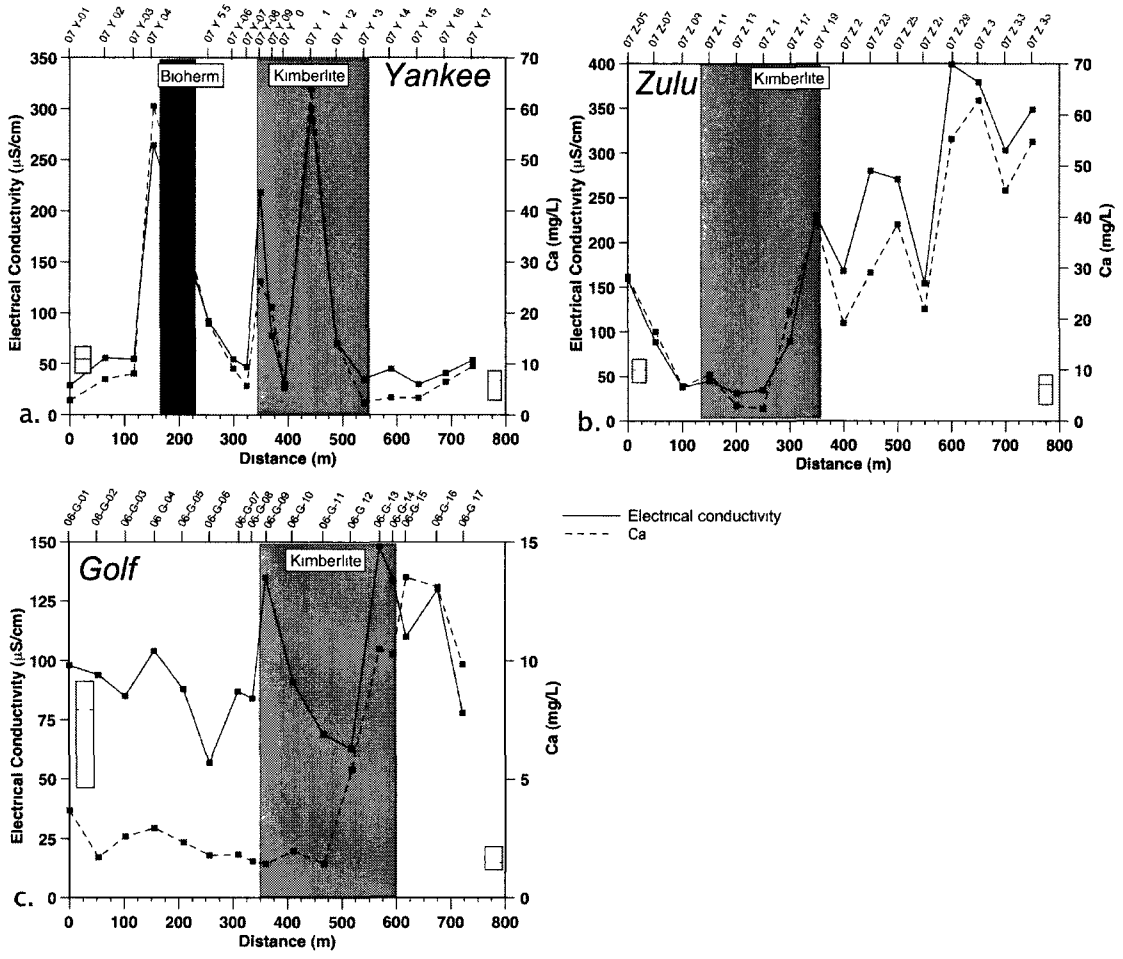

Figure 1-6. Profiles of electrical conductivity and Ca along transects over. (a) Yankee, (b) Zulu, and (c) Golf kimberlites. Electrical conductivity and Ca correlate well and indicate sites of upwelling minerotrophic groundwaters. Box plots represent the mean, first and third quartile values for baseline ombrotrophic peat groundwaters

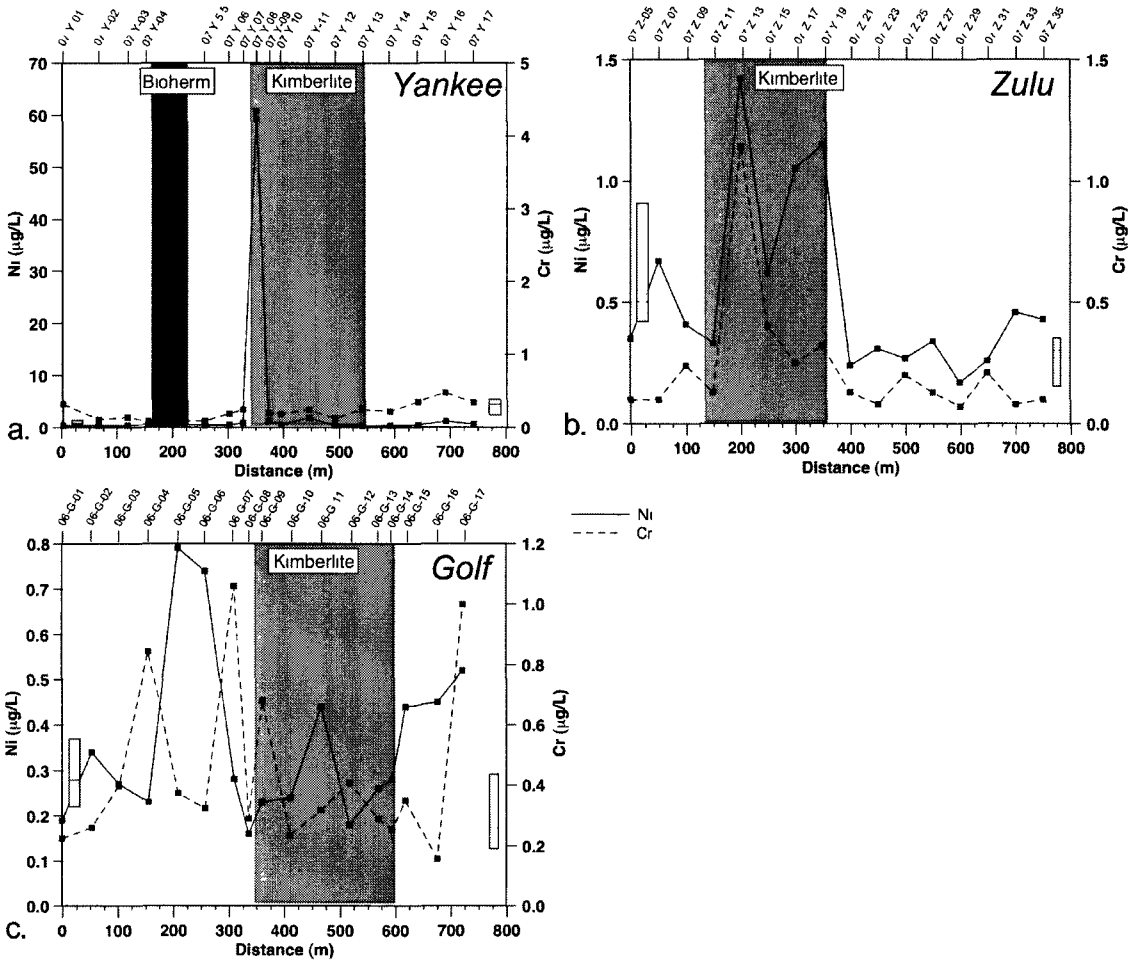

Figure 1-7. Concentrations of Cr and Ni in peat groundwater along transects over: (a) Yankee, (b) Zulu, and (c) Golf kimberlites. Ni and Cr are typically observed at sites of upwelling at kimberlite margins. Box plots represent the mean, first and third quartile values for baseline ombrotrophic peat groundwaters.

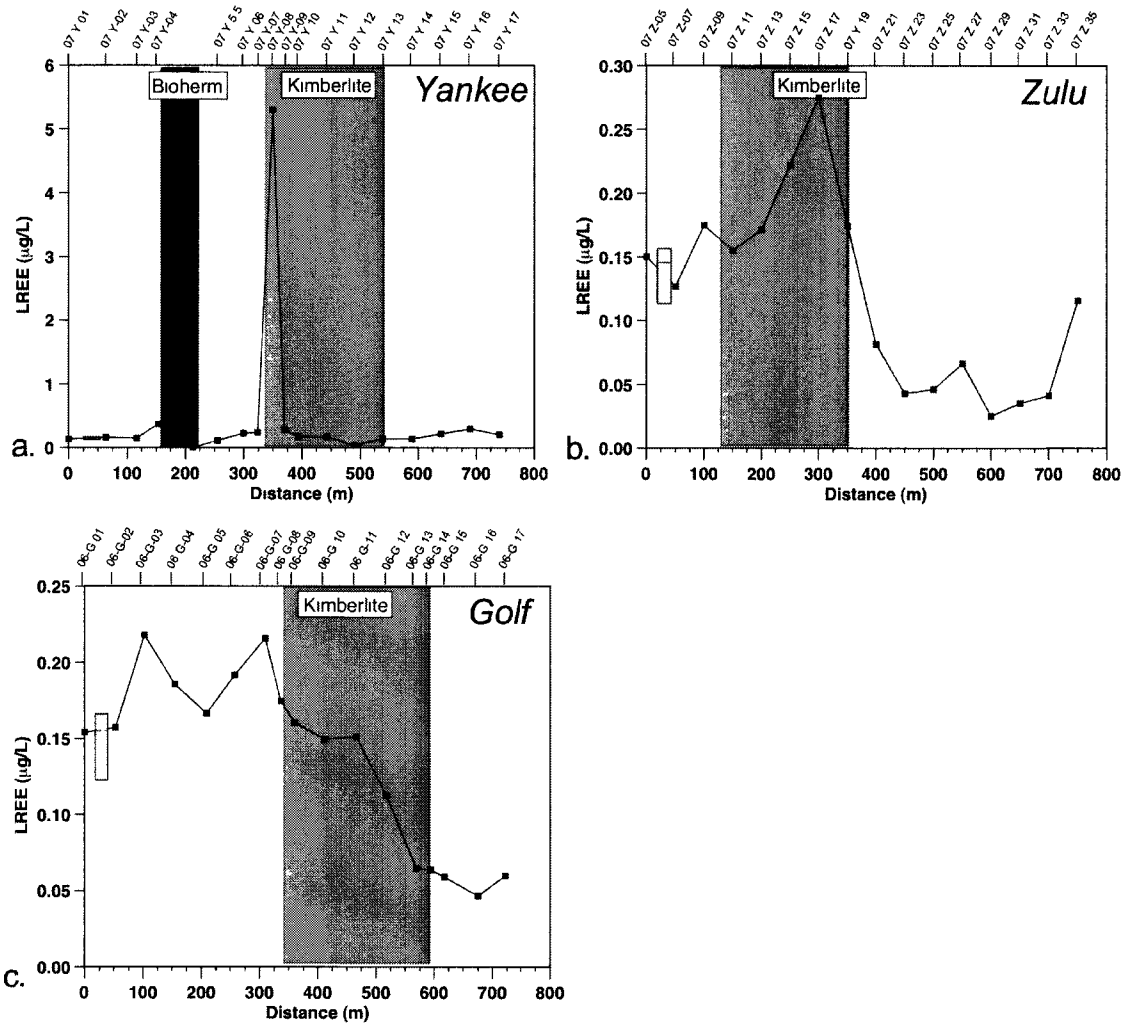

Figure 1-8. Concentrations of LREEs (La-Sm) in peat groundwater along transects over: (a) Yankee, (b) Zulu, and (c) Golf kimberlites Light REEs have similar profiles to Ni and Cr and are typically observed at the kimberlite margins Box plots represent the mean, first and third quartile values for baseline ombrotrophic peat groundwaters

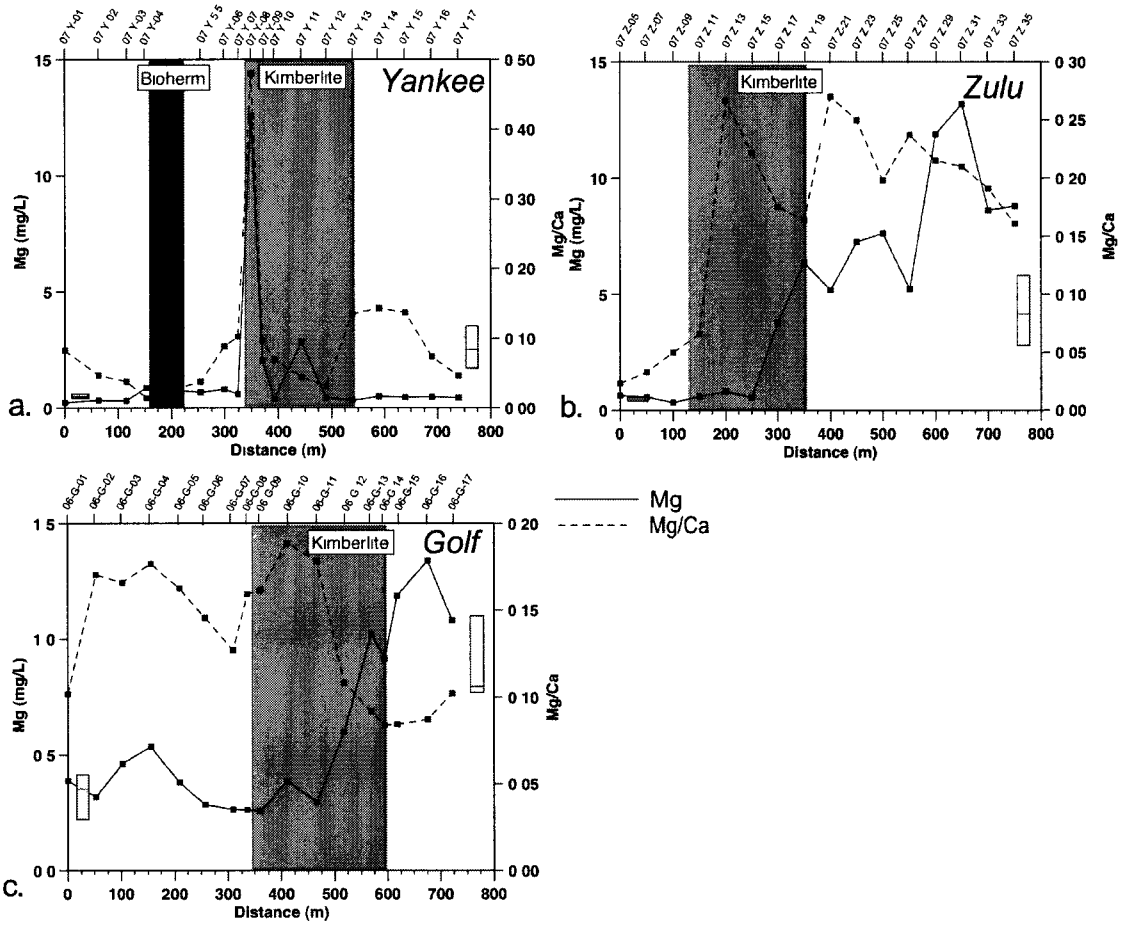

Figure 1-9. Concentrations of Mg and Mg/Ca in peat groundwater along transects over (a) Yankee, (b) Zulu, and (c) Golf kimberlites With the exception of Yankee, Mg indicates locations of upwelling minerotrophic groundwater The broad elevated Mg/Ca peaks along transects suggest waters rich in Mg relative to Ca may be coming from buried kimberlite Box plots represent the mean, first and third quartile values for baseline ombrotrophic peat groundwaters

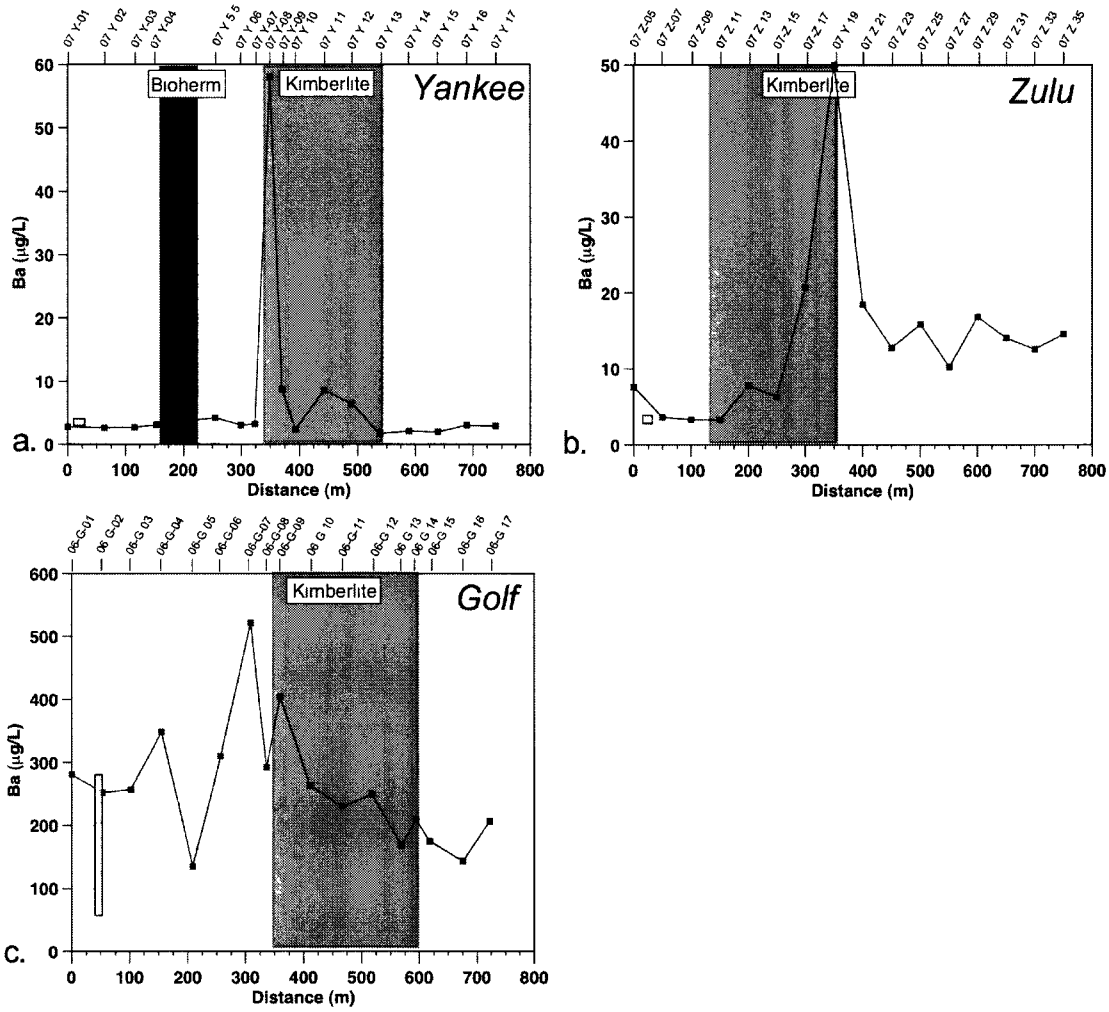

Figure 1-10. Concentrations of Ba in peat groundwater along transects over: (a) Yankee, (b) Zulu, and (c) Golf kimberlites. Barium is typically elevated only a kimberlite margins and their profiles differ compared with other alkaline earth metals (i.e Ca and Mg) at Zulu and Golf. Box plots represent the mean, first and third quartile values for baseline ombrotrophic peat groundwaters.

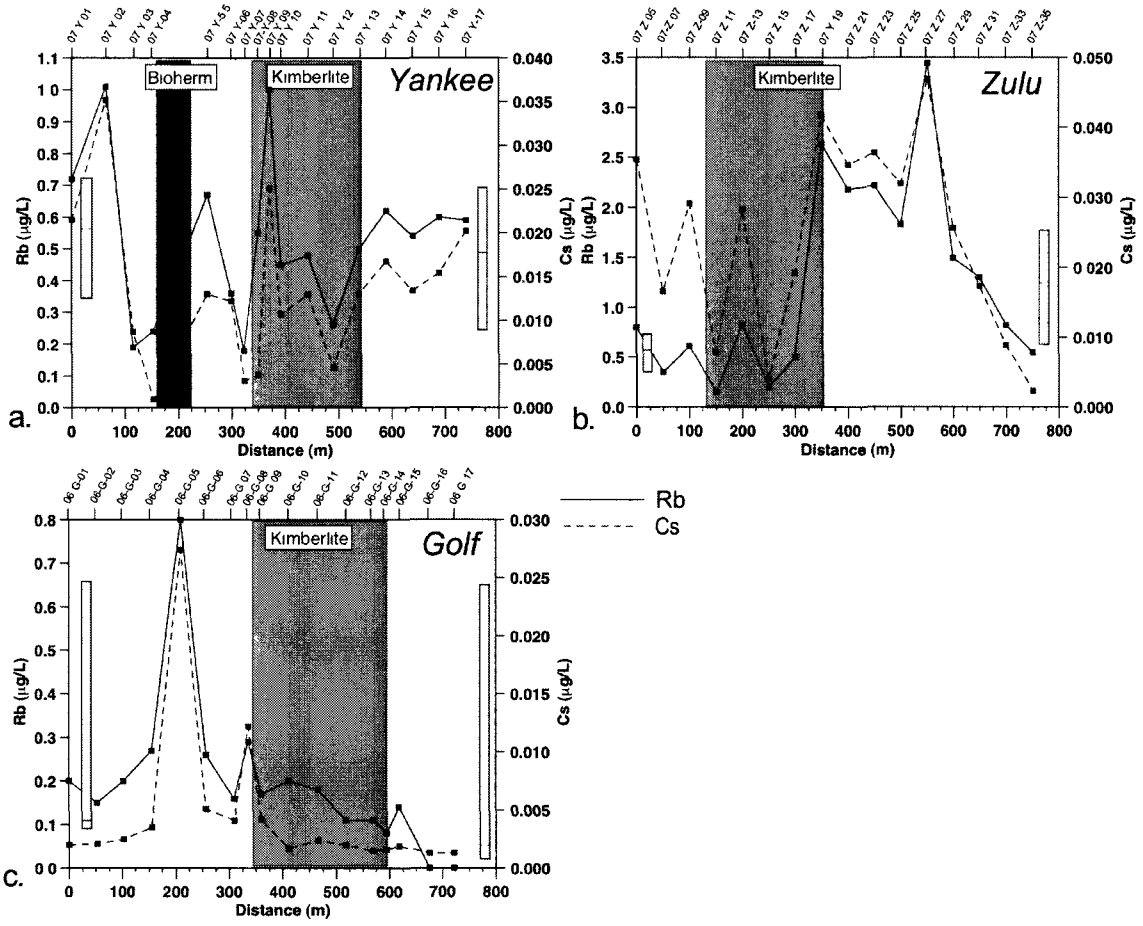

Figure 1-11. Concentrations of Rb and Cs in peat groundwater along transects over: (a) Yankee, (b) Zulu, and (c) Golf kimberlites. Although alkalis at Golf are marginally elevated relative to baseline values at 06-G-08 the concentration was prominent relative to other sites along the transect. Box plots represent the mean, first and third quartile values for baseline ombrotrophic peat groundwaters.

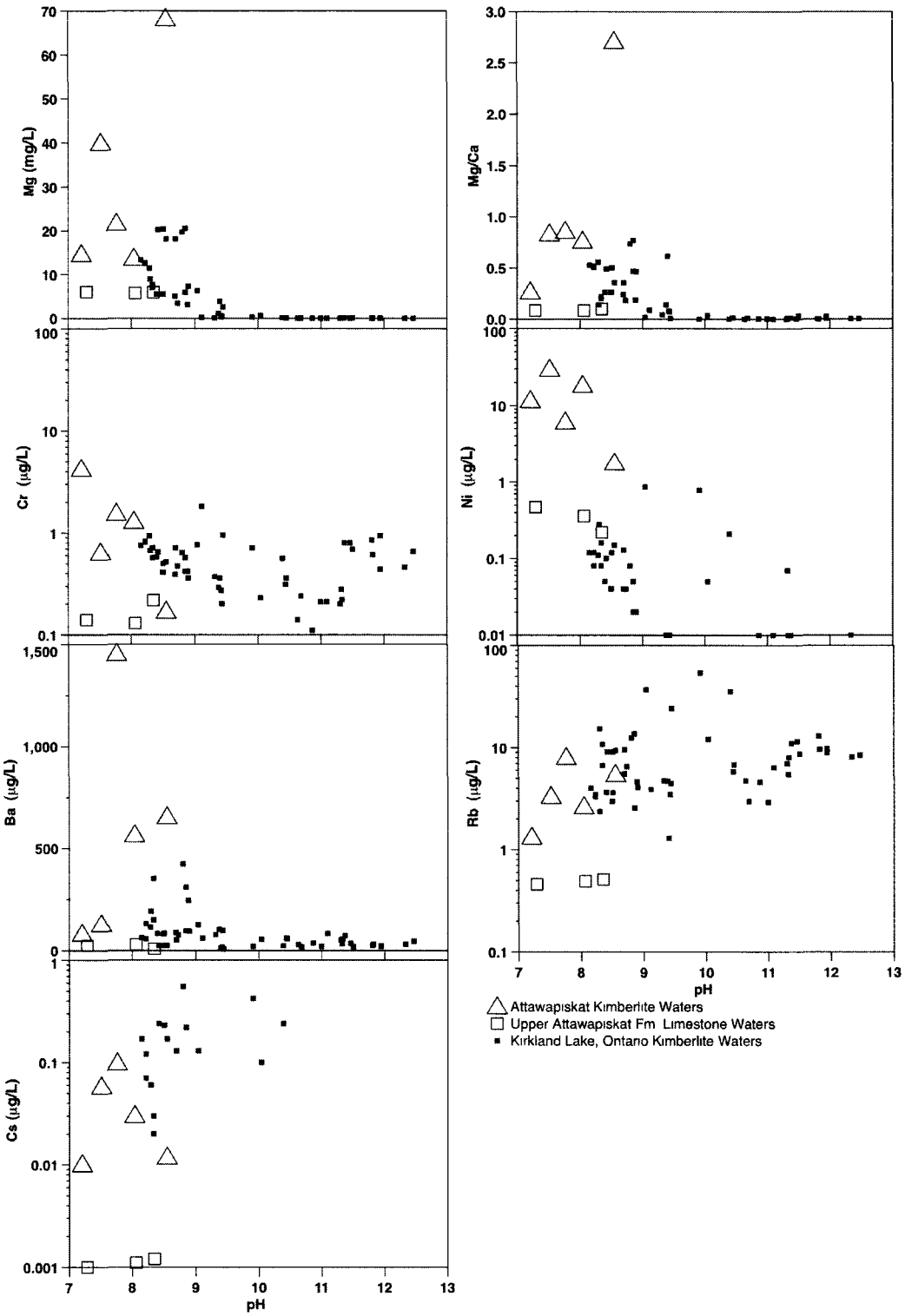

Figure 1-12. Comparison of Mg, Mg/Ca, Cr, Ni, Ba, Rb, and Cs in groundwaters from Attawapiskat kimberlites, Upper Attawapiskat Fm. limestone, and Kirkland Lake kimberlites, Ontario. Metals from almost all Attawapiskat kimberlite water samples follow the same trend as metals in lower pH (7 to 9) waters from Kirkland Lake kimberlites. Kirkland Lake kimberlite water data from Sader *et al.* (2007a).

1.10 TABLES

Table 1-1. The geochemistry of groundwaters in peat, TSS, and boreholes from the Attawapiskat kimberlite region. Detection limit presented is the laboratory method detection limit.
(Continued on next page)

Table 1.

Sample	Method	Detection Limit	07-Y-01	07-Y-02	07-Y-03	07-Y-04	07-Y-05 5	07-Y-06	07-Y-07	07-Y-08	07-Y-09	07-Y-10	07-Y-11	07-Y-12	07-Y-13	07-Y-14	07-Y-15	07-Y-16	07-Y-17
Distance along transect			0	64	116	153	255	299	324	349	370	393	443	489	539	589	639	689	739
water type			peat	peat	peat	peat	peat	peat	peat	peat	peat	peat	peat	peat	peat	peat	peat	peat	peat
Lat			52 8455	52 7743	52 7743	52 7744	52 7747	52 7749	52 7750	52 7751	52 7751	52 7752	52 7756	52 7760	52 7764	52 7768	52 7771	52 7776	52 7779
Long			-83 7915	-83 8772	-83 8765	-83 8759	-83 8745	-83 8739	-83 8735	-83 8732	-83 8729	-83 8726	-83 8723	-83 8720	-83 8716	-83 8712	-83 8709	-83 8706	-83 8702
Temp °C			8 7	9 8	9 0	9 5	8 8	8 1	7 9	7 7	6 3	7 4	6 7	8 2	10 4	8 0	7 2	7 6	4 2
pH			5 49	5 87	5 89	7 71	6 41	5 59	5 77	7 15	6 53	6 21	7 37	6 83	5 71	6 40	6 11	6 21	7 10
Eh (mV)			332	316	316	260	303	317	316	240	299	316	224	258	325	266	303	294	302
EC (uS/cm)			29	56	55	264	92	55	47	218	78	30	301	71	35	45	30	41	54
DO (mg/L)			1 24	2 23	3 11	4 47	4 48	4 39	2 56	2 72	1 72	1 90	2 66	1 19	4 00	1 97	0 77	8 00	3 13
DIC (mg/L)			7 36	na	15 31	36 00	22 67	na	11 68	30 30	20 37	9 82	47 88	25 61	10 14	13 66	19 05	12 95	na
mg/L																			
Ca	ICP-ES	0 03	2 91	7 07	8 12	60 54	17 89	9 15	5 75	26 18	21 12	5 49	63 91	14 01	2 52	3 43	3 36	6 50	9 54
Mg	ICP-ES	0 01	0 24	0 33	0 31	0 88	0 68	0 81	0 59	12 55	2 04	0 38	2 84	0 45	0 34	0 49	0 46	0 48	0 44
K	ICP-ES	0 18	0 35	0 36	0 00	0 00	0 26	0 00	0 00	0 00	0 31	0 00	0 00	0 00	0 25	0 45	0 26	0 19	0 27
Na	ICP-ES	0 05	0 34	0 44	0 36	0 42	0 80	0 52	0 39	0 66	0 47	0 26	0 85	0 33	0 34	0 33	0 44	0 43	0 50
SO_4^{2}	IC	0 04	0 36	na	0 21	0 39	0 04	na	0 29	1 09	0 09	0 15	0 07	0 12	0 39	0 38	3 97	0 33	
Cl	IC	0 03	0 59	na	0 76	0 63	0 12	na	1 24	0 71	0 89	0 71	0 87	0 22	2 05	1 2	0 73	1 68	
ug/L																			
Fe	ICP MS	3	155	409	258	25	302	256	171	400	586	111	4052	4726	119	140	151	448	1428
Mn	ICP-MS	1	18	23	7	65	6	14	33	78	34	17	74	129	19	12	14	36	26
S	ICP-ES	300	318	bd	bd	510	bd	348	bd	467	bd	bd	433	bd	341	bd	358	373	394
Cr	ICP-MS	0 02	0 32	0 11	0 14	0 09	0 09	0 19	0 24	4 23	0 20	0 18	0 24	0 13	0 25	0 22	0 35	0 48	0 34
Ba	ICP-MS	0 02	2 80	2 62	2 69	3 11	4 25	3 04	3 26	58 06	8 65	2 41	8 57	6 41	1 71	2 11	2 00	3 05	2 92
Ni	ICP-MS	0 10	0 40	0 40	0 42	0 66	0 51	0 46	0 87	60 76	1 22	0 56	1 87	0 40	0 35	0 42	0 51	1 18	0 64
Rb	ICP-MS	0 005	0 717	1 009	0 193	0 240	0 670	0 363	0 176	0 553	1 002	0 446	0 481	0 260	0 498	0 624	0 540	0 599	0 586
Cs	ICP-MS	0 0005	0 0215	0 0352	0 0087	0 0010	0 0130	0 0122	0 0031	0 0038	0 0251	0 0107	0 0130	0 0046	0 0131	0 0168	0 0134	0 0154	0 0202
La	ICP-MS	0 001	0 030	0 037	0 033	0 092	0 032	0 053	0 050	1 715	0 071	0 036	0 032	0 010	0 029	0 032	0 046	0 072	0 052
Ce	ICP-MS	0 002	0 059	0 069	0 068	0 150	0 047	0 097	0 109	2 386	0 123	0 077	0 075	0 017	0 063	0 065	0 102	0 132	0 100
Pr	ICP-MS	0 0004	0 0071	0 0098	0 0089	0 0215	0 0058	0 0127	0 0134	0 2467	0 0148	0 0095	0 0095	0 0020	0 0081	0 0076	0 0122	0 0158	0 0102
Nd	ICP-MS	0 003	0 031	0 035	0 031	0 092	0 026	0 051	0 054	0 823	0 056	0 040	0 039	0 009	0 032	0 028	0 048	0 064	0 034
Sm	ICP-MS	0 001	0 007	0 006	0 007	0 016	0 005	0 009	0 011	0 126	0 013	0 008	0 009	0 003	0 008	0 009	0 011	0 011	0 006

na = not analysed
bd = below detection

Table 1-1. Continued.

Sample	Method	Detection Limit	07-Z-05	07-Z-07	07-Z-09	07-Z-11	07-Z-13	07-Z-15	07-Z-17	07-Z-19	07-Z-21	07-Z-23	07-Z-25	07-Z-27	07-Z-29	07-Z-31	07-Z-33	07-Z-35
Distance along transect			0	50	100	150	200	250	300	350	400	450	500	550	600	650	700	750
water type			peat	peat	peat	peat	peat	peat	peat	peat	peat	peat	peat	peat	peat	peat	peat	peat
Lat			52 7298	52 7297	52 7297	52 7297	52 7296	52 7296	52 7296	52 7295	52 7296	52 7294	52 7294	52 7294	52 7294	52 7293	52 7293	52 7292
Long			-83 8354	-83 8345	-83 8338	-83 8331	-83 8324	-83 8316	-83 8309	-83 8301	-83 8294	-83 8286	-83 8279	-83 8271	-83 8264	-83 8256	-83 8249	-83 8241
Temp °C			11 2	12 0	9 7	10 8	11 0	9 9	10 0	11 2	9 1	6 5	8 9	9 7	10 1	9 6	4 6	10 5
pH			5 90	5 60	5 27	5 46	5 27	5 41	5 90	6 15	6 44	6 06	5 74	5 77	5 90	6 21	6 39	5 93
Eh (mV)			257	291	327	313	325	310	267	125	190	224	242	239	232	198	190	183
EC (uS/cm)			159	88	38	45	31	35	90	229	168	280	271	154	399	379	303	349
DO (mg/L)			bd	0 57	1 00	0 00	0 13	bd	bd	bd	bd	bd	bd	0 29	0 31	0 57	bd	0 32
DIC (mg/L)			35 56	31 65	26 72	20 16	17 97	19 63	25 39	51 61	38 50	49 85	56 45	43 91	70 10	65 99	54 47	55 44
mg/L																		
Ca	ICP-ES	0 03	28 28	17 52	6 82	9 11	3 04	2 52	21 52	38 74	19 23	29 07	38 55	22 00	55 23	62 80	45 15	54 76
Mg	ICP-ES	0 01	0 65	0 58	0 34	0 60	0 81	0 56	3 77	6 35	5 19	7 26	7 63	5 22	11 88	13 19	8 62	8 80
K	ICP-ES	0 18	0 37	0 00	0 27	0 00	0 43	0 00	0 50	2 51	2 62	2 48	1 78	2 65	2 22	1 63	1 03	0 81
Na	ICP-ES	0 05	1 05	0 60	1 14	0 75	1 06	0 35	3 32	12 54	11 40	20 99	14 07	11 02	28 55	25 51	30 59	25 80
SO_4^{2}	IC	0 04	0 22	0 21	0 25	0 23	0 40	0 20	0 27	0 53	0 20	0 22	0 80	0 20	0 17	0 22	0 22	0 29
Cl	IC	0 03	1 81	0 81	1 20	1 60	1 05	0 81	0 28	2 52	1 67	2 02	2 69	2 71	14 60	16 84	25 43	18 72
ug/L																		
Fe	ICP-MS	3	1507	1111	513	622	261	138	526	235	249	1042	1609	877	2235	3588	2763	3551
Mn	ICP-MS	1	18	17	8	10	10	6	17	25	6	22	30	54	80	112	40	91
S	ICP-ES	300	bd	332	bd	bd	bd	bd	328	bd	bd	bd	bd	bd	bd	bd	bd	bd
Cr	ICP-MS	0 02	0 10	0 10	0 24	0 13	1 14	0 40	0 25	0 32	0 13	0 08	0 20	0 13	0 07	0 21	0 08	0 10
Ba	ICP-MS	0 02	7 60	3 66	3 32	3 29	7 80	6 31	20 72	49 97	18 49	12 83	15 89	10 29	16 90	14 07	12 62	14 57
Ni	ICP-MS	0 10	0 35	0 67	0 41	0 33	1 42	0 62	1 05	1 15	0 24	0 31	0 27	0 34	0 17	0 26	0 46	0 43
Rb	ICP-MS	0 005	0 795	0 352	0 605	0 149	0 831	0 202	0 497	2 638	2 184	2 223	1 831	3 435	1 491	1 297	0 822	0 550
Cs	ICP-MS	0 001	0 035	0 017	0 029	0 008	0 028	0 004	0 019	0 042	0 035	0 036	0 032	0 047	0 026	0 017	0 009	0 002
La	ICP-MS	0 001	0 036	0 029	0 039	0 036	0 040	0 047	0 073	0 046	0 022	0 008	0 011	0 016	0 007	0 008	0 010	0 029
Ce	ICP-MS	0 002	0 069	0 058	0 076	0 070	0 078	0 099	0 123	0 077	0 033	0 017	0 020	0 027	0 009	0 016	0 018	0 054
Pr	ICP-MS	0 000	0 007	0 007	0 009	0 009	0 009	0 013	0 014	0 011	0 004	0 002	0 002	0 003	0 001	0 002	0 002	0 006
Nd	ICP-MS	0 003	0 033	0 026	0 043	0 032	0 036	0 053	0 055	0 035	0 018	0 014	0 010	0 017	0 006	0 007	0 009	0 023
Sm	ICP-MS	0 001	0 005	0 007	0 008	0 008	0 008	0 010	0 010	0 005	0 005	0 002	0 003	0 003	0 002	0 002	0 002	0 004

na = not analysed
bd = below detection

Table 1-1 Continued.

Table 1 Con't

Sample	Method	Detection	07-MWA-01	07-MW-A-01F	07-MWA-11	07-MW-A-11F	07-MWA-12	07-MW-A-12F	07-MW-C-01F	07-MWY-01	07-MW-Y-01F
Distance along transect			0	0	469	469	518	518	na	0	0
water type			TSS	TSS	TSS	TSS	TSS	TSS	TSS	TSS	TSS
over/outside kimberlite			outside	outside	over	over	over	over	outside	outside	outside
Lat			52 6907	52 6907	52 6938	52 6938	52 6939	52 6939	52 8455	52 7743	52 7743
Long			-83 7810	-83 7810	-83 7769	-83 7769	-83 7762	-83 7762	-83 7915	-83 8781	-83 8781
Temp °C			13 3	14 5	8 8	7 6	11 5	8 5	16 5	8 4	6 2
pH			7 12	7 51	7 53	6 24	6 71	7 19	7 44	8 25	6 98
Eh (mV)			103	263	101	244	209	279	276	60	192
EC (uS/cm)			481	474	524	377	448	248	285	440	410
DO (mg/L)			0 32	1 42	0 38	2 45	6 64	4 91	5 42	0 60	0 84
DIC (mg/L)			68 33	76 52	77 93	62 93	70 99	61 28	73 90	na	64 64
mg/L											
Ca	ICP-ES	0 03	110 94	112 39	85 65	25 34	78 02	50 90	na	103 17	102 94
Mg	ICP-ES	0 01	2 22	2 21	10 01	6 45	21 40	15 28	na	7 91	8 63
K	ICP-ES	0 18	1 05	1 08	1 64	3 06	0 45	0 38	na	0 48	0 29
Na	ICP-ES	0 05	3 21	5 06	27 62	50 55	1 75	1 30	na	1 56	1 04
SO_4^{2-}	IC	0 04	1 20	0 46	4 74	12 97	0 49	0 49	na	2 16	0 35
Cl	IC	0 03	9 56	1 89	4 28	10 31	3 70	1 02	na		1 64
ug/L											
Fe	ICP-MS	3	9035	5428	2430	256	4794	7063	na	836	672
Mn	ICP-MS	1	181	172	94	32	148	109	na	47	43
S	ICP-ES	300	626	465	1218	2804	584	334	na	679	591
Cr	ICP-MS	0 02	1 33	0.29	0 51	0 42	6 89	11 85	na	1 21	0 91
Ba	ICP-MS	0 02	8 83	15 58	5 29	8 60	14 86	13 06	na	8 19	14 68
Ni	ICP-MS	0 10	12 51	5 65	9 40	18 15	41 88	38 81	na	9 75	4 63
Rb	ICP-MS	0 005	1 372	1 396	3 143	4 281	2 901	2.404	na	1 184	0 895
Cs	ICP-MS	0 0005	0 0127	0 0104	0 0139	0 0260	0 0190	0 0166	na	0 0094	0 0069
La	ICP-MS	0 001	0 019	0 006	0 015	0 007	0 795	0 984	na	0 067	0 101
Ce	ICP-MS	0 002	0 034	0 012	0 037	0 013	1 408	1 831	na	0 133	0 208
Pr	ICP-MS	0 0004	0 0040	0 0015	0 0043	0 0018	0 1603	0 2033	na	0 0167	0 0268
Nd	ICP-MS	0 0030	0 0180	0 0050	0 0260	0 0080	0 5720	0 7610	na	0 0650	0 1060
Sm	ICP-MS	0 001	0 003	0 001	0 007	0 001	0 106	0 127	na	0 014	0 023

na = not analysed
bd = below detection

Table 1-1 Continued.

Table 1 Cont'd

Sample	07-MWY-10	07-MW-Y-10F	07-MWY-11 5	07-MW-Y-11 5	07-MWZ-05	07-MW-Z-05F	07-MWZ-15	07-MW-Z-15F	07-MW-Z-17F	07-MW-B-01F	07-MW-B-02F	07-MW-B-03F
Distance along transect	393	393	466	466	0	0	250	250	300	na	na	na
water type	TSS	TSS	TSS	TSS	TSS	TSS	TSS	TSS	TSS	TSS	TSS	TSS
over/outside kimberlite	over	over	over	over	outside	outside	over	over	over	over	outside	over
Lat	52 7752	52 7752	52 7759	52 7759	52 7298	52 7298	52 7296	52 7296	52 7296	52 8647	52 8636	52 8651
Long	-83 8725	-83 8725	-83 8721	-83 8721	-83 8354	-83 8354	-83 8316	-83 8316	-83 8309	-83 9390	-83 9387	-83 9395
Temp °C	18 4	5 4	16 8	6 5	16 4	16 4	na	7 1	6 5	9 6	6 2	15 1
pH	9 06	7 40	8 92	8 17	6 57	7 67	na	7 24	7 66	6 77	6 71	7 54
Eh (mV)	210	237	224	212	102	175	na	281	241	341	306	303
EC (uS/cm)	409	475	407	411	479	304	na	440	874	434	977	600
DO (mg/L)	1 62	4 15	6 52	2 87	0 00	1 95	na	2 72	0 56	6 82	7 69	1 90
DIC (mg/L)	57 70	68 85	53 62	56 41	126 16	32 06	78 14	84 00	153 36	61 46	130 06	70 22
mg/L												
Ca	116 19	112 86	94 91	87 84	103 89	43 62	82 21	82 60	150 65	64 42	179 63	107 80
Mg	6 03	5 86	4.27	3 98	3 09	2 49	27 35	24 45	41 85	15 62	10 84	8 36
K	0 58	0 55	0 68	0 88	2 37	3 21	0 22	0 00	11 96	0 64	5 34	1 40
Na	1 88	1 42	2 55	2 23	3 58	8 26	1 24	0 89	38 14	3 00	15 40	4 46
SO_4^{2}	0 16	0 21	0 27	0 27	0 20	0 97	0 16	0 04	1 24	0 49	1 28	0 57
Cl	1 76	1 34	1 53	1 39		2 15	1 34	0 93	3 74	2 63	8 85	2 46
ug/L												
Fe	1044	490	526	589	1981	224	5997	5863	111	130	105	43
Mn	80	70	166	185	180	46	149	155	223	63	328	203
S	671	606	500	483	886	336	612	547	bd	492	bd	474
Cr	1 65	1 16	0 22	0 24	2 09	0 80	18 05	14 96	0 36	0 43	0 28	0 23
Ba	17 95	16 80	15 46	19 90	28 57	10 82	314.24	269 03	45 96	15 43	31 25	27 41
Ni	18 45	5 08	29 38	7 65	28 34	20 90	5 01	2 86	25 08	82 37	11 48	15 19
Rb	1 425	1 018	0 746	0 749	2 844	2 161	0 787	0 600	4 996	1 686	3 821	1 923
Cs	0 0060	0 0060	0 0044	0 0036	0 0385	0 0103	0 0174	0 0101	0 0086	0 0115	0 0104	0 0115
La	0 098	0 126	0 011	0 012	0 367	0 197	0 663	0 599	0 007	0 350	0 004	0 056
Ce	0 205	0 261	0 021	0 023	0 695	0 371	1 281	1 106	0 011	0 682	0 007	0 102
Pr	0 0260	0 0328	0 0030	0 0030	0 0759	0 0435	0 1223	0 1041	0 0016	0 0783	0 0010	0 0120
Nd	0 1220	0 1320	0 0150	0 0120	0 2950	0 1510	0 4810	0 4160	0 0190	0.2910	0 0110	0 0460
Sm	0 020	0 026	0 004	0 004	0 051	0 028	0 078	0 085	0 001	0 050	0 002	0 010

na = not analysed
bd = below detection

Table 1-1. Continued.

Table 1 *Con't*

Sample	Method	Detection Limit	07-B1-07-08C-F	07-X-07-014C	07-Z-07-12C	07-Z-07-12C-F	07-Y-07-7H	07-Y-07-7H-F	07-07-C-01 5F	07-07-C-01F
Distance along transect			na	na	na	na	na	na	na	na
water type			borehole	borehole	borehole	borehole	borehole	borehole	peat	peat
limestone or kimberlite			kimberlite	kimberlite	kimberlite	kimberlite	limestone	limestone		
Lat			52 8649	52 7960	52 7290	52 7290	52 7756	52 7756	52 8449	52 8455
Long			-83 9393	-83 8537	-83 8317	83 8317	-83 8737	-83 8737	-83 7905	-83 7915
Temp °C			9 6	9 0	12 4	16 9	7 5	16 9	14 8	16 4
pH			8 55	7 76	7 51	8 04	8 06	7 29	5 54	4 93
Eh (mV)			226	23	68	136	-4	95	276	290
EC (uS/cm)			597	198	945	247	377	na	69	29
DO (mg/L)			2 48	bd	bd	1 26	bd	1 27	2 79	2 05
DIC (mg/L)			74 12	37 96	76 14	23 34	49 53	53 02	20 58	32 41
mg/L										
Ca	ICP-ES	0 03	25 19	25 18	47 99	17 94	68 25	72 37	5 99	3 23
Mg	ICP-ES	0 01	68 25	21 64	39 91	13 70	5 74	6 04	0 60	0 48
K	ICP-ES	0 18	5 33	0 40	9 47	1 28	0 46	0 46	bd	bd
Na	ICP-ES	0 05	7443 23	832 83	117766 12	9572 27	1172 30	999 68	430 72	429 12
SO_4^{2}	IC	0 04	0 24	0 67	13 09	3 92	0 43	0 04	0 38	0 19
Cl	IC	0 03	6 00	0 50	158 31	14 98	1 00	0 77	0 94	0 89
ug/L										
Fe	ICP-MS	3	73	299	444	1370	12373	12799	104	252
Mn	ICP-MS	1	20	19	16	20	116	122	8	6
S	ICP-ES	300	bd	537	939	823	462	382	428	301
Cr	ICP-MS	0 02	0 17	1 56	0 64	1 29	0 13	0 14	0 25	0 35
Ba	ICP-MS	0 02	654 57	1455 47	127 74	566 93	30 13	24 60	2 83	2 48
Ni	ICP-MS	0 10	1 79	6 18	29 65	18 41	0 36	0 47	0 48	0 48
Rb	ICP-MS	0 005	5 488	8 050	3 330	2 654	0 494	0 464	0 160	0 397
Cs	ICP-MS	0 0005	0 0119	0 0991	0 0579	0 0302	0 0011	0 0005	0 0087	0 0124
La	ICP-MS	0 001	0 026	0 102	0 060	0 925	0 009	0 005	0 026	0 030
Ce	ICP-MS	0 002	0 012	0 120	0 090	1 276	0 015	0 007	0 050	0 069
Pr	ICP-MS	0 0004	0 0009	0 0120	0 0091	0 1209	0 0022	0 0011	0 0071	0 0091
Nd	ICP-MS	0 003	0 006	0 038	0 030	0 402	0 011	0 000	0 028	0 032
Sm	ICP-MS	0 001	0 004	0 016	0 005	0 050	0 002	0 001	0 006	0 009

na = not analysed
bd = below detection

ADDENDUM TO CHAPTER 1 – IN RESPONSE TO COMMENTS RAISED DURING THE THESIS DEFENSE

Additional information on well installation and water sampling procedures

Installation of piezometers was conducted by pushing a 1.5 m length of white (environmental grade) polyvinyl chloride (PVC) or grey PVC into the peat 1.1 meters below ground surface (mbgs). The PVC piping has an inside diameter of 19 mm and no slots or screening within the pipe. Slots and screening was not required, as there was no mineral soil, and thus no sediment entered into the pipe following installation. The installation technique that was used permitted a simple and effective method for sampling peat groundwater from a given depth. Equilibration time for water level recovery in peizometers ranged from about 30 minutes to 3 hours.

The first step in the construction and installation of monitoring wells (MW) was the use of a soil sampling spoon to determine the depth of the peat to the TSS. The length of pipe needed for MW installation was determined by adding 0.7 m (depth of installation into the TSS below the peat), and 1.3 m (height of standpipe) to the determined peat thickness. The construction of MWs consisted of 19 mm inside diameter iron pipe, which was attached to a 40 cm long stainless steel drive point (Solinst Canada) that was screened approximately 25 cm from the drive point tip. The 19 mm iron pipe was purchased from a building supply store and is commonly used for residential natural gas purposes. A 12 mm inside diameter low or high density polyethylene tube, approximately 30 cm longer than the iron pipe was fastened onto a barbed fitting on the drive point. The polyethylene tubing was subsequently fed through the prepared length of iron pipe and the drive point was screwed tightly onto the iron pipe using pipe wrenches. At the top part of the pipe, a solid iron pipe length with a

pass-through for the polyethylene tubing was screwed on. This piece functioned to prevent mushrooming of the iron pipe while using the slide hammer to hammer the MW to 0.7 m below the peat/TSS contact. Following advancement of the MW to 0.7 m below the peat/TSS contact, the solid iron pipe was removed and a check valve was inserted into the top of the polyethylene tubing. This valve permitted the degassing of the MW, but prevented air from entering.

Recovery of the MWs was slow and typically no water was detected in the MWs 5 days following well installation. Due to the slow recovery, MWs installed in the summer of 2007 could only be sampled in fall 2007. It is reasonable to suggest that there was little or no leakage from the overlying peat, as the recovery of the MWs was slow. A hydrogeological survey over Golf kimberlite was not conducted during fieldwork conducted by Brauneder, 2007.

Exploration boreholes were cased through the overburden sediment using NQ steel casings. These wells were drilled approximately 1 year prior to sampling.

Clarification on detection of upwelling groundwater

Vertical hydraulic gradient

The vertical hydraulic gradient (i) for MWs that have positive values indicate upward flow, and conversely, negative values indicate a downward flow of groundwater. At site 07-MW-Z-17 i= 0.08 and indicates upwelling, and at sites 07-Z-05 and 15 the gradients are negative (i = -0.59 and -0.11), respectively (Fig. AD-1). At the Yankee transect, the vertical hydraulic gradient is positive at sites 07-Y-01 and 11.5 (i = 0.09, and 0.04 respectively), and it is negative at site 07-Y-10 (i = -0.01) (Fig. AD-1). The vertical gradients for all kimberlites in

this study (Yankee, Zulu, Alpha-1, Bravo-1, and Control) from fall 2007 are listed in Table AD-1. It has also been specified in Figure AD-1 that flow indicated is shallow flow within the peat.

Geochemical indicators for inferred upwelling:

The EC of peat groundwaters increase sharply with increases in the vertical gradient, with the exception of one sample (Fig. AD-2). This positive correlation indicates that upwelling minerotrophic groundwater is contributing to the otherwise ombrotrophic peat groundwaters at these sites. The trend in Figure AD-2 also suggests that upwelling minerotrophic groundwater may be inferred at sites where elevated EC, Ca, pH and lower Eh values in peat groundwaters are present. It may then be inferred that sites such as those between 07-Z-17 to 35 (with elevated EC, Ca, pH and lower Eh values) have upwelling of minerotrophic groundwaters.

It should be noted that not all sites with minerotrophic peat groundwaters are from kimberlites or have strong indicators of kimberlites. For example, although sample 07-Y-04 (Yankee) is minerotrophic and upward movement of groundwater inferred, it does not contain high concentrations of pathfinder metals either in peat groundwater or in peat (Hattori and Hamilton, 2008).

Clarification on the possibility of perceived locations of upwelling groundwater

In this thesis, perceived locations of upwelling groundwater (commonly at kimberlite margins) were interpreted to be due to fractured host rock surrounding kimberlites, and up to 200 m beyond their margins. However, it is important to note that perceived locations of

upwelling may also be due to the relative magnitude of horizontal versus vertical velocity of groundwater in the TSS and the peat.

Below is an example of possible displacement of pathfinder metal anomalies and indicators of minerotrophic groundwater down gradient of the Zulu kimberlite from site 07-Z-17. Note that in the following calculations K values and porosities have been estimated from the literature (Fig. AD-3).

1) Based on the assumption that the horizontal gradient is the same as the water table, the horizontal velocity of groundwater in the TSS is $6.5 * 10^{-10}$, or **0.02 cm/year**. Based on that velocity, groundwater has only migrated horizontally approximately 100 cm in the last 5000 years (since the retreat of the Tyrell Sea).
2) Based on the vertical gradient of 0.08 at monitoring well 07-MW-Z-17 at Zulu (Table AD-1), the vertical velocity of groundwater is **0.3 cm/year**. This velocity was calculated based on an estimated K value of $1*10^{-7}$ cm/s, and an estimated porosity (*n*) of 0.7 (Freeze and Cherry 1979).
3) The vertical and horizontal vectors for groundwater velocity in the TSS were used to solve for the angle of upwelling groundwater from the TSS. This angle of upwelling was calculated to be 4° from vertical (Fig. AD-3). Therefore, groundwater movement is almost vertical.
4) Using K_{peat} values of peat (ranging from 10^{-3} to 10^{-6}) (Ingram, 1983; Hoag and Price, 1995; Price, 2003), a K_{TSS} value of 10^{-7} (Freeze and Cherry 1979), and an angle of upwelling from TSS of 4° (θ_{TSS}), the angle of groundwater movement in the peat (θ_{pcat}) has been determined for site 07-Z-17 using the following equation:

$$(K_{TSS}/ K_{peat}) = (\tan\theta_{TSS}/\tan\theta_{peat})$$

The following represents table represents the angles (from vertical) that groundwater upwelling from TSS to peat is expected to have:

Peat K value cm/s	angle of upwelling degrees
1E-03	89.99
1E-04	89.95
1E-05	89.50
1E-06	85.03

These values indicate that once waters have upwelled from TSS into peat, they will likely travel dominantly in a horizontal direction with only a small vertical componant.

5) The angle of flow in the peat of 89.5° (approximated) (from vertical) (Fig. AD-3), and an average peat thickness of 2 m (distance between the peat/TSS boundary and the depth peat groundwater sampling below ground surface) was used to calculate the horizontal distance that discharging groundwater will travel from the TSS before being identified in the piezometers. Based on a piezometer installation depth of 1.1 mbgs, upwelling TSS water from 07-MW-Z-17 will be identified 230 m down gradient (site 07-Z-27). This is schematically demonstrated in Figure AD-3. Alternatively, using Darcy Flux equations, water discharging from the TSS into the peat will be observed approximately only 0.5, down gradient, as the angle of upwelling in the peat is 15° (from vertical).

Clarification on time constraints on upward movement of groundwater from kimberlite, through the TSS and into the peat

Due to the inferred low hydraulic conductivity in the TSS ($1*10^{-7}$ cm/s), upward groundwater movement is slow compared with other sediment types such as sand, till, and peat (Freeze and Cherry 1979). Therefore, upward movement of groundwater through the TSS could potentially take thousands of years. In this study, where a positive vertical hydraulic gradient was identified (Table AD-1), the upward movement of groundwater through the TSS in 5000 years (time since retreat of the Tyrell Sea) is between 10 and 22 m (depending on gradient). As the TSS is between 2 and 21 m in thickness, there is a strong possibility that there has been adequate time for groundwaters from kimberlites to migrate through the TSS.

It should be noted that the TSS is assumed to have a homogenous consistency, and therefore the same K value throughout. However, TSS samples recovered with the soil sampling spoon (used during MW installation) had some variability in grain size. Medium pebbles to fine sand were occasionally identified in the silty clay TSS. This grain size variability suggests that the K value $1*10^{-7}$ cm/s used here may be a maximum, as this value represents marine clay (Freeze and Cherry 1979). Additionally, the identification of anomalous high concentrations of kimberlite pathfinder metals over or near kimberlites (Chapter 1) coupled with an upward travel distance calculated to be between 10 and 22 m suggests that a K value of $1*10^{-7}$ cm/s may be appropriate approximation for the TSS.

Clarification on the horizontal gradient of the water table and velocity in peat groundwater

The horizontal flow direction of water in the peat can only be estimated (approximated) at Yankee kimberlite, as it is only measured in the direction of the transect. In order to identify the true regional peat groundwater horizontal gradient and precise horizontal groundwater velocity, more peat groundwater elevation measurements various locations on either side of the transect are required.

At Zulu, there is a short transect of peizometers installed north – south that intersect the longer east – west transect. The intersecting transects permit a more defined peat groundwater horizontal gradient and velocity. The peat groundwater flow direction and gradient has been revised as per the following calculations:

North – South Zulu Transect Gradient

Distance along N-S transect: 215 m

Change in elevation of peat groundwater: -0.12 m along the transect south

Gradient: -0.00056 along the transect south

North – South Zulu Transect Velocity

Velocity: $v=(-Ki)/n$, where K is the hydraulic conductivity of the peat, i is the gradient, and n is peat porosity. The calculation used a hydraulic conductivity value of 0.001 cm/s based on measurements from northern sphagnum bogs and spring fens (Chason and Siegel, 1986). An active peat porosity (n) value of 0.3 was used based on measurements of the catotelum from sphagnum peat bogs (Hoag and Price, 1995; 1997).

$v = 1.87 \times 10^{-6}$ south direction of the N-S transect

Peat groundwater horizontal gradients and estimated horizontal velocity at Zulu based on N-S and E-W transects

E-W gradient: -1.95×10^{-3} east (from Ch. 1)

N-S gradient: -5.6×10^{-4} south

Gradient = $SQRT((-1.95 \times 10^{-3})^2 + (-5.6 \times 10^{-4})^2)$

$= -2.03 \times 10^{-3}$ cm/s trending 106°

Velocity $= 6.76 \times 10^{-6}$ cm/s trending 106°

Therefore, the calculations suggest that peat groundwater likely flows almost parallel with the E-W transect at Zulu.

Clarification on standing water as an indicator of upwelling

The elevation of groundwater in piezometers is greater than standing water at some locations at Yankee (07-Z-01, 04, 08, and 12). At Zulu site 07-Z-17, the water level in the peizometer was also greater than standing water. Piezometer water elevations ranged from 1 to 3 cm higher than standing water. Therefore, higher elevations of piezometer water elevations than the standing water are considered to be sites of upwelling groundwater.

Clarification on the definition of relative standard deviation (RSD)

RSD = (SDV x 100)/Mean,

where SDV is standard deviation.

Clarification on detection limits

The detection limit for metals was determined by the laboratory (Geoscience Laboratories of the Ministry of Northern Development of Mines). Values for analyzed blanks (background noise) are required for calculation of detection limits. It is possible that the *practical detection limits* (calculated from blanks) could be as much as 10 times higher than laboratory values.

Clarification on scales for metals along transects

Metal concentrations along transects were initially plotted using variable scales for the same metals at different sites (i.e. Yankee, Zulu, or Golf). In order to more easily identify metal anomalies along transects, metals have been re-plotted with the same scale (Fig. AD-4 to 10). However, it should be noted in instances where there were orders of magnitude differences in metal concentrations between transects, log plots of metal concentrations were used.

Clarification on differences in metal concentrations in TSS groundwaters over kimberlite compared with sites over limestone

Box percentile plots with distribution indicate comparisons of the data from TSS over kimberlite and limestone (Fig AD-11). The majority of kimberlite pathfinder metals are elevated in TSS groundwaters over kimberlites compared with sites over limestone, however, Rb and Cs appear to have similar concentrations. Due to the small and variable sample set of groundwaters over limestone (n = 8) compared to the sample set over kimberlites (n = 15), no statistical analyses such as the Wilcoxon matched pairs signed-ranks test (see Appendix 3) were conducted.

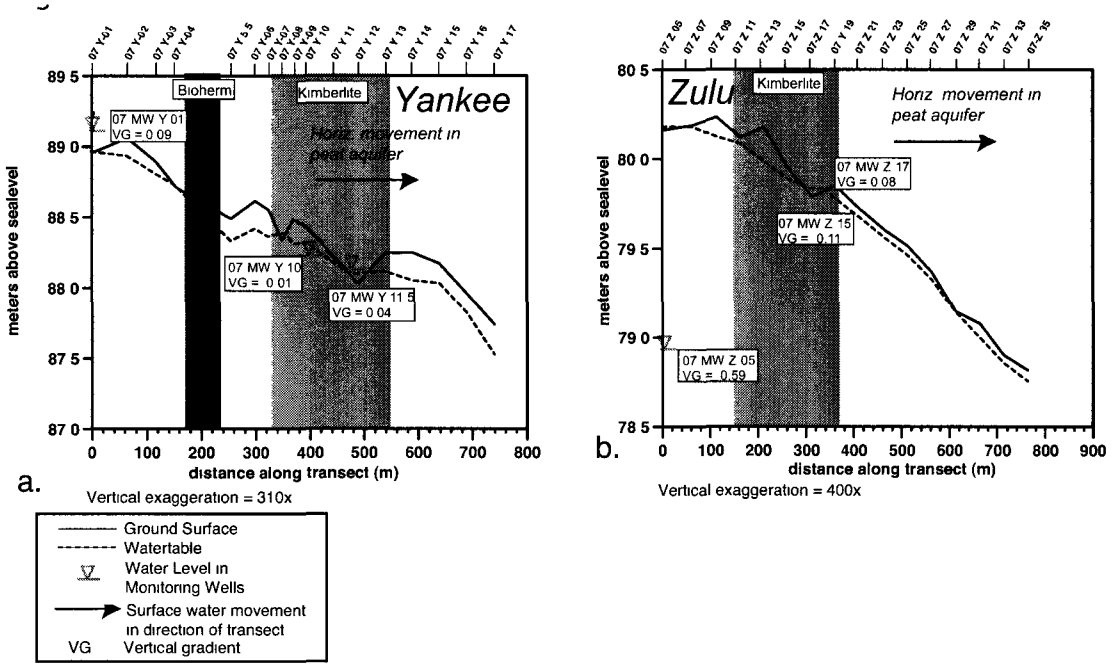

Figure AD-1. Profiles of the ground surface, the water table, and potentiometric surfaces along the transects at (a) Yankee and (b) Zulu kimberlites Negative vertical gradient numbers indicate downward flow and positive numbers indicate upward flow

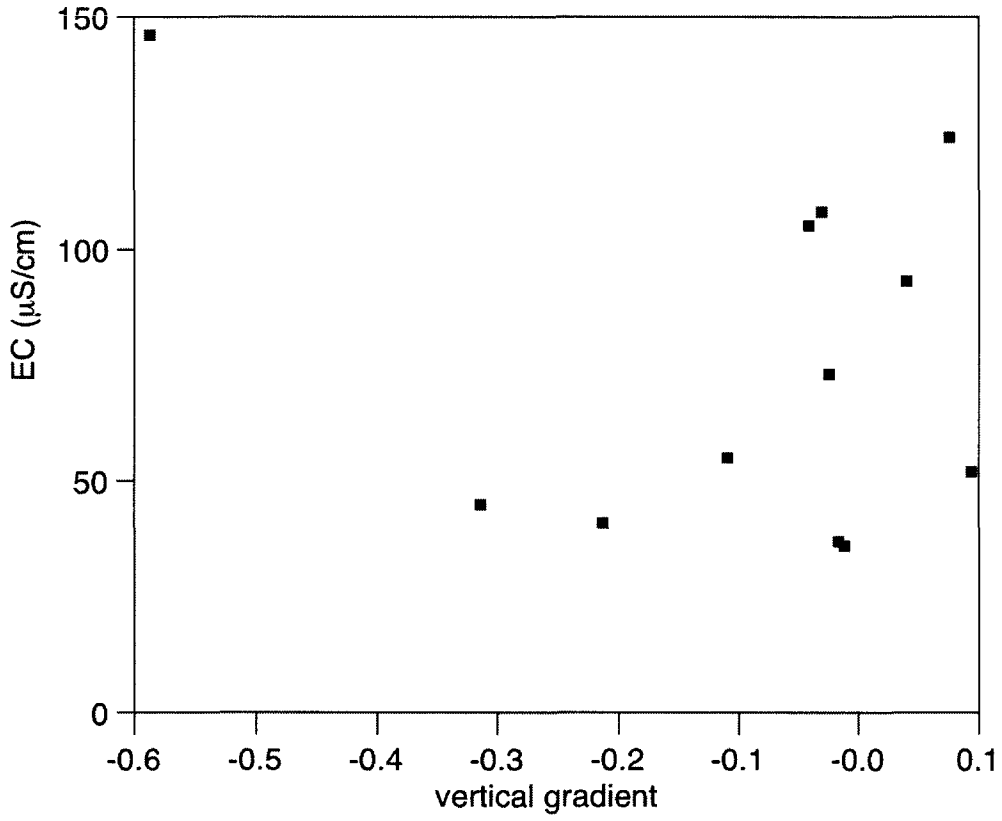

Figure AD-2. Plot of peat groundwater EC values versus vertical gradients of monitoring wells that were installed within 30 cm of piezometers The positive correlation for all but one samples indicates that with increasing vertical gradient, there is a greater input of minerotrophic groundwater into the ombrotrophic peat groundwater

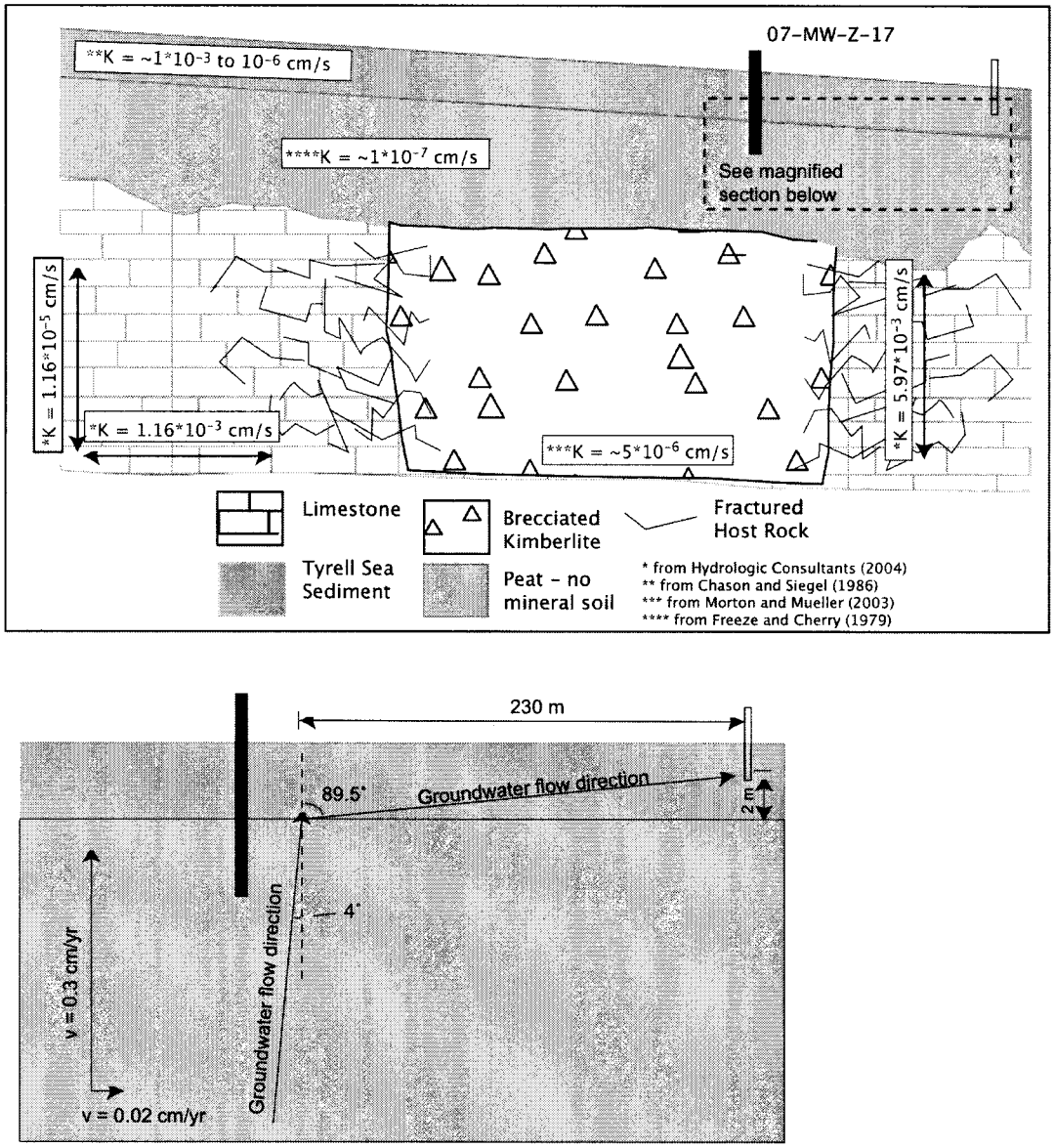

Figure AD-3. Schematic diagram of interpreted groundwater movement within the TSS and peat at Zulu. The diagram indicates a possibility that there may be a significant shift in the perceived areas of groundwater upwelling from the TSS at monitoring well 07-MW-Z-17. Diagram is not to scale.

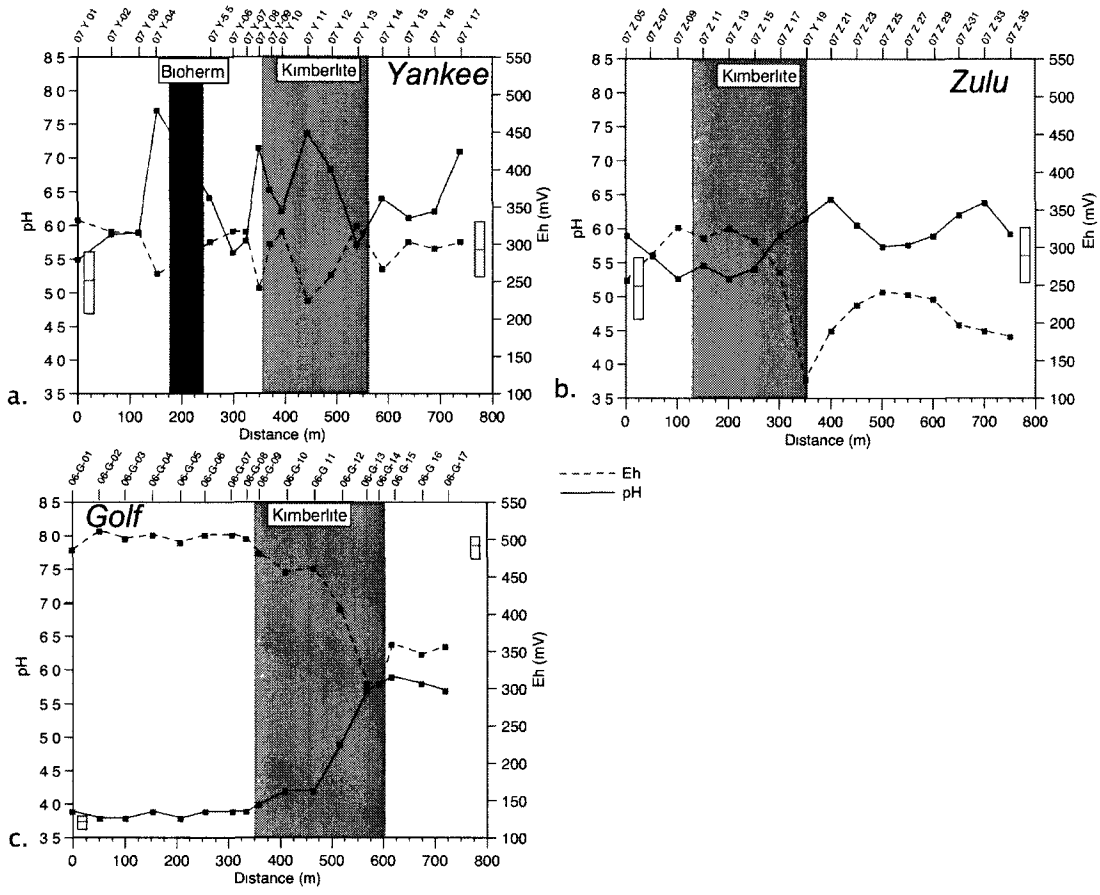

Figure AD-4. Profiles of pH and Eh along transects over: (a) Yankee, (b) Zulu, and (c) Golf kimberlites. Typically, pH and Eh indicate sites of upwelling groundwater and a shift from ombrotrophic to minerotrophic peat groundwater conditions. Box plots represent the mean, first and third quartile values for baseline ombrotrophic peat groundwaters.

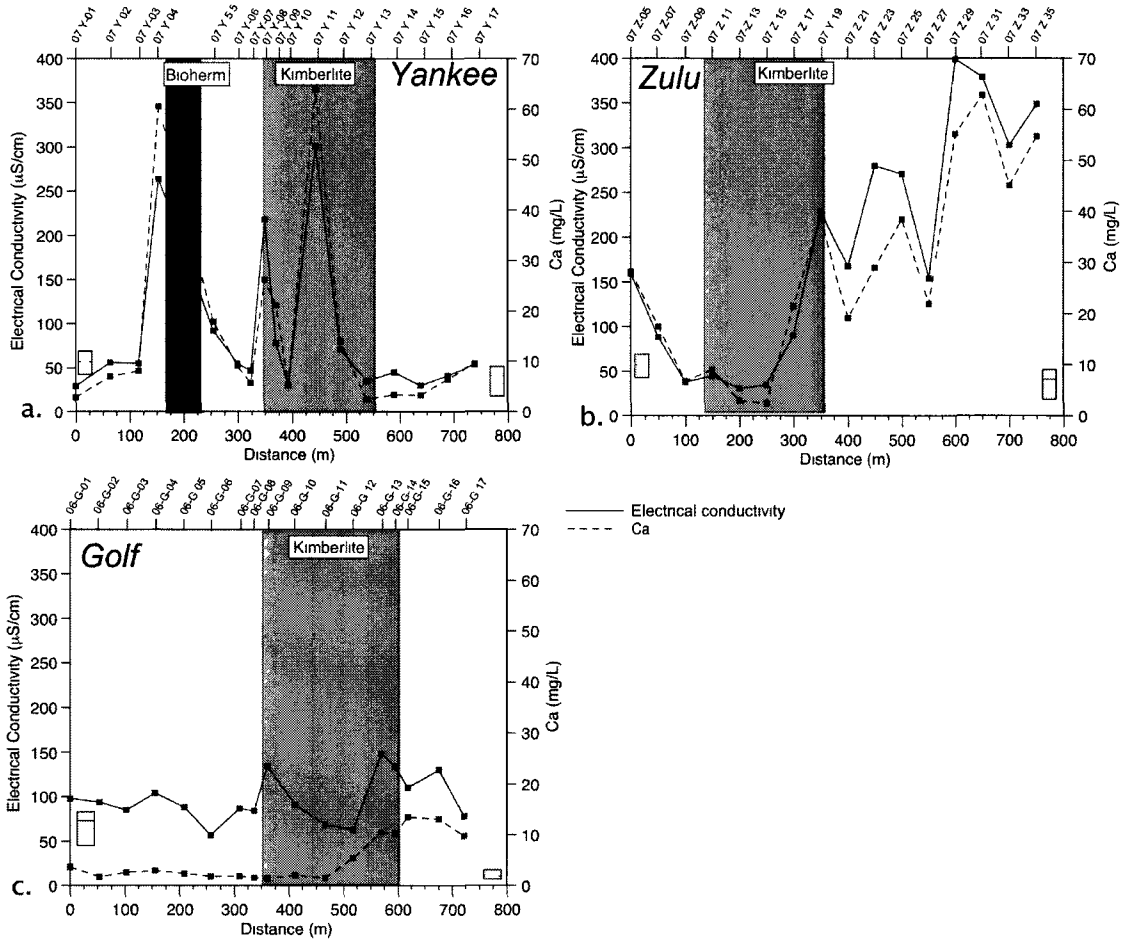

Figure AD-5. Profiles of electrical conductivity and Ca along transects over (a) Yankee, (b) Zulu, and (c) Golf kimberlites Electrical conductivity and Ca correlate well and indicate sites of upwelling minerotrophic groundwaters Box plots represent the mean, first and third quartile values for baseline ombrotrophic peat groundwaters

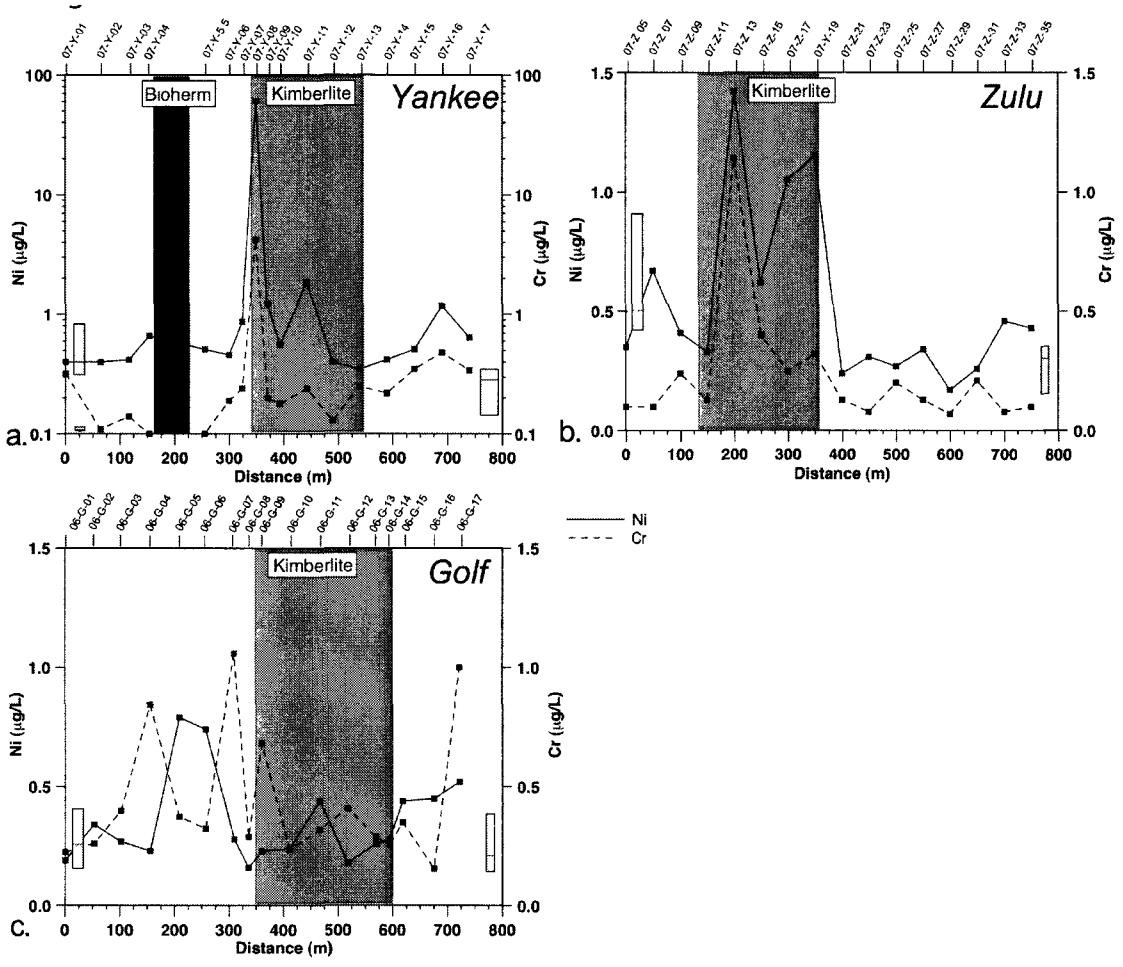

Figure AD-6. Concentrations of Cr and Ni in peat groundwater along transects over: (a) Yankee, (b) Zulu, and (c) Golf kimberlites. Ni and Cr are typically observed at sites of upwelling at kimberlite margins. Box plots represent the mean, first and third quartile values for baseline ombrotrophic peat groundwaters.

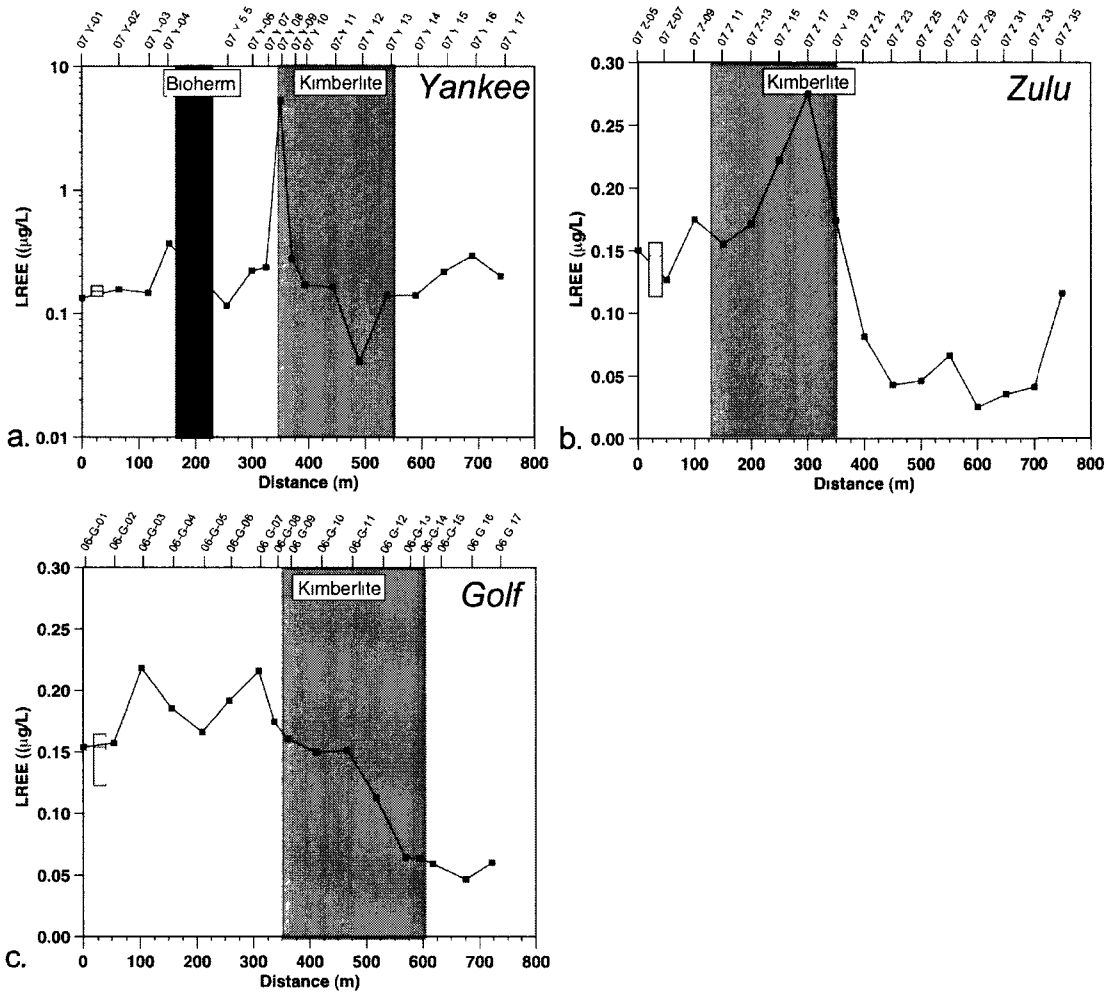

Figure AD-7. Concentrations of LREEs (La-Sm) in peat groundwater along transects over: (a) Yankee, (b) Zulu, and (c) Golf kimberlites. Light REEs have similar profiles to Ni and Cr and are typically observed at the kimberlite margins. Box plots represent the mean, first and third quartile values for baseline ombrotrophic peat groundwaters.

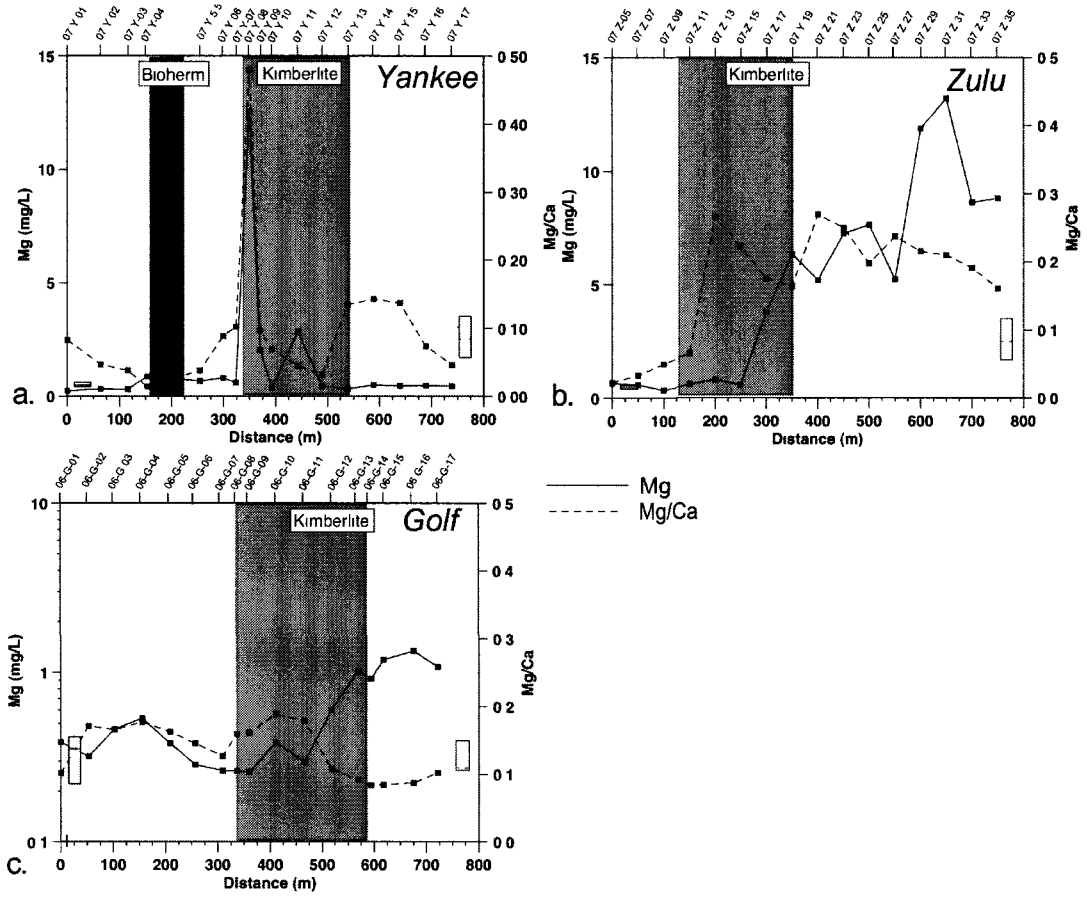

Figure AD-8. Concentrations of Mg and Mg/Ca in peat groundwater along transects over (a) Yankee, (b) Zulu, and (c) Golf kimberlites With the exception of Yankee, Mg indicates locations of upwelling minerotrophic groundwater The broad elevated Mg/Ca peaks along transects suggest waters rich in Mg relative to Ca may be coming from buried kimberlite Box plots represent the mean, first and third quartile values for baseline ombrotrophic peat groundwaters

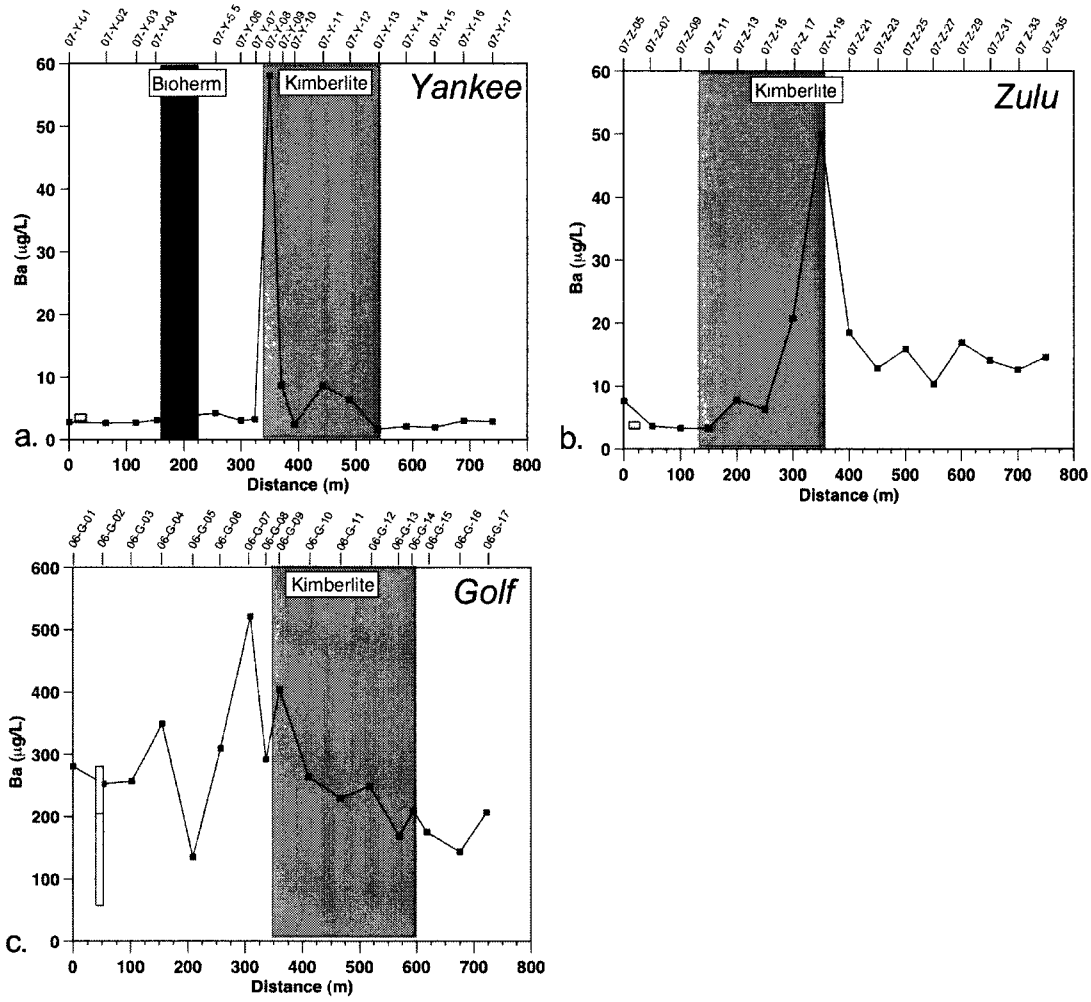

Figure AD-9. Concentrations of Ba in peat groundwater along transects over: (a) Yankee, (b) Zulu, and (c) Golf kimberlites. Barium is typically elevated only a kimberlite margins and their profiles differ compared with other alkaline earth metals (i.e. Ca and Mg) at Zulu and Golf. Box plots represent the mean, first and third quartile values for baseline ombrotrophic peat groundwaters.

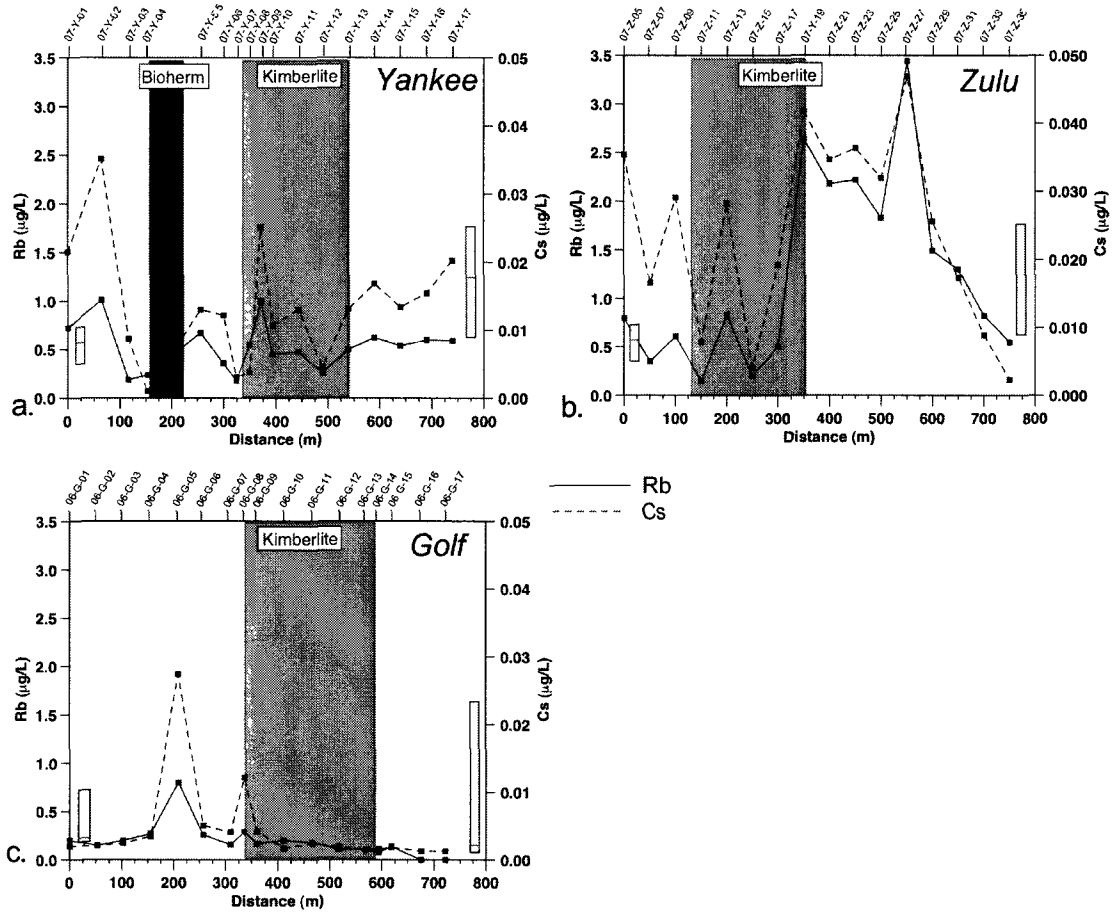

Figure AD-10. Concentrations of Rb and Cs in peat groundwater along transects over: (a) Yankee, (b) Zulu, and (c) Golf kimberlites. Although alkalis at Golf are marginally elevated relative to baseline values at 06-G-08 the concentration was prominent relative to other sites along the transect. Box plots represent the mean, first and third quartile values for baseline ombrotrophic peat groundwaters.

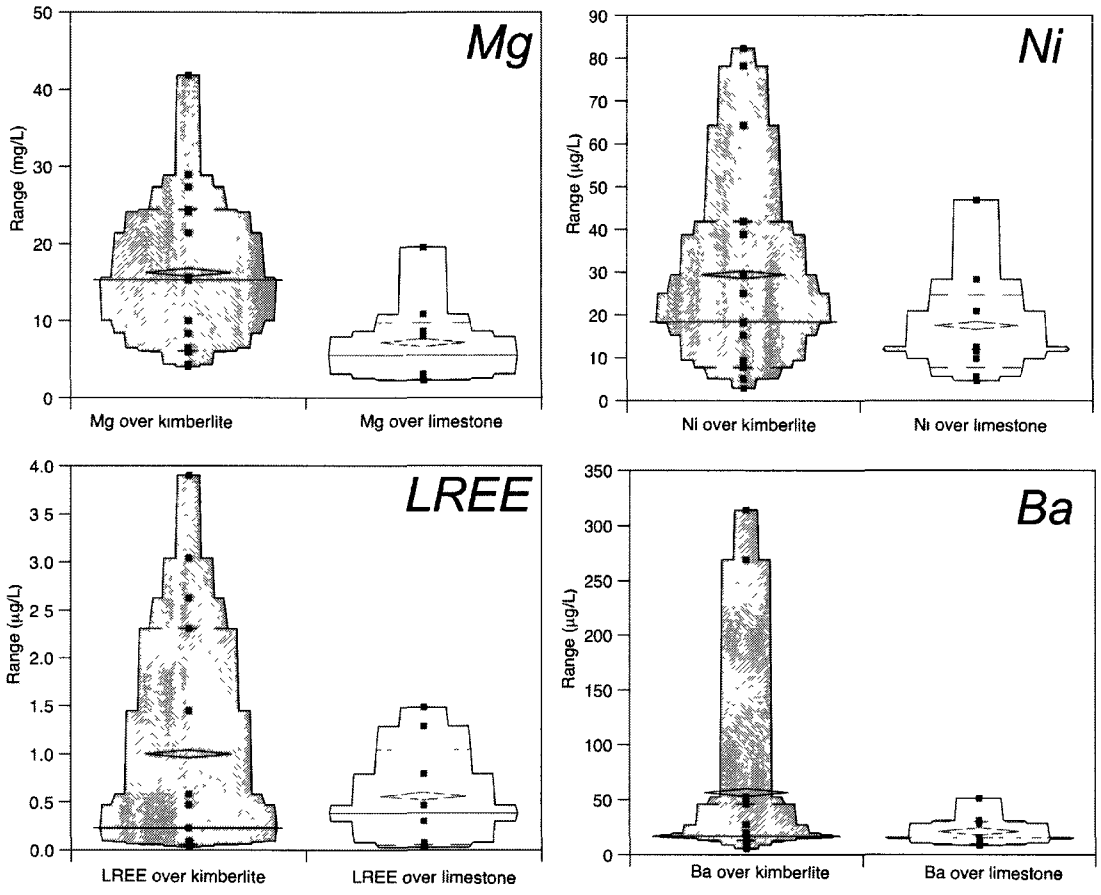

Figure AD-11. Box percentile plots with distribution for Mg, Ni, LREE, Ba, Cr, Mg/Ca, Rb and Cs. The plots indicate that all metals and ratios, with the exception of the alkalis in groundwater samples from TSS over kimberlites are elevated with respect to TSS groundwater samples over limestone. n = 15 for samples over kimberlite and n = 8 for samples over limestone. Continued on next page.

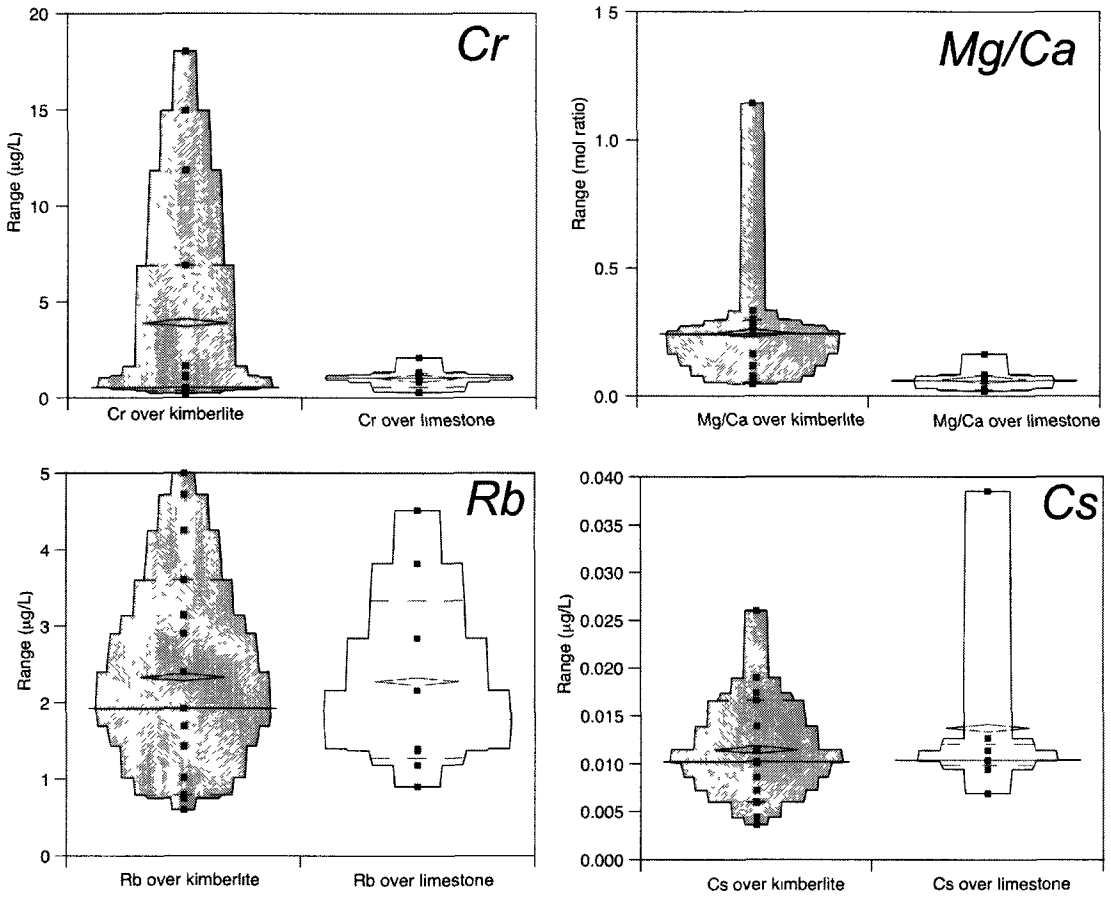

Figure AD-11. Continued.

Table AD-1. Vertical gradients for monitoring wells. Hydrogeological data from the Fall of 2007.

		Water Level Elevation	Groundsurface Elevation	Installation Depth	Vertical Gradient
Zulu					
07-Z-05F	masl	80.22	80.16	79.06	
07-MW-Z-05F	masl	78.94	80.28	76.88	-0.59
07-Z-15F	masl	79.89	79.95	78.85	
07-MW-Z-15F	masl	79.74	80.03	77.53	-0.11
07-Z-17F	masl	79.84	79.79	78.69	
07-MW-Z-17F	masl	80.00	79.92	76.52	0.08
Alpha-1					
07-A-01F	masl	86.43	86.66	85.56	
07-A-MW-01F	masl	86.39	86.66	83.26	-0.02
07-A-11F	masl	86.55	86.57	85.47	
07-A-MW-11F	masl	86.06	86.57	83.17	-0.21
07-A-12F	masl	86.63	86.69	85.59	
07-A-MW-12F	masl	86.19	86.69	84.19	-0.31
Yankee					
07-Y-1F	masl	88.97	88.95	87.85	
07-MWY-01F	masl	89.16	89.03	85.83	0.09
07-Y-10F	masl	88.32	88.44	87.34	
07-MWY-10.5F	masl	88.29	88.05	84.85	-0.01
07-Y-12F	masl	88.10	88.03	86.93	
07-MWY-11.5F	masl	88.18	88.11	84.91	0.04
Bravo-1					
07-B-01F	masl	86.25	86.25	85.15	
07-B-MW-01F	masl	86.17	86.25	83.25	-0.04
07-B-02F	masl	86.46	86.46	85.36	
07-B-MW-02F	masl	86.41	86.49	83.34	-0.02
07-B-03F	masl	86.53	86.58	85.48	
07-B-MW-03F	masl	86.47	86.55	83.55	-0.03
Control					
07-C-01F	m	99.85	100.30	99.20	
07-MW-C-01F	m	99.66	100.30	97.87	-0.14

masl = meters above sea level

Chapter 2

METAL-DISSOLVED ORGANIC MATTER COMPLEXATION AND FERRIHYDRITE ADSORPTION IN SHALLOW PEAT GROUNDWATERS: APPLICATION TO DIAMOND EXPLORATION IN THE JAMES BAY LOWLANDS, CANADA

Jamil A. Sader[1*], Keiko Hattori[1], Stewart Hamilton[2], Kerstin Brauneder[1]

[1]University of Ottawa, Earth Sciences Department, Ottawa, Ontario, K1N 6N5, Canada
[2]Sedimentary Geoscience Division, Ontario Geological Survey, Sudbury, Ontario, P3E 2G9, Canada

Manuscript submitted for publication in Applied Geochemistry

2.1 ABSTRACT

The speciation and solubility of kimberlite pathfinder metals (Ni, Nd, Ba, and K) in shallow peat groundwaters is investigated over the Yankee, Zulu, and Golf kimberlites in the Attawapiskat region, James Bay Lowlands, Canada. The purpose of this study is to examine the relationship between dissolved organic matter (DOM) complexation with kimberlite pathfinder metals and determine the spatial distribution of those metals in shallow peat groundwaters along sampling transects over subcropping kimberlites. Nickel, Nd, Ba, and K complexation with DOM and the adsorption of these metals onto ferrihydrite were calculated using Visual MINTEQ 3.0 and the NICA-Donnan database. Calculations predict almost 100% of soluble Nd, Ni, and Ba form complexes with DOM at sampling sites with little to no contribution from upwelling groundwater (i.e., dissolved organic carbon (DOC) concentrations = 40 to 132 mg/L, pH = 3.9 to 5.5, and log ionic strength = < -3). In only the most ombrotrophic peat groundwater conditions does a majority fraction of K bind to DOM. By contrast, under conditions with large contributions from upwelling groundwaters (i.e., DOC concentrations = < 40 mg/L, pH = 5.5 to 6.5, and log ionic strength = -3 to -2), as little as 10% of Nd and Ni, and 0% K and Ba are predicted to complex with DOM. The modeling calculations suggest the dominant control on metal-DOM complexation, particularly with respect to Ni and Nd, is competitive effects for DOM binding sites due to elevated ionic strength at sites of strong groundwater upwelling. MINTEQ modeling of metal adsorption on ferrihydrite surfaces predicts that under strong upwelling conditions, Ni and Nd are scavenged from solution due to inferred increased ferrihydrite precipitation and decreased fractions of metals complexed with DOM. Analytical geochemical data are consistent with model predictions of metal adsorption on ferrihydrite. Total Ni and Nd concentrations at

sites of strong upwelling are typically 5 times lower than waters with little to no upwelling and log ferrihydrite saturation indices ($logSI_{ferr}$) strongly indicate precipitation (values up to 5) at sites of strong groundwater upwelling. Where the majority of Ni and Nd complex with DOM and ferrihydrite is highly under saturated ($logSI_{ferr}$ -18 to -5), the concentrations of total Ni and Nd are elevated in peat groundwaters compared to other sites along sampling transects. Metal complexation with DOM effectively inhibits metal scavenging from solution via adsorption or from forming secondary mineral precipitates. Also, because alkaline earth metals do not compete strongly with Ni and Nd for adsorption sites on ferrihydrite surfaces, but do compete strongly for insoluble organic sites, Ni and Nd are more likely to adsorb onto ferrihydrite.

2.2 INTRODUCTION

Dissolved organic matter (DOM) in natural waters can strongly affect metal speciation, but this process is commonly overlooked. In biological applications, metal DOM complexes have the ability to render potentially harmful dissolved metals non-toxic, as these complexes are typically bio-unavailable to organisms (Bruland *et al.*, 1991; Bell *et al.*, 2002; Paquin *et al.*, 2002; Perdue and Ritchie, 2005). Metal-DOM complexes also can prevent metal scavenging due to formation of secondary mineral precipitates or adsorption to insoluble substances (Cornell and Schwertmann, 1979; Ravichandran *et al.*, 1999; Hoch *et al.*, 2000; Tipping, 2002; Cornell and Schwertmann, 2003). Metal-DOM complexation is best exemplified in wetland environments, where dissolved organic carbon (DOC) is a major component of the dissolved ions in peat groundwaters.

In mineral exploration, the ability of mobile ions to adsorb or precipitate onto mineral soil in the shallow subsurface (Mann *et al.*, 1998; Cameron *et al.*, 2004b;

McClenaghan *et al.*, 2006; Hattori *et al.*, 2009; Sader *et al*, 2009) or peat (Hattori and Hamilton, 2008) is effectively used to detect buried mineral deposits. Determining factors related to metal solubility such as pH and Eh are important when using water as an exploration tool to locate blind mineral deposits (Leybourne and Cameron, 2010). With the exception of peat, most groundwater geochemical studies have not accounted for DOM influences on metal solubilities, as the majority of natural groundwaters have low DOM concentrations. Additionally, soils for geochemical exploration are typically collected from locations that are above the water table. However, in wetland environments, high DOC concentrations are an integral part of metal solubility (Tipping, 2002; Johannesson *et al.*, 2004) and may significantly impact the behaviour of potential ore deposit pathfinder metals in the shallow subsurface.

A previous geochemical study of peat groundwaters along sampling transects over Attawapiskat kimberlites identified elevated concentrations of Ni, Cr, light rare earth metals (LREEs), Ba, Rb, and Cs, and high Ca/Mg ratios indicative of the presence of buried kimberlite (Sader *et al.*, 2010). This study demonstrated pathfinder metals in peat groundwaters correlated with sites of upwelling minerotrophic groundwaters primarily identified at or near the margins of kimberlites. The authors noted that Ni, Cr, LREEs, and Ba are generally elevated at sites at or near kimberlite margins, where there is only a small contribution from upwelling groundwater (based on geochemical parameters). Along sampling transects, high Ba, Rb, and Cs concentrations were commonly observed at locations different from those with high Ni, Cr, and LREEs. The ratios of Mg/Ca were high at sites where transition, alkaline earth, and alkali pathfinder metals were also high.

Herein we examine the influences that high DOC content in peat groundwaters may exert on pathfinder metal solubilities along sampling transects over subcropping kimberlites in the Attawapiskat kimberlite field, James Bay Lowlands, Canada. Peat groundwater metal concentrations and model calculations for metal speciation and the adsorption of soluble ions on ferrihydrite surfaces are presented. We explore the interrelationship between metal-DOM complexes, and adsorption to ferrihydrite as a potential major sink for dissolved metals associated with buried kimberlite. The goals of this paper are to: 1) identify the dominant controls related to variable metal-DOM complexation in peat groundwaters; 2) compare metal-DOM speciation calculations to analytical data; and 3) suggest possible mechanisms for scavenging metals from solution.

2.3 LOCATION AND GEOLOGY

2.3.1 Geological setting, geology, and mineralogy of kimberlites

The kimberlites in this study are located in the James Bay Lowlands in north-central Canada, approximately 90 km west of the community of Attawapiskat, Ontario, and are within 15 km of DeBeers' Victor diamond mine (Fig. 2-1). The kimberlites intruded Paleozoic sedimentary rocks, predominantly composed of limestone, and underlying Archean igneous and metamorphic rocks in the mid-Jurassic (~170 Ma) (Norris, 1993; Webb *et al.*, 2004) (Fig. 2-2). Host rock to the kimberlite at the bedrock surface is limestone of the Upper Attawapiskat Formation (Fig. 2-2) that locally crops out in the form of bioherms that stand up to 2 m above the surrounding ground surface. Bioherms are reef cores composed of coral and skeletal remains of other marine organisms (Cowell, 1983). Kimberlites in this study form round to ellipsoid areal extents that range from 200 to 300 m in diameter (Fig. 2-3) and subcrop, with the exception of the Zulu kimberlite, which crops out along its southern

margin. A thin sheet of till (< 1 m) and Tyrell Sea glaciomarine sediment (2.1 to 21 m) (DeBeers, unpublished data) overlies the host Upper Attawapiskat Formation limestone and kimberlites in the study area (Fig. 2-2).

The region was glaciated during the Quaternary. During this period bedrock erosion took place and a thin till layer (<1 m) was deposited on the limestone and kimberlite surfaces. Tyrell Sea sediment (TSS) is comprised of fine-grained marine sand, silt and clay. The TSS was deposited between 10 and 5 ka following the end of glaciation. At that time, the shoreline of James Bay (referred to as the Tyrell Sea during that period) extended inland approximately 300 km west and southwest of its present location. Since the retreat of the Laurentide ice sheet in the Attawapiskat region, isostatic rebound resulted in ground surface elevation rises of 100 to 300 m (Shilts, 1986). The present-day ground surface elevation is 80 to 90 m above sea level. Overlying the TSS is sphagnum peat, approximately 2.5 to 3.4 m thick, has been accumulating since the retreat of the Tyrell Sea approximately 5000 years BP. The peat becomes increasingly more humified with depth (i.e., the sphagnum is increasingly less recognizable below 0.5 m).

The Yankee kimberlite is located between outcropping bioherms southwest and northeast of the kimberlite (Fig. 2-3). The ground surface forms a gently sloping bowl-shape depression over the kimberlite that extends 150 m beyond its margin. The Zulu kimberlite is located east of a lobate raised bog and north of a small bioherm (Fig. 2-3). Ground surface at the Golf kimberlite is similar to that at Zulu, as both slope gently from west to east. No bioherms were observed near the Golf transect.

The mineralogy of the Attawapiskat kimberlites consists of abundant olivine macrocrysts, ilmenite, garnet, Cr-diopside, phlogopite, and spinel (Kong *et al.*, 1999; Sage,

2000a; Armstrong *et al.*, 2004). Kimberlite groundmass mainly consists of carbonate, spinel, and serpentine with lesser monticellite, mica, apatite, and perovskite (Kong et al., 1999). All kimberlites in the Attawapiskat field are either hypabyssal or volcaniclastic (Kong *et al.*, 1999; van Straaten *et al.*, 2009). Kimberlites sampled in this study (Yankee, Zulu, and Golf) are altered hypabyssal facies (Sage, 2000a).

2.3.2 Peat groundwater hydrogeology and geochemical parameters

Hydrogeological measurements in the peat and TSS groundwaters of the Yankee and Zulu transects have been previously reported by Sader et al. (2010). To summarize, the water table gradient at both Yankee and Zulu indicates peat groundwater flows in an eastern direction along the length of each transect. The flow rate ranges from a minimum of approximately 2 cm/year to a maximum of 200 cm/year along the length of the transect at a sample depth of 1.1 meters below ground surface (mbgs). The upwelling of deep minerotrophic groundwaters into peat was recognized by observation of a higher groundwater elevation in deeper monitoring wells installed in the TSS compared with the water table elevation measured in the piezometers installed in peat. In peat groundwater samples, the pH values vary from 3.80 to 7.10 and Eh values range from 125 to 512 mV. High pH and low Eh values are generally demonstrate upwelling groundwater along each transect in the peat groundwaters, as these values contrast with more acidic pH values and more oxidizing conditions in ombrotrophic peat groundwaters. Samples from the Golf transect, as a whole, have the most oxidized peat groundwater conditions (lowest pH and highest Eh values), likely a result of the shallow (0.4 mbgs) water collection depth.

Peat groundwater electrical conductivity (EC) values are highly variable and are elevated at sites of upwelling deep groundwater. High EC values are commonly used to

identify sites of minerotrophic groundwaters in wetlands (Ingram, 1983, Hill and Siegel, 1991, Hoag and Price, 1995) Boelter and Verry (1977) define EC values in peat groundwaters up to 80 µS/cm as being ombrotrophic and values greater than 100 µS/cm as having a contribution from minerotrophic groundwaters In this study, we define ombrotrophic conditions as those with EC values less than 100 µS/cm and we define peat groundwaters with minerotrophic groundwater contributions as those with EC values greater than 100 µS/cm Electrical conductivity values higher than this reflect greater minerotrophic groundwater contributions

Based on the combined hydrogeological and geochemical peat groundwater data in Sader *et al* (2010), upwelling occurs as isolated point sources at 0, 153, 349, 370 and 489 m along the Yankee transect and near the kimberlite margin at 300 m, extending to the east end of the Zulu transect Upwelling occurs between sites at 300 and 400 m and extends to the east end of the Golf sampling transect

2.4 METHODS

2.4.1 Field Procedures

Peat groundwater samples were collected during the summers of 2006 (early August) and 2007 (August 14-23) along transects over Yankee, Zulu, and Golf kimberlites Samples collected in 2006 and 2007 are denoted by the prefixes *06* and *07*, respectively Samples along Yankee, Zulu, and Golf transects are denoted by the prefixes *Y*, *Z*, and *G*, respectively All geochemical data for water samples collected in 2006 have been reported by Brauneder (2007) The compositional data for water samples collected in 2007 are presented in Table 2-1

Field sampling methods from Sader et al. (2010) for peat groundwaters are summarized below. Shallow piezometers used for peat groundwater sampling were constructed from 1.5 m lengths of either 19 mm (¾ inch) inner diameter white (environmental grade) or grey polyvinyl chloride (PVC) piping. Piezometers were installed 1.1 mbgs into the peat along sampling transects across the Yankee and Zulu kimberlites, and 0.4 mbgs along the Golf kimberlite transect. Shallow piezometers were installed approximately every 25 to 50 m along each sampling transect and at least 200 m beyond the kimberlite margins (Fig. 2-3). Peat groundwater samples were collected from each of the installed piezometers.

The pH, oxidation-reduction potential (ORP), electrical conductivity, dissolved oxygen content (DO), and temperature were measured on-site with a Hanna^{TM} HI-9828 multi parameter water quality portable meter. Probes for pH, DO, and EC were calibrated daily. ORP values have been corrected to the standard hydrogen electrode (SHE) for waters at 10 °C by adding 207 mV, and are reported as Eh.

Water samples were collected in 60 and 30 mL Nalgene high-density polyethylene (HDPE) bottles for cation and anion analysis, respectively. Samples for dissolved inorganic carbon (DIC) and dissolved organic carbon (DOC) analysis were collected in 40 mL brown borosilicate bottles with a silicone- polytetrafluoroethylene (PTFE) septa cap. An additional PTFE and rubber septa from Chromatographic Specialties Inc. was inserted underneath the septa cap to prevent DIC loss (silicone is gas permeable). All water samples were filtered through Millipore^{TM} 0.45 μm filters and were kept cool in ice-packed coolers or refrigerated until they were analyzed. Prior to analysis water samples for cation analysis were acidified to 1% using Baseline-grade HNO_3 from Seastar Chemicals.

2.4.2 Laboratory Procedures

Waters were analyzed to determine concentrations of DIC and DOC at the University of Ottawa G.G. Hatch Stable Isotope Laboratory using a Finnigan-Mat Delta Plus mass spectrometer and the 2 σ analytical precision is $\pm$ 0.002 ppm. Elemental analyses of groundwaters for cations and anions were conducted at the Geoscience Laboratories, Ontario Ministry of Northern Development of Mines, Sudbury, Canada. Calcium, Fe, K, Mg, Mn, Na, and S were analyzed by ICP-ES; Ti, Cr, Ni, Rb, Sr, Nd, Ba, Cu, Zn, and Y were analyzed by ICP-MS; and Cl^- and SO_4^{2-} were analyzed by IC. A precision of < 5% relative standard deviation (RSD) was achieved for all metals and anions with the exception of Mn (7%), Zn (6%), and Ti (11%). A full description of cation and anion analytical procedures including quality assurance and quality control procedures, have been reported elsewhere (Sader *et al.*, 2010).

2.4.3 Speciation calculations and modeling

The nonideal competitive adsorption model (NICA) and Donnan database in Visual MINTEQ 3.0 (Gustafsson, 2010) was used to calculate Nd, Ni, Ba, and K complexation with DOM. This model is based on the combination of two active processes. The NICA model simulates metal complexation and was first developed by Koopal et al. (1994), and assumes that binding sites to humic substances are heterogeneous and treats them as continuous functions. It also takes into consideration competition effects between metals and other ions in the solution, which is represented by ionic strength. The Donnan database model (Benedetti et al., 1996) concerns electrostatic interactions of ions and assumes that the dissociation of carboxylic and phenolic groups results in an electrical potential around those

substances and that organic matter is in a gel phase The negative charge around these molecules exerts a binding effect for ions (Kinniburgh et al., 1999). The MINTEQ default settings were used in the calculations, which assumes that the ratio of DOM to DOC is 1.4 and 100% of the DOM is fulvic acid. Peat groundwater samples were clear to light yellow in colour and indicate fulvic acid is likely the dominant organic acid, as humic acids are darker in colour (Stevenson, 1994). Additionally, based on visual observation, peat groundwater samples acidified to ~1 pH for cation analysis did not result in humic acid precipitates in all but two samples. Humic acids are only soluble at pH values greater than 2, whereas fulvic acids are soluble throughout the pH range. Appreciable concentrations of acetic acid (CH_3COOH) is not likely in the peat groundwater samples, although this organic substance is colourless and soluble throughout the pH range. Charge balance calculations assuming DOC is entirely dissociated acetic acid (CH_3COO^-) (i.e. each DOC has a valence of -0.5) does not result in balanced charges for cations and anions. Therefore, it likely that DOC is dominantly composed of larger fulvic acid molecules.

The binding constants (logK) used in this model calculation for Ni, Ba, and K are from Milne et al. (2003) and are in the MINTEQ - NICA-Donnan database. However, logK values for Nd, derived by Sonke and Salters (2004), were added separately, as they are not included in the original database.

Visual MINTEQ 3.0 was used to calculate the fraction of dissolved metals that adsorbed on ferrihydrite. Based on the activity of Fe and the pH of the peat groundwaters, ferrihydrite is the Fe-oxide most likely to precipitate (Cornell and Schwertmann, 2003) and is the inferred Fe-oxide in this paper. The *feo-dlm_2008.vdb* database uses the 2-pK Diffuse Layer Model. Dzombak and Morel (1990) derived the ferrihydrite surface complexation

constants for Ni and Ba. Because a constant for Nd was not included in the database, an experimentally derived constant for Nd by Tang and Johannesson (2005) was used. No constant was available for K, however, it has little affinity to be adsorbed on ferrihydrite surfaces (Kinniburgh et al., 1976). The Dzombak and Morel (1990) model assumes that ferrihydrite has a specific surface area of 600 m^2/g. Table 2-1 lists the dissolved metal concentrations and geochemical parameters from Yankee and Zulu peat groundwaters that were input into the NICA-Donnan and ferrihydrite surface complexation models. The geochemical data for Golf are from Brauneder (2007).

2.5 RESULTS

2.5.1 Peat groundwater geochemistry

Dissolved organic carbon concentrations range from 15.8 to 132.2 mg/L and are elevated in peat groundwaters that receive little to no contribution from upwelling minerotrophic groundwater (EC < 100 μS/cm). The low DOC concentrations are generally associated with sites that have high contributions from upwelling minerotrophic groundwater (EC >100 μS/cm). Transition metals such as Ni, Ti, Cr, and Nd are elevated with concentrations up to 1.8, 4.0, 1.1, and 0.10 μg/L, respectively, in peat groundwaters at or near kimberlite margins. The exception is site 349 m (07-Y-08) at Yankee, which has transition metal concentrations that are 4 to 60 times greater and are more similar to groundwaters from the TSS (Sader *et al.*, 2010). The elevated values are notably higher than local baseline values in ombrotrophic peat groundwaters (Sader *et al.*, 2010). Collectively, peat groundwaters from all sites show that Ni, Ti, Cr, and Nd concentrations increase with increases in DOC where EC is lower (Fig. 2-4). Concentrations of alkaline earth metals such as Mg and Ca have negative correlations with DOC concentrations and positive correlations with EC (Fig. 2-4). The

negative correlations are likely a result of the high Mg and Ca concentrations (up to 13.2 and 62.8 mg/L, respectively) that are common in upwelling groundwaters. At most sampling sites Mg and Ca reflect upwelling regardless of whether the waters are spatially related to locations of buried kimberlite. Elevated Ba concentrations (10 to 50 μg/L) also reflect upwelling groundwater, however, unlike the majority of Mg or Ca, the greatest concentrations are located at sites at or near the kimberlite margins. Note that the Ba concentrations at Golf are 2 orders of magnitude greater than Yankee or Zulu. All waters collected during summer 2006 have high Ba values (Brauneder, 2007). Although the reason is not known, we have ruled out the possibility of contamination, or analytical artifact. Laboratory QA and QC results indicated an relative standard deviation (RSD) of < 5% for Ba and analytical runs for Ba using ICP-MS and runs using ICP-AES had almost identical concentrations. Furthermore, Ba concentrations in peat groundwaters from 2006, which were collected at 0.4 mbgs along the Yankee transect, had similar profile shape compared with the Yankee profile in this study. Variable Ba solubility is also ruled out, as neither witherite (barium carbonate), barite (barium sulfate) are favoured from any peat groundwaters in this study.

Concentrations of alkali metals such as K and Rb are commonly elevated at sites with elevated EC and low DOC. However, compared to Ca and Mg, these concentrations correlate poorly with EC and DOC concentrations (Fig. 2-4). Alkaline earth metals, specifically Ca and Mg, strongly contribute to ionic strength (I) values in peat groundwater and the correlation between Ca+Mg and ionic strength is strong (r=0.98). Elevated log$I$ values (-3 to ~ -2) are inferred to occur at sites of strong upwelling along each of the 3 sampling transects (Table 2-2).

Sulfate concentrations are low at all sites (mean = 0.35, median = 0.3, max = 3.97 mg/L); and total sulfur concentrations in waters are also low (mean = 0.4, max = 0.9, many samples less than the detection limit of 0.3 mg/L) (Table 2-1). Chloride concentrations are low and range from 0.12 to 25.43 mg/L with mean and median concentrations of 3.6 and 2.0 mg/L, respectively.

2.5.2 Geochemical model calculations

2.5.2.1 Mineral saturation

The computer modeling software package Visual MINTEQ 3.0 (Gustafsson, 2010) was used to calculate ferrihydrite saturation indices ($logSI_{ferr}$), and calcite saturation indices ($logSI_{calcite}$) in the presence of DOC for each peat groundwater sample (Table 2-2). Saturation indices were calculated based on the fraction of dissolved Fe^{3+} and Ca^{2+} that were not bound to DOM. The $logSI_{ferr}$ values are elevated (~ -5 to 5) at locations which have significant contributions from upwelling minerotrophic groundwaters (EC > 100 µS/cm) (Fig. 2-5). Typically, the greater the minerotrophic groundwater contribution, the higher the $logSI_{ferr}$ values are. Overall lower $logSI_{ferr}$ values along the Golf transect are likely due to the shallower depth of sample collection and more acidic pH. Sites that show strong ombrotrophic characteristics (EC < 100 µS/cm) have lower $logSI_{ferr}$ values, which range from -5 to -18. Calcite is not predicted to precipitate from any peat groundwaters, as $logSI_{calcite}$ values for all peat groundwater samples are < 0 (Fig. 2-5; Table 2-2). The lack of favorability for calcite precipitation is a function of the acidic pH values for peat groundwaters. Dolomite is highly under saturated (the highest $logSI_{dolomite}$ value is -5.5 for peat groundwater samples), and thus, is not considered in this study.

A number of oxide phases have not been considered in this study. Mn-oxyhydroxides are not considered for SI calculations, as concentrations in peat total dissolution are low, and are 19 and 5 ppm (vol.) (mean and median, respectively) (Hattori and Hamilton, 2008). Additionally, the mean and median concentrations in peat groundwaters are 31 and 18 μm/L. These low concencentrations in peat and peat groundwater indicate that Mn-oxyhydroxides are not common solid phases in peat. The other common Fe-oxyhydroxide phase, geothite, was not considered. Geothite is favored to preciptate only at pH values of 0 to 3.5 at log a_{Fe} of -5 (average activity for soluble Fe in this study) (Kinniburgh *et al.*, 1976; Cornell and Schwertmann, 2003). Whereas, ferrihydrite is favored to precipitate between the pH values of 3.5 and 14 at log a_{Fe} of -5. Although it is likely that ferrihydrite will age to geothite and may compose some of the Fe in peat, fractions of various Fe-oxyhydroxides are not known.

2.5.2.2 Metal speciation calculations

Metal-DOM complexation calculations were conducted using MINTEQ for Nd, Ni, Ba, and K in peat groundwater samples along the Yankee, Zulu and Golf transects. These four metals were selected as they represent kimberlite pathfinder metals that are high in peat and peat groundwaters overlying kimberlites relative to sites distal to kimberlites in the Attawapiskat kimberlite field (Hattori and Hamilton, 2008; Sader *et al.*, 2010). They are also different metal types and have established binding constants (Milne et al., 2003; Sonke and Salters, 2004).

Dissolved metals were calculated as organic complexes and free ions. The model calculations indicate that aqueous sulfate and carbonate complexes comprise less than 0.5% of the total dissolved metals in the groundwater samples. The fraction of total dissolved metal complexed with DOM along transects at Yankee, Zulu and Golf decreases with

increases in pH, increases in *I*, and decreases in DOC concentrations (Fig. 2-6). Under conditions with little to no contribution from upwelling groundwater, where DOC concentrations are high, pH is low, and *I* is low, almost all soluble Nd, Ni, and Ba complex with DOM in groundwaters collected over the Yankee, Zulu and Golf transects. Under these conditions, a significantly lower fraction of K forms DOM complexes compared with the other metals and is as low as 30% at Golf (Fig. 2-6). Conversely, at sites of strong groundwater upwelling (lower DOC, higher pH, and higher *I*) the fraction of Nd and Ni bound to DOM is around 40 to 50% and sites of upwelling at Yankee are as low as 10%. The fraction of Ba bound to DOM is also lower (15 to <5%), and virtually all K is calculated to exist as free ions (Fig. 2-6). Decreases in the fraction of total Ni and Nd bound to DOM correspond to decreases in the concentration of these metals in the peat groundwater. However these sites are accompanied by increases in concentrations of Ni and Nd in peat total digestion significantly greater than baseline values, and was reported by Hattori and Hamilton (2008).

2.5.2.3 Ferrihydrite – metal adsorption calculations

Modeling was conducted to simulate the behaviour of pathfinder metals as peat groundwater geochemistry evolves from conditions with only minor contributions from upwelling groundwaters to conditions where these contributions dominate. The Zulu and Golf kimberlite transects were used for these calculations because they both have progressively greater eastward contributions from upwelling groundwater along their transects starting at site 300, and 307 m at Zulu and Golf, respectively based on increasing EC, pH, and Ca values and decreasing Eh values (Sader *et al.*, 2009). Pathfinder metal concentrations (Nd, Ni, K and Ba) at Zulu and Golf were held constant and modeled with the geochemical

conditions (i.e. pH and Eh), DOC and DIC, and major ions (i.e. Ca, Mg, Na, Fe, Al) observed in successive peat groundwater samples eastward along each transect. Concentrations of ferrihydrite were set at 1 g/L for sites with low contributions from upwelling groundwaters (EC < 100 μS/cm) and 10 g/L at sites of upwelling minerotrophic waters (EC > 100 μS/cm). These ferrihydrite concentrations were chosen because total Fe contents in peat reported by Hattori and Hamilton (2008) along the same Yankee and Golf transects as this study ranged from 0.05 to 0.15% where EC < 100 μS/cm and ranged from 0.7 to 3.19% where EC > 100 μS/cm. It is unclear where the Fe, which has precipitated on peat surfaces, originated from. Possible sources include pyrite in the TSS or limestone. The source of Fe could also be kimberlites due to the hydration of olivine provided redox conditions were favourable for Fe^{2+}, however, Fe in Attawapiskat kimberlite waters are commonly favoured to precipitate as Fe-oxyhydroxides. The formation of Fe-oxyhydroxides is also favoured in other kimberlite waters (i.e., Sader *et al.*, 2007a).

We assume that the majority of total Fe exists as secondary precipitated ferrihydrite because no residual mineral grains were visually identified in the peat, however, no specific Fe mineral phases were investigated. For Zulu model calculations, the ferrihydrite content at sites 300, 350, and 400 m were set at 1 g/L and at sites 450 to 750 m the content was set at 10 g/L. For Golf, ferrihydrite content was set at 1 g/L at sites 309 to 569 m and at sites 594 to 722 m it was set at 10 g/L.

The model calculations indicate progressively greater fractions of Ni and Nd are adsorbed onto ferrihydrite with increasing contributions from upwelling groundwaters and increasing ferrihydrite inputs into the model calculations (i.e. 1 or 10 g/L) (Fig. 2-7). Increases in Ni and Nd fraction adsorbed to ferrihydrite are roughly inversely proportional to

the fraction of dissolved Ni and Nd complexed with DOM and to total dissolved metal concentrations (Fig. 2-6). No K and only a small fraction of Ba are calculated to be adsorbed onto ferrihydrite (Fig. 2-7) and likewise, there is no relationship with analyzed K and Ba concentrations (Fig. 2-6).

2.6 DISCUSSION

2.6.1 Controls on Metal speciation

MINTEQ calculations indicate the fraction of total dissolved Nd, Ni, Ba, and K complexed with DOM in peat groundwaters decreases with increased contributions of minerotrophic groundwaters. Our model calculations suggest the binding strength and ion selectivity for DOM, in order from strongest to weakest, is: Nd > Ni > Ba > K. The calculated strong binding of Ni and Nd to DOM is consistent with their affinity to form strong coordinate linkages with DOM molecules (Stevenson, 1994). Our MINTEQ speciation calculations provide a reasonable estimation of metal-DOM speciation and compare favourably with other studies. Rare earth element – DOM speciation modeling of peat groundwaters from the Great Dismal Swamp, Virginia conducted by Johannesson et al. (2004) indicated that Nd – DOM species accounted for between 60 and nearly 100% of the total metal concentration. They reported pH, ionic strength and DOC concentrations similar to values reported in the present study. Additionally, Unsworth et al. (2006) compared experimentally derived concentrations of Ni – DOM complexes with MINTEQ calculated Ni – DOM concentrations for the same waters. Their results showed similar values for calculated and modeled Ni-DOM fractions, suggesting MINTEQ accurately predicts metal – DOM complexation.

Metal – DOM complexation profiles along sampling transects indicate concentrations of Ba and K are more sensitive to changes in the peat groundwater geochemistry compared

with concentrations of Nd and Ni (Fig. 2-6). Modeling calculations predict the fraction of K bound to DOM is typically less than 50%, and only under the most ombrotrophic conditions do the total concentrations approach 100% DOM – bound. Smaller contributions of minerotrophic groundwater result in a much greater decrease in Ba and K DOM complexes in the calculations compared with Nd and Ni, and this is likely due to the lower DOM binding affinities of Ba and K. Alkali metals only bind via electrostatic forces, whereas alkaline earth metals bind at specific sites. However, alkaline earth metals do not bind as strongly to DOM as transition metals due to the ion spherical symmetry and low polarizability of alkaline earth metals (Clymo, 1983; Stevenson, 1994; Tipping, 2002).

There are four factors that may limit the ability of metals to complex with DOM: 1) variability in pH; 2) type of DOM (i.e. fulvic or humic acid); 3) the ionic strength of peat groundwaters; and 4) variations in DOC concentrations. Research has previously shown that increases in pH result in a greater capacity for metals to bind to DOM (Lu and Allen, 2002; Tipping, 2002; Pourret *et al.*, 2007). Higher pH values in waters typically result in less competition by H^+ for DOM binding sites. With less competition, a greater fraction of dissolved Ni and Nd can bind to DOM because they can fill more available binding sites. Conversely, under low pH conditions, elevated H^+ ion activity exerts stronger competitive effects and commonly fills more of the available binding sites on organic molecules. Competition from H^+ effectively inhibits other dissolved metals from binding with DOM, resulting in greater concentrations of free ions in water. However, our study indicates that the calculated fraction of metal-DOM species decreases with increasing pH (Fig. 2-6), suggesting that pH is not likely a limiting factor in metal complexation with DOM, particularly at sites of upwelling. It is possible the poor association of pH with metal-DOM

complexation is due to elevated carbonate alkalinity in minerotrophic peat groundwaters such as 300 m to the end of the Zulu transect, 307 m to the end of Golf, and at point-source locations along Yankee (Fig. 2-6; Table 2-1). Concentrations of HCO_3^- and CO_3^{2-} can consume H^+ and will buffer low pH peat groundwaters.

Elevated carbonate alkalinity (based on DIC concentrations and pH) at these sites likely buffers the normally acidic peat groundwaters. The source of the high alkalinity could be from groundwater interactions with kimberlite, limestone or Tyrell Sea sediment, or some combination of these sources. Additionally, Tang and Johannesson (2010) showed that carbonate ions can outcompete fulvic acid for REEs, but not humic acids.

The most likely explanation for the decrease in metal – DOM complexation at sites with elevated upwelling minerotrophic groundwater is a combination of lower DOM concentrations coupled with increased ionic strength. This combination likely enhances competition effects, as there are more metal ions in the peat groundwaters competing for fewer DOM binding sites. The correlation between increases in ionic strength and decreases in the calculated fraction of Ni and Nd - DOM complexes is statistically significant ($r = -0.71$ and -0.94, respectively). The lower correlation coefficient for Ni compared with that for Nd might be attributed to the lower affinity of divalent Ni to bind to DOM. Elevated concentrations of alkaline earth metals such as Ca and Mg (major contributors to ionic strength) can induce strong competitive effects that inhibit metal binding to DOM (Cabaniss and Shuman, 1988b; a; Tipping, 2002). In our study, Ca and Mg concentrations are up to 25 times more elevated in minerotrophic peat groundwaters than in peat groundwaters with little to no detectable upwelling groundwater, and are 6 to 7 orders of magnitude greater than concentrations of Ni and Nd.

2.6.2 Controls on metal solubility

2.6.2.1 Metal binding and adsorption

The results of this study suggest that metal speciation is a key determining factor in kimberlite pathfinder metal solubility in peat groundwaters. The concomitant decrease in total Ni and Nd concentrations and decrease in the calculated fraction of these metals complexed with DOM (Fig. 2-6) suggests they may have been scavenged from solution due to their presence in greater proportions as free ions. Conversely, metals complexed with DOM are generally inhibited from participating in adsorption processes (Sholkovitz and Copland, 1981; Lofts and Tipping, 1998; Radovanovic and Koelmans, 1998) and therefore they tend to remain in solution. For example, elevated Ni and Nd concentrations along sampling transects occur at the east and west margins at Zulu and Golf, respectively and at 350 m at Yankee (Fig. 2-6). With the exception of the Yankee sample site, these sites represent only small contributions from upwelling groundwaters and have high predicted fractions of Ni and Nd – DOM complexes. However, where upwelling of minerotrophic groundwater is greater, such as 400 to 700 m at Zulu, 400 to 700 m at Golf, and 443 and 489 m at Yankee, total Ni and Nd concentrations are commonly lower than local baseline peat groundwater values determined by Sader et al. (2010). The low Ni and Nd concentrations suggest that they have been scavenged from solution. Further evidence for metal scavenging is the elevated concentrations of Nd and Ni in peat digestion (Hattori and Hamilton, 2008), and these coincide with sites where total Ni and Nd concentrations and Ni and Nd fractions complexed with DOM are low (Fig. 2-6).

The formation of ferrihydrite at sites of upwelling is likely critically important in scavenging metals where they dominantly exist as free ions. Peat groundwaters are close to

or greater than saturation with respect to ferrihydrite at sites of high groundwater contributions (EC > 100 μS/cm), but well below saturation where conditions indicate little to no groundwater contribution (EC > 100 μS/cm) (Fig. 2-5). Overall, the $logSI_{ferr}$ values are lower along the Golf sampling transect, and this is likely a function of the shallow sampling depth (0.4 mbgs) and lower pH. Additionally, the $logSI_{ferr}$ correlates moderately well (r=0.72) with peat Fe content from total peat digestion reported by Hattori and Hamilton (2008), and supports the validity of $logSI_{ferr}$ calculations.

Decreases in total Ni and Nd and decreases in the calculated fraction of these metals complexed with DOM, coupled with increases in ferrihydrite suggest metals may be adsorbing on ferrihydrite where they exist as free ions. A plot of Nd versus $logSI_{ferr}$ (Fig. 2-8) defines a trend of decreasing concentration with increasing $logSI_{ferr}$. Nickel concentrations also decrease with increasing $logSI_{ferr}$, however, the trend is not as defined as Nd, and this is likely because Nd is trivalent and has a stronger affinity to adsorb on Fe-oxyhydroxides (Stevenson, 1994). Conversely, alkali and alkaline earth metals (K and Ba) do not generally have a high affinity to adsorb on ferrihydrite (Kinniburgh *et al.*, 1976; Cornell and Schwertmann, 2003), especially in the acidic pH peat groundwaters of this study. Laboratory tests by Kinniburgh et al. (1976) indicated the pH must be greater than 8.1 for 50% of dissolved Ca and Mg to adsorb onto the surfaces of Fe gels. Based on that observation, they suggested alkaline earth metals have a low selectivity for adsorption on Fe-oxyhydroxides. Likewise, little association exists between peat groundwater Ba concentrations and $logSI_{ferr}$ in this study (Fig. 2-8).

The MINTEQ calculated predictions of metal adsorption on ferrihydrite surfaces along the Zulu and Golf sampling transects support our analytical results. Calculations

predict Ni and Nd are increasingly scavenged onto ferrihydrite surfaces at sites with greater upwelling groundwater contributions (Fig. 2-7). Calculations reveal that up to 90 and 95% of soluble Ni and Nd, respectively, may adsorb onto ferrihydrite surfaces. Additionally, sample sites with high predicted adsorption (up to 95%) represent the lowest fractions (~20%) of soluble Ni and Nd complexed with DOM. Calculations of metal-DOM speciation and adsorption to ferrihydrite surfaces (Fig. 2-6 & 2-7) suggest decreases in Ni and Nd complexation coupled with an inversely proportional increase in Ni and Nd bound to ferrihydrite is due to the increased availability of free metal ions. Conversely, the calculations predict Ba and K do not adsorb strongly due to their lack of adsorption affinity for ferrihydrite. The results and modeling of metal adsorption on ferrihydrite surfaces in this study compares favourably with sequential leach results of sphagnum peat from a peat bog in Estonia (Syrovetnik et al., 2007). These authors concluded that a significant fraction of the transition metals Pb, Zn, and Mn had adsorbed to Fe-oxyhydroxides, whereas adsorption of alkaline earth metals was negligible.

Adsorption of metals onto insoluble humic substances may be partly responsible for scavenging metals where groundwaters are upwelling. Metals typically have a strong affinity to adsorb onto insoluble organic matter. The cation exchange capacity of sphagnum peat ranges from 0.6 to 2 meq/g at pH 7 and peat can retain high concentrations of metals (Sikora and Keeney, 1983; Hill and Siegel, 1991). However, we suggest Ni and Nd may be more likely to adsorb onto ferrihydrite rather than insoluble organics. Alkali and alkaline earth metals are highly effective competitors for insoluble organic adsorption sites and will invariably compete strongly with Ni and Nd for insoluble organic adsorption sites. This competition is likely strongest at sites of upwelling where alkaline earth concentrations are

up to 25 times higher than ombrotrophic peat groundwaters. However, these metals will not compete strongly for ferrihydrite adsorption sites.

It is also possible that all insoluble organic adsorption sites have been filled where groundwater upwelling is strong. Hill and Siegel (1991) noted that insoluble organic cation exchange sites are full in spring-fen condition sphagnum peat bogs. In our study, the elevated Ca and Mg at sites of strong upwelling may indicate a similar scenario, where all insoluble organic adsorption sites are filled. The contribution rate of alkali and alkaline earth metal inputs to peat groundwaters at sites of strong groundwater upwelling may exceed the rate of peat humification and production of insoluble organic substances. The ~3 m layer of peat in the study area accumulated over approximately 5000 years. If these adsorption sites were full, transition metals would have an additional further affinity to adsorb to ferrihydrite because of the lack of insoluble organic adsorption sites.

2.6.2.2 Secondary mineral precipitation

Carbonate and sulfide mineral precipitation are capable of scavenging metals from solution in many environments. However, in this study it is reasonable to exclude these processes as possible scavengers of dissolved metal. The $\log SI_{calcite}$ for all peat groundwater samples is < 0 and therefore calcite is not favoured to form. It should, however, be noted that loss on ignition and ammonium acetate leach analyses of Attawapiskat peat (Brauneder, 2007; Hattori and Hamilton, 2008) provide evidence of carbonate precipitation in peat samples collected at 0.6 mbgs along sampling transects nearly identical to those in this study. However, peat groundwater samples in this study were collected at 1.1 mbgs at Yankee and Zulu and 0.4 mbgs at Golf and likely represent different geochemical zones within the peat. Peat groundwater geochemistry such as Ca concentration, pH and alkalinity can vary

substantially over small changes in depth (Clymo, 1983), which will impact the calcite saturation.

Sulfide minerals are not thought to appreciably scavenge soluble metals in this study. Both sulfate and total sulfur concentrations are low in the peat groundwaters and no correlation exists between concentrations of sulfate and sulfur, and sites of upwelling groundwaters (Table 2-1). Additionally Hattori and Hamilton (2008) noted that total sulfur content in the peat is below 0.1% at all of their sample sites.

2.7 SUMMARY AND IMPLICATIONS FOR MINERAL EXPLORATION

This study highlights the importance of metal - DOM complexation and the effect those complexes can have on the solubility of metals in water saturated environments such as wetlands. The saturated nature of wetlands and the high DOC concentrations in peat groundwaters adds another level of complexity, as dissolved metals are not only governed by adsorption processes onto solid media, but by abundant metal – DOM complexes that can prevent metal adsorption and increase solubility. For example, we have shown that Nd concentrations are elevated at sample sites with minor contributions of upwelling groundwaters at or near kimberlite margins at Zulu and Golf. At these sites our modeling calculations indicate nearly 100% of the transition metals form DOM complexes. Conversely, where our modeling calculations indicate low Nd and Ni – DOM complexes, such as at site 07-Y-12 at Yankee, and at the east ends of Zulu and Golf sampling transects, the metal concentrations in peat groundwater are less than baseline values. Modeling calculations predict that the low metal concentrations at these sites are due to a greater affinity for Ni and Nd (which exist as free ions) to adsorb on ferrihydrite surfaces.

In contrast to the high DOM, water saturated peat bog environment of this study, soluble metals in groundwaters employed in mineral exploration typically do not consider DOM concentrations (Sader *et al.*, 2007a; Leybourne and Cameron, 2010). Dissolved organic matter concentrations are low in most natural groundwaters (Freeze and Cherry, 1979) and therefore they do not control soluble metal behaviour. Our findings also contrasts with the findings of geochemical studies of soil collected above the water table for mineral exploration. In these environments, adsorption onto solid phase organics and ferrihydrite are more important aspects for detecting pathfinder metals.

This study has implications for surficial geochemical exploration for mineral deposits, as metal speciation and metal adsorption affinities are important aspects must be considered when establishing effective sampling methodologies. It also has implications for the spatial distribution of metals in soils, peat, and groundwaters where high DOM conditions exist. In wetland environments, our results indicate that the most effective means to accurately detect kimberlite pathfinder metals is to collect samples from both peat and peat groundwater samples along sampling transects. The collection of both media likely provides a more accurate delineation of metals associated with a buried kimberlite. If the peat groundwaters are dominantly ombrotrophic with only minor contributions from kimberlite groundwaters, metals are more likely to remain highly soluble as metal – DOM complexes. A geochemical sampling program that only focuses on peat may overlook important geochemical responses, as the formation of metal-DOM complexes may inhibit metal adsorption or incorporation into secondary mineral precipitates. Conversely, if only peat groundwaters are collected, a kimberlite geochemical response may also be overlooked where kimberlite pathfinder metals are migrating upwards into peat groundwaters that have

the potential to scavenge dissolved metals (more minerotrophic conditions) Our results suggest scavenging of metals, which exist as free ions by ferrihydrite or insoluble organic matter, is the most likely pathway.

2.8 ACKNOWLEDGEMENTS

We thank DeBeers Canada for providing financial and logistical support for the project. Julie Kong, Ed Francisco, and Brad Wood were particularly helpful. Financial support was also provided by a NSERC Discovery grant and a NSERC Collaborative Research grant to Keiko Hattori. Jamil Sader received financial support from an Ontario Graduate Scholarship and a student research grant from the Society of Economic Geologists. Fieldwork was assisted by Katherine Mellor. We thank M. Beth McClenaghan and Jan Peter (Geological Survey of Canada), Matt Leybourne (GNS New Zealand), and Karen Johannesson (Tulane University) for reviews of the manuscript.

2.9 FIGURES

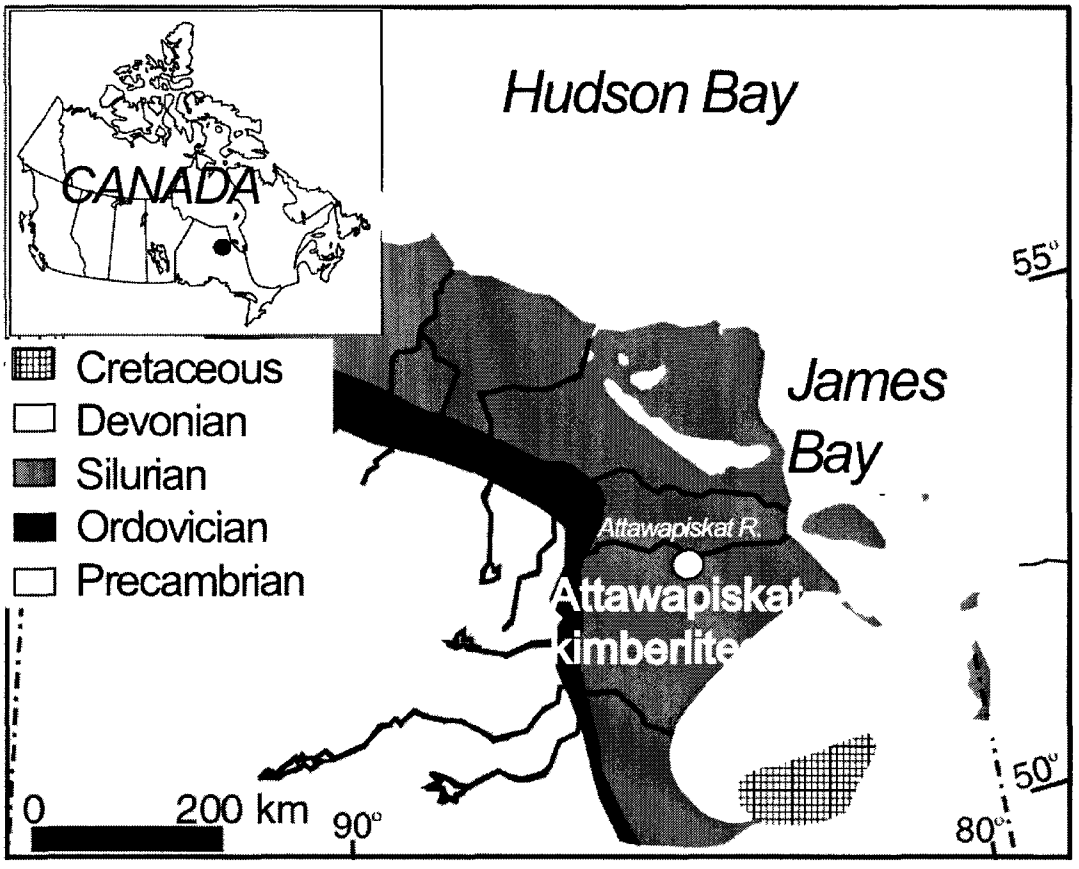

Figure 2-1. Regional bedrock geology of the James Bay Lowlands and location of the Attawapiskat kimberlite field in north central Canada (geological map modified from Bellefleur et al. (2005)).

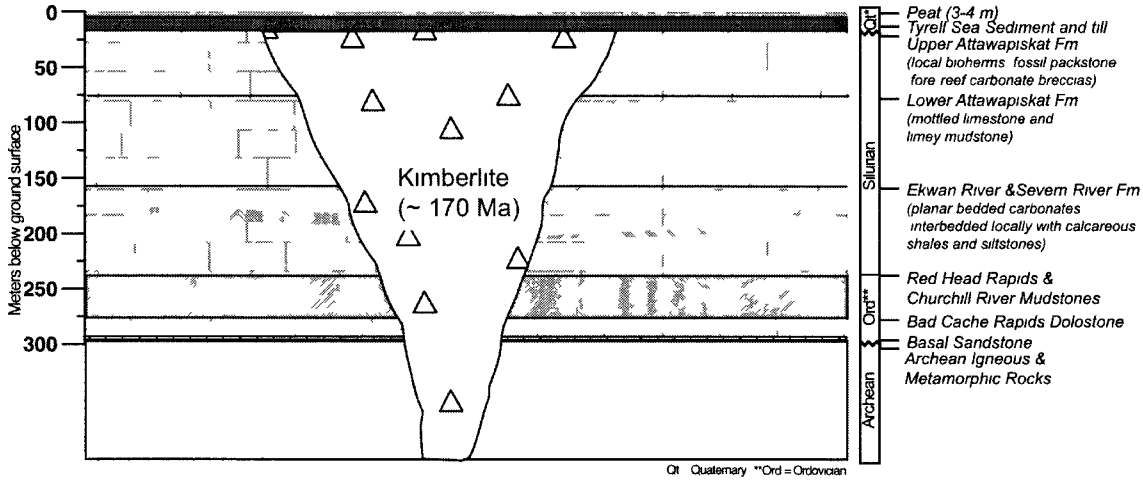

Figure 2-2. Schematic vertical section of rocks and sediment of which Attawapiskat kimberlites are emplaced into Kimberlite and host rocks are overlain by a thin till, Tyrell Sea sediment (10 to 5 Ka), and peat (5 Ka to present) Diagram from (Sader *et al* , 2010), geology from Norris (1993)

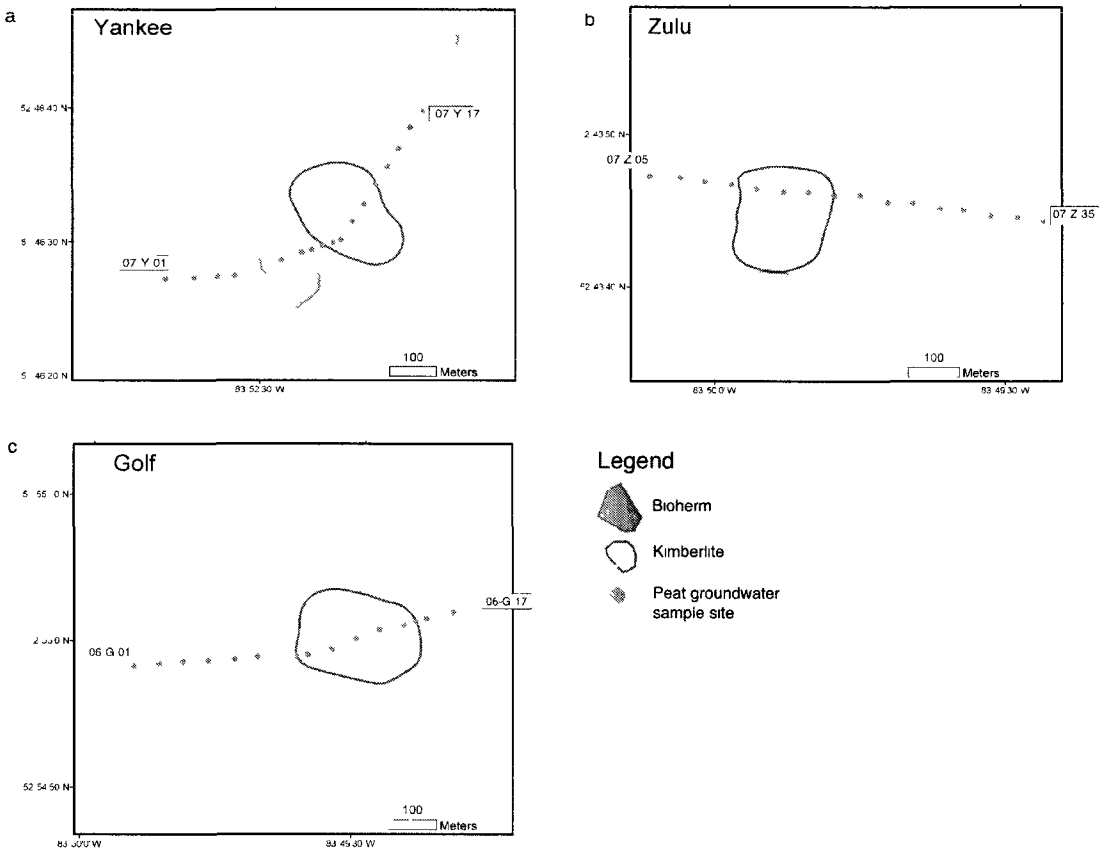

Figure 2-3. Location of the (a) Yankee, (b) Zulu, and (c) Golf kimberlites, and peat groundwater sample sites The aerial extent of each kimberlite was determined using geophysical data and exploration drilling by DeBeers Canada Figures modified from Sader et al (2010)

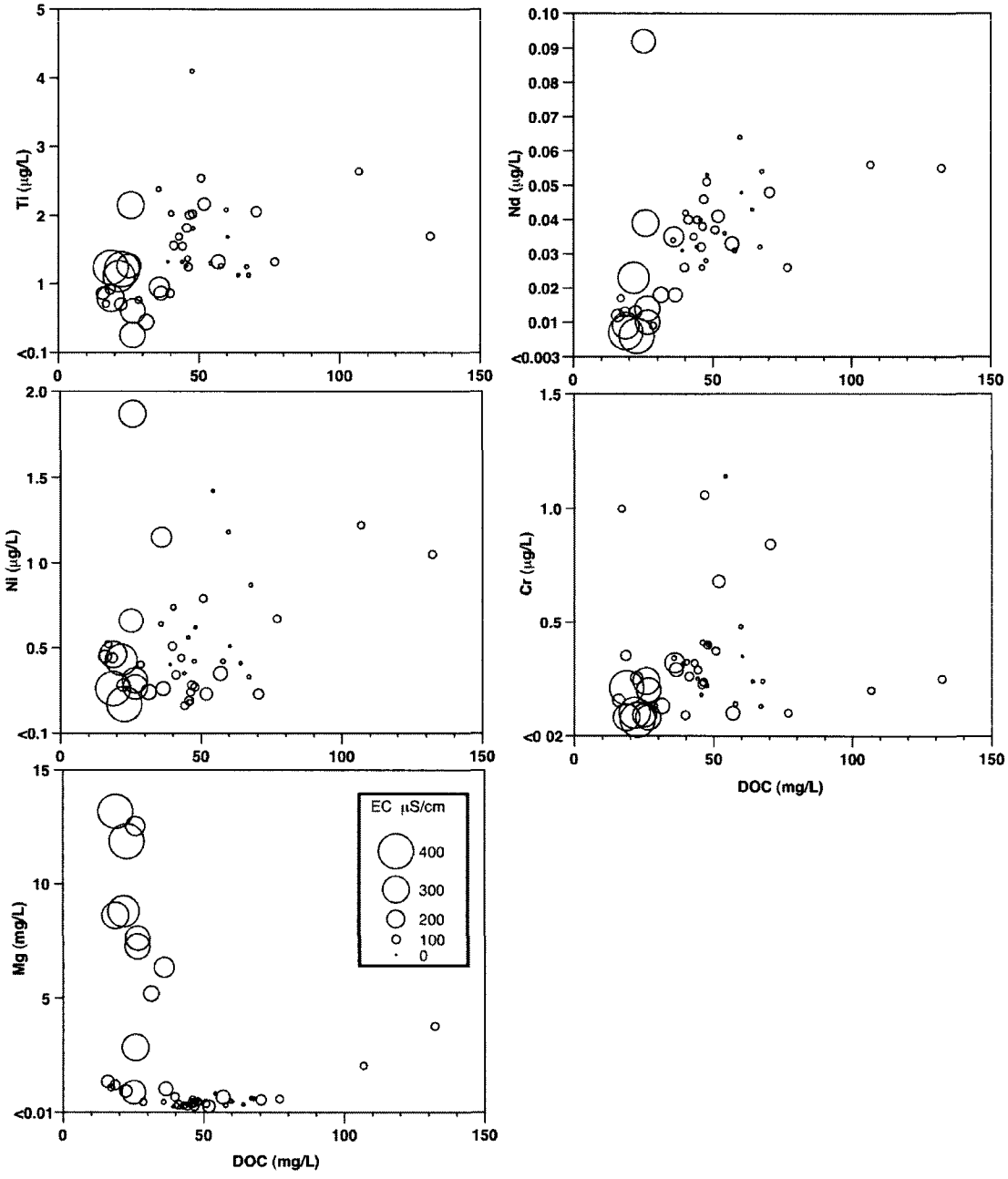

Figure 2-4. DOC versus major, minor and trace elements in peat groundwaters for Yankee, Zulu, and Golf kimberlites (n=50) Increases in DOC and decreases in EC coincide with increased concentrations of Ti, Nd, Ni, and Cr Concentrations of Mg, Ca, Ba, K, and Rb display the opposite trend. (Continued on next page)

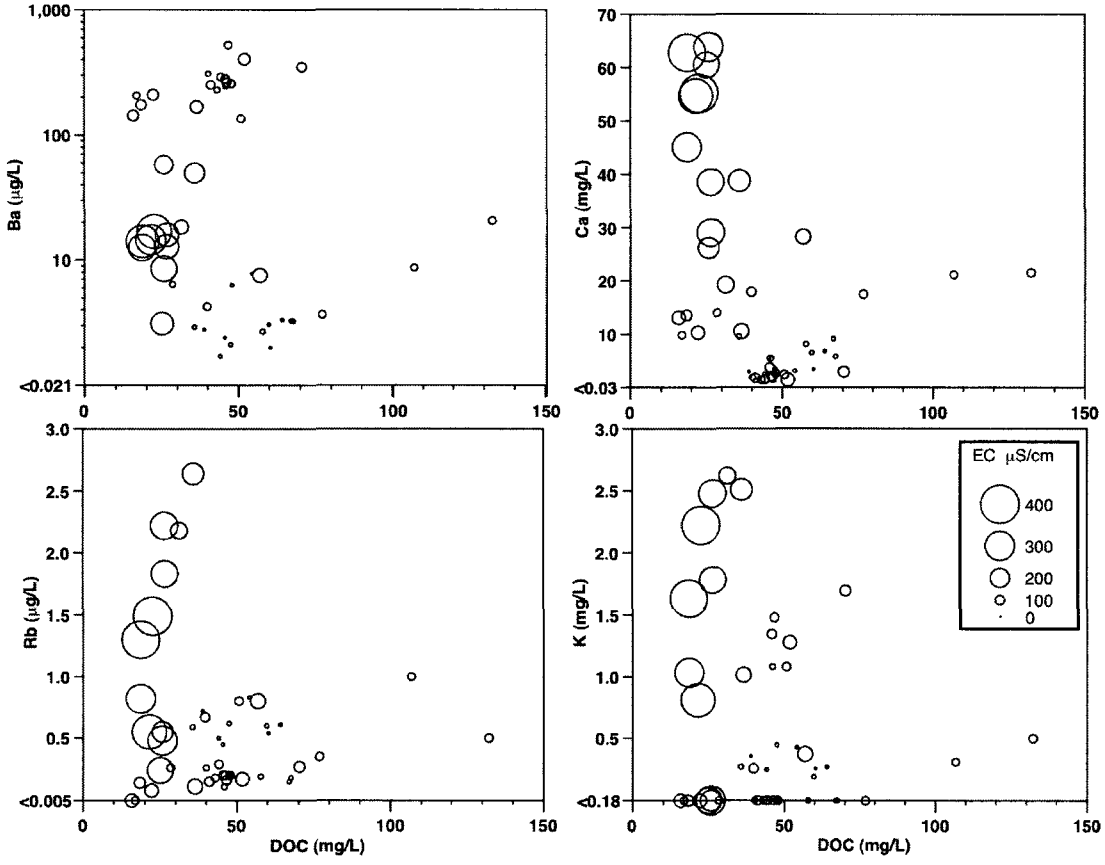

Figure 2-4: Continued.

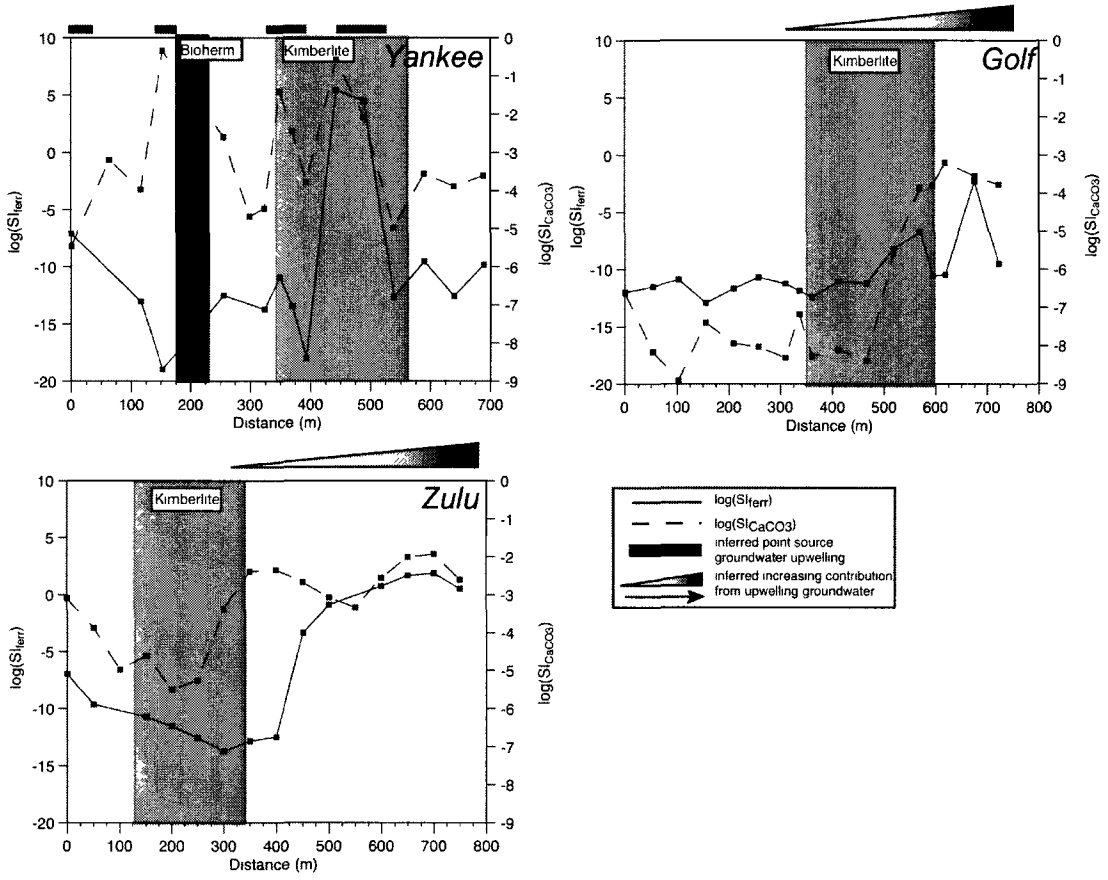

Figure 2-5. Profiles of SI_{ferr} and SI_{CaCO3} in peat groundwater at Yankee, Zulu and Golf kimberlites. The highest saturation indices are located at sites along transects which have elevated contributions from upwelling groundwaters. Ferrihydtite is commonly near or greater than saturation at sites of strong upwelling. No samples are saturated with respect to calcite.

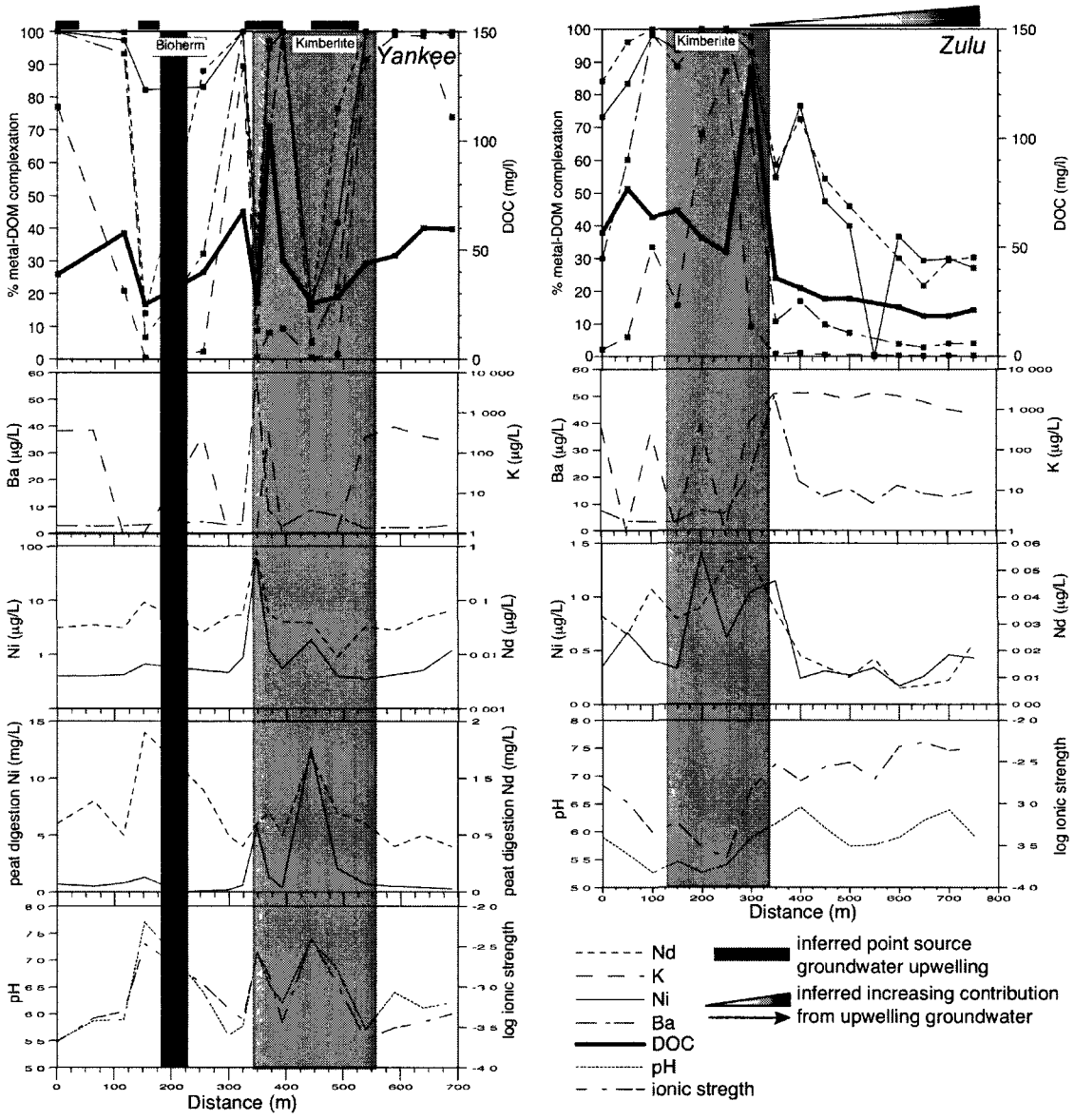

Figure 2-6. The profiles of MINTEQ-calculated metal-DOM speciation shown as a percentage of total metal content in peat groundwater along transects over Yankee, Zulu, and Golf kimberlites. The profiles indicate that at sites of strong upwelling the fraction of metals bound to DOC decrease. At these sites, peat groundwater Ni, Nd, and DOC concentrations are low. However pH and ionic strength in peat groundwaters, and Ni and Nd in peat digestion are elevated at the sites of upwelling, suggesting Ni and Nd may be scavenged from solution when they do not exist as metal-DOM complexes. On the other hand, concentrations of Ba tend to be elevated at most sites of upwelling along Yankee, Zulu, and Golf transects and especially at kimberlite margins or over them. Potassium concentrations reflect the fact that alkali metals neither bind strongly to DOM, nor are they strongly scavenged from solution. Concentrations of Ni and Nd in peat total digestion at Yankee and Golf are from Hattori and Hamilton (2008). (Continued on next page).

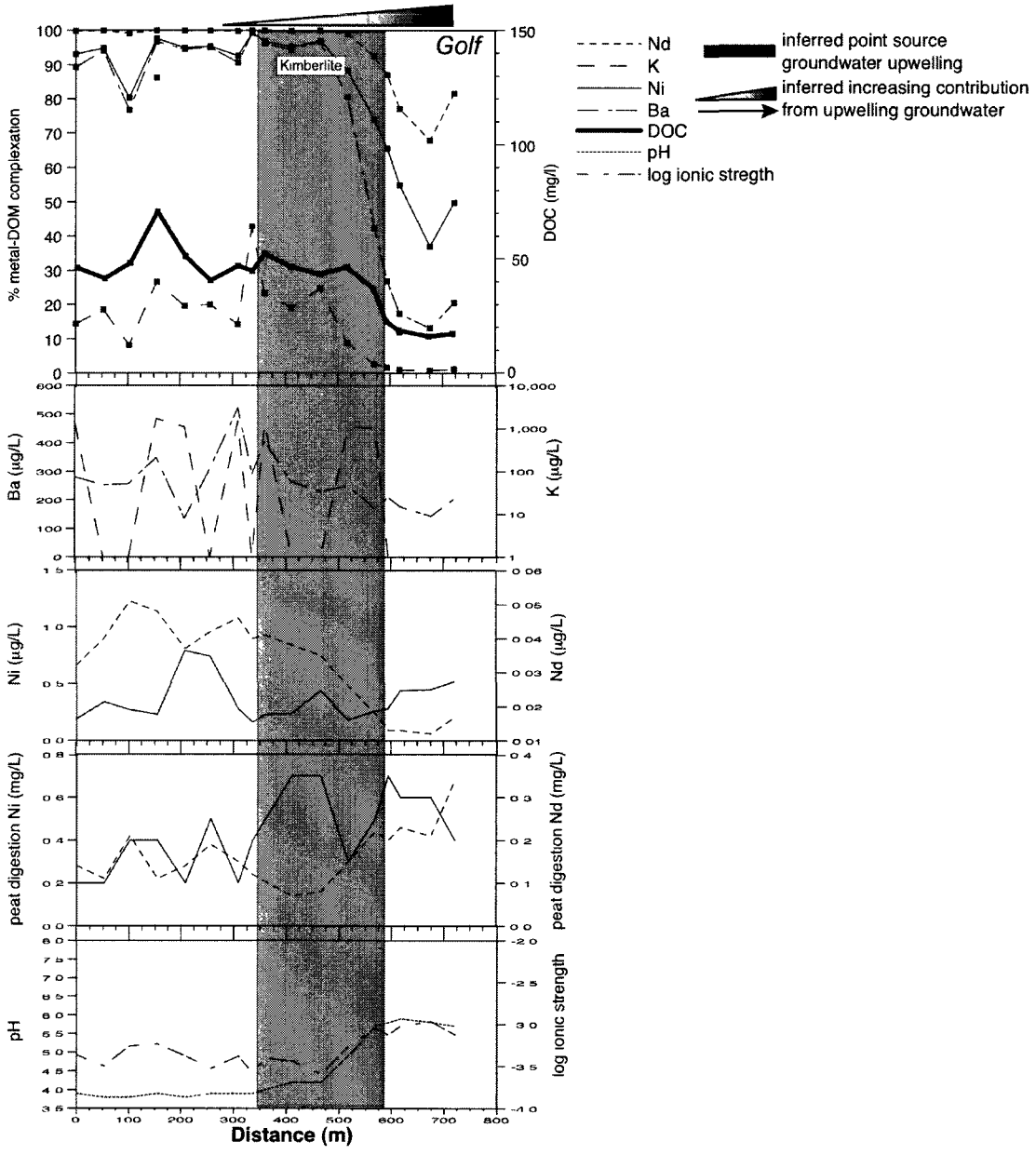

Figure 2-6: Continued.

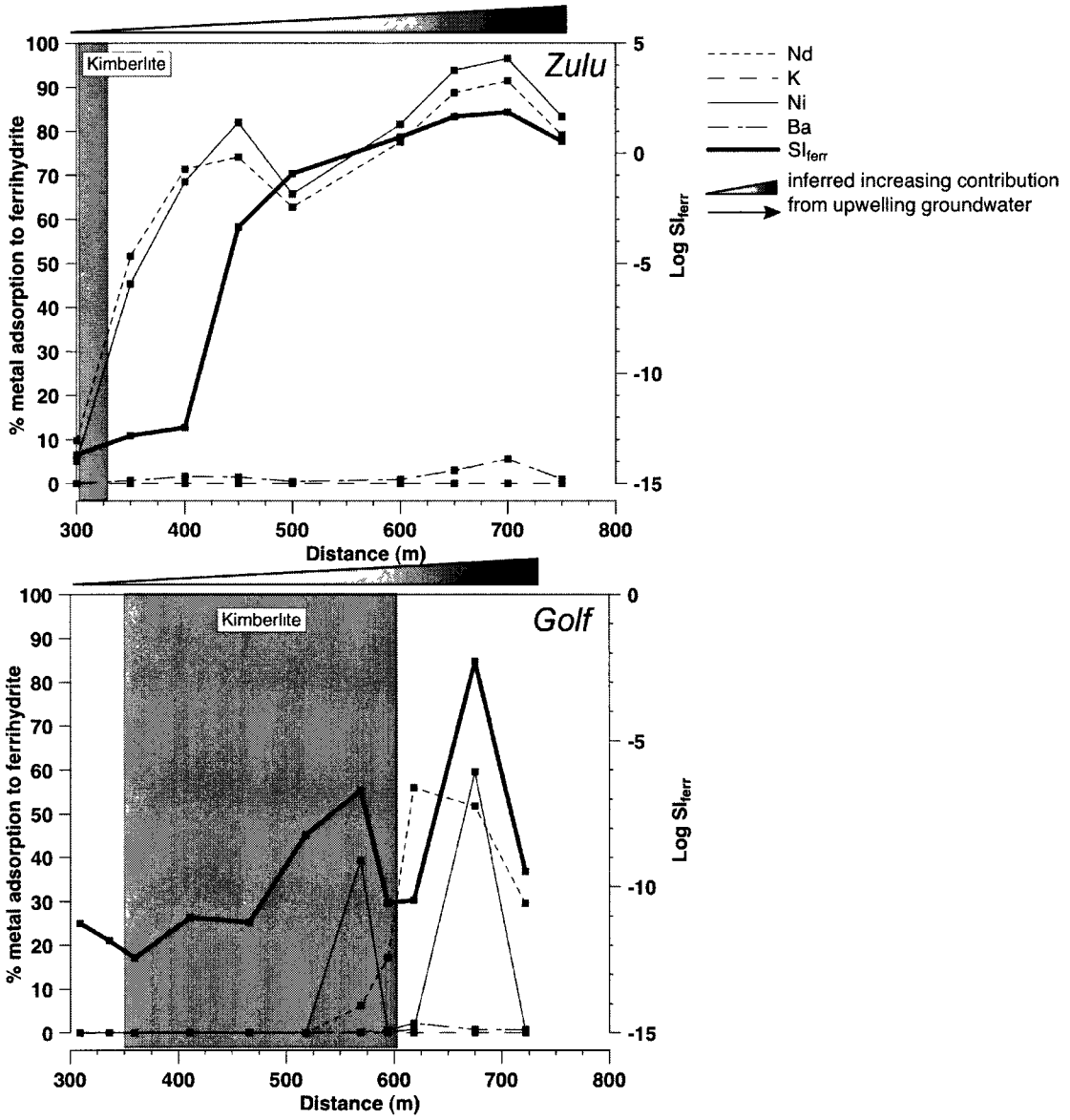

Figure 2-7. Profiles of MINTEQ-calculated adsorption of Nd, Ni, Ba, and K onto ferrihydrite surfaces along portions of the Zulu and Golf transects starting at 300 and 307 m respectively (sites of increasing contributions from upwelling groundwater). The fraction of Ni and Nd calculated to adsorb to ferrihydrite increases with increasing ferrihydrite saturation indices. Barium and K are not calculated to adsorb strongly to ferrihydrite.

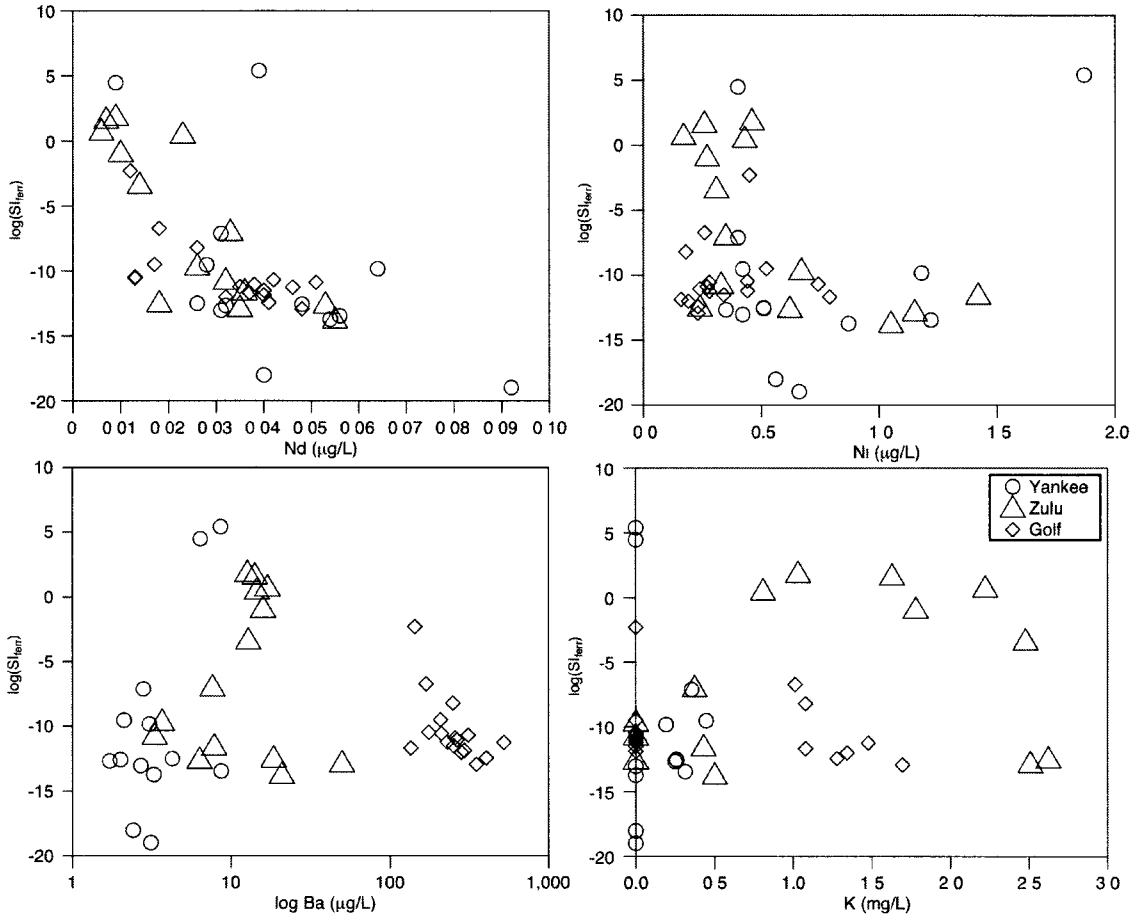

Figure 2-8. Plots of Nd and Ni versus SI_{ferr} for peat groundwater samples from Yankee, Zulu and Golf (n=42) indicate the highest concentrations of these metals are usually found where the SI_{ferr} is the lowest, likely due to their affinity to bind to ferrihydrite. Conversely, there is little correlation of SI_{ferr} with Ba suggesting Ba and no correlation with K.

2.10 TABLES

Table 2-1. Compositions of peat groundwaters along sampling transects over the Yankee and Zulu kimberlites.
Continued next page.

Table 1

Sample	Detection Limit	07-Y-01	07-Y-02	07-Y-03	07-Y-04	07-Y-05 5	07-Y-06	07-Y-07	07-Y-08	07-Y-09	07-Y-10	07-Y-11	07-Y-12	07-Y-13	07-Y-14	07-Y-15	07-Y-16	07-Y-17
Distance along transect (m)		0	64	116	153	255	299	324	349	370	393	443	489	539	589	639	689	739
Upwelling groundwater sites		upwelling	ombrotrophic	ombrotrophic	upwelling	ombrotrophic	ombrotrophic	ombrotrophic	upwelling	upwelling	ombrotrophic	upwelling	upwelling	ombrotrophic	ombrotrophic	ombrotrophic	ombrotrophic	ombrotrophic
Bedrock substrate		limestone	limestone	limestone	limestone	limestone	limestone	limestone	kimberlite	kimberlite	kimberlite	kimberlite	kimberlite	kimberlite	kimberlite	limestone	limestone	limestone
Lat		52 8455	52 7743	52 7743	52 7744	52 7747	52 7749	52 7750	52 7751	52 7751	52 7752	52 7756	52 7760	52.7764	52 7768	52 7771	52 7776	52 7779
Long		-83 7915	-83 8772	-83 8765	-83 8759	-83 8745	-83 8739	-83 8735	-83 8732	-83 8729	-83 8726	-83 8723	-83 8720	-83 8716	-83 8712	-83 8709	-83 8706	-83 8702
Temp °C		8 7	9 8	9 0	9 5	8 8	8 1	7 9	7 7	6 3	7 4	6 7	8 2	10 4	8 0	7 2	7 6	4 2
pH		5 49	5 87	5 89	7 71	6 41	5 59	5 77	7 15	6 53	6 21	7 37	6 83	5 71	6 40	6 11	6 21	7 10
Eh (mV)		332	316	316	260	303	317	316	240	299	316	224	258	325	266	303	294	302
EC (µS/cm)		29	56	55	264	92	55	47	218	78	30	301	71	35	45	30	41	54
DO (mg/L)		1 24	2 23	3 11	4 47	4 48	4.39	2 56	2 72	1 72	1 90	2 66	1 19	4 00	1 97	0 77	8 00	3 13
DIC (mg/L)		7 36	na	15 31	36 00	22 67	na	11 68	30 30	20 37	9 82	47 88	25 61	10 14	13 66	19 05	12 95	na
DOC (mg/L)		38 80	na	57 74	25 00	39 72	na	67 57	25 64	106 78	45 46	25 62	28 42	43 98	47 38	60 21	59 68	35 62
mg/L																		
Ca	0 03	2 91	7 07	8 12	60 54	17 89	9 15	5 75	26 18	21 12	5 49	63 91	14 01	2 52	3 43	3 36	6 50	9 54
Mg	0 01	0 24	0 33	0 31	0 88	0 68	0 81	0 59	12 55	2 04	0 38	2 84	0 45	0 34	0 49	0 46	0 48	0 44
K	0 18	0 35	0 36	bd	bd	0 26	bd	bd	bd	0 31	bd	bd	bd	0 25	0 45	0 26	0 19	0 27
Na	0 05	0 34	0 44	0 36	0 42	0 80	0 52	0 39	0 66	0 47	0 26	0 85	0 33	0 34	0 33	0 44	0 43	0 50
SO_4^{2-}	0 04	0 36	na	0 21	0 39	0 04	na	0 29	1 09	0 09	0 15	0 07	0 12	0 39	0 38	3 97	0 33	na
Cl	0 03	0 59	na	0 76	0 63	0 12	na	1 24	0 71	0 89	0 71	0 87	0 22	2 05	1 2	0 73	1 68	na
ug/L																		
Fe	3	155	409	258	25	302	256	171	400	586	111	4052	4726	119	140	151	448	1428
Mn	1	18	23	7	65	6	14	33	78	34	17	74	129	19	12	14	36	26
Al	5	157	81	74	28	33	69	141	156	135	84	12	14	66	133	100	121	79
S	300	318	bd	bd	510	bd	348	bd	467	bd	bd	433	bd	341	bd	358	373	394
Cr	0 02	0 32	0 11	0 14	0 09	0 09	0 19	0 24	4 23	0 20	0 18	0 24	0 13	0 25	0 22	0 35	0 48	0 34
Ba	0 02	2 80	2 62	2 68	3 11	4 25	3 04	3.26	58 06	8 65	2 41	8 57	6 41	1 71	2 11	2 00	3 05	2 92
Ni	0 10	0 40	0 40	0 42	0 66	0 51	0 46	0 87	60 76	1 22	0 56	1 87	0 40	0 35	0 42	0 51	1 18	0 64
Rb	0 005	0 717	1 009	0 193	0 240	0 670	0 363	0 176	0 553	1 002	0 446	0 481	0 260	0 498	0 624	0 540	0 599	0 586
Nd	0 003	0 031	0 035	0 031	0 092	0 026	0.051	0 054	0 823	0 056	0 040	0 039	0 009	0 032	0 028	0 048	0 064	0 034
Cu	0 2	18 8	1 9	1 3	0 8	1 8	3 1	7 5	3 2	2 6	4 0	5 1	3 0	3 4	2 9	5 3	9 7	3 9
Zn	1	18 9	4 0	3 3	1 6	6 1	7 0	11 7	1 7	7 9	5 9	6 4	6 3	21 8	5 0	8 2	10 9	7 3
Sr	0 1	3 67	7 22	7 20	43 32	20 05	9 17	6 53	137 55	23 88	5 23	46 69	11 32	2 84	3 60	3 98	6 07	7 95
Y	0 0005	0 0215	0 0212	0 0247	0 0895	0 0227	0 0352	0 0324	0 3144	0 0408	0 0304	0 0483	0 0071	0 0313	0 0629	0 0294	0 0382	0 0348
Pb	0 05	0 52	0 66	0 53	0 10	0 38	1 28	0 98	0 17	0 59	0 72	0 39	0 22	0 30	0 47	0 40	0 81	0 32

na = not analysed
bd = below detection

Table 2-1: Continued.

Table 1 - Con't

Sample	Detection Limit	07 Z-05	07 Z-07	07-Z-09	07-Z 11	07-Z-13	07 Z-15	07 Z-17	07 Z-19	07-Z 21	07-Z-23	07 Z-25	07 Z 27	07 Z 29	07 Z 31	07-Z-33	07-Z-35
Distance along transect (m)		0	50	100	150	200	250	300	350	400	450	500	550	600	650	700	750
Upwelling groundwater sites		ombrotrophic	ombrotrophic	ombrotrophic	ombrotrophic	ombrotrophic	ombrotrophic	upwelling	upwelling	upwelling	upwelling	upwelling	upwelling	upwelling	upwelling	upwelling	upwelling
Bedrock substrate		limestone	limestone	limestone	kimberlite	kimberlite	kimberlite	kimberlite	limestone	limestone	limestone	limestone	limestone	limestone	limestone	limestone	limestone
Lat		52 7298	52 7297	52 7297	52 7297	52 7296	52 7296	52 7296	52 7295	52 7296	52 7294	52 7294	52 7294	52 7294	52 7293	52 7293	52 7292
Long		-83 8354	-83 8345	-83 8338	-83 8331	-83 8324	-83 8316	-83 8309	-83 8301	-83 8294	-83 8286	-83 8279	-83 8271	-83 8264	-83 8256	-83 8249	-83 8241
Temp °C		11 2	12 0	9 7	10 8	11 0	9 9	10 0	11 2	9 1	6 5	8 9	9 7	10 1	9 6	4 6	10 5
pH		5 90	5 60	5 27	5 46	5 27	5 41	5 90	6 15	6 44	6 06	5 74	5 77	5 90	6 21	6 39	5 93
Eh (mV)		257	291	327	313	325	310	267	125	190	224	242	239	232	198	190	183
EC (µS/cm)		159	88	38	45	31	35	90	229	168	280	271	154	399	379	303	349
DO (mg/L)		bd	0 57	1 00	0 00	0 13	bd	bd	bd	bd	bd	bd	0 29	0 31	0 57	bd	0 32
DIC (mg/L)		35 56	31 65	26 72	20 16	17 97	19 63	25 39	51 61	38 50	49 85	56 45	43 91	70 10	65 99	54 47	55 44
DOC (mg/L)		56 78	76 84	63 98	66 85	54 14	47 80	132 21	35 81	31 30	26 40	26 50	na	22 47	18 63	18 55	21 40
mg/L																	
Ca	0 03	28 28	17 52	6 82	9 11	3 04	2 52	21 52	38 74	19 23	29 07	38 55	22 00	55 23	62 80	45 15	54 76
Mg	0 01	0 65	0 58	0 34	0 60	0 81	0 56	3 77	6 35	5 19	7 26	7 63	5 22	11 88	13 19	8 62	8 80
K	0 18	0 37	bd	0 27	bd	0 43	bd	0 50	2 51	2 62	2 48	1 78	2 65	2 22	1 63	1 03	0 81
Na	0 05	1 05	0 60	1 14	0 75	1 06	0 35	3 32	12 54	11 40	20 99	14 07	11 02	28 55	25 51	30 59	25 80
SO_4^{2}	0 04	0 22	0 21	0 25	0 23	0 40	0 20	0 27	0 53	0 20	0 22	0 80	0 20	0 17	0.22	0 22	0 29
Cl	0 03	1 81	0 81	1 20	1 60	1 05	0 81	0 28	2 52	1 67	2 02	2 69	2 71	14 60	16 84	25 43	18 72
ug/L																	
Fe	3	1507	1111	513	622	261	138	526	235	249	1042	1609	877	2235	3588	2763	3551
Mn	1	18	17	8	10	10	6	17	25	6	22	30	54	80	112	40	91
Al	5	46	72	58	64	59	67	79	13	365	6	7	13	6	10	9	23
S	300	bd	332	bd	bd	bd	bd	328	bd	bd	bd	bd	bd	bd	bd	bd	bd
Cr	0 02	0 10	0 10	0 24	0 13	1 14	0 40	0 25	0 32	0 13	0 08	0 20	0 13	0 07	0.21	0 08	0 10
Ba	0 02	7 60	3 66	3 32	3 29	7 80	6 31	20 72	49 97	18 49	12 83	15 89	10 29	16 90	14 07	12 62	14 57
Ni	0 10	0 35	0 67	0 41	0 33	1 42	0 62	1 05	1 15	0 24	0 31	0 27	0 34	0 17	0 26	0 46	0 43
Rb	0 005	0 795	0 352	0 605	0 149	0 831	0 202	0 497	2 638	2 184	2 223	1 831	3 435	1 491	1.297	0 822	0 550
Nd	0 003	0 033	0 026	0 043	0 032	0 036	0 053	0 055	0 035	0 018	0 014	0 010	0 017	0 006	0 007	0 009	0 023
Cu	0 2	1 0	0 7	4 0	1 3	9 8	6 0	6 8	3 0	3 0	0 9	3 9	1 9	1 2	3 2	0 9	1 5
Zn	1	8 6	2 6	6 2	2 6	20 3	7 7	7 7	16 3	4 9	12 5	10 9	6 6	1 8	10 7	2 4	3 0
Sr	0 1	39 87	22 84	12 25	14 08	8 02	8 82	71 62	164 01	90 54	117 39	127 93	69 79	191 83	203 05	128 19	125 35
Y	0 0005	0 0208	0 0184	0 0220	0 0246	0 0298	0 0312	0 0357	0 0193	0 0135	0 0083	0 0090	0 0096	0 0088	0 0170	0 0093	0 0173
Pb	0 05	0 24	0 43	0 81	0 47	1 25	1 22	1 08	0 39	0 65	0 17	0 22	0 16	0 09	0 17	0 13	0 18

na = not analysed
bd = below detection

Table 2-2. Log *I*, $LogSI_{ferr}$, and $LogSI_{CaCO3}$ values calculated for sampling transects over Yankee, Zulu, and Golf kimberlites

Table 2

Sample	Distance along transect (m)	Upwelling groundwater sites	Log *I*	Log SI_{ferr}	Log SI_{CaCO3}
Yankee					
07-Y-01	0	upwelling	-3 68	-7 12	-5 46
07-Y-02	64	ombrotrophic	-3 39	nc	-3 21
07-Y-03	116	ombrotrophic	-3 31	nc	-3 97
07-Y-04	153	upwelling	-2 47	-18 96	-0 34
07-Y-05 5	255	ombrotrophic	-2 97	-12 49	-2 60
07-Y-06	299	ombrotrophic	-3 26	nc	-4 68
07-Y-07	324	ombrotrophic	-3 41	-13 73	-4 47
07-Y-08	349	upwelling	-2 58	-10 91	-1 41
07-Y-09	370	upwelling	-2 86	-13 44	-2 44
07-Y-10	393	ombrotrophic	-3 44	-18 00	-3 79
07-Y-11	443	upwelling	-2 40	5 40	-0 58
07-Y-12	489	upwelling	-2 97	4 48	-2 09
07-Y-13	539	ombrotrophic	-3 65	-12 67	-4 98
07-Y-14	589	ombrotrophic	-3 51	-9 52	-3 55
07-Y-15	639	ombrotrophic	-3 43	-12 56	-3 89
07-Y-16	689	ombrotrophic	-3 33	-9 82	-3 61
07-Y-17	739	ombrotrophic	nc	nc	nc
Zulu					
07-Z-05	0	ombrotrophic	-2 78	-6 98	-3 09
07-Z-07	50	ombrotrophic	-2 99	-9 61	-3 87
07-Z-09	100	ombrotrophic	-3 34	nc	-4 98
07-Z-11	150	ombrotrophic	-3 23	-10 72	-4 60
07-Z-13	200	ombrotrophic	-3 53	-11 53	-5 49
07-Z-15	250	ombrotrophic	-3 65	-12 55	-5 25
07-Z-17	300	upwelling	-2 81	-13 71	-3 38
07-Z-19	350	upwelling	-2 53	-12 84	-2 39
07-Z-21	400	upwelling	-2 73	-12 46	-2 35
07-Z-23	450	upwelling	-2 56	-3 36	-2 68
07-Z-25	500	upwelling	-2 51	-0 92	-3 07
07-Z-27	550	upwelling	-2 71	nc	-3 35
07-Z-29	600	upwelling	-2 32	0 74	-2 56
07-Z-31	650	upwelling	-2 27	1 67	-2 01
07-Z-33	700	upwelling	-2 36	1 87	-1 94
07-Z-35	750	upwelling	-2 34	0 53	-2 60
Golf					
06G-01	0	ombrotrophic	-3 37	-11 99	-6 01
06G-02	53	ombrotrophic	-3 50	-11 51	-7 54
06G-03	102	ombrotrophic	-3 26	-10 89	-8 30
06G-04	155	ombrotrophic	-3 24	-12 94	6 79
06G-05	209	ombrotrophic	-3 38	-11 67	-7 33
06G-06	257	ombrotrophic	-3 53	-10 70	-7 41
06G-07	309	upwelling	-3 38	-11 25	-7 71
06G-08	336	upwelling	-3 58	-11 86	-6 57
06G-09	360	upwelling	-3 41	-12 44	-7 66
06G-10	411	upwelling	-3 44	-11 06	-7 50
06G-11	466	upwelling	-3 59	-11 22	-7 78
06G-12	518	upwelling	-3 27	-8 22	-4 96
06G-13	569	upwelling	-3 04	-6 72	-3 26
06G-14	594	upwelling	-3 13	-10 55	-3 18
06G-15	618	upwelling	-3 01	-10 46	-2 58
06G-16	675	upwelling	-2 97	-2 29	-2 93
06G-17	722	upwelling	-3 12	-9 48	-3 16

nc = not calculated

Chapter 3

THE INFLUENCE OF BURIED KIMBERLITE ON METHANE PRODUCTION IN OVERLYING SEDIMENT, ATTAWAPISKAT REGION, JAMES BAY LOWLANDS, ONTARIO

Jamil A. Sader[1*], Keiko H. Hattori[1], Kerstin Brauneder[1], Stewart M. Hamilton[2]

[1]University of Ottawa, Earth Sciences Department, Ottawa, Ontario, K1N 6N5, Canada
[2]Sedimentary Geoscience Division, Ontario Geological Survey, Sudbury, Ontario, P3E 2G9, Canada
**Corresponding author (e-mail: jamilsader@yahoo.com)*

Manuscript in preparation for submission to a refereed journal

3.1 ABSTRACT

Shallow groundwaters were collected over and near buried kimberlites in the Attawapiskat River region of the James Bay Lowlands, Ontario, Canada in order to study the impact kimberlites have on CO_2 – CH_4 systematics. Groundwaters collected from boreholes in kimberlites and limestone, and from groundwaters in overlying Tyrell Sea sediment (TSS) were analyzed for $\delta^{13}C_{DIC}$, $\delta^{2}H_{H2O}$, $\delta^{18}O_{H2O}$, dissolved inorganic carbon (DIC), and metal concentrations. Methane gas samples from borehole and TSS groundwaters were analyzed for concentration, $\delta^{13}C_{CH4}$, and $\delta^{2}H_{CH4}$. The CH_4 concentrations and $\Delta^{13}C_{DIC\text{-}CH4}$ (isotope separation) values indicate biological carbonate reduction in TSS groundwaters overlying kimberlites. Conversely, groundwaters from TSS over limestone and from boreholes in limestone, and kimberlites have methane concentrations and $\Delta^{13}C_{DIC\text{-}CH4}$ values consistent with methane oxidation. All but one methane sample in TSS groundwater over kimberlite indicates *in situ* formation. Lower $\delta^{2}H_{H2O}$ values (greater than the local meteoric water line) are typically those from TSS over kimberlites, and suggests the reduction of DIC and production of CH_4, as biological DIC reduction requires H^+ ions from H_2O to form CH_4. The ratio of methane to calculated Fe^{3+} (as amorphous Fe hydroxide), SO_4^{2-}, and $O_{2(aq)}$ is largest in the majority of TSS groundwaters over kimberlites (where $\Delta^{13}C_{DIC\text{-}CH4}$ values indicate CH_4 production). Low temperature serpentinization of olivine in kimberlite is not considered for CH_4 production, as redox conditions in kimberlite groundwaters do not support abiogenic methane production. Our data suggest that kimberlites indirectly influence the CO_2-CH_4 system by consuming oxidized ions in the TSS overlying kimberlites. These results imply that variable lithology underlying sediment cover can impact methane production.

3.2 INTRODUCTION

Methane formation pathways typically occur via reduction (fermentative) of dissolved organic carbon (DOC) or reduction of dissolved inorganic carbon (DIC). These styles of methane formation occur because there are few redox-sensitive ionic species other than carbonate species. Therefore, DOC or DIC reduction commonly proceeds with bacteria as the catalyst (Clymo, 1984; Jakobsen and Postma, 1999; Beer and Blodau, 2007). However, the presence of electron acceptors, such as SO_4^{2-}, Fe^{3+} or dissolved oxygen (DO) can result in the oxidation of methane or the inhibition of its formation (Whiticar and Faber, 1986; Segers, 1988; Miura *et al.*, 1992; Kumaraswamy *et al.*, 2001; Yu *et al.*, 2007).

Previous studies (Reeve *et al.*, 1996; Rejmankova and Post, 1996) have suggested that chemical weathering processes of soil or rock underlying wetlands can indirectly influence near surface methane flux due to the release of oxidized ions. Additionally, several studies have shown that mineralized zones in crystalline rock emit CH_4 and other hydrocarbons that can be detected at surface (Lovell *et al.*, 1983; McCarthy *et al.*, 1986; Cameron *et al.*, 2004a; Sader *et al.*, 2009).

Variable methane concentrations and isotopic compositions may be useful as indicators to pin-point kimberlite bodies that are buried under sequences of sediment. This study investigated the carbon isotope system in Tyrell Sea sediment (TSS), and groundwaters in kimberlite and limestone, over and near known kimberlites in the James Bay Lowlands of northern Ontario, Canada. The goals of this study are to: 1) identify variations in CO_2 – CH_4 systematics; 2) investigate controls on the CH_4 – CO_2 system in TSS; 3) establish the origin of methane in the Tyrell Sea sediment; and 4) suggest how buried kimberlites influence (either directly through gas migration, or indirectly through

changes in redox conditions) the carbon system in overlying sediment. Redox chemistry, CH_4 and CO_2 concentrations, and $\delta^{13}C$ $\delta^{18}O$, and $\delta^{2}H$ isotopes are used to evaluate CO_2-CH_4 cycling over buried kimberlite and limestone.

3.3 LOCATION AND GEOLOGY

Kimberlites investigated in this study are located in the James Bay Lowlands in central Canada, approximately 90 km west of the community of Attawapiskat, Ontario. The kimberlites in this study are also within 15 km of the DeBeers' Victor diamond mine (Fig. 3-1). The kimberlites intruded into Paleozoic sedimentary rocks, predominantly composed of limestone, and underlying basement Archean igneous and metamorphic rocks in the mid-Jurassic (~170 Ma) (Norris, 1993; Webb *et al.*, 2004) (Fig. 3-2). Host rock to the kimberlites at the bedrock surface is the Upper Attawapiskat Formation limestone. This unit occasionally outcrops in the form of bioherms (coral and skeletal remains) up to 2 m above the surrounding ground surface. All kimberlites in this study subcrop, with the exception of the Zulu kimberlite, which outcrops along its south margin. A thin sheet of till (<1 m) and TSS glaciomarine sediment (2 to 21 m in thickness) overlies the host Upper Attawapiskat Formation limestone and kimberlites (Fig. 3-2). Although the range in TSS thickness is highly variable, it is generally found to be approximately 13 m thick (DeBeers, pers. comm.).

The region was glaciated during the Quaternary, during which time bedrock surface was eroded and a thin till layer (<1 m) was deposited. The TSS is composed of fine-grained marine sand, silt and clay deposited between 10 and 5 ka following the end of glaciation when the shoreline of James Bay (known as Tyrell Sea during that period) extended inland approximately 300 km west and southwest of its present location. Isostatic rebound resulted

in ground surface elevation increases of 100 to 300 m since the retreat of the Laurentide ice sheet in the Attawapiskat region (Shilts, 1986). The present-day ground surface elevation is 80 to 90 m above sea level. Peat approximately 2.5 to > 4.0 m thick overlies the TSS and has been accumulating since the retreat of the Tyrell Sea approximately 5000 BP. The peat is predominantly composed of sphagnum and becomes progressively more humified with depth (i.e., the sphagnum is increasingly less recognizable below 0.5 m).

The kimberlites consist of abundant olivine macrocrysts, and phenocrysts of ilmenite, garnet, Cr-diopside, phlogopite, and spinel (Kong *et al.*, 1999; Sage, 2000a; Armstrong *et al.*, 2004). Kimberlite groundmass mainly consists of carbonate, spinel, and serpentine with lesser monticellite, mica, apatite, and perovskite (Kong et al., 1999). All known kimberlites in the Attawapiskat region are either hypabyssal or volcaniclastic (Kong *et al.*, 1999; van Straaten *et al.*, 2009). Kimberlites sampled in this study (Yankee, Zulu, Alpha-1, Golf, and Bravo-1) are altered hypabyssal facies (Sage, 2000a).

3.3.1 Site Conditions

The Yankee kimberlite is located between outcropping bioherms southwest and northeast of the kimberlite and the ground surface elevation is slightly lower over the kimberlite compared to immediately surrounding ground surfaces that overly limestone along the transect. The Zulu kimberlite is located east of a lobate raised bog and north of a small bioherm. The site of the Alpha-1 is composed of two bodies (Alpha-1 and Alpha-1 north). The indicator minerals from the two bodies are very similar (Sage, 2000a) and suggest they may have been emplaced simultaneously. The ground surface over Alpha-1 and Alpha-1 north has little topographic relief and is a raised bog. The area is bounded by lower elevation

fens on the west and east sides of the raised bog. The surface conditions at Bravo-1 kimberlite indicate a slight topographic low and there is standing water up to 30 cm deep at many areas over the kimberlite. In addition to sites of known kimberlites, samples were also collected from the Control site, a location with no known kimberlite in the vicinity (based on geophysical data). This site grades gently towards the Attawapiskat River, approximately 600 m to the north. Ground surface and surface drainage at the Golf kimberlite is similar to that of Zulu (from west to east). The east end of the Golf sampling transect and is within 100 m of a bioherm.

3.4 METHODS

3.4.1 Field Procedures

Field sampling and laboratory analytical methods for waters are summarized below from Sader *et al.* (2010). Monitoring wells were installed into the TSS 0.7 m below the peat/TSS boundary in summer 2007 using stainless steel drive points, iron casings, and low or high-density polyethylene tubing. Three monitoring wells were installed at the Yankee, Zulu, Alpha-1, and Bravo-1 sites; two over each kimberlite and one adjacent to each kimberlite (Fig. 3-3). One well was installed at the Control site (Fig. 3-3f). There are no known kimberlites in the region surrounding the Control site. Samples from Yankee, Zulu, Alpha-1, Bravo-1 and Control are denoted by the prefixes of Y, Z, A, B, and C, respectively, and samples collected in the Fall are denoted by the suffix *F*. Monitoring wells installed during Summer 2007 could not be sampled until Fall 2007, as water levels were slow to recover.

Groundwater samples were collected from existing exploration boreholes (cased through peat, TSS, and till) located approximately 10 m outside and up gradient of the

Yankee kimberlite margin (07-Y-07-7H); south of the center of the Zulu kimberlite (07-Z-07-12C); in the southeast part of Alpha-1 (07-A-BH-06); and near the center of Bravo-1 kimberlite (07-B1-07-08C); (Fig. 3-3). Borehole groundwaters were collected at a depth of 14 mbgs. Groundwater was collected from one natural spring (06-Spring) at the Control site.

The pH, oxidation-reduction potential (ORP), electrical conductivity (EC), dissolved oxygen (DO), and temperature was measured on-site for each water sample. A peristaltic pump was used to pump water into a vessel, which contained the pH, ORP, EC, DO and temperature probes. Oxidation reduction potential values have been corrected to the standard hydrogen electrode (SHE) for waters at 10 °C by adding 207 mV to the ORP values, and are reported as Eh. Waters were collected in Nalgene^{TM} high-density polyethylene bottles for cations and anions. Samples for dissolved inorganic carbon (DIC) analysis were collected in 40 mL brown tinted borosilicate bottles with a silicone - polytetrafluoroethylene (PTFE) septum cap. An additional PTFE and rubber septum (Chromatographic Specialties Inc.) was inserted underneath the septum cap to prevent DIC loss (silicone is gas-permeable). All water samples were filtered through 0.45 μm Sterivex-HV^{TM} filters (Millipore Corporation).

Methane gas samples were collected using gas diffusion samplers in boreholes and monitoring wells. The gas samplers were constructed of two 10 cm lengths of copper tubing with a 10 cm length of gas-permeable silicone tubing fastened in between. The two outside ends of the copper tubing (not fastened to the silicone) were crimped and soldered. The samplers were suspended approximately 15 cm above the drive point in monitoring wells and approximately 14 mbgs in boreholes in summer 2007. During the time between installation and collection, gas diffused into the samplers submerged in groundwater. Immediately after retrieval in the Fall of 2007, the open ends of the copper tubing fastened to

the silicone tubing were crimped or clamped, thereby sealing the diffused gas in the copper tubing. The gas samplers were collected from all monitoring wells and boreholes with the exception of the Bravo-1 borehole (07-B1-07-08C).

3.4.2 Analytical Procedures

Waters were analyzed for DIC concentration, and $\delta^{13}C_{DIC}$, $\delta^{2}H_{H20}$, and $\delta^{18}O_{H20}$ values at the University of Ottawa G.G. Hatch Stable Isotope Laboratory using a Finnigan-Mat Delta Plus mass spectrometer. The 2σ analytical precision is ± 0.002 ppm for DIC, ± 0.2‰ for $\delta^{13}C_{DIC}$ values, ± 2‰ for $\delta^{2}H_{H20}$, and ± 0.15‰ for $\delta^{18}O_{H20}$. Methane gas samples were analyzed at the G.G. Hatch Laboratory for $\delta^{13}C_{CH4}$ and $\delta^{2}H_{CH4}$ compositions and CH_4 concentrations using a gas chromatograph consisting of a Porabond Q column, connected to a XP Finnigan-MAT IR mass spectrometer. Calibrations were carried out using two international reference standards (NGS1-8559 & NGS2-8560) and one internal reference standard for both C and H isotope analysis. The precision is 7.7, 3.0, and 2.4% relative standard deviation (RSD), respectively for methane concentrations. The 2σ analytical precision for $\delta^{13}C_{CH4}$ and $\delta^{2}H_{CH4}$ is ± 0.2‰. All $\delta^{13}C$ values are presented in ‰ relative to VPDB and all $\delta^{2}H$ values are relative to VSMOW. Semi-quantitative hydrogen gas concentrations were determined from mass spectrometry data. Quantitative data was not determined, as H standards were not run prior to and during analysis of gas samples. Therefore, the hydrogen concentrations were determined based on the existence of well-defined hydrogen peaks along mass spectrometer profiles and are considered semi-quantitative.

Elemental analyses of groundwaters were conducted at the Ontario Geoscience Laboratories, Ministry of Northern Development and Mines, Sudbury, Canada. Water

samples for cations were acidified to 1% concentration prior to analysis using Baseline-grade HNO_3 from Seastar Chemicals. Waters were analyzed for Fe using an inductively coupled plasma mass spectrometer (ICP-MS), and for Na using a Spectro inductively coupled plasma emission spectrometer (ICP-ES). Sulfate and chloride were analyzed using a Dionex ion chromatograph (IC). Analysis of certified reference standard SLRS-4 from the National Research Council of Canada (ICP-MS), FP83MI1 and FP83TE1 (ICP-ES), and internal standards (IC) before, during, and after the run indicated a precision of less than 5% relative standard deviation (RSD) for each metal or species.

3.5 RESULTS

3.5.1 Isotopic compositions of TSS, kimberlite, and limestone groundwaters

The concentration of DIC in TSS groundwaters over kimberlite and limestone ranges from 2.7 to 12.8 mmol/L, whereas groundwaters from boreholes in kimberlites and limestone have lower DIC concentrations and range from 1.8 to 6.2 mmol/L. The $\delta^{13}C_{DIC}$ values in TSS groundwaters range from -9.8 to 4.6‰ and have a high degree of variability compared with $\delta^{13}C_{DIC}$ values in groundwaters from kimberlite and limestone, which only varied from -13.7 to -11.4‰ (Table 3-1). Monitoring wells and borehole groundwaters collected in 2006 have $\delta^{13}C_{DOC}$ values that are consistently -26 ±1‰ and were similar to values in peat groundwaters (-27 ±1‰) (Brauneder, 2007).

Methane concentrations in TSS and borehole groundwaters are variable and range from less than detection limit (0.01 mmol/L) to 0.63 mmol/l. These concentrations are below methane saturation at 10 °C for samples collected from monitoring wells and boreholes. Saturation is reached at 1.73 and 2.03 mmol/l for monitoring wells and borehole sample

collection depths, respectively. Methane concentrations from boreholes within Zulu and Alpha-1 kimberlites are lower compared to methane concentrations in the TSS over the respective kimberlites. The concentrations of H_2 range from non-detect (no indication of a profile peak) to 2.2 mmol/L and increase with in increasing CH_4 concentrations for approximately half of the total gas samples (Fig. 3-4). However, samples from boreholes within the Zulu and Alpha-1 kimberlites, and some samples in the TSS have no detectable H_2, yet have concentrations of CH_4 up to 0.63 mmol/L (Fig. 3-4).

The $\delta^{13}C_{CH4}$ values are low (-82.4 to -62.5‰) and the $\delta^{2}H_{CH4}$ values range from -289 to -253‰ (Table 3-1). $\delta^{13}C_{CH4}$ and $\delta^{2}H_{CH4}$ isotope values in the boreholes within Zulu and Alpha-1, and the borehole in limestone near Yankee do not differ significantly from those samples collected in the TSS. The isotope separation between $\delta^{13}C_{DIC}$ and $\delta^{13}C_{CH4}$ ($\Delta^{13}C_{DIC\text{-}CH4}$) versus CH_4 concentration indicates two trends (Fig. 3-5a). Small decreases in the $\Delta^{13}C_{DIC\text{-}CH4}$ values are accompanied by a significant increase in CH_4 concentrations, consistent with CO_2 reduction (Whiticar, 1999). By comparison, $\Delta^{13}C_{DIC\text{-}CH4}$ values that are highly variable (range = 55 to 74‰) have sharply decreasing CH_4 concentrations and follow a trend of CH_4 oxidation (Fig. 3-5a). One sample, 07-Z-07-12C-F (Zulu borehole sample), is the exception, as it has low $\Delta^{13}C_{DIC\text{-}CH4}$, but a CH_4 concentrations of 0.31 mmol/L.

Rayleigh fractionation curves were calculated for biological CH_4 production via CO_2 reduction (Equation 1) and methane oxidation (Equation 2).

$$\delta^{13}C_{CH4(f)} = \delta^{13}C_{DIC(i)} + \varepsilon^{13}C_{DIC\text{-}CH4} \cdot (1+\ln(1-f)) \quad (1)$$

$$\delta^{13}C_{CH4(f)} = \delta^{13}C_{CH4(i)} + \varepsilon^{13}C_{CH4} \cdot (1+\ln(1-f)) \quad (2)$$

The $\delta^{13}C_{CH4(f)}$ is the resulting $\delta^{13}C_{CH4}$ value after CO_2 reduction. $\delta^{13}C_{DIC(i)}$ is the average initial value in deep groundwaters collected from kimberlites and limestone. The $\varepsilon^{13}C_{DIC\text{-}CH4}$ variable represents the isotope fractionation between DIC and CH_4. A value of 71.8‰ was used, as it represents the $\Delta^{13}C_{DIC\text{-}CH4}$ isotope separation average for samples that plot along a CO_2 reduction trend in Figure 3-5a. It is also similar to the average value of 75‰ for biological CH_4 production via CO_2 reduction in waters (Clark and Fritz, 1997). "*f*" denotes the fraction of methane produced. For Equation 2, $\delta^{13}C_{CH4(i)}$ is the initial methane value before oxidation; the lowest $\delta^{13}C_{CH4}$ value measured, -82.4‰, was used. The isotope fractionation value of $\varepsilon^{13}C_{CH4}$ (4‰) for residual methane was previously empirically estimated based on CH_4 collected from marine, brackish, and freshwater environments (Whiticar, 1999). The samples that have an isotope separation of approximately 72‰ (Fig. 3-5a) also plot along a Rayleigh fractionation curve for biological CO_2 reduction (Fig. 3-5b). Conversely, samples that have an isotope separation < 72‰ plot along the methane oxidation Rayleigh fractionation curve.

A local meteoric water line (LMWL) of $\delta^{2}H_{H2O}$ and $\delta^{18}O_{H2O}$ values in kimberlite, limestone, and TSS groundwaters has a similar slope to that of the Bonner Lake meteoric water line (BLMWL) (Fig. 3-6). The similarity indicates that Attawapiskat groundwaters are likely meteoric. The BLMWL was generated from precipitation data collected by Birks *et al.* (2003) at Bonner Lake, Ontario (49.38° N; 82.12° W) and was the closest precipitation monitoring station to the Attawapiskat sample locations. The difference in slope between the two water lines (Fig. 3-6) is likely due to the fact Bonner Lake is 400 km south of the study area in a slightly different climatic zone. The magnified inset in Figure 3-6 indicates that TSS waters from all but one site over kimberlites, 07-MW-B-01F (Bravo-1), plot above the

BLMWL and display less negative δ^2H_{H2O} values compared with TSS samples collected over limestone. It should be noted that the Bravo-1 sample has CH_4 concentrations that are below the detection limit. Sample 07-MW-A-12F, which has the highest concentration of methane in this study (0.63 mmol/L), also has δ^2H_{H2O} values that deviate the most from the BLMWL. Borehole samples from within Alpha-1 and in limestone near Yankee have isotopic values that plot on or slightly below the BLMWL. However, the borehole sample from the Zulu kimberlite plots above the BLMWL.

The plot of δ^2H_{CH4} and δ^2H_{H2O} (Fig. 3-7) indicates that origin of CH_4 measured in this study, which is either forming or being oxidized, was almost entirely derived from carbonate reduction. Samples from the Zulu kimberlite borehole, and TSS samples 07-MW-A-12A and 07-MW-Y-11.5F (over kimberlites) appear to have a contribution from methyl fermentation and plot on or near an 80% carbonate reduction, 20% methyl fermentation slope (Whiticar, 1999). During bacterial CO_2 reduction, bacteria will utilize the H^+ in water during methane formation. Fractionation between δ^2H_{H2O} and δ^2H_{CH4} during bacterial DIC reduction is consistently -160 ±10‰ (Schoell, 1980; Whiticar *et al.*, 1986; Whiticar, 1999) and is demonstrated through the following linear relationship (Equation 3):

$$\delta^2H_{CH4} = \delta^2H_{H2O} - 160‰ \qquad (3)$$

Conversely, methane from methyl fermentation only uses one H^+ from H_2O and three H^+ ions derived from the organic acid, and is therefore dominantly reliant on the δ^2H values of the organic acids rather than water (Whiticar 1986). Had the majority of H^+ been derived through methyl fermentation for these samples, they would likely comprise more negative

δ^2H_{CH4} values of approximately -380 to -390‰. The samples would then plot nearer to the %C:%M = 0:100 line (Fig. 3-7).

3.5.2 Geochemical geochemical compositions of TSS, kimberlite, and limestone groundwaters

The pH values in TSS, kimberlite, and limestone groundwaters are circumneutral to slightly alkaline (7.1 to 9.1 with an average of 7.5). The Eh values in TSS groundwaters (average 217 mV) are typically more elevated compared with Eh values in boreholes from kimberlites (average = 90 mV) (Table 3-1). Sulfate concentrations in borehole and TSS groundwaters are low. The mean, maximum, and minimum SO_4^{2-} concentrations are 14.7 μmol/L, 135 μmol/L, and at detection limit (0.4 μmol/L), respectively. In contrast, Fe concentrations in TSS and borehole groundwaters were typically 4 to 5 times greater than SO_4^{2-} concentrations (Table 3-1). The speciation of Fe^{2+} and Fe^{3+} was calculated using Geochemists WorkBench (Bethke, 2002) and varied from dominantly ferric to dominantly ferrous Fe in all groundwaters.

3.6 DISCUSSION

3.6.1 CH_4 isotope systematics and biological DIC reduction

3.6.1.1 $\delta^{13}C_{CH4}$ and $\delta^{13}C_{DIC}$ systematics

The consistent $\Delta^{13}C_{DIC\text{-}CH4}$ values of approximately 72‰ for almost all TSS groundwaters over kimberlites, coupled with increases in CH_4 concentrations, suggest CH_4 production via biological reduction of DIC (Fig. 3-5a). The high and consistent $\Delta^{13}C_{DIC\text{-}CH4}$ values typically indicate bacterial DIC reduction because the $\delta^{13}C_{DIC}$ values become higher at approximately the same rate that $\delta^{13}C_{CH4}$ values become equally higher in a closed system (Whiticar, 1999).

Bacterial CO_2 reduction is further suggested because the same groundwaters that have $\Delta^{13}C_{DIC\text{-}CH4}$ of approximately 72‰ plot near a trend of Rayleigh fractionation for CO_2 reduction (Fig. 3-5b).

For most TSS groundwater samples outside kimberlite (over limestone), and deeper groundwaters from kimberlite and limestone, a sharp decrease in $\Delta^{13}C_{DIC\text{-}CH4}$ values is accompanied by a decrease in CH_4 concentrations (Fig. 3-5a). This trend suggests CH_4 is most likely being consumed by methanotrophic bacteria, and is characteristic of bacterial methane oxidation in both freshwater and marine environments (Whiticar, 1999). The decrease in $\Delta^{13}C_{DIC\text{-}CH4}$ values is due to the preferential use of ^{12}C by methanotrophic bacteria, thereby resulting in higher $\delta^{13}C_{CH4}$ values as CH_4 concentrations decrease along the Rayleigh fractionation trend (Fig. 3-5b).

The addition of DIC with low values (closer to that of $\delta^{13}C_{CH4}$) could also result in variable (and lower) $\Delta^{13}C_{DIC\text{-}CH4}$ values, and could indicate methane oxidation, as shown in Figure 3-5a. However, samples that plot along the trend of CH_4 oxidation in the plot of $\Delta^{13}C_{DIC\text{-}CH4}$ versus CH_4 concentration (Fig. 3-5a) are the same samples that plot along the Rayleigh fractionation trend of CH_4 oxidation in Figure 3-5b. As calculation of the Rayleigh fractionation trend for methane oxidation does not involve $\delta^{13}C_{DIC}$ values, low $\Delta^{13}C_{DIC\text{-}CH4}$ associated with inputs of isotopically light DIC is not likely.

Sample 07-MW-Z-15, collected over the Zulu kimberlite, is the only monitoring well groundwater sample collected over kimberlite where methane oxidation is indicated. This sample may have been contaminated by peat pore water close to the peat/TSS boundary, as the monitoring well drive point could not be fully driven into the marine sediment below the peat. Low Na and Cl concentrations in the water compared to groundwater samples from

other monitoring wells at Zulu are consistent with a contribution from ombrotrophic peat groundwater (Sader *et al.*, 2010).

The only sample that does not fit a trend of CH_4 oxidation or production in Figure 3-5a & b is 07-Z-07-12C-F (groundwater from Zulu kimberlite borehole). Rather, this sample has a low $\Delta^{13}C_{DIC\text{-}CH4}$ value of 60.7‰, but the methane concentration is high (0.31 mmol/L) and the sample plots near the intersection of the Rayleigh fractionation trends for CO_2 reduction and methane oxidation (Fig. 3-4a & b). There are two possible explanations as to why the data for sample 07-Z-07-12C-F are ambiguous compared with other samples. It is possible that the sample represents mixing between methane from two different sources. Figure 3-7 indicates that as much as 20% of this methane sample may have been produced via methyl fermentation. The addition of methane from low-temperature serpentinization of olivine in kimberlite could also potentially result in lower $\Delta^{13}C_{DIC\text{-}CH4}$ and $\delta^{13}C_{CH4}$ values. Methane is commonly favoured to form through the process of low temperature serpentinization of olivine in ultramafic rocks (Barnes *et al.*, 1972; Abrajano *et al.*, 1988; Fritz *et al.*, 1992; Sader *et al.*, 2007a) (Equation 4). However, a serpentinization pathway is

$$15\ (Mg,Fe)_2SiO_4\ (FO_{90}) + 20\ H_2O + 0.25\ CO_2 \rightarrow$$
$$Fe_3O_4 + 7.5\ Mg_3Si_2O_5(OH)_4 + 4.5Mg(OH)_2 + 0.25\ CH_4 \qquad (4)$$

not suggested for this study, and therefore the production of abiogenic CH_4 is not likely. Abiogenic CH_4 typically forms under redox conditions that are significantly lower (Eh $\leq$ -200 mV at pH values of 6 to 7) than occurs in the kimberlites in this study. The Eh values observed in Attawapiskat kimberlite groundwaters (this study) range from 23 to 272 mV.

Sader *et al.* (2007a) suggested that kimberlite groundwaters that had bicarbonate alkalinity and pH only 1 to 2 units greater than 7 and oxidizing Eh values may be a result of short groundwater residence time within kimberlites. Low residence time could result in less water - kimberlite (olivine) interactions.

The $\delta^{13}C_{CH4}$ values in samples from kimberlite do not support an abiogenic source, as the values are low (-73 and -68.7‰ at 07-Z-07-12C-F and 07-A-BH-06, respectively). The $\delta^{13}C_{CH4}$ values typically associated with serpentinization reactions and abiogenic methane formation range between -10 and -20‰ (Abrajano et al., 1988; Fritz et al., 1992; Proskurowski et al., 2008).

3.6.1.2 $\delta^{18}O_{H2O}$ and $\delta^{2}H_{H2O}$ evidence for CH_4 production

The plot of $\delta^{18}O_{H2O}$ and $\delta^{2}H_{H2O}$ (Fig. 3-6) provides further evidence for bacterial DIC reduction processes in TSS samples collected over kimberlites. All but one TSS sample collected over kimberlites, and the borehole within the Zulu kimberlite (07-Z-7-12C) has $\delta^{2}H_{H2O}$ values that plot above the BLMWL (less negative) (Fig. 3-6). Conversely, samples from TSS over limestone or from the Yankee borehole within limestone plot closer to or below the BLMWL. The less negative $\delta^{2}H_{H2O}$ associated with TSS samples over kimberlites suggests Rayleigh fractionation of H isotopes as methane is produced. During the biological reduction of DIC, the methane that is produced derives all its hydrogen atoms from water (Whiticar, 1999). Methanogenic bacteria will preferentially use lighter $^{1}H_{H2O}$, thereby fractionating to less negative $\delta^{2}H_{H2O}$ values. The effect of this process has been shown in studies where CH_4 is being produced through the biological reduction of DIC (Clark and Fritz, 1997; Siegel *et al.*, 2001).

Isotopic mass balance calculations were conducted to estimate the CH_4 that would be produced based the deviation of δ^2H_{H2O} towards less negative values (samples that plot above the BLMWL) in Figure 3-6. The fractionation equation used is:

$$\delta_f{}^2H_{H2O} = \delta_o{}^2H_{H2O} + 10^3 \cdot (\alpha^2H_{H2O\text{-}CH4} - 1)\ln f$$

Where $\delta_f{}^2H_{H2O}$ is the measured isotopic value and $\delta_o{}^2H_{H2O}$ is the value if it plotted along the BLMWL (no fractionation). The variable $\alpha^2H_{H2O\text{-}CH4}$ is 2.26, and was empirically determined by Bottinga (1969), and "*f*" is the fraction of CH_4 produced per litre H_2O. The calculated CH_4 concentrations based on the fractionation of δ^2H_{H2O} to more positive values from the BLMWL in Figure 3-6 is on the order of mol/L of CH_4 and is roughly 3 orders of magnitude higher than the measured CH_4 concentrations (Fig. 3-8). However, for samples collected over kimberlites and from the Zulu kimberlite, there is a linear correlation (r=0.80) between the measured and calculated methane concentrations (increasing measured CH_4 with increasing calculated CH_4). This correlation suggests that the production of methane did result in a positive shift in δ^2H_{H2O} values. However, the 3 orders of magnitude difference between calculated and measured methane concentrations may be related to methane loss over time due to diffusion or ebullation of gas from formation waters. Siegel *et al.* (2001) indicated that calculated methane production (based on δ^2H_{H2O} values, which plotted above the LMWL for sites from a bog in Minnesota) was approximately an order of magnitude greater than measured methane. In that study it was suggested that loss occurred due to methane migration or their gas samplers did not collect a portion of gas dissolved in groundwater. Although methane was observed in groundwaters from TSS over limestone

and from the Yankee borehole in limestone, they do not demonstrate a correlation with the calculated values (Fig. 3-8). This lack of correlation may indicate that water carrying dissolved methane migrated to into TSS and underwent oxidation. It is possible the source overlying peat groundwaters containing dissolved methane.

3.6.2 Geochemical influences on in situ methane production and oxidation

Variations in concentrations of oxidized ions such as SO_4^{2-}, Fe^{3+}, and $O_{2(aq)}$ relative to CH_4 are likely controlling *in situ* formation or oxidation of CH_4. Ratios of CH_4/Fe^{3+}, CH_4/SO_4^{2-}, and $CH_4/O_{2(aq)}$ typically remain low (< 10, 5, and 1, respectively) where the $\delta^{13}C_{DIC\text{-}CH4}$ values are < 72‰ (Fig. 3-9). As these low ratios are typically spatially associated with TSS samples collected over limestone.

Where $\Delta^{13}C_{DIC\text{-}CH4}$ values are approximately 72‰ (mostly samples from TSS over kimberlites), the molar ratios of CH_4/Fe^{3+}, CH_4/SO_4^{2-}, and $CH_4/O_{2(aq)}$ increase up to 400 (Fig. 3-9). This pattern suggests the consistent and high $\Delta^{13}C_{DIC\text{-}CH4}$ values (indicative of CH_4 production) are due to decreases in concentrations of oxidized ions, thereby making conditions more favourable for the reduction of DIC. The migration of reduced ions and kimberlite pathfinder metals upwards from kimberlites to TSS via upward groundwater movement has been suggested (Sader *et al.*, 2010). Most groundwaters over limestone and in boreholes have low ratios of CH_4/Fe^{3+}, CH_4/SO_4^{2-}, and $CH_4/O_{2(aq)}$ (Fig. 3-9). These low ratios suggest that conditions are favourable for CH_4 oxidation. Additionally, the samples with low CH_4/Fe^{3+}, CH_4/SO_4^{2-}, and $CH_4/O_{2(aq)}$ ratios are the same ones that plot along a trend of biological methane oxidation (sharp decreases in methane concentrations with decreases

in the $\Delta^{13}C_{DIC\text{-}CH4}$ values; Fig. 3-5a). These relationships suggest methane oxidation may be due to anaerobic or aerobic methanotrophs.

The reduction of DIC results in lower energy yields for bacteria compared to bacterial reduction of SO_4^{2-}, Fe^{3+}, or $O_{2(aq)}$. Therefore, where Fe^{3+}, SO_4^{2-}, and $O_{2(aq)}$ concentrations are elevated relative to CH_4, the oxidized ions likely inhibit or suppress methanogenic bacteria in favour of methanotrophs due to competitive effects (Whiticar and Faber, 1986; Segers, 1988; Achtnich *et al.*, 1995). However, in the absence of oxidized ions such as SO_4^{2-}, Fe^{3+}, and $O_{2(aq)}$ methanogens are commonly more predominant (Segers, 1988). The occurrence of CH_4 in low concentrations (< 0.2 mmol/L), which exist in the presence of elevated oxidized ions and represent samples along the methane oxidation trend (Fig. 3-5a), may represent residual methane that is not oxidized by bacteria. Methane concentrations < 0.15 mmol/L have been documented to commonly coexist with Fe^{3+} and SO_4^{2-} reducing bacteria (Martens and Berner, 1977; Jakobsen and Postma, 1999). Whiticar and Faber (1986) suggest this coexistence is attributed to CH_4 concentrations that are too low for methanotrophic bacteria to utilize.

3.6.3 Sources of H_2 for methane production

In order to reduce DIC and produce CH_4, methanogenic bacteria require H_2 to function as an electron donor. Appreciable abiogenic H_2 production by low-temperature serpentinization of olivine is unlikely, given that the redox conditions do not favour the hydrolysis of H_2O. Additionally, abiogenic H_2 produced by low temperature serpentinization, as noted in Kirkland Lake kimberlites (Sader *et al.*, 2007b), typically has low δ^2H_{H2} values ranging from -599 to -800‰ (Abrajano *et al.*, 1988; Fritz *et al.*, 1992;

Sader *et al.*, 2007b). If methanogenic bacteria had utilized H_2 from this source much lower δ^2H_{CH4} values would be expected to be present. Instead, the decomposition of organic material and the production of H_2 is the most likely source and may be utilized by bacteria to reduce DIC. Environments with high concentrations of organics are commonly major sources for H_2 (Clark and Fritz, 1997). Although CH_4 and H_2 only correlate positively for approximately half the gas samples (Fig. 3-4), it is reasonable to suspect that H_2 is available and is being utilized to reduce DIC. Measureable H_2 concentrations are not always indicative of a dominant electron accepting process (in this case DIC oxidation) (Jakobsen *et al.*, 1998; Jakobsen and Postma, 1999; Hansen *et al.*, 2001). In each of these studies, the calculated energy yield was too low for the biological production of methane (low H_2 concentrations), yet the studies show strong evidence for *in situ* CH_4 formation.

3.6.4 Origin of methane outside kimberlites

The source of CH_4 in TSS outside kimberlites and in limestone in this study is difficult to delineate. It is unlikely that CH_4 is migrating upwards from limestone, given that upward migration of CH_4 at sites over kimberlite is not supported by the redox conditions in kimberlite waters. The most likely source of CH_4 is the peat overlying the TSS, as drainage of peat groundwater could transport methane that is dissolved in peat groundwaters to the TSS. The reduction of DIC is generally considered the dominant pathway for the production of CH_4 in deeper peat zones (the catetolem) (Lansdown *et al.*, 1992; Hornibrook *et al.*, 2000; Beer and Blodau, 2007). This pathway is consistent with the methane samples in this study, as between 80 and 100% of the in CH_4 (regardless of whether the samples were collected

over kimberlite or limestone) have been derived from the groundwaters in which DIC reduction is taking place (Fig. 3-7).

3.7 SUMMARY AND CONCLUSION

In summary, buried kimberlites likely influence the redox environment in TSS overlying kimberlites, which results in changes in the CO_2-CH_4 system in the TSS groundwater. The schematic diagram in Figure 3-10 shows our interpretation of the CO_2-CH_4 system for groundwater in the TSS overlying kimberlite and limestone.

This study provides evidence that buried kimberlites from James Bay lowlands can alter the CO_2-CH_4 system in sediment overlying kimberlites. $\delta^{13}C_{DIC\text{-}CH4}$ values of approximately 72‰ coupled with increases in methane concentrations indicated CO_2 reduction for the majority of TSS groundwater samples over kimberlites. The same samples with $\delta^{13}C_{DIC\text{-}CH4}$ values of 72‰ are also those that plot along a Rayleigh fractionation curve for CO_2 reduction. Data suggest that methane in all but one sample was due to *in situ* methane formation. Common methane formation at these locations likely results from reduced ions in the underlying kimberlite groundwaters. Sites with low $\delta^{13}C_{DIC\text{-}CH4}$ values commonly had low CH_4/Fe^{3+}, CH_4/SO_4^{2-}, and $CH_4/O_{2(aq)}$ ratios.

Hydrocarbons have been used successfully to delineate buried kimberlites in the Ville-Marie region of western Quebec (Sader *et al.*, 2009). McCarthy et al. (1986) indicated CH_4 anomalies near surface were associated with a buried sulfide deposit. Additionally, a number of commercial laboratory packages exist to delineate blind mineralization using reduced gas. However, the geochemical processes that are producing the gas anomalies are not fully understood. The results of this study have implications for geochemical exploration and the origin of reduced gas anomalies over mineralization. The use of isotopes and CH_4

gas concentrations, coupled with isotopic values of DIC in groundwaters over Attawapiskat kimberlites provides further insight into processes that are responsible for these gas anomalies. Our work suggests that methane anomalies over kimberlites are related to *in situ* formation within the TSS over the kimberlites, and not directly due to water – kimberlite reactions.

Further research into mechanisms controlling the CO_2-CH_4 system over various rock types is required. The identification of redox and methane gradients by collecting groundwaters and gas samples systematically along vertical profiles within the TSS would provide additional information on the upward movement of redox sensitive ions and methane fluxes over kimberlites versus outside them. Additionally, the collection of methane in peat over and outside kimberlites would provide more information on the methane formation or oxidation in peat groundwaters.

3.8 ACKNOWLEDGEMENTS

We thank DeBeers Canada for providing financial and logistical support for the project. Julie Kong, Ed Francisco, and Brad Wood were particularly helpful. Financial support was also provided by a NSERC Discovery grant and a NSERC Collaborative Research grant to Keiko Hattori. Jamil Sader received financial support from an Ontario Graduate Scholarship and a student research grant from the Society of Economic Geologists. A scholarship awarded to Jamil from the G.G. Hatch Laboratory (University of Ottawa) covered partial isotope analytical costs. Fieldwork was assisted by Katherine Mellor. We thank M. Beth McClenaghan (Geological Survey of Canada) and Matthew Leybourne (GNS New Zealand) for reviews of the manuscript.

3.9 FIGURES

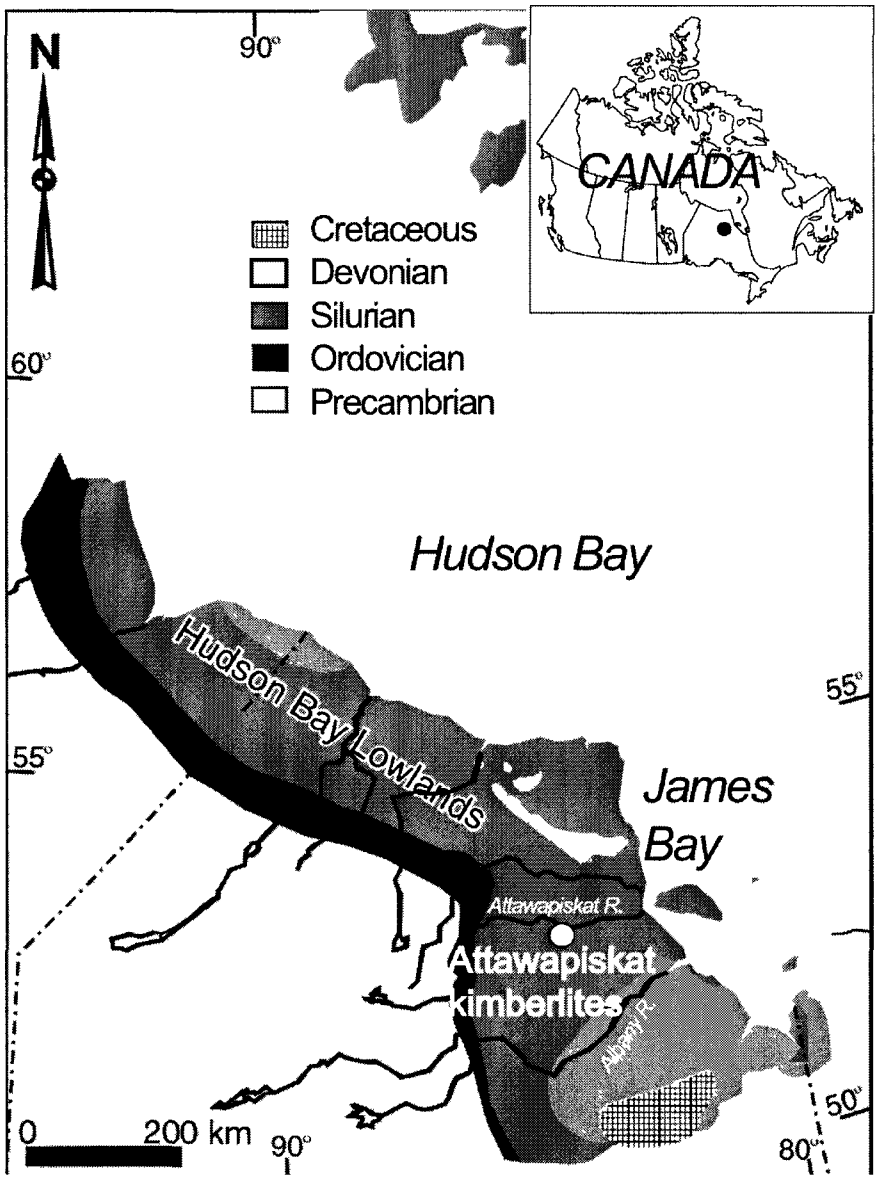

Figure 3-1. Regional bedrock geology of the James Bay Lowlands and location of the Attawapiskat kimberlite field in north central Canada. Figure modified from Bellefleur *et al.* (2005).

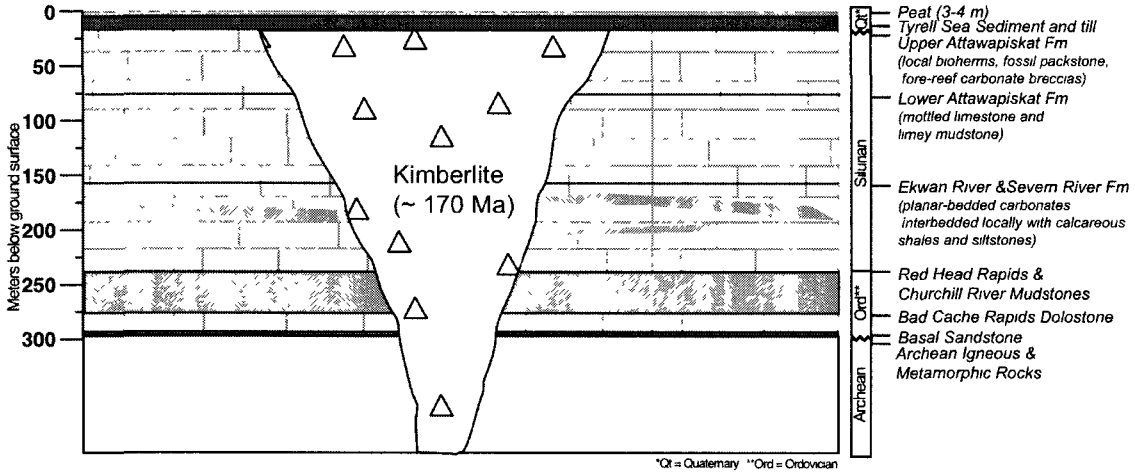

Figure 3-2. Schematic vertical section of rocks and sediment of which Attawapiskat kimberlites are emplaced into. Kimberlite and host rocks are overlain by a thin till, Tyrell Sea sediment (12 to 5 Ka), and peat (5 Ka to present). Diagram from (Sader *et al.*, 2010); Geology from Norris (1993).

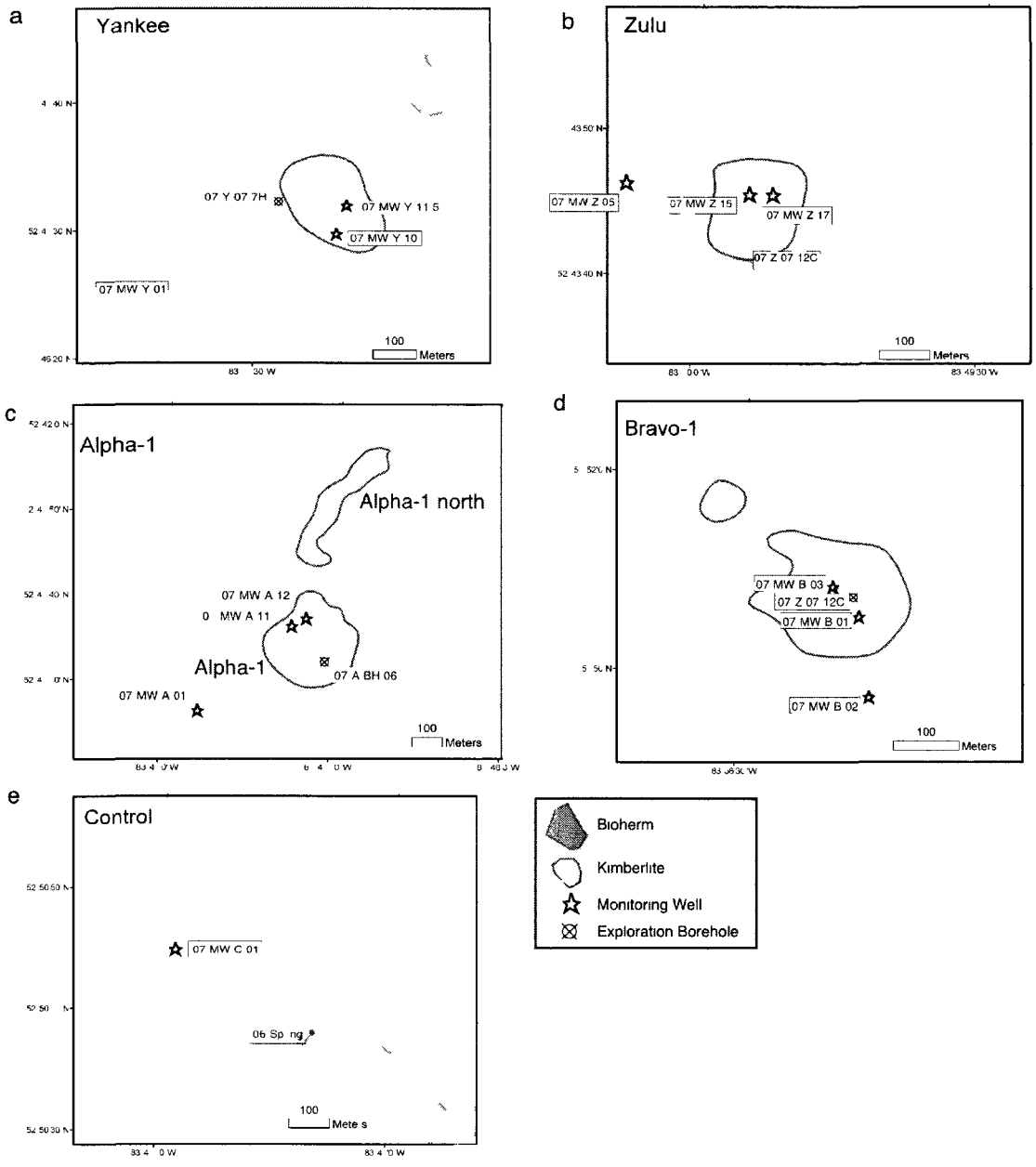

Figure 3-3. Location of kimberlites a) Yankee, b) Zulu, c) Golf, d) Alpha-1, e) Bravo-1, and f) Control Site, boreholes, Tyrell Sea sediment, and peat groundwater sample sites Areal extent of each kimberlite was determined using geophysical data and exploration drilling by DeBeers Canada

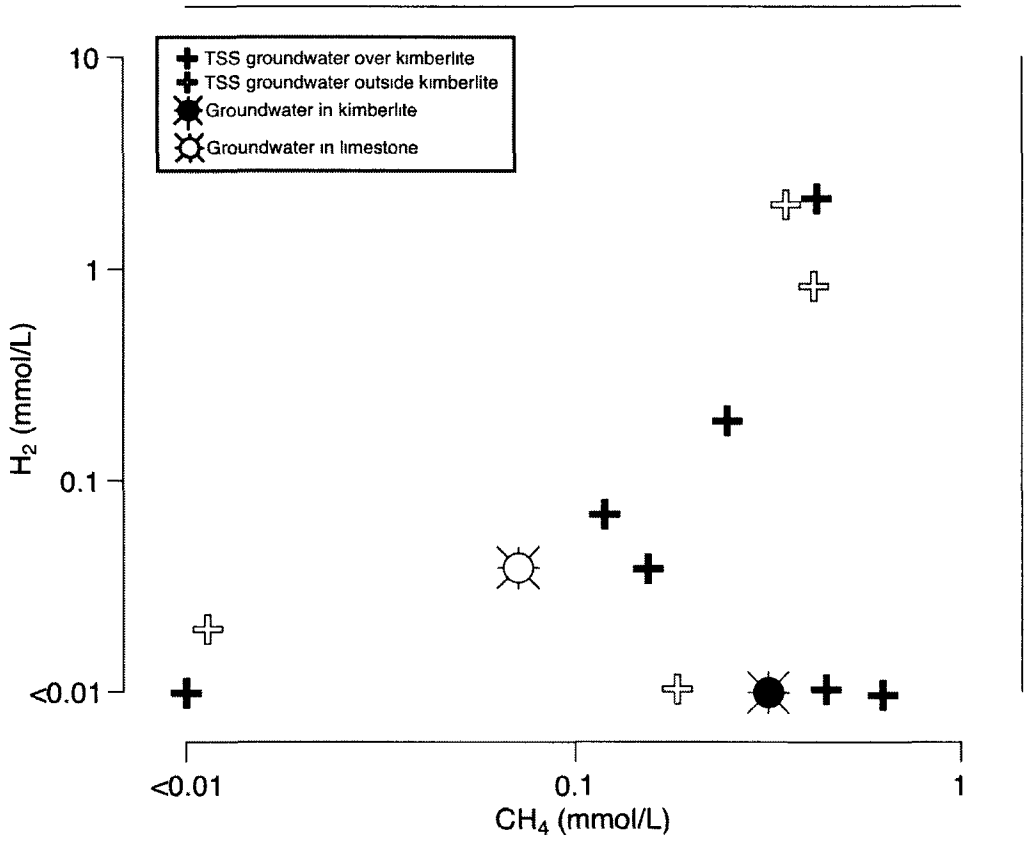

Figure 3-4. A plot of CH_4 versus H_2 for TSS and monitoring well gas samples. The diagram indicates that for approximately half the samples, H_2 increases with increasing CH_4 concentrations. However, there are a number of samples that demonstrate high CH_4 concentrations, but H_2 is below detection.

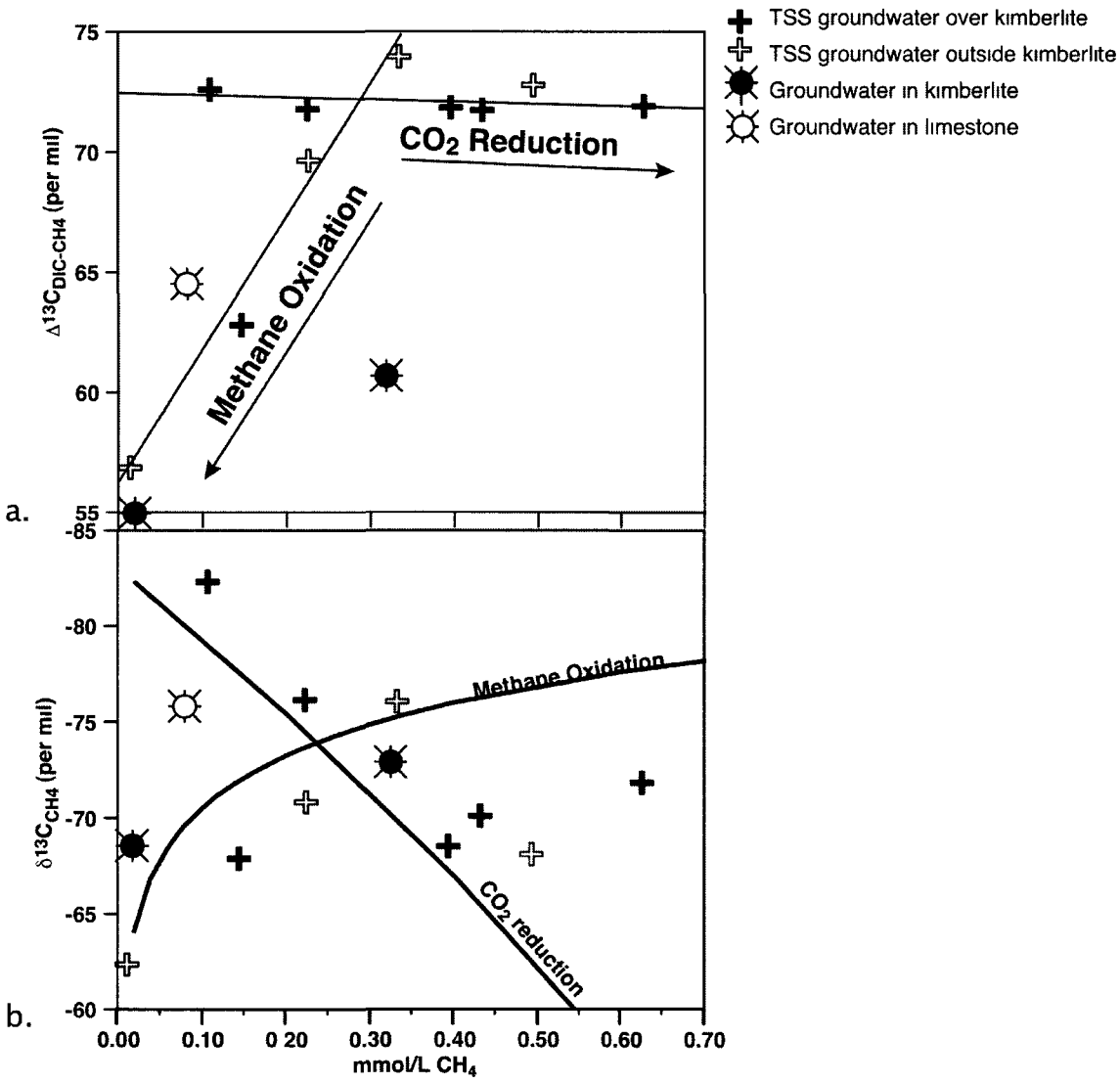

Figure 3-5. a) A plot of $\delta^{13}C_{DIC\ CH4}$ values versus methane content for monitoring wells and boreholes The small decrease in isotope separation with increase in methane concentrations suggests methane production Conversely, the sharp decline in isotope separation with decreases in methane concentrations suggests methane oxidation **b)** Plot of methane content versus $\delta^{13}C_{CH4}$ Thick black lines indicate trends for Rayleigh fractionation for $\delta^{13}C_{CH4}$ during CO_2 reduction (Equation 1) and methane oxidation (Equation 2) Samples that plot along the Rayleigh fractionation curve for CO_2 reduction also display isotope separation of approximately 72‰ Samples less than 72‰ plot along the methane oxidation Rayleigh fractionation curve Methane saturation is 2 03 mmol/l CH_4 at sampling pressure and temperature conditions

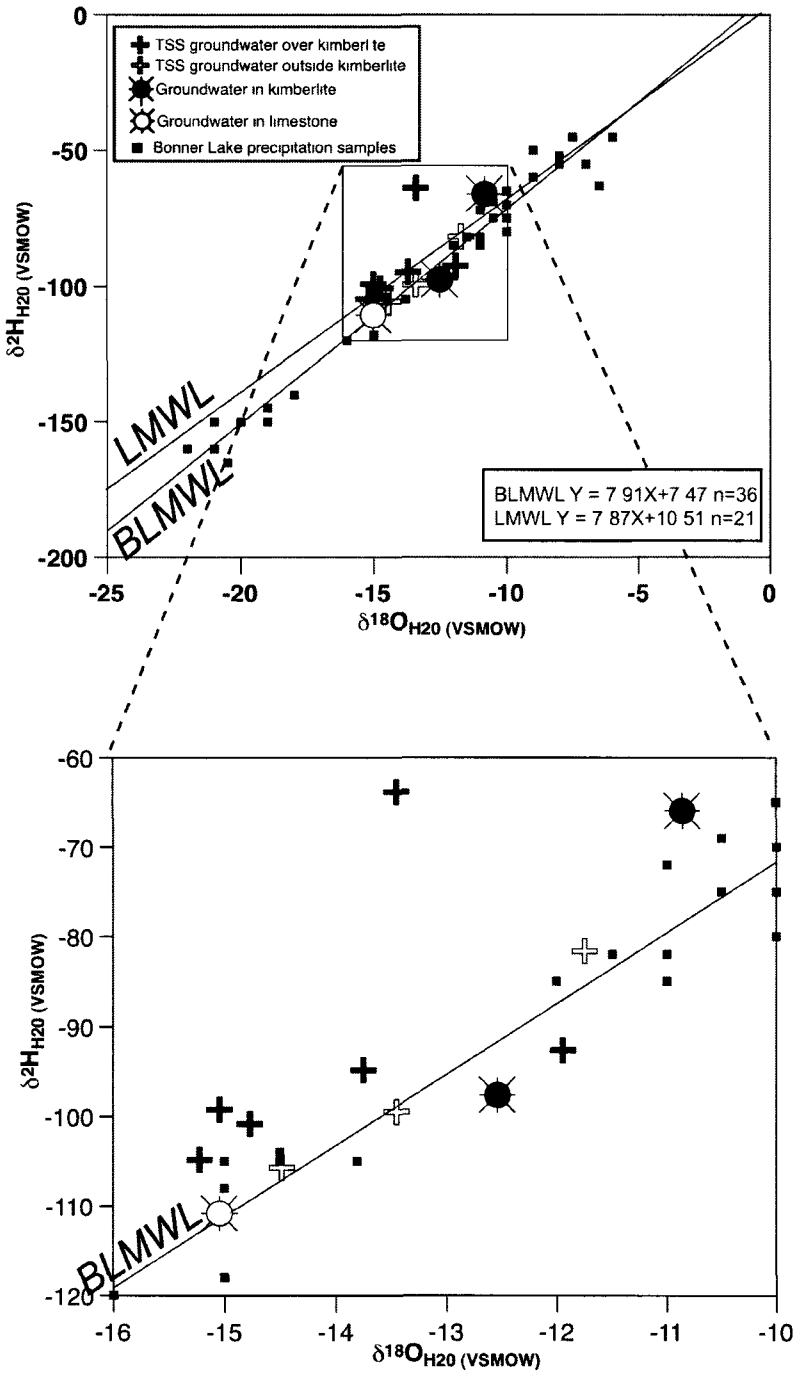

Figure 3-6. The δ^2H_{H2O} and $\delta^{18}O_{H2O}$ values from kimberlite, limestone, and TSS groundwaters plot on a local water line (LMWL) The slope of the LMWL is similar to the Bonner Lake meteoric water line (BLMWL) based on precipitation data from Bonner Lake, Ontario (49 38° N, 82 12° W) The expanded plot indicates that the majority of samples collected from the TSS over kimberlite plot above the LMWL and have heavier δ^2H_{H2O} values The similarity of the two slopes indicates groundwaters in this study are meteoric Data for construction of the BLMWL obtained from Birks et al (2003)

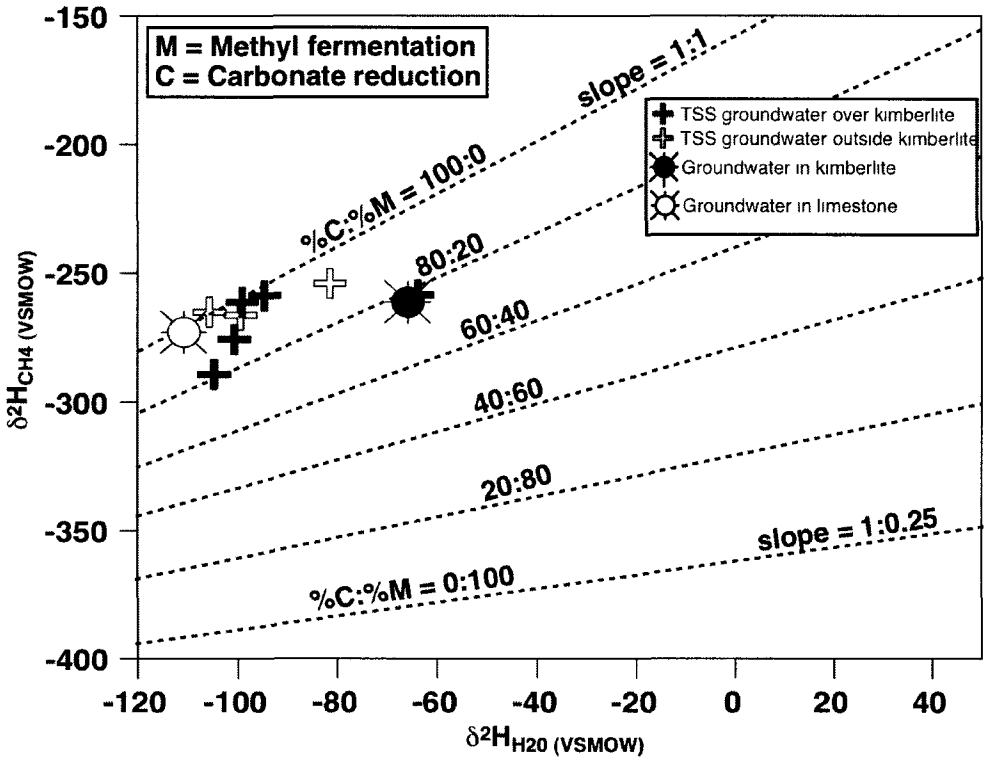

Figure 3-7. The δ^2H_{CH4} and δ^2H_{H2O} values in groundwaters from TSS, limestone, and kimberlite plot near the 1 1 slope, indicating a biological CO_2 reduction origin of the methane The ratios of carbonate reduction versus methyl fermentation and slopes are from Whiticar (1999)

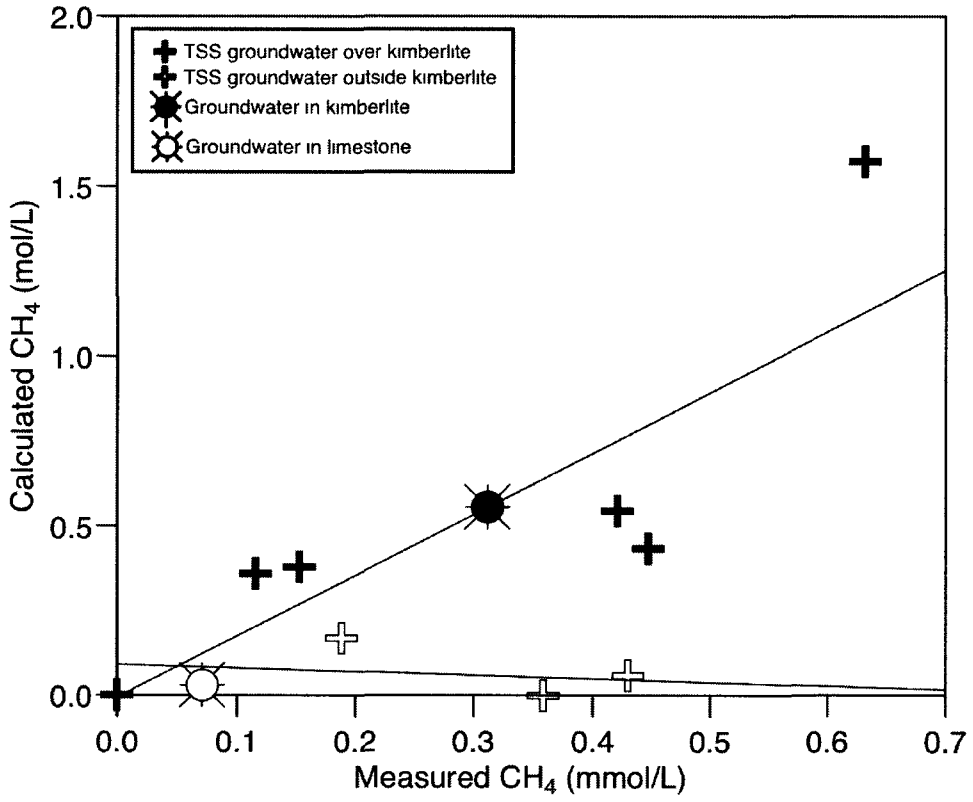

Figure 3-8. The calculated versus measured CH_4 for groundwater samples from TSS and boreholes Calculations for CH_4 are based on the how much heavier δ^2H_{H2O} values are compared with the BLMWL (see Fig. 3-6) Note that samples that plot on or below the BLMWL are considered to have a value of 0 calculated CH_4. Additionally, note that the calculated methane is approximately 3 orders of magnitude greater than measured methane

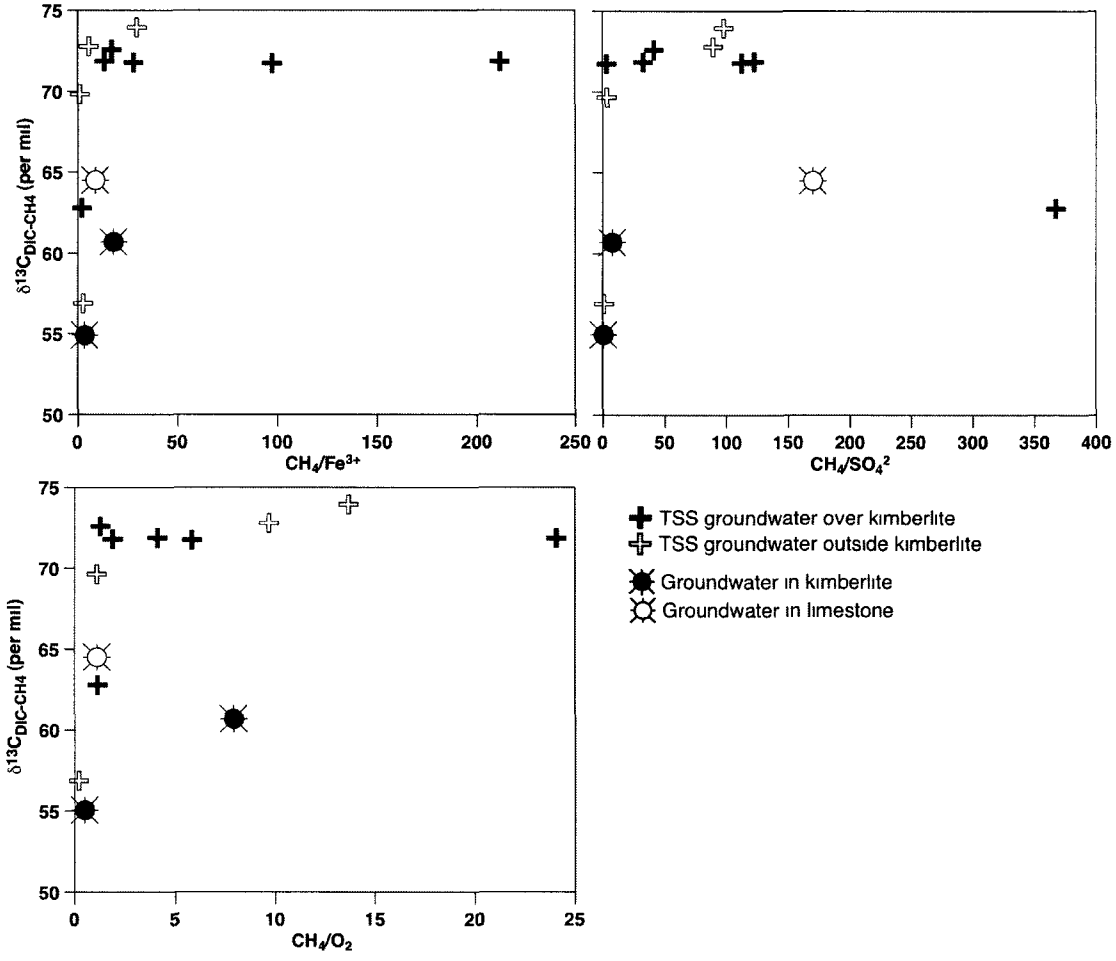

Figure 3-9 Plots of low CH_4/Fe^{3+} and CH_4/SO_4^{2} ratios coupled with low $\delta^{13}C_{DIC\ CH4}$ suggest that methane oxidation is occurring due to the high concentrations of oxidized ions Conversely, samples with high CH_4/Fe^{3+} and CH_4/SO_4^{2} and high $\delta^{13}C_{DIC\ CH4}$ are dominantly those collected in TSS over kimberlites and suggests kimberlites may be consuming oxidized ions This may provide bacteria with more suitable conditions for CO_2 reduction All ratios are molar ratios

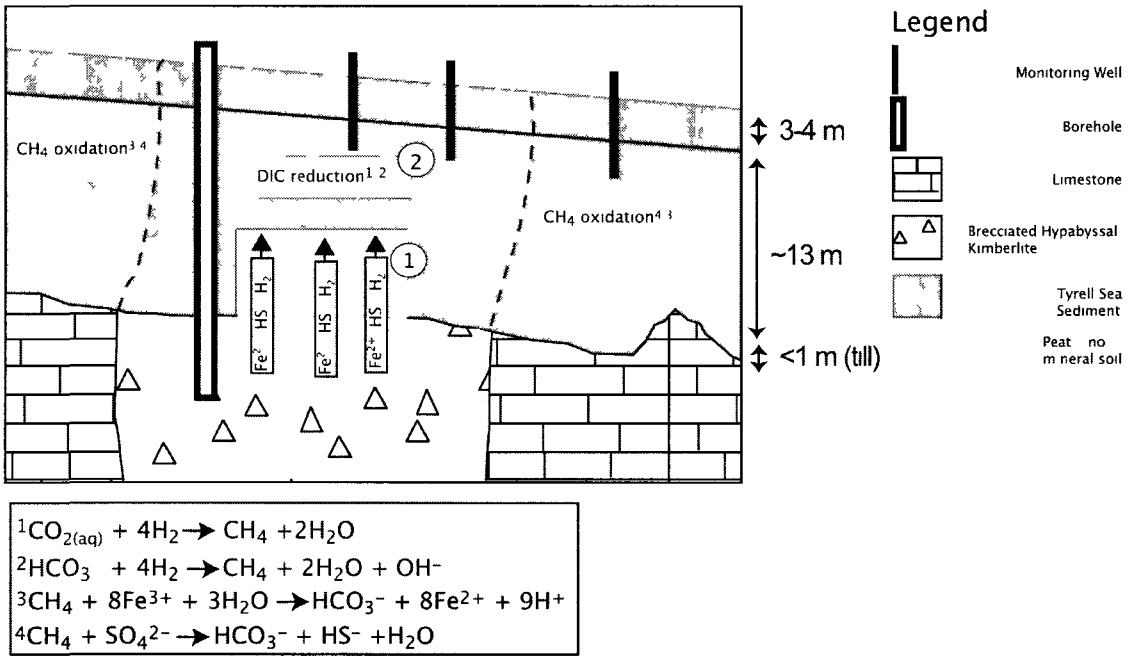

Figure 3-10. Schematic cross-section of a kimberlite in the Attawapiskat field and their influence on CO_2 – CH_4 systematics Numbers in white circles correspond to the following **1)** More reducing groundwaters within kimberlites migrate upwards into the TSS and consume oxidized ions such as Fe^{3+}, SO_4^{2}, and O_2, **2)** The resulting depletion of oxidized ions promotes bacterial reduction of DIC, which results in elevated methane relative to Fe^{3+}, SO_4^{2}, and O_2 in the TSS groundwaters over kimberlites

3.10 TABLES

Table 3-1. Geochemical and isotopic compositions of groundwaters from TSS and boreholes at Yankee, Zulu, Golf, Alpha-1, Bravo-1, and Control (Continued on next page)

Table 1

Sample	Kimberlite m	Water type	Location	Latitude degrees	Longitude degrees	Temp °C	pH	Eh (mV) mV	EC µS/cm	DO mmol/L	Na µmol/L	Fe total µmol/L
07-MWA 01	Alpha 1	TSS	limestone	52 6907	83 7810	13 3	7 12	103	481	0 010	139	161 8
07-MW-A-01F	Alpha-1	TSS	limestone	52 6907	83 7810	14 5	7 51	263	474	0 044	220	97 2
07 MWA-11	Alpha 1	TSS	kimberlite	52 6938	83 7769	8 8	7 53	101	524	0 012	1201	43 5
07 MW A-11F	Alpha 1	TSS	kimberlite	52 6938	83 7769	7 6	6 24	244	377	0 077	2198	4 6
07-MWA 12	Alpha-1	TSS	kimberlite	52 6939	83 7762	11 5	6 71	209	448	0 208	76	85 8
07 MW A-12F	Alpha 1	TSS	kimberlite	52 6939	83 7762	8 5	7 19	279	248	0 153	57	126 5
07 MW C 01F	Control	TSS	limestone	52 8455	83 7915	16 5	7 44	276	285	0 169	na	na
07 MWY 01	Yankee	TSS	limestone	52 7743	83 8781	8 4	8 25	60	440	0 019	68	15 0
07 MW Y 01F	Yankee	TSS	limestone	52 7743	83 8781	6 2	6 98	192	410	0 026	45	12 0
07 MWY 10	Yankee	TSS	kimberlite	52 7752	83 8725	18 4	9 06	210	409	0 051	82	18 7
07 MW Y 10F	Yankee	TSS	kimberlite	52 7752	83 8725	5 4	7 40	237	475	0 130	62	8 8
07 MWY-11 5	Yankee	TSS	kimberlite	52 7759	83 8721	16 8	8 92	224	407	0 204	111	9 4
07 MW-Y-11 5F	Yankee	TSS	kimberlite	52 7759	83 8721	6 5	8 17	212	411	0 090	97	10 5
07 MWZ 05	Zulu	TSS	limestone	52 7298	83 8354	16 4	6 57	102	479	bd	156	35 5
07 MW Z 05F	Zulu	TSS	limestone	52 7298	83 8354	16 4	7 67	175	304	0 061	359	4 0
07 MWZ 15	Zulu	TSS	kimberlite	52 7296	-83 8316	na	na	na	na	bd	54	107 4
07 MW Z 15F	Zulu	TSS	kimberlite	52 7296	-83 8316	7 1	7 24	281	440	0 085	39	105 0
07-MW-Z 17F	Zulu	TSS	kimberlite	52 7296	83 8309	6 5	7 66	241	874	0 018	1658	2 0
07 MW B 01F	Bravo 1	TSS	kimberlite	52 8647	-83 9390	9 6	6 77	341	434	0 213	130	2 3
07 MW B 02F	Bravo 1	TSS	limestone	52 8636	-83 9387	6 2	6 71	306	977	0 240	670	1 9
07 MW B 03F	Bravo 1	TSS	kimberlite	52 8651	83 9395	15 1	7 54	303	600	0 059	194	0 8
07 B1 07 08C F	Bravo 1	borehole	kimberlite	52 8649	83 9393	9 6	8 55	226	597	0 078	324	1 3
07 X 07-014C	X Ray	borehole	kimberlite	52 7960	83 8537	9 0	7 76	23	198	bd	36	5 4
07 Z-07 12C	Zulu	borehole	kimberlite	52 7290	83 8317	12 4	7 51	68	945	bd	51	221 6
07 Z-07-12C-F	Zulu	borehole	kimberlite	52 7290	83 8317	16 9	8 04	136	247	0 040	43	229 2
07-Y-07 7H	Yankee	borehole	kimberlite	52 7756	83 8737	7 5	8 06	4	377	bd	5120	8 0
07 Y 07 7H F	Yankee	borehole	kimberlite	52 7756	83 8737	16 9	7 29	95	na	0 039	416	24 5
07 A BH 06	Alpha-1	borehole	kimberlite	52 6922	83 7752	9 1	7 21	272	na	na	842	66 2

na = not analyzed
bd = below detection

Table 3-1. Continued

Table 1 Con t

Sample	Fe^{2+} µmol/L	Fe^{3+} µmol/L	SO_4^{2} µmol/L	Cl µmol/L	CH_4 µmol/L	H_2 µmol/L	$\delta^{13}C_{CH4}$ per mil	$\delta^{2}H_{CH4}$ per mil	DIC mmol/L	$\delta^{13}C_{DIC}$ per mil	$\delta^{2}H_{H2O}$ per mil	$\delta^{18}O_{H2O}$ per mil
07-MWA-01	136 9	24 9	12 5	269 3	na	na	na	na	5 69	4 3	na	na
07-MW-A-01F	23 3	73 9	4 8	53 2	429 6	0 9	-68 2	-265 2	6 37	4 6	-105 7	-14 5
07-MWA-11	23 3	20 2	49 4	120 6	na	na	na	na	6 49	-3 9	na	na
07-MW-A-11F	0 0	4 6	135 1	290 4	447 1	bd	-70 2	-258 7	5 24	1 5	94 8	-13 8
07-MWA-12	59 1	26 8	5 1	104 2	na	na	na	na	5 91	0 9	na	na
07-MW-A-12F	41 3	85 2	5 1	28 7	632 4	bd	-71 9	-258 6	5 10	0 0	-63 8	-13 5
07-MW-C-01F	na	na	na	na	187 7	bd	70 9	-254 2	6 15	-1 3	-81 6	-11 8
07-MWY-01	na	na	22 5	bd	na	na	na	na	na	na	na	na
07-MW-Y-01F	0 0	12 0	3 6	46 2	358 4	2 0	-76 2	-266 4	5 38	-2 2	-99 5	-13 5
07-MWY-10	1 1	17 6	1 7	49 6	na	na	na	na	4 80	-7 0	na	na
07-MW-Y 10F	0 0	8 8	2 2	37 7	246 6	0 2	-76 3	-269 7	5 73	4 5	na	na
07-MWY-11 5	0 0	9 4	2 8	43 1	na	na	na	na	4 46	-9 2	na	na
07-MW-Y-11 5F	0 0	10 5	2 8	39 2	116 1	0 1	-82 4	-289 2	4 70	-9 8	-104 8	-15 2
07 MWZ-05	13 5	22 0	2 1	bd	na	na	na	na	10 50	-7 8	na	na
07-MW-Z-05F	0 0	4 0	10 1	60 6	11 3	0 0	-62 5	253 0	2 67	-5 6	na	na
07-MWZ-15	na	na	1 7	37 7	na	na	na	na	6 51	-2 6	na	na
07-MW-Z-15F	31 2	73 8	0 4	26 2	153 1	0 0	-68 0	-275 7	6 99	-5 2	-100 8	-14 8
07-MW-Z-17F	0 0	2 0	12 9	105 4	421 3	2 2	-68 6	-261 4	12 77	3 2	99 2	15 0
07-MW-B-01F	0 0	2 3	5 1	74 1	bd	bd	bd	bd	5 12	-5 4	-92 6	-12 0
07-MW-B-02F	0 0	1 9	13 3	249 3	bd	bd	bd	bd	10 83	3 2	na	na
07-MW-B-03F	0 0	0 8	5 9	69 3	bd	bd	bd	bd	5 85	-3 5	na	na
07-B1-07-08C-F	0 0	1 3	2 5	169 0	na	na	na	na	6 17	-7 2	-97 6	-12 5
07-X-07-014C	0 0	5 4	7 0	14 1	na	na	na	na	3 16	-2 0	na	na
07-Z-07-12C	214 6	6 9	4 5	28 2	na	na	na	na	4 12	-10 3	na	na
07-Z-07-12C-F	221 3	7 9	0 4	21 7	71 0	bd	-75 9	-272 9	4 41	-11 4	-65 9	-10 9
07-Y-07-7H	0 9	7 1	136 4	4459 4	na	na	na	na	6 34	12 6	na	na
07-Y-07-7H-F	7 2	17 3	40 8	422 0	311 8	0 5	-73 0	-261 2	1 94	-12 3	-110 8	-15 0
07-A-BH-06	26 8	39 3	11 6	182 8	10 0	na	-68 7	-287 1	1 81	-13 7	na	na

na = not analyzed

bd = below detection

Chapter 4 - Summary and Implications

SUMMARY

High concentrations of kimberlite pathfinder metals consisting of Ni, Cr, Ti, LREEs, Ba, Rb, Cs, and the ratio of Mg/Ca are observed at sites along sampling transects proximal to the aerial margin of buried kimberlites. This research suggests that the physical upward movement of groundwater from kimberlites to the shallow subsurface is the dominant transport mechanism for pathfinder metals. Elevated pathfinder metals in groundwaters from kimberlite are due to the chemical weathering of olivine, pyroxene, and phlogopite (Sader *et al.*, 2007a). These metals in kimberlite-impacted waters could be migrating preferentially upwards along fractures in host rock up to 200 m from kimberlite margins.

Spatial variations among pathfinder metals exist at sites of upwelling groundwaters (i.e. not all pathfinder metals are elevated in peat groundwaters at the same sites of upwelling). These differences are due to variable metal solubility under conditions that range from dominantly ombrotrophic (low contributions from upwelling groundwaters) to dominantly minerotrophic (high contributions from upwelling groundwaters). Modeling calculations and analytical data indicate that under conditions of low upwelling contributions, pathfinder metals (particularly transition metals) in peat groundwaters remain soluble due to high metal fractions that are complexed with DOM. In contrast, at sites of high upwelling groundwater contributions, metal-DOM complexation is lower. The greater concentrations of free ions (metals not complexed with DOM) are likely to adsorb to ferrihydrite, resulting in low metal solubility. Alkaline earth and alkali pathfinders have lower binding affinities to DOM and adsorption affinities to ferrihydrite, and thus indicate different sites of elevated concentrations along peat groundwater sampling transects.

In addition to influencing metal concentrations in peat groundwaters, kimberlites influence the CH_4-CO_2 system in the overlying TSS. The CH_4 production via biological reduction of DIC in TSS over kimberlites is likely due to the upward migration of reduced ions from kimberlite. In contrast, TSS groundwaters over limestone show evidence to suggest CH_4 is oxidizing, as the ratio of CH_4 to oxidized ions consisting of Fe^{3+}, SO_4^{2-}, and $O_{2(aq)}$ is low.

IMPLICATIONS

Elevated kimberlite pathfinder metals in peat groundwaters have significant implications for diamond exploration in northern boreal regions. As these regions commonly have vast wetlands, peat groundwaters could be utilized as a geochemical exploration tool in conjunction with geophysical methods. Although geophysical methods are useful in determining potential kimberlite targets in the James Bay region, they may falsely indicate kimberlites (syenite and mafic dykes may show geophysical features similar to kimberlites). This research suggests that near surface water geochemistry could assist by providing additional information about a buried geophysical feature and whether there is geochemical evidence to suggest the buried anomaly is kimberlite before the commencement of drilling. Peat and groundwater geochemistry were not determined over other intrusive igneous bodies however, it is likely that geochemistry could discriminate these intrusive bodies from kimberlites. Minerals within kimberlites are more susceptible to chemical weathering versus other intrusive igneous rocks. Therefore, it is likely that groundwater within kimberlites will require less residence time to develop a geochemical kimberlite signature compared with other bodies such as syenite or diabase, which have minerals that are more resistant to chemical weathering.

There are some limitations to using peat groundwater as an exploration tool for the detection of hidden kimberlite bodies. Because the concentrations of some metal pathfinders in the shallow peat groundwaters are low (sub - μm/L concentrations), they could be influenced by air pollution. Potential sites located down wind from industrial areas could potentially mask geochemical signals. Another limitation to the method, which was addressed in Chapter 2, is the various mechanisms in the shallow subsurface (i.e. adsorption and incorporation into secondary minerals), which have the potential to scavenge metals from groundwater.

Due to the unusual sampling environment (saturated sphagnum peat), this study has identified several methods for geochemical exploration surveys in peat bogs.

1) Hydrogeological survey

A hydrogeological survey of areas near a potential buried kimberlite body is suggested. Over Attawapiskat kimberlites, the installation of piezometers and monitoring wells is useful to identify upwelling groundwaters. Although the detection of variations in geochemical parameters such as EC, Eh, and pH are also useful in the identification of sites of upwelling, hydrogeological measurements are typically more precise. However, monitoring well installation is physically demanding, time-consuming, and requires some heavy equipment (i.e. iron pipe, iron slide hammer, large pipe wrenches). As it is not feasible to install monitoring wells at each site, it is important to rely on both geochemical parameters and hydrogeology to detect groundwater upwelling. All upwelling groundwaters have high EC, pH, ionic strength, and low Eh compared with ombrotrophic peat groundwaters. It should, however, be noted that geochemical parameters that indicate upwelling may have traveled a distance down gradient from where upwelling groundwaters enter the peat from the TSS.

2) Extent of sampling transect

Results suggest peat groundwater samples should be collected at least 200 m beyond the suspected kimberlite margins where possible, as fractured host rock may extend as far as 150 m from the margin. Additionally, the geochemical data from samples > 200 m from the suspected kimberlite body are useful in deriving local baseline metal concentrations.

3) Peat and peat groundwater sampling

The most effective means to accurately detect kimberlite pathfinder metals in high DOC wetlands is to collect samples of the solid media (peat) and peat groundwater along sampling transects. In Attawapiskat peat groundwaters, metal solubility is variable. Therefore, It is possible a geochemical sampling program that only focuses on peat may overlook important metal pathfinders. Metals that are dominantly complexed with DOM are to likely remain soluble as they may inhibit metal adsorption to surfaces such as ferrihydrite. Conversely, if only peat groundwaters are collected, a kimberlite geochemical response may also be overlooked. Where free ions are dominant, metals are more likely to be scavenged from solution, or are more likely to be incorporated into precipitating minerals.

4) Methane – CO_2 system

The results of this study suggest buried lithology can impact methane emissions in overlying sediment. Hydrocarbons have been used successfully to delineate buried kimberlites and buried sulfide deposits. Additionally, a number of commercial laboratory packages exist to delineate blind mineralization using reduced gas variations over suspected mineralization. The use of isotopes and CH_4 gas concentrations, coupled with isotopic values of DIC in groundwaters over Attawapiskat kimberlites provides further insight into processes that are responsible for variable CH_4 concentrations and isotopic signatures and

suggest that these signatures over or near kimberlites may be a secondary effect of groundwater – kimberlite interaction.

References

2007. Environment Canada - National Climate Data and Information Archive.

ABRAJANO, T. A., STURCHIO, N. C., BOHLKE, J. K., LYON, G. L., POREDA, R. J. and STEVENS, C. M., 1988. Methane-hydrogen gas seeps, Zambales ophiolite, Philippines: deep or shallow origin? *Chemical Geology*. **71**, 211-222.

ACHTNICH, C., BAK, F. and CONRAD, R., 1995. Competition for electron donors among nitrate reducers, ferric iron reducers, sulfate reducers, and methanogens in anoxic paddy soil. *Biology and Fertility of Soils*. **19**(1), 65-72.

ARMSTRONG, J. P., WILSON, M., BARNETT, R. L., NOWICKI, T. and KJARSGAARD, B. A., 2004. Mineralogy of primary carbonate-bearing hypabyssal kimberlite, Lac de Gras, Slave Province, Northwest Territories, Canada. *Lithos*. **76**, 415-433.

BARNES, I. and O'NEIL, J. R., 1969. The relationship between fluids in some fresh alpine-type ultramafics and possible modern serpentinization, western United States. *Geological Society of America Bulletin*. **80**, 1947-1960.

BARNES, I., RAPP, J. B. and O'NEIL, J. R., 1972. Metamorphic assemblages and the direction of flow of metamorphic fluids in four instances of serpentinization. *Contributions to Mineralogy and Petrology*. **35**, 263-270.

BEER, J. and BLODAU, C., 2007. Transport and thermodynamics constrain belowground carbon turnover in a northern peatland. *Geochimica et Cosmochimica Acta*. **71**, 2989-3002.

BELL, R. A., OGDEN, N. and KRAMER, J. R., 2002. The biotic ligand model and a cellular approach to class B metal aquatic toxicity. *Comparative Biochemistry and Physiology C: Pharmacology Toxicology and Endocrinology*. **133**(1-2), 175-188.

BELLEFLEUR, G., MATTHEWS, L., ROBERTS, B. et al., 2005. Downhole seismic imaging of the Victor Kimberlite, James Bay Lowlands, Ontario; a feasibility study. *Open File Report 2005-C1, Geological Survey of Canada*, 7.

BENEDETTI, M. F., VAN RIEMSDIJK, W. H., KOOPAL, L. K., KINNIBURGH, D. G., GOODDY, D. C. and MILNE, C. J., 1996. Metal ion binding by natural organic matter: From the model to the field. *Geochimica et Cosmochimica Acta*. **60**(14), 2503-2513.

BETHKE, C. M., 2002. *The Geochemist's Workbench - Release 4.0*. University of Illinois.

BIRKS, S. J., EDWARDS, T. W. D., GIBSON, J. J., MICHEL, F. A., DRIMMIE, R. J. and MACTAVISH, D., 2003. Canadian Network for Isotopes in Precipitation. University of Waterloo/Meteorological Service of Canada, Waterloo, Ontario.

BOELTER, D. H. and VERRY, E. S., 1977. *Peatland and water in the northern Lake States, General Technical Report NC-31*, U.S. Department fo Agriculture, Forest Service, St. Paul, MN.

BOTTINGA, Y., 1969. Calculated fractionation factors for carbon and hydrogen isotope exchange in the system calcite-carbon dioxide-graphite-methane-hydrogen-water vapor. *Geochimica et Cosmochimica Acta*. **33**(1), 49-64.

BRAUNEDER, K., 2007. *Characterization of peatland waters overlying concealed kimberlites in the Attawapiskat region, northern Ontario*. B.Sc. Hon. Thesis, University of Ottawa, Ottawa, 76 pp.

BRULAND, K. W., DONAT, J. R. and HUTCHINS, D. A., 1991. Interactive influences of bioactive trace metals on biological production in oceanic waters. *Limnology and Oceanography*. **36**(8), 1555-1577.

CABANISS, S. E. and SHUMAN, M. S., 1988a. Copper binding by dissolved organic matter: I. Suwannee River fulvic acid equilibria. *Geochimica et Cosmochimica Acta*. **52**(1), 185-193.

CABANISS, S. E. and SHUMAN, M. S., 1988b. Copper binding by dissolved organic matter: II. Variation in type and source of organic matter. *Geochimica et Cosmochimica Acta*. **52**(1), 195-200.

CAMERON, E. M., HAMILTON, S. M., LEYBOURNE, M. I., HALL, G. E. M. and MCCLENAGHAN, M. B., 2004a. Finding deeply buried deposits using geochemistry. *Geochemistry - Exploration, Environment, Analysis*. **4**(1), 7-32.

CAMERON, E. M., HAMILTON, S. M., LEYBOURNE, M. I., HALL, G. E. M. and MCCLENAGHAN, M. B., 2004b. Finding deeply buried deposits using geochemistry. *Geochemistry: Exploration, Environment, Analysis*. **4**(1), 7-32.

CHASON, D. B. and SIEGEL, D. I., 1986. Hydraulic conductivity and related physical properties of peat, Lost River peatland, northern Minnesota. *Soil Science*. **142**(2), 91-99.

CLARK, I. D. and FRITZ, P., 1997. *Environmental Isotopes in Hydrogeology*. Lewis Publishers, Boca Raton, New York, 328 pp.

CLYMO, R. S., 1983. Peat. In: A.J.P. GORE (Editor), *Mires: Swamp, bog, fen and moor*. Elsevier Scientific Publishing Company, Amsterdam, Oxford, New York, pp. 440.

CLYMO, R. S., 1984. The limits to peat bog growth. *Philosophical Transactions of the Royal Society of London, Series B: Biological Sciences*. **303**(1117), 605-654.

CORNELL, R. M. and SCHWERTMANN, U., 1979. Influence of organic anions on the crystallization of ferrihydrite. *Clays and Clay Minerals*. **27**(6), 402-410.

CORNELL, R. M. and SCHWERTMANN, U., 2003. *The iron oxides; structure, properties, reactions, occurrence and uses*. Wiley-VCH, Weinheim, 664 pp.

COWELL, D. W., 1983. Karst hydrogeology within a subarctic peatland: Attawapiskat River, Hudson Bay lowland, Canada. *Journal of Hydrology*. **61**(1-3), 169-175.

DZOMBAK, D. A. and MOREL, F. M. M., 1990. *Surface complexation modeling; hydrous ferric oxide*. John Wiley & Sons, New York, NY, USA.

FRASER, C. J. D., ROULET, N. T. and MOORE, T. R., 2001. Hydrology and dissolved organic carbon biogeochemistry in an ombrotrophic bog. In: M. WOO, P. MARSH and D. MOORE (Editors), *Hydrological Processes*. John Wiley & Sons, New York, pp. 3151-3166.

FREEZE, R. A. and CHERRY, J. A., 1979. *Groundwater*. Prentice-Hall, Inc., Englewood Cliffs, N.J., 604 pp.

FRENZEL, B., 1983. Mires - Repositories of Climatic Information or Self-Perpetuating Ecosystems. In: A.J.P. GORE (Editor), *Mires: Swamp, bog, fen and moor*. Elsevier Scientific Publishing Company, Amsterdam, Oxford, New York, pp. 440.

FRITZ, P., CLARK, I. D., FONTES, J.-C., WHITICAR, M. J. and FABER, E., 1992. Deuterium and (super 13) C evidence for low temperature production of hydrogen and methane in a highly alkaline groundwater environment in Oman. In: Y.K. KHARAKA and A.S. MAEST (Editors), *Proceedings - International Symposium on Water-Rock Interaction, vol.7*, pp. 793-796.

GUSTAFSSON, J. P., 2010. Visiual MINTEQ 3.0 For Windows XP/7.

HANSEN, L. K., JAKOBSEN, R. and POSTMA, D., 2001. Methanogenesis in a shallow sandy aquifer, Romo, Denmark. *Geochimica et Cosmochimica Acta*. **65**(17), 2925-2935.

HATTORI, K. H. and CAMERON, E. M., 2004. Using the high mobility of palladium in surface media in exploration for platinum group element deposits; evidence from the Lac des Iles region, northwestern Ontario. *Economic Geology and the Bulletin of the Society of Economic Geologists*. **99**(1), 157-171.

HATTORI, K. H. and HAMILTON, S., 2008. Geochemistry of peat over kimberlites in the Attawapiskat area, James Bay Lowlands, northern Canada. *Applied Geochemistry*. **23**(12), 3767-3782.

HATTORI, K. H., HAMILTON, S. M., KONG, J. and GRAVEL, J., 2009. Soil geochemical survey over concealed kimberlites in the Attawapiskat area in northern Canada. *Geochemistry: Exploration, Environment, Analysis*. **9**(2), 139-150.

HILL, B. M. and SIEGEL, D. I., 1991. Groundwater flow and the metal content of peat. *Journal of Hydrology*. **123**(3-4), 211-224.

HOAG, R. S. and PRICE, J. S., 1995. A field-scale, natural gradient solute transport experiment in peat at a Newfoundland blanket bog. *Journal of Hydrology*. **172**(1-4), 171-184.

HOAG, R. S. and PRICE, J. S., 1997. The effects of matrix diffusion on solute transport and retardation in undisturbed peat in laboratory columns. *Journal of Contaminant Hydrology*. **28**(3), 193-205.

HOCH, A. R., REDDY, M. M. and AIKEN, G. R., 2000. Calcite crystal growth inhibition by humic substances with emphasis on hydrophobic acids from the Florida Everglades. *Geochimica et Cosmochimica Acta*. **64**(1), 61-72.

HORNIBROOK, E. R. C. and BOWES, H. L., 2007. Trophic status impacts both the magnitude and stable carbon isotope composition of methane flux from peatlands. *Geophysical Research Letters*. **34**(21).

HORNIBROOK, E. R. C., LONGSTAFFE, F. J. and FYFE, W. S., 2000. Evolution of stable carbon isotope compositions for methane and carbon dioxide in freshwater wetlands and other anaerobic environments. *Geochimica et Cosmochimica Acta*. **64**(6), 1013-1027.

HYDROLOGIC CONSULTANTS, I., 2004. *Dewatering of Victor diamond project: Predicted engineering, cost, and environmental factors*, Consultant Report, 109.

INGRAM, H. A. P., 1983. Hydrogeology. In: A.J.P. GORE (Editor), *Mires: Swamp, bog, fen and moor*. Elsevier Scientific Publishing Company, Amsterdam, Oxford, New York, pp. 440.

JAKOBSEN, R. and POSTMA, D., 1999. Redox zoning, rates of sulfate reduction and interactions with Fe-reduction and methanogenesis in a shallow sandy aquifer, Rømø, Denmark. *Geochimica et Cosmochimica Acta*. **63**, 137-151.

JAKOBSEN, R., ALBRECHTSEN, H.-J. R., RASMUSSEN, M., BAY, H., BJERG, P. L. and CHRISTENSEN, T. H., 1998. H2 Concentrations in a Landfill Leachate Plume (Grindsted, Denmark):,Äâ In Situ Energetics of Terminal Electron Acceptor Processes. *Environmental Science & Technology*. **32**(14), 2142-2148.

JANSE, A. J. A. and SHEAHAN, P. A., 1995. Catalogue of world wide diamond and kimberlite occurrences; a selective and annotative approach. *Journal of Geochemical Exploration*. **53**(1-3), 73-111.

JOHANNESSON, K. H., TANG, J., DANIELS, J. M., BOUNDS, W. J. and BURDIGE, D. J., 2004. Rare earth element concentrations and speciation in organic-rich blackwaters of the Great Dismal Swamp, Virginia, USA. *Chemical Geology*. **209**(3-4), 271-294.

KINNIBURGH, D. G., JACKSON, M. L. and SYERS, J. K., 1976. Adsorption of alkaline earth, transition, and heavy metal cations by hydrous oxide gels of iron and aluminum. *Soil Science Society of America Journal*. **40**(5), 796-799.

KINNIBURGH, D. G., VAN RIEMSDIJK, W. H., KOOPAL, L. K., BORKOVEC, M., BENEDETTI, M. F. and AVENA, M. J., 1999. Ion binding to natural organic matter: competition, heterogeneity, stoichiometry and thermodynamic consistency. *Colloids and Surfaces A: Physicochemical and Engineering Aspects*. **151**(1-2), 147-166.

KONG, J. M., BOUCHER, D. R. and SCOTT SMITH, B. H., 1999. Exploration and geology of the Attawapiskat Kimberlites, James Bay Lowland, northern Ontario, Canada. In: J.J. GURNEY, J.L. GURNEY, M.D. PASCOE and S.H. RICHARDSON (Editors), *Proceedings of the International Kimberlite Conference*, pp. 452-467.

KOOPAL, L. K., VAN RIEMSDIJK, W. H., DE WIT, J. C. M. and BENEDETTI, M. F., 1994. Analytical Isotherm Equations for Multicomponent Adsorption to Heterogeneous Surfaces. *Journal of Colloid and Interface Science*. **166**(1), 51-60.

KUCHLING, K., CHORLEY, D. and ZAWADZKI, W., 2000. *Hydrogeological modeling of mining operations at the Diavik Diamonds project*, Consultant Report, 8.

KUMARASWAMY, S., RAMAKRISHNAN, B. and SETHUNATHAN, N., 2001. Methane Production and Oxidation in an Anoxic Rice Soil as Influenced by Inorganic Redox Species. *J Environ Qual*. **30**(6), 2195-2201.

LANSDOWN, J. M., QUAY, P. D. and KING, S. L., 1992. CH (sub 4) production via CO (sub 2) reduction in a temperate bog; a source of (super 13) C-depleted CH (sub 4). *Geochimica et Cosmochimica Acta*. **56**(9), 3493-3503.

LEHTONEN, M. L., MARMO, J. S., NISSINEN, A. J., JOHANSON, B. S. and PAKKANEN, L. K., 2005. Glacial dispersal studies using indicator minerals and till geochemistry around two Eastern Finland kimberlites. *Journal of Geochemical Exploration.* **87**(1), 19-43.

LEYBOURNE, M. I. and CAMERON, E. M., 2006. Composition of groundwaters associated with porphyry-Cu deposits, Atacama Desert, Chile: Elemental and isotopic constraints on water sources and water-rock reactions. *Geochimica et Cosmochimica Acta.* **70**, 1616-1635.

LEYBOURNE, M. I. and CAMERON, E. M., 2010. Ground water in geochemical exploration. *Geochemistry: Exploration, Environment, Analysis.* **10**(2), 99-118.

LEYBOURNE, M. I., BOYLE, D. R. and GOODFELLOW, W. D., 2003. Interpretation of stream water and sediment geochemistry in the Bathurst Mining Camp, New Brunswick. *Economic Geology Monograph.* **11**, 741-762.

LOFTS, S. and TIPPING, E., 1998. An assemblage model for cation binding by natural particulate matter. *Geochimica et Cosmochimica Acta.* **62**(15), 2609-2625.

LOVELL, J. S., HALE, M., WEBB, J. S. and PARSLOW, G. R., 1983. Soil air carbon dioxide and oxygen measurements as a guide to concealed mineralizations in semi-arid and arid regions, *Journal of Geochemical Exploration.* Elsevier, Amsterdam-New York, pp. 305-317.

LU, Y. and ALLEN, H. E., 2002. Characterization of copper complexation with natural dissolved organic matter (DOM)--link to acidic moieties of DOM and competition by Ca and Mg. *Water Research.* **36**(20), 5083-5101.

MANN, A. W., BIRRELL, R. D., MANN, A. T., HUMPHREYS, D. B. and PERDRIX, J. L., 1998. Application of the mobile metal ion technique to routine geochemical exploration. *Journal of Geochemical Exploration.* **61**, 87-102.

MARTENS, C. S. and BERNER, R. A., 1977. Interstitial water chemistry of anoxic Long Island Sound sediments; 1, Dissolved gases. *Limnology and Oceanography.* **22**(1), 10-25.

MCCARTHY, J. H., JR., LAMBE, R. N. and DIETRICH, J. A., 1986. A case study of soil gases as an exploration guide in glaciated terrain; Crandon massive sulfide deposit, Wisconsin. *Economic Geology and the Bulletin of the Society of Economic Geologists.* **81**(2), 408-420.

MCCLENAGHAN, M. B., HAMILTON, S. M., HALL, G. E. M., BURT, A. K. and KJARSGAARD, B. A., 2006. Selective Leach Geochemistry of Soils Overlying the 95-2, B30, and A4 Kimberlites, Northeastern Ontario. *Geological Survey of Canada - Open-File Report 5069*, 31.

MILNE, C. J., KINNIBURGH, D. G., VAN RIEMSDIJK, W. H. and TIPPING, E., 2003. Generic NICA - Donnan Model Parameters for Metal-Ion Binding by Humic Substances. *Environmental Science and Technology*. **37**(5), 958-971.

MITCHELL, R. H., 1986. *Kimberlites: Mineralogy, Geochemistry, and Petrology*. Plenum Publishing Corp., New York, 442 pp.

MIURA, Y., WATANABE, A., MURASE, J. and KIMURA, M., 1992. Methane production and its fate in paddy fields II. Oxidation of methane and its coupled ferric oxide reduction in subsoil. *Soil Science and Plant Nutrition*. **38**(4), 673-679.

MORTON, K. L. and MUELLER, S., 2003. Hydrogeology of the Venetia diamond mine, South Africa. *South African Journal of Geology*. **106**(2-3), 193-204.

NORRIS, A. W., 1993. Hudson Platform; Introduction. In: D.F. STOTT and J.D. AITKEN (Editors), *Sedimentary cover of the craton in Canada*. Geol. Surv. Canada, Ottawa.

O'BRIEN, H. E. and TYNI, M., 1999. Mineralogy and geochemistry of kimberlites and related rocks from Finland. In: J.J. GURNEY, J.L. GURNEY, M.D. PASCOE and S.H. RICHARDSON (Editors), *Proceedings of the International Kimberlite Conference*. publisher varies, location varies, pp. 625-636.

PALANDRI, J. L. and REED, M. H., 2004. Geochemical models of metasomatism in ultramafic systems: serpentinization, rodingitization, and sea floor carbonate chimney precipitation. *Geochimica et Cosmochimica Acta*. **68**(5), 1115 - 1133.

PAQUIN, P. R., GORSUCH, J. W., APTE, S. et al., 2002. The biotic ligand model: a historical overview. *Comparative Biochemistry and Physiology C: Pharmacology Toxicology and Endocrinology*. **133**(1-2), 3-35.

PERDUE, E. M. and RITCHIE, J. D., 2005. Dissolved Organic Matter in Freshwaters. In: J.I. DREVER (Editor), *Surface and Ground Water, Weathering, and Soils*. Elsevier Ltd., Oxford, UK, pp. 626.

POURRET, O., DAVRANCHE, M., GRUAU, G. and DIA, A., 2007. Rare earth elements complexation with humic acid. *Chemical Geology*. **243**, 1-2.

PRICE, J. S., 2003. Role and character of seasonal peat soil deformation on the hydrology of undisturbed and cutover peatlands. *Water Resources Research*. **39**(9), 10.

PROSKUROWSKI, G., LILLEY, M. D., SEEWALD, J. S. et al., 2008. Abiogenic Hydrocarbon Production at Lost City Hydrothermal Field. *Science*. **319**(5863), 604-607.

RADOVANOVIC, H. and KOELMANS, A. A., 1998. Prediction of In Situ Trace Metal Distribution Coefficients for Suspended Solids in Natural Waters. *Environmental Science and Technology*. **32**(6), 753-759.

RAVICHANDRAN, M., AIKEN, G. R., RYAN, J. N. and REDDY, M. M., 1999. Inhibition of Precipitation and Aggregation of Metacinnabar (Mercuric Sulfide) by Dissolved Organic Matter Isolated from the Florida Everglades. *Environmental Science and Technology*. **33**(9), 1418-1423.

REEVE, A. S., SIEGEL, D. I. and GLASER, P. H., 1996. Geochemical controls on peatland pore water from the Hudson Bay Lowland; a multivariate statistical approach. *Journal of Hydrology*. **181**(1-4), 285-304.

REJMANKOVA, E. and POST, R., 1996. Methane in sulfate-rich and sulfate-poor wetland sediments. *Biogeochemistry*. **34**(2), 57-70.

SADER, J. A., LEYBOURNE, M. I., MCCLENAGHAN, M. B. and HAMILTON, S. M., 2007a. Low-temperature serpentinization processes and kimberlite ground water signatures in the Kirkland Lake and Lake Timiskiming kimberlite fields, Ontario, Canada; implications for diamond exploration. *Geochemistry: Exploration, Environment, Analysis*. **7**(1), 3-21.

SADER, J. A., LEYBOURNE, M. I., MCCLENAGHAN, M. B. and HAMILTON, S. M., 2007a. Low-temperature serpentinization processes and kimberlite ground water signatures in the Kirkland Lake and Lake Timiskiming kimberlite fields, Ontario, Canada; implications for diamond exploration. *Geochemistry - Exploration, Environment, Analysis*. **7**(1), 3-21.

SADER, J. A., ANDERSON, H. S. I., FENSTERMACHER, R. F. and HATTORI, K. H., 2009. Imaging a buried diamondiferous kimberlite using conventional geochemistry and Amplified Geochemical Imaging Technology. In: D.R. LENTZ, THORNE, K.G., AND BEAL, K. (Editor), *24th International Applied Geochemistry Symposium*. Association of Applied Geochemists, Fredericton, NB, Canada.

SADER, J. A., HATTORI, K. H., KONG, J. M. and HAMILTON, S. M., 2010. Geochemical responses in peat groundwater over Attawapiskat kimberlites, James Bay Lowlands, Canada and their application to diamond exploration. *Geochemistry: Exploration, Environment, Analysis*. **Accepted**.

SADER, J. A., LEYBOURNE, M. I., MCLENAGHAN, M. B., CLARK, I. D. and HAMILTON, S. M., 2007b. Antacid belches from northeastern Ontario: Generation of high pH groundwaters and H2 gas, *International Applied Geochemical Symposium*, Ovideo, Spain, June 14 - 19, 2007.

SAGE, R. P., 2000a. Kimberlites of the Attawapiskat Area, James Bay Lowlands, Northern Ontario. *Ontario Geological Survey, Open File Report 6019*, 341.

SAGE, R. P., 2000b. Kimberlites of the Lake Timiskaming structural zone; supplement. *Ontario Geological Survey, Open File Report 6018*, 123.

SCHOELL, M., 1980. The hydrogen and carbon isotopic composition of methane from natural gases of various origins. *Geochimica et Cosmochimica Acta*. **44**(5), 649-662.

SEGERS, R., 1988. Methane production and methane consumption: a review of processes underlying wetland methane fluxes. *Biogeochemistry*. **41**, 23-51.

SHILTS, W. W., 1986. Glaciation of the Hudson Bay Region. In: I.P. MARTINI (Editor), *Canadian Inland Seas*. Elsevier Science Plublishers B.V., Amsterdam, The Netherlands, pp. 494.

SHOLKOVITZ, E. R. and COPLAND, D., 1981. The coagulation, solubility and adsorption properties of Fe, Mn, Cu, Ni, Cd, Co and humic acids in a river water. *Geochimica et Cosmochimica Acta*. **45**(2), 181-189.

SIEGEL, D. I., CHANTON, J. P., GLASER, P. H., CHASAR, L. S. and ROSENBERRY, D. O., 2001. Estimating methane production rates in bogs and landfills by deuterium enrichment of pore water. *Global Biogeochemical Cycles*. **15**(4), 967-975.

SIKORA, L. J. and KEENEY, D. R., 1983. Further Aspects of Soil Chemsitry Under Anaerobic Conditions. In: A.J.P. GORE (Editor), *Mires: Swamp, bog, fen and moor*. Elsevier Scientific Publishing Company, Amsterdam, Oxford, New York, pp. 440.

SJORS, H., 1963. *Bogs and fens on Attawapiskat river, northern Ontario*, Department of Northern Affairs and National Resources Canada, National Museum of Canada, 45-133.

SONKE, J. E. and SALTERS, V. J. M., 2004. Determination of neodymium-fulvic acid binding constants by capillary electrophoresis inductively coupled plasma mass spectrometry (CE-ICP-MS). *Journal of Analytical Atomic Spectrometry*. **19**(2), 6.

STEVENSON, F. J., 1994. *Humus Chemsitry: Genesis, Composition, Reactions*. John Wiley & Sons, Inc., New York, 512 pp.

SYROVETNIK, K., PUURA, E. and NERETNIEKS, I., 2004. Accumulation of heavy metals in Oostriku peat body, Estonia; site description, conceptual modelling and geochemical modelling of the source of the metals. *Environmental Geology*. **45**(5), 731-740.

SYROVETNIK, K., MALMSTROM, M. E. and NERETNIEKS, I., 2007. Accumulation of heavy metals in the Oostriku peat bog, Estonia: Determination of binding processes by means of sequential leaching. *Environmental Pollution*. **147**(1), 291-300.

SYROVETNIK, K., MALMSTROM, M. E. and NERETNIEKS, I., 2008. Modelling retention of heavy metals in the Oostriku peat bog, Estonia; comparison of predicted and observed results. *Applied Geochemistry*. **23**(6), 1498-1512.

TANG, J. and JOHANNESSON, K. H., 2005. Adsorption of rare earth elements onto Carrizo sand: Experimental investigations and modeling with surface complexation. *Geochimica et Cosmochimica Acta*. **69**(22), 5247-5261.

TANG, J. and JOHANNESSON, K. H., 2010. Ligand extraction of rare earth elements from aquifer sediments: Implications for rare earth element complexation with organic matter in natural waters *Geochimica et Cosmochimica Acta*. **Accepted**.

TIPPING, E., 2002. *Cation binding by humic substances*. Cambridge Environmental Chemistry Series, **12**. Cambridge University Press, 434 pp.

UNSWORTH, E. R., WARNKEN, K. W., ZHANG, H. et al., 2006. Model Predictions of Metal Speciation in Freshwaters Compared to Measurements by In Situ Techniques. *Environmental Science and Technology*. **40**(6), 1942-1949.

VAN STRAATEN, B. I., KOPYLOVA, M. G., RUSSELL, J. K., WEBB, K. J. and SMITH, B. H. S., 2009. Stratigraphy of the intra-crater volcaniclastic deposits of the Victor Northwest kimberlite, northern Ontario, Canada. *Lithos*. **112**(Supplement 1), 488-500.

WEBB, K. J., SCOTT SMITH, B. H., PAUL, J. L. and HETMAN, C. M., 2004. Geology of the Victor Kimberlite, Attawapiskat, northern Ontario, Canada; cross-cutting and nested craters. *Lithos*. **76**, 29-50.

WHITICAR, M. J., 1999. Carbon and hydrogen isotope systematics of bacterial formation and oxidation of methane. *Chemical Geology*. **161**(1-3), 291-314.

WHITICAR, M. J. and FABER, E., 1986. Methane oxidation in sediment and water column environments; isotope evidence. *Organic Geochemistry*. **10**, 759-768.

WHITICAR, M. J., FABER, E. and SCHOELL, M., 1986. Biogenic methane formation in marine and freshwater environments; CO (sub 2) reduction vs. acetate fermentation; isotope evidence. *Geochimica et Cosmochimica Acta*. **50**(5), 693-709.

WILSON, L. and HEAD, J. W. I., 2007. An integrated model of kimberlite ascent and eruption. *Nature*. **447**, 53-57.

YU, K., BOHME, F., RINKLEBE, J., NEUE, H.-U. and DELAUNE, R. D., 2007. Major Biogeochemical Processes in Soils-A Microcosm Incubation from Reducing to Oxidizing Conditions. *Soil Science Society of America Journal*. **71**(4), 1406-1417.

Appendices

APPENDIX 1 – EXTENDED ABSTRACT FROM THE 24TH INTERNATIONAL APPLIED GEOCHEMISTRY SYMPOSIUM

Imaging a buried diamondiferous kimberlite using conventional geochemistry and Amplified Geochemical Imaging[SM] Technology

Jamil. A. Sader[1], Harry. S. Anderson II[2], Ray. F. Fenstermacher[2] & Keiko Hattori[1]

[1]*University of Ottawa, Earth Sciences Department, Ottawa, Ontario K1N 6N5, Canada (e-mail:*

[2]*W. L. Gore & Associates, Inc. 100 Chesapeake Blvd, Elkton, MD, USA*

ABSTRACT: Accurate mapping of mineral deposits buried by tens to hundreds of meters of overburden will focus an exploration program, minimizing costs and time expended. Traditional surface geochemical techniques often focus on measuring and mapping metal ions in the soil or vegetation, water/soil chemical properties, and by-product gases such as oxygen and carbon dioxide. A new technique, Amplified Geochemical Imaging[SM] Technology, focuses on high sensitivity measurements of volatile compounds emanating from the mineral deposit itself, its contact zone, or associated redox systems. Compounds ranging from light sulphur species to organics with 18 carbon atoms, which are found at the surface, are collected and analyzed using a sensitive and sophisticated analytical technique. Differentiation of compounds associated with the mineralization and a robust image of the buried deposit are then obtained by processing the data using advanced modelling systems and multivariate statistical methods. This new technique works well with high content sulphur minerals such as those deposits hosted in Volcanogenic Massive Sulphide, porphyry Cu, Mississippi Valley-type, and some gold systems. In this paper, Amplified Geochemical Imaging[SM] Technology, along with conventional surface geochemical analysis, was used to image a kimberlite.

KEYWORDS: *diamond, kimberlite, soil geochemistry, imaging, volatile*

INTRODUCTION

In regions where bedrock is covered by thick sediments, application of surficial geochemical exploration methods has led to a great deal of success. This paper identifies responses of Gore Amplified Geochemical Imaging[SM] (GAGI) compounds ranging from light sulphur species to organics with 18 carbon atoms (Anderson 2006) over kimberlites, which correlate well with geochemical responses in soil.

GEOLOGICAL SETTING

The Honerat kimberlite is approximately 45 km east of the town of Ville-Marie, western Quebec, Canada (Fig. 1). Gravity surveys and drilling have indicated that the kimberlite was emplaced along a normal fault structure trending NW-SE. Kimberlites in this region are of Jurassic age. The Honerat kimberlite is approximately 85 m in diameter, based on company drill logs. The subcropping surface of the kimberlite consists of hypabyssal facies kimberlite. Country rocks are dominantly Archean felsic to intermediate metavolcanics and the surficial sediments sampled at Honerat consisted of clay with minor silt to silt with minor clay. Continental-scale glaciation has affected the region several times during the Quaternary. The most recent glaciation retreated from the study area approximately 8000 years BP (Veillette 1994), during which time thick deposits (45 to 90 m) of unconsolidated glacial,

glaciofluvial and glaciolacustrine sediments were deposited over the Honerat kimberlite.

A second location approximately 5 km south of the Honerat kimberlite was also studied (named Unknown) (Fig. 1).

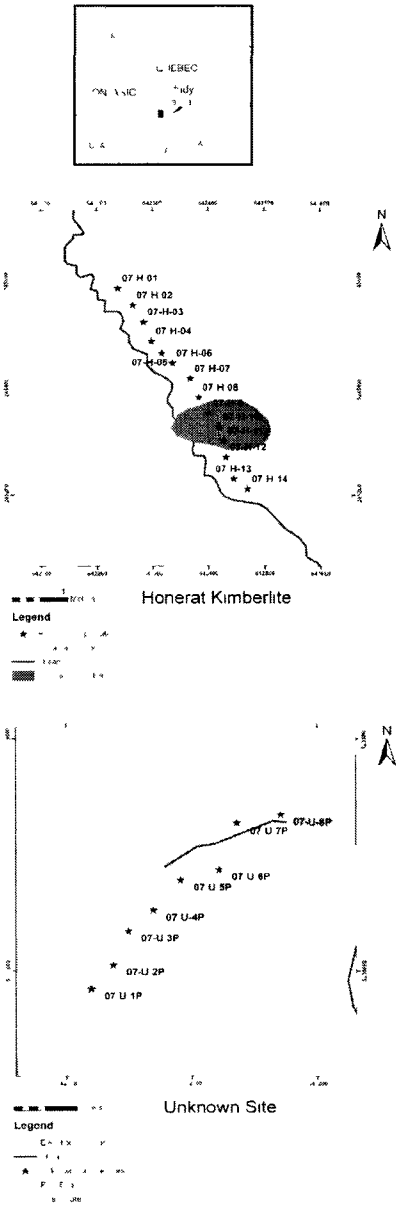

Fig. 1. The Honerat kimberlite and the Unknown Site are located in western Quebec, Canada. The labeled points represent sample collection sites along transects at Honerat and Unknown.

Although no kimberlite is known of in this second area, kimberlite boulders and elevated kimberlite indicator mineral counts in glacial sediments have been found within 300 m of the Unknown site. This location was also interpreted to be a possible site for a kimberlite pipe because it is along a NE-SW trending graben structure. The terrain at Unknown is saturated peat, between 1 and 4 m deep, which overlies fine gravel. Depth to bedrock at this test site is not known.

METHODS

Soil samples were collected along a traverse over the Honerat kimberlite and extended off the kimberlite approximately 75 m SE and 225 m NW from the pipe's centre (Fig. 1). Although it is common practice to collect samples from upper B-horizon soil (Levinson 1980; Bajc 1998; Mann *et al.* 2005) our samples were collected from C-horizon soil because GAGI samplers were placed at a depth of 60 cm (well below the B horizon). Within 8 hours of sampling, a portion of each soil sample was mixed with Milli-Q water (1:1) to create a slurry. The values of pH and oxidation-reduction potential (ORP) were determined in each slurry. Ammonia acetate leach of the soil samples were performed at Acme Analytical Laboratories, Vancouver, where 20 ml of ammonium acetate was mixed with 1 g soil sample and elements were determined by inductively coupled plasma-mass spectrometry. The GAGI samplers installed at Unknown were placed in piezometers and submerged in water at a depth of approximately 1 m below ground surface.

The GAGI samplers, installed along traverses at both Honerat and Unknown, were left in place for 5 months before being retrieved. Retrieved samplers from both locations were sent to Gore Laboratories where they were heated, and compounds were thermally desorbed and analyzed with a gas chromatograph/mass spectrometer (GC/MS).

RESULTS AND DISCUSSION

Soil slurry ORP values are lower over the Honerat kimberlite (near 0 mV) compared to other locations along the sampling traverse (up to 100 mV). Over this kimberlite there is also a marked depletion in concentrations of a variety of elements such as Ni, Mg, Co, K, and total REEs in soil directly over the kimberlite (Fig. 2). Conversely, enrichments of these elements at the margin(s) of the kimberlite are evident. The elemental results are similar to the soil geochemical signature over the 95-2 kimberlite, approximately 60 km to the west (McClenaghan *et al.* 2006).

Reduced ions from the Honerat kimberlite are accumulating in the surface soil producing low ORP values. Low ORP values over the kimberlite with high values near the margins suggest the presence of a "reduced chimney" (Hamilton *et al.* 2004a, 2004b), where reduced species (such as Fe^{2+}) are migrating from the underlying kimberlite through glacial sediments to surface.

The partial leach results from soil samples identify the location of the buried Honerat kimberlite. The depletion of Ni, Mg, Co, K, and total REEs in C-horizon soils over the Honorat kimberlite suggests that numerous kimberlite pathfinder elements are not adsorbed on to soil particles. Instead, they are remaining in the dissolved phase in solution due to the more reducing environment inside compared with outside the kimberlite. However, as elements migrate out of the kimberlite "reduced chimney" environment into a more oxidizing environment, they may adsorb to soil particles, possibly oxyhydroxide complexes and produce elevated element responses at the margins of the kimberlite.

The data obtained by GAGI correlate well with soil geochemical data for the Honorat kimberlite. Individual components of the Gore analysis such as elevated dimethyl sulfide, and lower concentrations of methyl butane (Fig. 3a & b) are found at the same locations as low relative element concentrations and more reducing conditions. The spatial correlation between changes in the redox conditions, the depletion of metals, and some GAGI compounds suggests either the upward migration of GAGI compounds from the kimberlite or their formation/depletion in soil due to changing redox conditions. We suggest the latter interpretation based on the variation of $\delta^{13}C$ for dissolved inorganic carbon (DIC) in peat groundwaters from Unknown. The values of $\delta^{13}C$ compared with concentrations of sulfide and hydrocarbons suggest biogenic reactions with inorganic carbon.

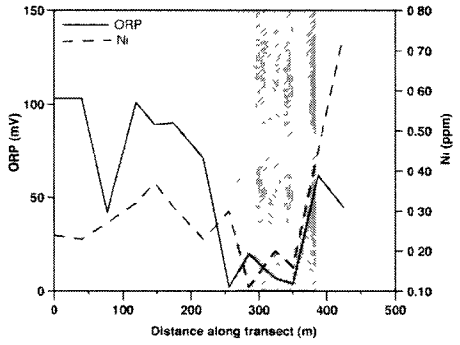

Fig. 2. Low relative ORP values correlate with low Ni values in soils over the Honerat kimberlite (depicted as the grey zone).

CONCLUSIONS

This paper demonstrates that, in addition to soil geochemical exploration techniques, Gore Amplified Geochemical Imaging[SM] is another tool for the exploration geochemist.

1) Kimberlite bodies can be identified at ground surface using soil geochemistry where 90 m of glacial sediment overlies a kimberlite. This is based on variations in element concentrations of pathfinder elements such as Ni, Mg, Co, K, and total REEs over versus off a kimberlite.

2) The Gore Amplified Geochemical Imaging[SM] technique, like soil geochemistry, shows anomalous concentrations of sulfides and hydrocarbons in soils over the kimberlite.

3) Values of $\delta^{13}C$-DIC correlate with some hydrocarbons at the Unknown Site and suggest that Amplified Geochemical

Imaging[SM] responses could be the result of surficial bacterial communities that thrive over kimberlites.

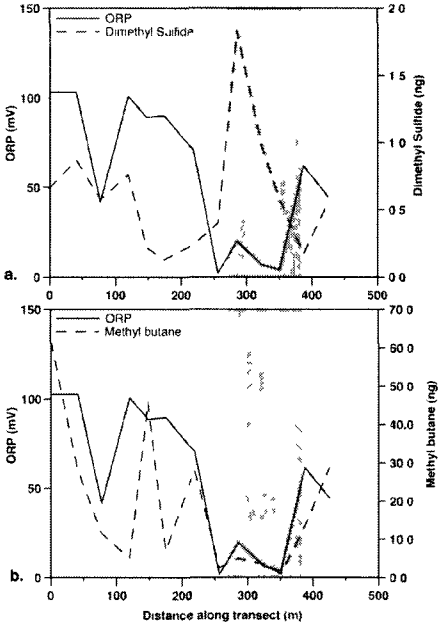

Fig. 3. High concentrations of dimethyl sulfide (a) and depleted concentrations of methyl butane (b) correlate with reducing soils over the kimberlite (depicted as the grey zone).

ACKNOWLEDGEMENTS

We thank Dr. Thomas Morris, President and CEO, and Mr. Matthew Sooley of Northern Superior Resources for providing information on, and access to the site. Field expenses and analytical costs were supported by an NSERC Discovery Grant.

Funding for this project was also provided in part by an Ontario Graduate Scholarship (support for Jamil Sader's Ph.D.) and a student research grant from the Society of Economic Geologists.

REFERENCES

ANDERSON, H.S. II. 2006. Amplified Geochemical Imaging: An Enhanced View to Optimize Outcomes. *EAGE First Break*, 24, August 2006, 77–80.

BAJC, A.F. 1998. A comparative analysis of enzyme leach and mobile metal ion selective extractions; case studies from glaciated terrain, northern Ontario. *Journal of Geochemical Exploration,* **61**, 113-148.

HAMILTON, S.M., CAMERON, E.M., MCCLENAGHAN, M.B., & HALL, G.E.M. 2004a. Redox, pH and SP variation over mineralization in thick glacial overburden. Part I: methodologies and field investigation at the Marsh Zone gold property. *Geochemistry: Exploration, Environment, Analysis,* **4**, 33-44.

HAMILTON, S.M., CAMERON, E.M., MCCLENAGHAN, M.B., & HALL, G.E.M. 2004b. Redox, pH and SP variation over mineralization in thick glacial overburden; Part II, Field investigation at Cross Lake VMS property. *Geochemistry - Exploration, Environment, Analysis,* **4**, 45-58.

LEVINSON, A.A. 1980. *Introduction to Exploration Geochemistry*. Applied Publishing, Wilmette, Illinois.

MANN, A.W., BIRRELL, R.D., FEDIKOW, M A.F., & DE SOUZA, H.A.F. 2005. Vertical ionic migration; mechanisms, soil anomalies, and sampling depth for mineral exploration. *Geochemistry - Exploration, Environment, Analysis,* **5**, 201-210.

MCCLENAGHAN, M.B., HAMILTON, S.M., HALL, G.E.M., BURT, A.K., & KJARSGAARD, B.A. 2006. Selective Leach Geochemistry of Soils Overlying the 95-2, B30, and A4 Kimberlites, Northeastern Ontario. *Geological Survey of Canada*, Open File 5069.

VEILLETTE, J.J. 1994. Evolution and paleohydrology of glacial lakes Barlow and Ojibway. *Quaternery Science Reviews,* **13**, 945-971.

APPENDIX 2 – KIMBERLITE PATHFINDER METAL PROFILES ALONG A TRANSECT AT CONTROL SITE

Peat groundwater pathfinder metals plotted for Control Site (Fig. A2-1 to 5) were collected in the Fall (September) of 2006 at 0.4 meters below ground surface (mbgs). This data was collected and reported by Brauneder (2007). As these samples were collected at 0.4 mbgs, they have not been included in the determination of baseline values for pathfinder metal in peat groundwater samples collected at 1.1 mbgs in Chapter 1. Geophysical data (DeBeers unpublished) suggest that there is no kimberlite in the vicinity of the Control site.

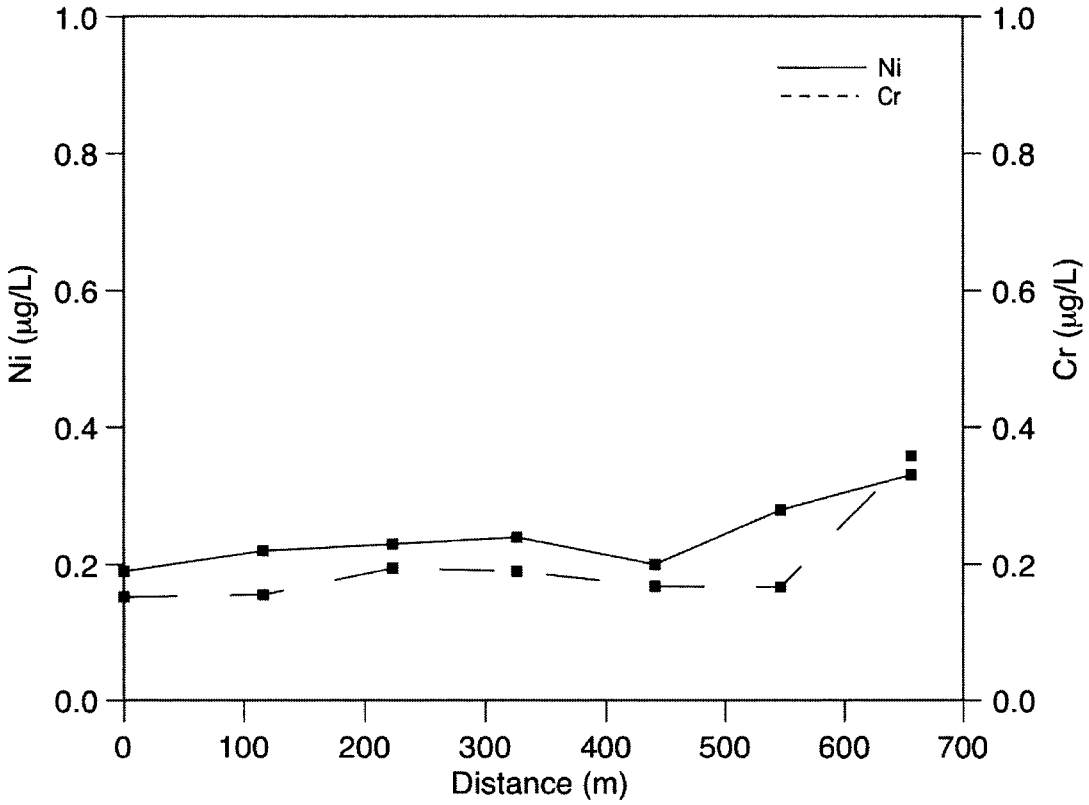

Figure A2-1. The profile of Ni and Cr along a transect over the Control site.

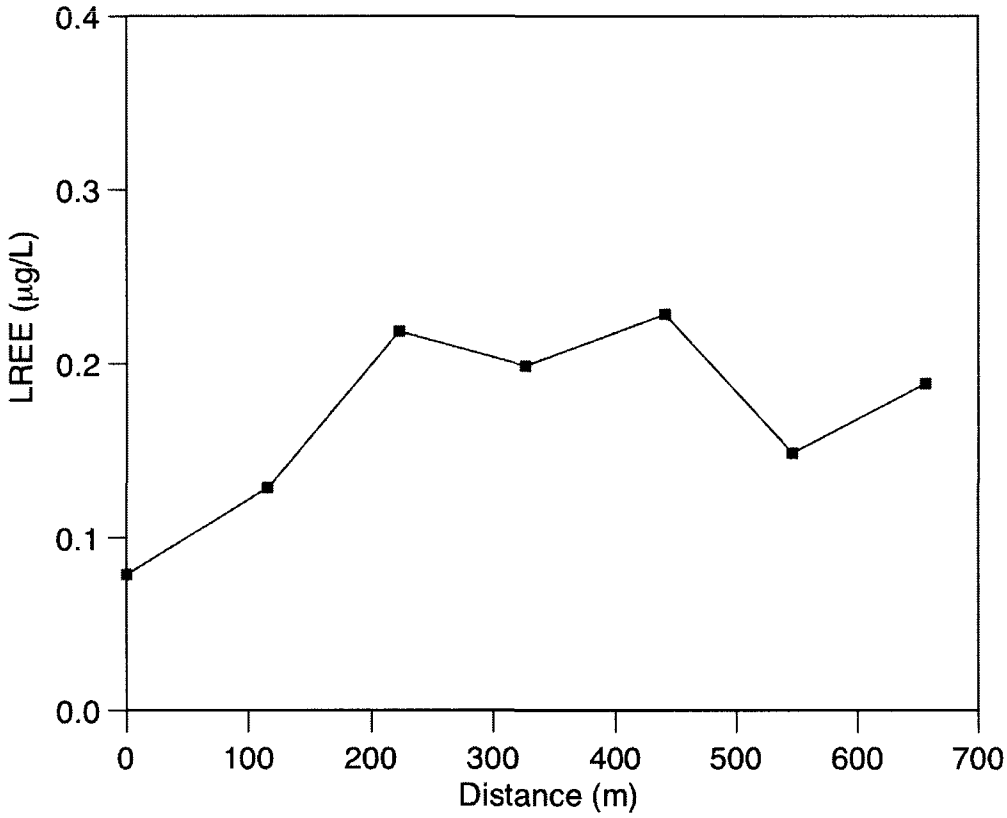

Figure A2-2. The profile of light rare earth elements (LREEs) along a transect over the Control site.

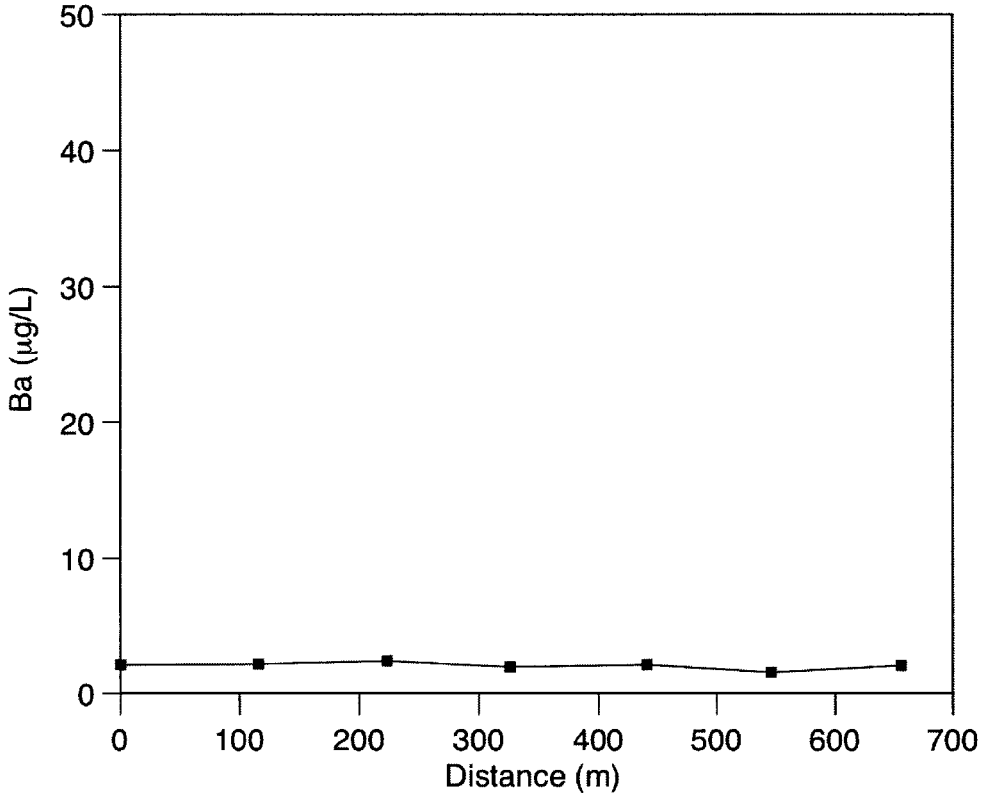

Figure A2-3. The profile of Ba along a transect over the Control site.

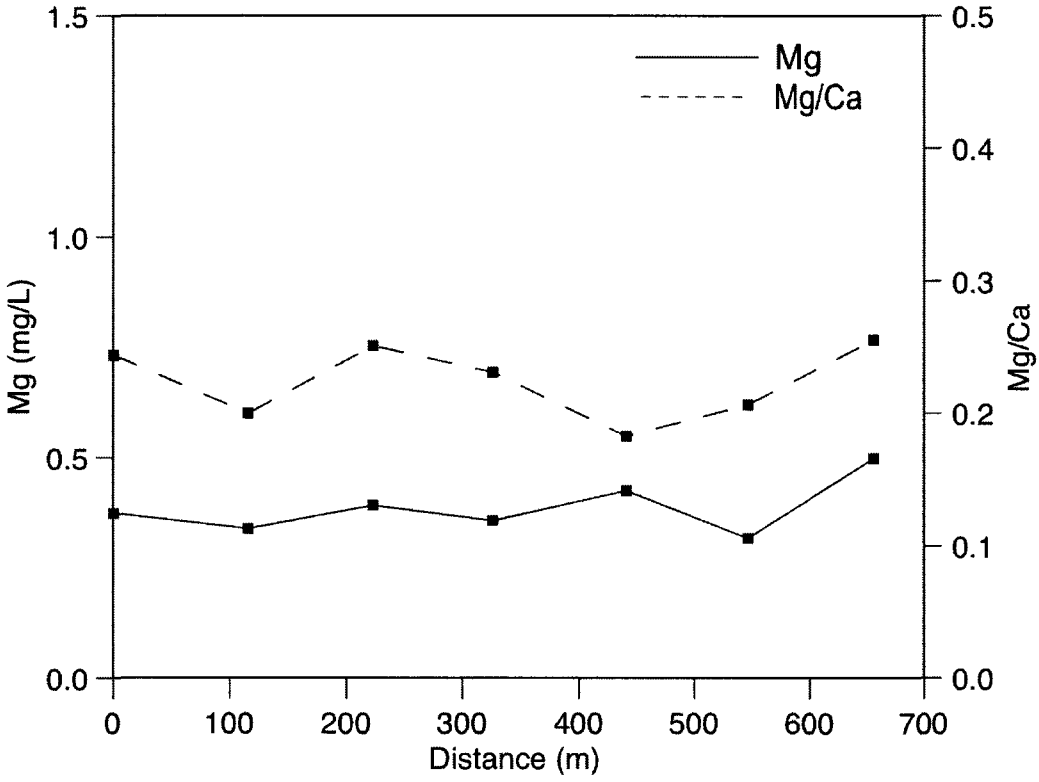

Figure A2-4. The profiles of Mg and Mg/Ca along a transect over the Control site.

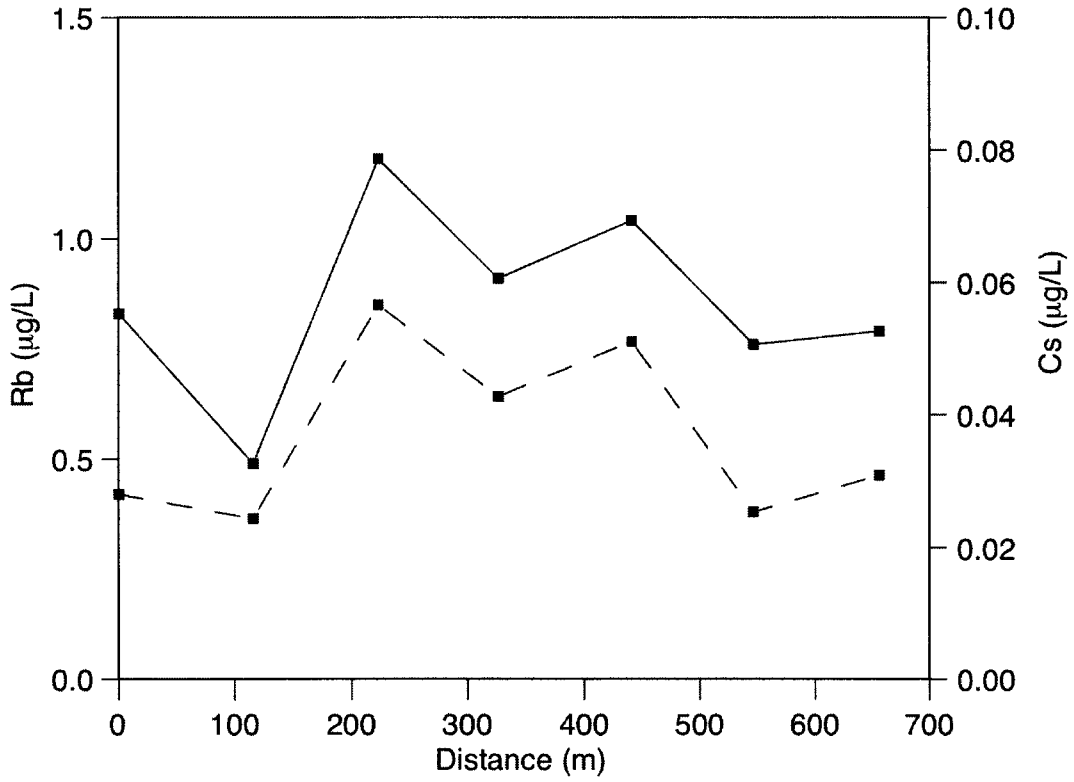

Figure A2-5. The profiles of Rb and Cs along a transect over the Control site

APPENDIX 3 - SEASONAL AND DEPTH CONTROLS ON METAL CONCENTRATIONS IN PEAT GROUNDWATER

Peat groundwater samples were collected at Attawapiskat kimberlites (Yankee, Golf and Alpha-1) in summer (early August) 2006. Select sample sites sampled in summer 2006 were also sampled in the Fall (late September) of 2006. All peat groundwater samples from 2006 (0.4 mbgs) were collected and reported by (Brauneder, 2007). Peat groundwater samples were also collected from Yankee, Zulu, Alpha-1, and Bravo-1 in the summer (August 14 - 23) of 2007. Select sites that were sampled in the Summer of 2007 were sampled in the Fall of 2007 (October 14-18). All samples from 2007 were collected at 1.1 mbgs.

A Wilcoxon matched pairs signed-ranks statistical analysis was conducted to compare summer 2006 to fall 2006, and summer 2007 to fall 2007 pathfinder metal concentrations. This statistical analysis was used because in many cases metal concentrations for a given sample set (i.e. summer or fall 2007) do not have a normal distribution. Definitions of each variable are listed in Table A3-1. "p" values < 0.05 indicate a statistical difference, and "p" values > 0.05 indicate there is little to no statistical difference to a 95% confidence interval between the sample sets of a given year.

Precipitation in the Summer and Fall of seasons of 2006 and 2007

Cumulative rainfall for the July and August 2006 was 172 mm. It was significantly lower (74.5 mm) for September and October 2006. During July and August 2007 rainfall was 179 mm and was almost identical to precipitation for the same period in 2006. However, the rainfall in September and October 2007 was significantly higher (262 mm), and Environment Canada (2007) indicated it was one of the wettest fall seasons on record for the

region. All rainfall data was collected by Environment Canada at the nearest monitoring station, Moosenee, Ontario (approximately 250 km SE of the study locations).

Seasonal differences in metal concentrations between the Summer and Fall of 2006

Peat groundwaters collected at 0.4 mbgs during summer 2006 contained lower concentrations of Mg, Rb, and Cl compared with samples collected in fall 2006 at the same locations and are statistically different (Fig. A3-1). The concentrations of the transition metals LREE and Cr are statistically higher in the summer compared with fall 2006 ($p < 0.05$). However, there is no statistical difference between the concentrations of Ni in the summer and fall of 2006 ($p > 0.05$) (Fig. A3-1).

Seasonal differences in metal concentrations between the Summer and Fall of 2007

For peat groundwater samples collected in summer and fall 2007 at 1.1 mbgs (within the deeper catetolem peat zone), the concentrations of Mg, Cr, and Ni are not statistically different (Fig. A3-2). Rubidium, Cl-, and LREEs differ between the 2 seasons and tend to be lower in the Fall of 2007, when rainfall amount for the combined months of September and October was high (262 mm).

Differences in metal concentrations in groundwaters collected at 0.4 and 1.1 mbgs at Yankee

Calcium, Mg and Rb concentrations in peat groundwaters collected at 0.4 mbgs in summer 2006 (Brauneder 2007) are on average only 33 and 23%, respectively, of concentrations in waters collected at 1.1 mbgs (summer 2007) along the transect over the Yankee kimberlite (Fig. A3-3). Transition metals (Ni, Cr, and LREEs) overall display similar concentrations at

0.4 and 1.1 mbgs. However, concentrations of Ni, Cr, and LREEs are particularly enhanced at sites of inferred groundwater upwelling (153, 349, 370 and 442 m) along the Yankee transect at 1.1 mbgs compared with 0.4 mbgs. The differences in metal concentrations between the summers of 2006 and 2007 is not likely due to variations in precipitation between the two years. The rainfall for the months of July and August 2006 and 2007 only varied by 7 mm, or 4% Environment Canada (2007).

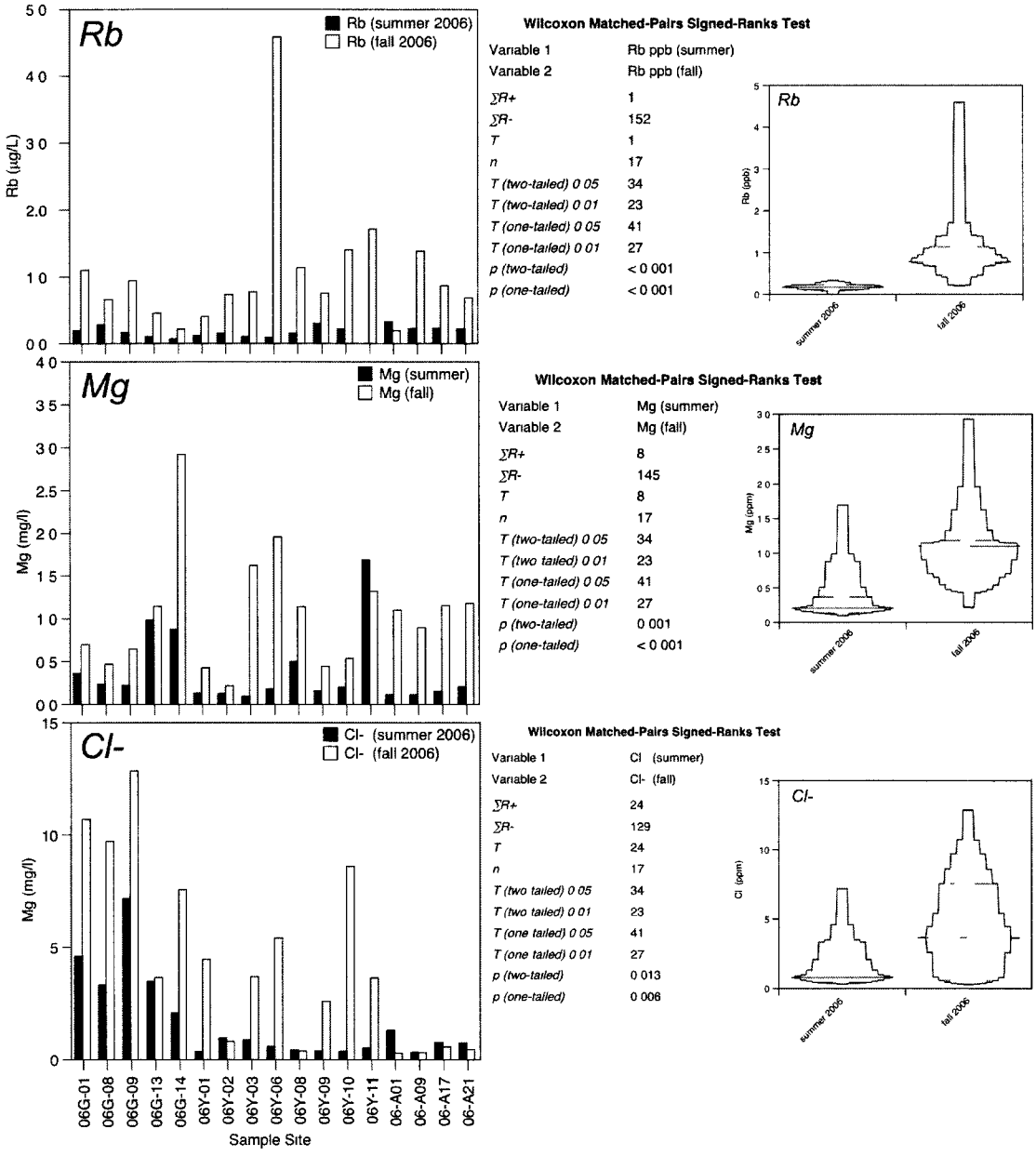

Figure A3-1. Bar charts and Wilcoxon matched-pairs signed-ranks test for Rb, Mg, Cl-, LREE, Cr, and Ni in peat groundwater samples collected in the Summer and Fall of 2006 at a depth of 0.4 mbgs. Continued on next page.

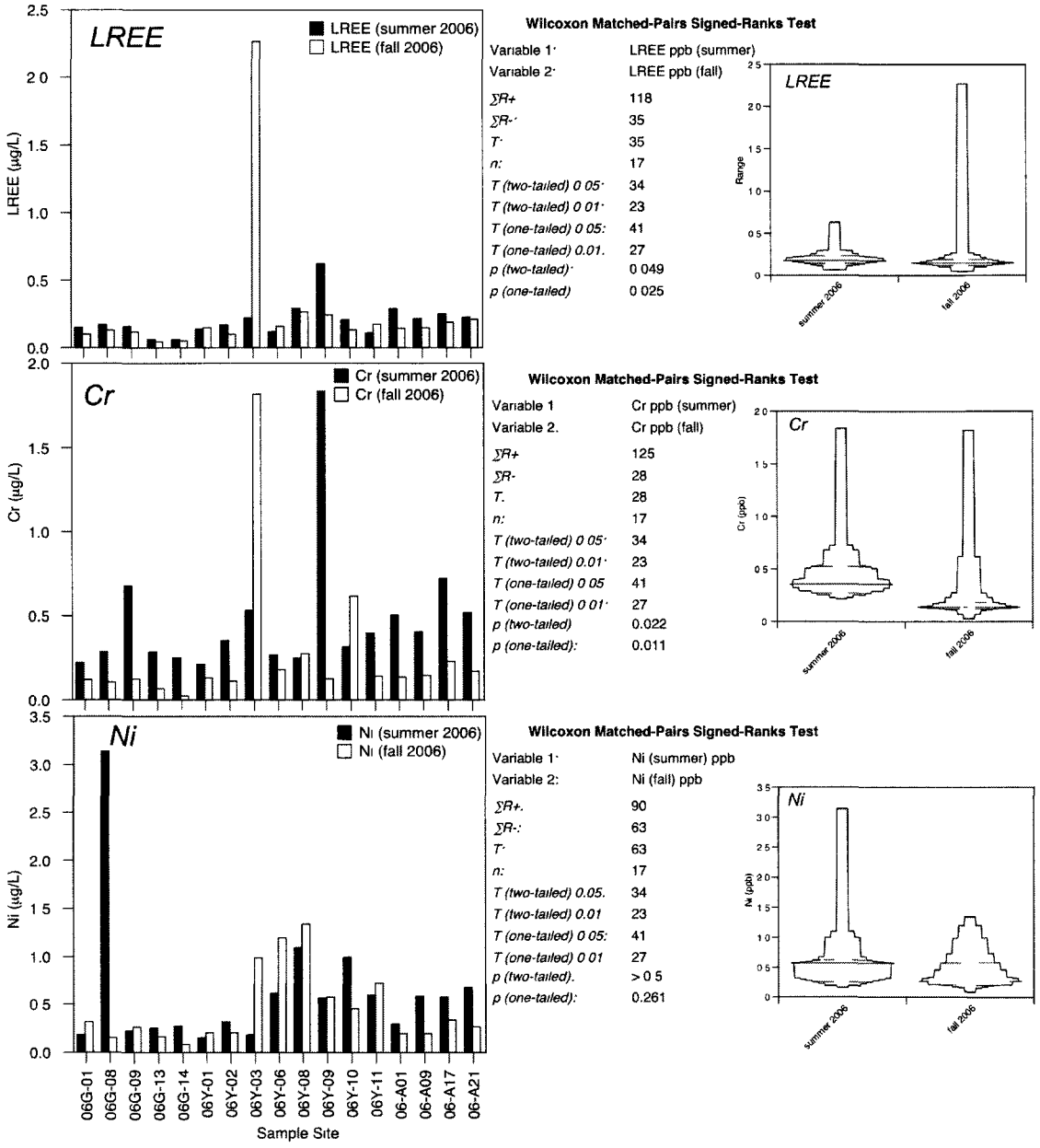

Figure A3-1. Continued.

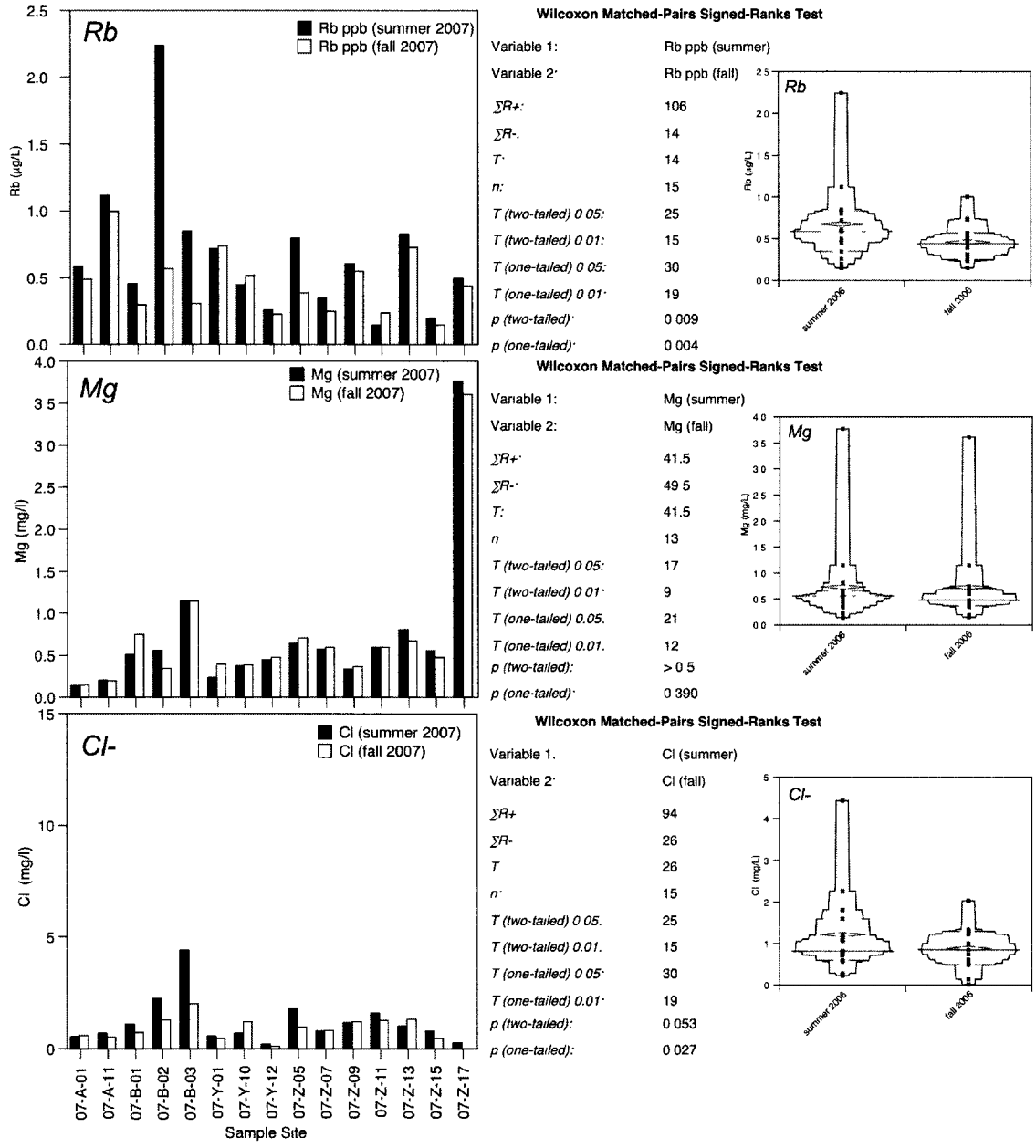

Figure A3-2. Bar charts and Wilcoxon matched-pairs signed-ranks test for Rb, Mg, Cl-, LREE, Cr, and Ni in peat groundwater samples collected in the Summer and Fall of 2007 at a depth of 1.1 mbgs. Continued on next page.

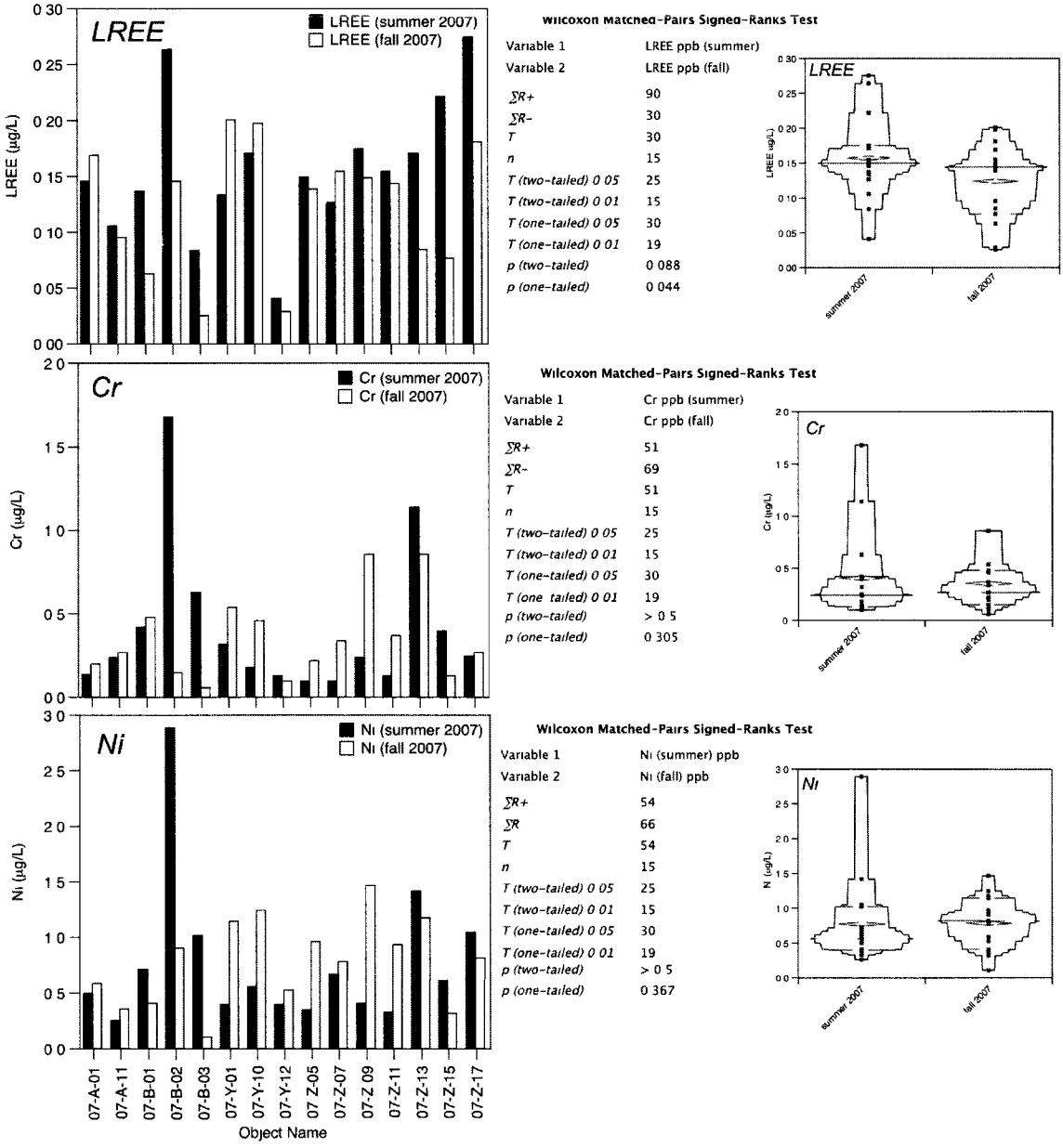

Figure A3-2. Continued.

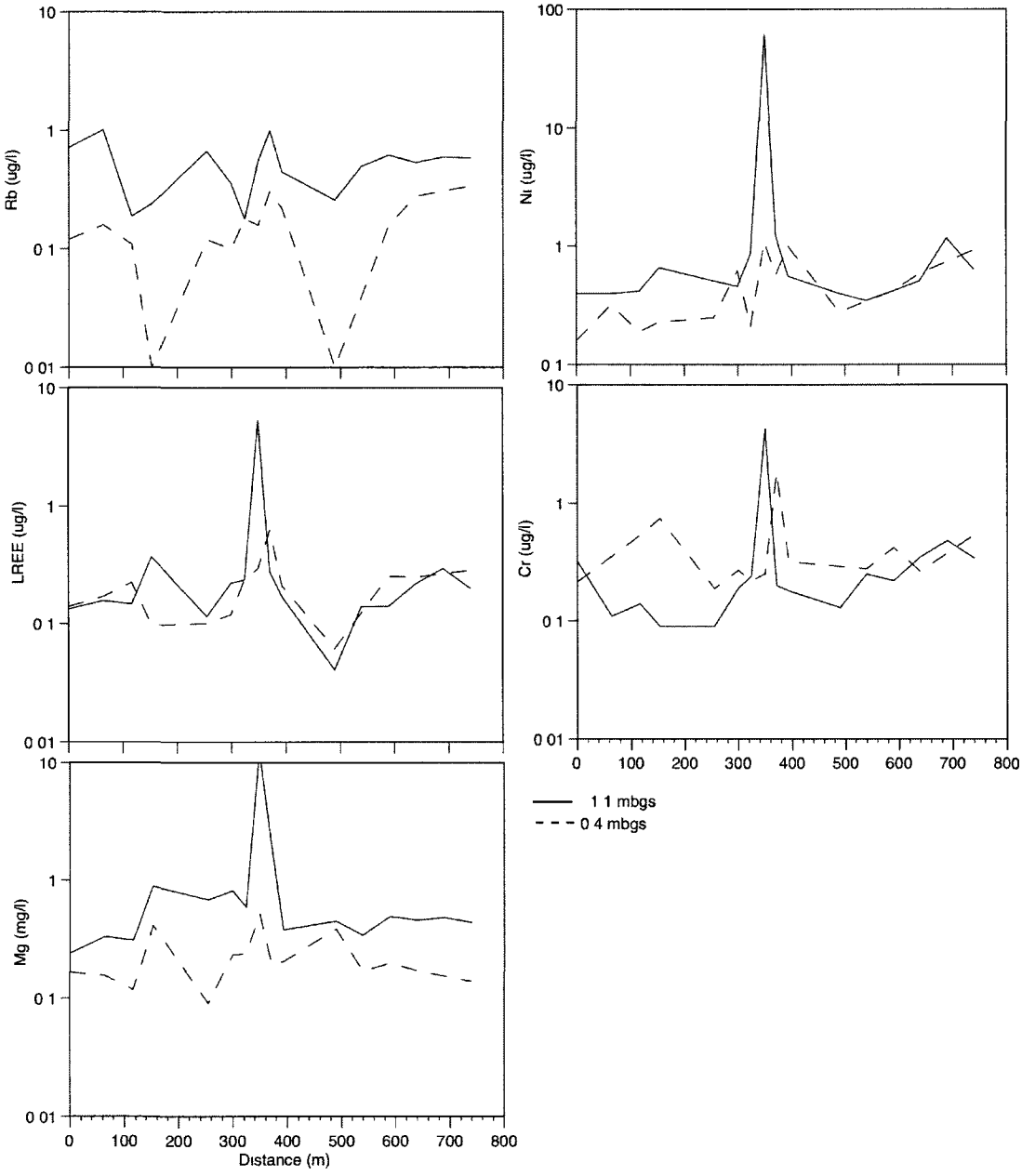

Figure A3-3. Profiles for Rb, LREEs, Mg, Ni, and Cr along the Yankee transect at 0.4 and 1 1 mbgs. Note that samples collected at 0.4 mbgs are from summer 2006 and samples collected at 1.1 mbgs were collected in summer 2007. Precipitation amounts for the months of July and August 2006 and 2007 were almost identical.

Table A3-1. Descriptions of variables used with the Wilcoxon matched-pairs signed-ranks tests

Variable	Description
Σ R+	The sum of positive rank differences
Σ R-	The sum of negative rank differences
T	The observed Wilcoxon T statistic
n	The number of non-zero differences
T (two-tailed) 0.05	Critical T (two-tailed) value at the 0.05 significane level
T (two-tailed) 0.01	Critical T (two-tailed) value at the 0.01 significane level
T (one-tailed) 0.05	Critical T one-tailed) value at the 0.05 significane level
T one-tailed) 0 01	Critical T one-tailed) value at the 0.01 significane level
p (two-tailed)	paired value to compare to a perscribed level of significance (0.05)
p one-tailed)	paired value to compare to a perscribed level of significance (0.05)

APPENDIX 4 - REDOX AND DEPTH CONTROLS ON $\delta^{13}C_{CO2}$ IN PEAT GROUNDWATERS

The $CO_{2(aq)}$ concentrations in peat groundwaters range from 0.15 to 4.5 mmol/L, averaging 1.4 mmol/L. The $\delta^{13}C_{CO2}$ along the Yankee sampling transect is saw-tooth shaped and low $\delta^{13}C_{CO2}$ values (-23.6, -16.0, and -18.6‰) exist over the kimberlite at sample sites 07-Y-08, 09, and 12, respectively, and also at 07-Y-04 (outside the kimberlite margin) (Fig. A4-1). Sample 07-Y-04 is a site of inferred groundwater upwelling near a bioherm based on elevated geochemical parameters and a peizometer water level that was greater than standing water (Sader *et al.*, 2010). The $\delta^{13}C_{CO2}$ values along the Zulu and Golf kimberlite transects are less variable. However, $\delta^{13}C_{CO2}$ values still fluctuate by 8 to 10‰ along the length of the transect (Fig. A4-1). The values of $\delta^{13}C_{CO2}$ trend to heavier values with increasing depth of peat groundwater sample collection below the saturated zone (Fig. A4-2). Note that the $\delta^{13}C_{DIC}$ values and DIC concentrations ($CO_2 + HCO_3^- + CO_3^{2-}$) for peat groundwaters were recalculated to represent $\delta^{13}C_{CO2}$ values and $CO_{2(aq)}$ based on pH, because of the wide range of pH values measured in the peat groundwaters. Normalizing peat groundwater $\delta^{13}C_{DIC}$ values to $\delta^{13}C_{CO2}$ removes the effect of pH on isotope values of soluble carbon species. $\delta^{13}C_{CO2}$ peat groundwater values vary widely (-22‰ to +4.5‰) (Table A4-1). The $\delta^{13}C_{DOC}$ values are consistently -27 ±1‰ for peat groundwaters (Brauneder, 2007).

The pH values in peat groundwaters range from 3.2 to 7.1 and the Eh values range from 125 to 550 mV (Table 4A-1). Samples from Golf have the lowest pH and highest Eh values of the three kimberlites; most likely a function of the shallower groundwater collection depth (0.4 mbgs). Concentrations of DO are on average low over Zulu and Yankee kimberlites compared to the concentrations outside their margins and ranged from

< 0.004 to 0.13 mmol/L (Table 4A-1). Sulfate concentrations in peat groundwater are an average 4.3 μmol/L. The maximum concentration is 11 μmol/L, and many peat groundwater samples were near the detection limit (0.4 μmol/L) (Table 4A-1). Iron concentrations in peat groundwaters vary from 2 to 80 μmol/L and on average are an order of magnitude greater than mean SO_4^{2-} concentrations. The percentage of Fe^{3+} relative to total Fe concentrations ($Fe^{3+}/Fe_{total}x100$) is high along transects over Zulu and Golf kimberlites (Fig. 4A-3; Table 4A-2). Iron speciation was calculated using Geochemist's WorkBench (Bethke, 2002). Percent Fe^{3+} values are highly variable along the Yankee transect (from 45 to 100%) and are elevated at the kimberlite margins, as well as a the groundwater discharge zone near the bioherm (07-Y-04) (Sader *et al.*, 2010). High percentages of Fe^{3+} and small variations along the transect at Golf relative to Yankee and Zulu (Fig. A4-3) is likely a function of the more oxidizing conditions due to the shallower sample depth.

The redox state of peat groundwaters is important in the CO_2-CH_4 cycle. $\delta^{13}C_{CO2}$ values (up to 4.5‰) in peat groundwater are most likely due to Rayleigh fractionation processes resulting from CO_2 reduction. The consumption of DO and the reduction of Fe^{3+} represent possible pathways responsible for the oxidation of CH_4 in the peat groundwaters. The lowest $\delta^{13}C_{CO2}$ values were observed where conditions dominantly consist of Fe^{3+}, and/or where DO was detected (Fig. A4-4). The increase in $\delta^{13}C_{CO2}$ values with decreasing DO and Fe^{3+} concentrations suggests CH_4 oxidation and Fe^{3+} reduction via Equation 5 and 6:

$$CH_4 + 2O_2 \rightarrow CO_2 + 2H_2O \quad (5)$$

$$CH_4 + 8Fe^{3+} + 3H_2O \rightarrow HCO_3^- + 8Fe^{2+} + 9H^+ \quad (6)$$

Elevated Fe^{3+} ions in the peat groundwater likely provide bacteria with a source of electron acceptors for CH_4 oxidation. It has been suggested that biological reduction of Fe^{3+} in rice paddies stimulates CH_4 oxidation and inhibits production (Miura *et al.*, 1992; Kumaraswamy *et al.*, 2001). Because SO_4^{2-} concentrations in peat groundwater are low (in many cases below the detection limit of 0.4 μmol/L), and because the S content of the peat is low (< 0.1%) (Hattori and Hamilton, 2008), it is unlikely that SO_4^{2-} plays a significant role in CH_4 oxidation within the peat.

The depth at which waters were collected below the water table may influence $\delta^{13}C_{CO2}$ values (and the redox conditions) observed along transects. Sites with the highest $\delta^{13}C_{CO2}$ values are those where samples were collected deepest below the water table and where the Eh values indicate conditions are most reducing. Progressively more reducing conditions and higher $\delta^{13}C_{CO2}$ values with depth of peat groundwater sample collection are consistent with other studies (Lansdown *et al.*, 1992; Beer and Blodau, 2007; Hornibrook and Bowes, 2007). These studies have shown that with increasing depth in peat groundwater, there are fewer oxidized ions and biological CO_2 reduction becomes a dominant redox process.

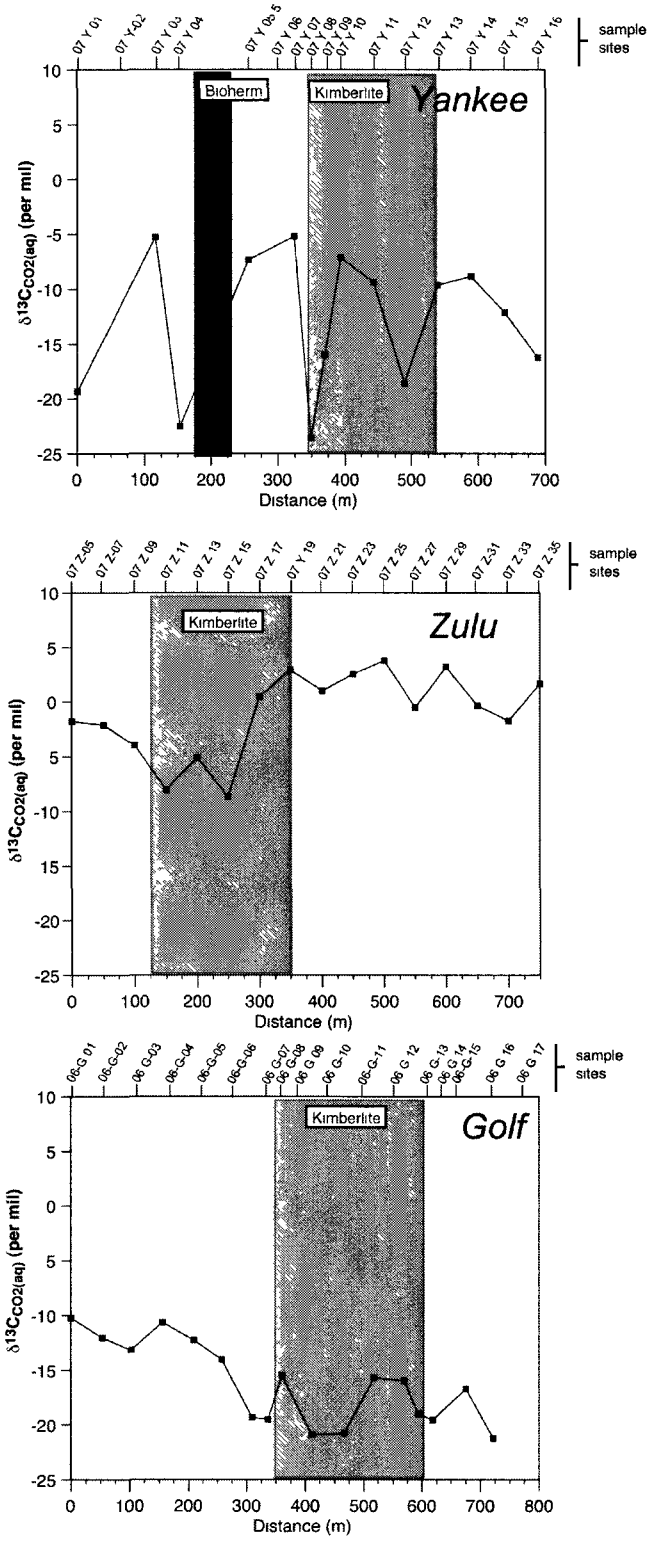

Figure A4-1. $\delta^{13}C_{CO2}$ profiles along transects over kimberlites a) Yankee, b) Zulu, and c) Golf

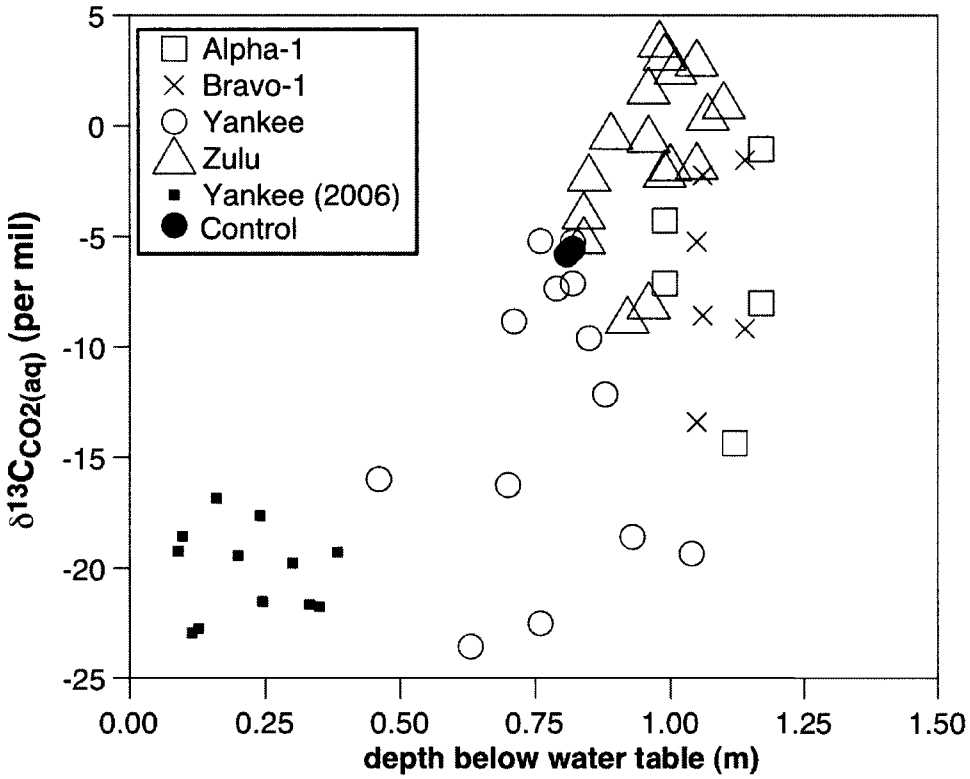

Figure A4-2. C isotopic values of CO_2 become heavier with increasing sample depth below the water table Note that Yankee (2006) data is from Brauneder (2007) The depths below water table for those data are based on water table elevations from 2007 This is a reasonable approximation of elevation, as summer 2006 and 2007 precipitation was almost identical for the 2 summers

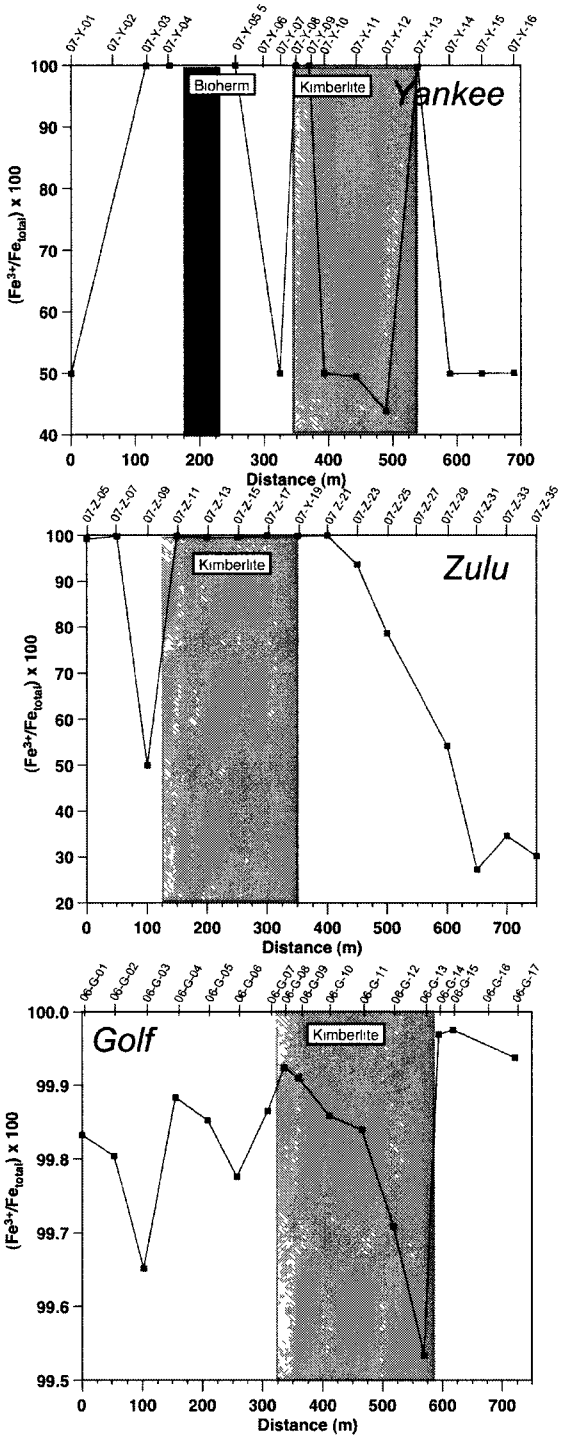

Figure A4-3. $(Fe^{3+}/Fe_{total}) \cdot 100$ ratios over kimberlites: a) Yankee, b) Zulu, and c) Golf. Ferric Fe is commonly elevated relative to total Fe at sites where the $\delta^{13}C_{CO2}$ values are lowest and where sample depth below the water table is least (Table A4-1). The Fe speciation data was calculated using Geochemists Workbench (Bethke, 2002).

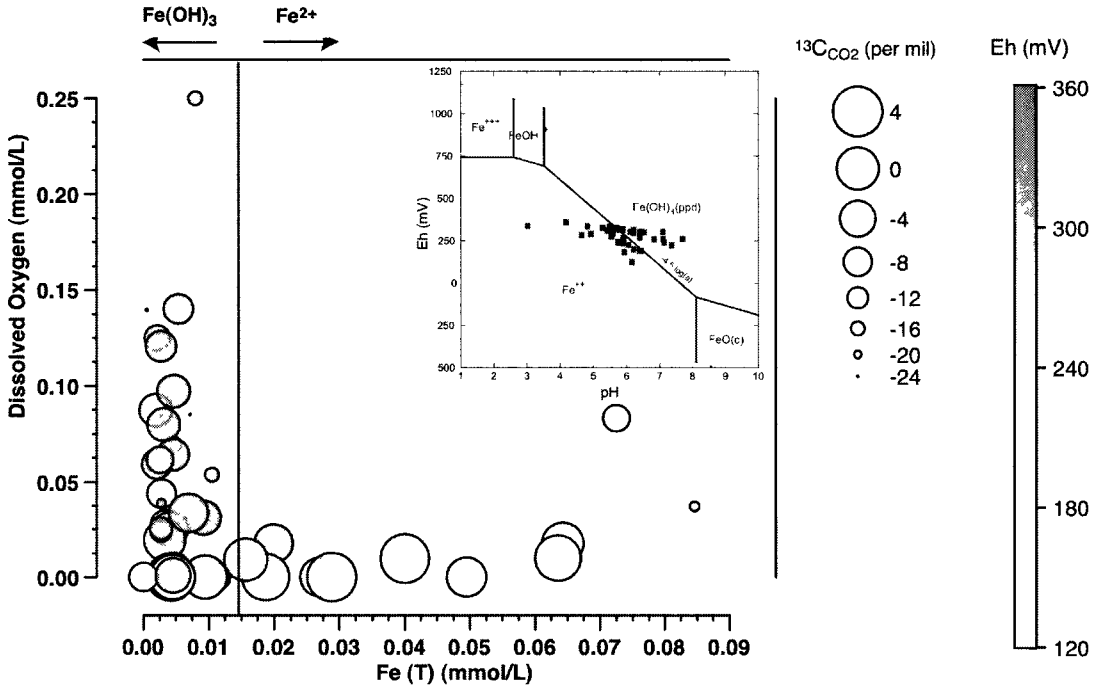

Figure A4-4. Low $\delta^{13}C_{CO2}$ values in this plot commonly occur where elevated DO or Fe^{3+} is present, suggesting that in the presence of oxidized ions, methane is consumed or inhibited from forming. The elevated $\delta^{13}C_{CO2}$ values in anoxic conditions and elevated Fe^{2+} suggest that CO_2 reduction is proceeding. The inset figure represents the stability of Fe^{2+} and amorphous Fe-oxyhydroxides in peat groundwaters at an average Fe log activity of -4.5. The -4.5 log(a) line is also represented by the vertical line in the bubble plot of total Fe versus DO.

Table A4-1. Geochemical and isotopic compositions of peat groundwaters at Yankee, Zulu Alpha-1, Bravo-1, and Control.

Table 2

Samples	Distance along transect (m)	Location	Latitude (degrees)	Longitude (degrees)	sample collection below water table (m)	Temp °C	pH	Eh (mV)	EC (µS/cm)	DO (mmol/L)	DIC (mmol/L)	$\delta\,^{13}C_{CO2}$ (per mil)	Na (µmol/L)	Cl (µmol/L)	SO_4^{2} (µmol/L)
Yankee															
07 Y-01	0	limestone	52 8455	83 7915	1 04	8 7	5 5	332	29	0 039	0 61	-19 3	14 73	16 62	0 00
07-Y-02	64	limestone	52 7743	83 8772	0 62	9 8	5 9	316	56	0 070	na	na	19 33	bd	bd
07-Y-03	116	limestone	52 7743	-83 8765	0 82	9 0	5 9	316	55	0 097	1 27	-5 3	15 81	21 41	0 00
07-Y-04	153	limestone	52 7744	-83 8759	0 76	9 5	7 7	260	264	0 140	3 00	22 5	18 38	17 75	0 00
07-Y-05 5	255	limestone	52 7747	-83 8745	0 79	8 8	6 4	303	92	0 140	1 89	-7 4	34 77	3 38	0 00
07 Y-06	299	limestone	52 7749	-83 8739	0 43	8 1	5 6	317	55	0 137	na	na	22 45	bd	bd
07-Y-07	*324*	*limestone*	*52 7750*	*83 8735*	*0 76*	*7 9*	*5 8*	*316*	*47*	*0 080*	*0 97*	*5 2*	*17 12*	*34 93*	*0 00*
07-Y-08	349	kimberlite	52 7751	-83 8732	0 63	7 7	7 2	240	218	0 085	2 52	-23 6	28 73	20 00	0 01
07-Y-09	370	kimberlite	52 7751	-83 8729	0 46	6 3	6 5	299	78	0 054	1 70	-16 0	20 58	25 07	0 00
07-Y 10	393	kimberlite	52 7752	-83 8726	0 82	7 4	6 2	316	30	0 059	0 82	7 1	11 09	20 00	0 00
07-Y-11	443	kimberlite	52 7756	-83 8723	na	6 7	7 4	224	301	0 083	3 99	9 4	37 07	24 51	0 00
07-Y-12	489	kimberlite	52 7760	-83 8720	0 93	8 2	6 8	258	71	0 037	2 13	18 6	14 15	6 20	1 25
07-Y-13	539	kimberlite	52 7764	-83 8716	0 85	10 4	5 7	325	35	0 125	0 84	9 6	14 57	57 75	4 06
07-Y-14	589	limestone	52 7768	-83 8712	0 71	8 0	6 4	266	45	0 062	1 14	8 8	14 17	33 80	3 96
07 Y-15	639	limestone	52 7771	-83 8709	0 88	7 2	6 1	303	30	0 024	1 59	12 1	19 03	20 56	41 35
07 Y-16	689	limestone	52 7776	-83 8706	0 70	7 6	6 2	294	41	0 250	1 08	16 2	18 74	47 32	3 44
07-Y-17	739	limestone	52 7779	-83 8702	0 37	4 2	7 1	302	54	na	na	na	21 88	na	na
Zulu															
07-Z-05	0	limestone	52 7298	-83 8354	1 00	11 2	5 9	257	159	bd	2 96	1 8	45 52	50 99	2 29
07 Z-07	50	limestone	52 7297	83 8345	0 99	12 0	5 6	291	88	0 018	2 64	-2 1	26 15	22 82	2 19
07 Z 09	100	limestone	52 7297	-83 8338	0 84	9 7	5 3	327	38	0 031	2 22	4 0	49 59	33 80	2 60
07-Z-11	150	kimberlite	52 7297	83 8331	0 96	10 8	5 5	313	45	bd	1 68	8 0	32 77	45 07	2 40
07-Z 13	200	kimberlite	52 7296	83 8324	0 84	11 0	5 3	325	31	0 004	1 50	5 1	45 91	29 58	4 17
07-Z 15	250	kimberlite	52 7296	83 8316	0 92	9 9	5 4	310	35	bd	1 63	8 7	15 02	22 82	2 08
07-Z 17	300	kimberlite	52 7296	-83 8309	1 07	10 0	5 9	267	90	bd	2 11	0 5	144 16	7 89	2 81
07-Z-19	350	kimberlite	52 7295	-83 8301	1 05	11 2	6 2	125	229	bd	4 30	2 9	545 07	70 99	5 52
07-Z-21	400	limestone	52 7296	-83 8294	1 10	9 1	6 4	190	168	bd	3 21	1 0	495 73	47 04	2 08
07-Z 23	450	limestone	52 7294	-83 8286	1 01	6 5	6 1	224	280	bd	4 15	2 6	912 56	56 90	2 29
07 Z-25	500	limestone	52 7294	-83 8279	0 98	8 9	5 7	242	271	bd	4 70	3 8	611 70	75 77	8 33
07-Z-27	550	limestone	52 7294	-83 8271	0 96	9 7	5 8	239	154	0 009	3 66	-0 5	478 92	76 34	2 08
07-Z-29	600	limestone	52 7294	-83 8264	0 99	10 1	5 9	232	399	0 010	5 84	3 2	1241 30	411 27	1 77
07-Z-31	650	limestone	52 7293	-83 8256	0 89	9 6	6 2	198	379	0 018	5 49	0 3	1109 22	474 37	2 29
07-Z-33	700	limestone	52 7293	-83 8249	1 05	4 6	6 4	190	303	bd	4 54	-1 7	1329 83	716 34	2 29
07-Z-35	750	limestone	52 7292	-83 8241	0 96	10 5	5 9	183	349	0 010	4 62	1 7	1121 77	527 32	3 02
Alpha-1															
07-A-01	na	limestone	52 6907	-83 7810	0 99	8 2	4 8	335	34	0 028	1 14	-7 1	16 33	15 77	3 13
07-A-01F	na	limestone	52 6907	-83 7810	0 99	14 4	5 6	272	37	0 025	2 45	4 3	15 87	17 18	bd
07-A-11	na	kimberlite	52 6938	83 7769	1 17	8 8	4 7	284	43	0 019	1 46	1 1	18 22	20 28	1 67
07-A-11F	na	kimberlite	52 6938	-83 7769	1 17	5 1	7 1	261	41	0 044	1 19	8 0	15 20	14 93	bd
07-A-12	na	kimberlite	52 6939	-83 7762	1 12	15 0	3 0	338	51	0 069	1 36	14 3	26 65	43 94	6 77
07-A-12F	na	kimberlite	52 6939	-83 7762	1 12	12 0	5 6	292	45	0 018	na	na	na	na	na
Bravo-1															0 00
07-B-01	na	kimberlite	52 8647	-83 9390	1 14	17 3	5 6	308	56	0 088	2 01	-1 6	33 59	31 27	0 21
07 B-01F	na	kimberlite	52 8647	-83 9390	1 14	12 8	6 5	293	105	0 138	2 14	9 2	34 33	20 85	bd
07 B 02	na	limestone	52 8636	-83 9387	1 06	17 1	5 0	323	51	0 119	1 00	-8 6	135 54	63 66	1 46
07-B-02F	na	limestone	52 8636	83 9387	1 06	7 1	5 3	332	73	0 008	1 30	2 3	49 79	36 62	0 21
07 B 03	na	kimberlite	52 8651	-83 9395	1 05	17 5	5 7	246	75	0 017	1 40	5 3	70 83	124 79	7 08
07-B 03F	na	kimberlite	52 8651	-83 9395	1 05	12 8	6 5	330	108	0 079	3 87	-13 4	44 39	57 18	0 42
Control															
07 C 01	na	limestone	52 8455	-83 7915		17 3	4 2	360	58	na	na	na	na	na	na
07 C 01F	na	limestone	52 8455	-83 7915	0 82	16 4	4 9	290	29	0 064	2 70	5 8	18 66	25 07	1 98
07 C 01 5F	na	limestone	52 8449	83 7905	0 83	14 8	5 5	276	69	0 087	1 71	5 5	18 73	26 48	3 96

na = not analysed
bd = below detection

Table A4-2. Total Fe concentrations and calculated concentrations of ferrous and ferric Fe. Total Fe concentrations for Golf from Brauneder (2007). All concentrations are in µmol/L

	Distance along transect (m)	Location	Fe (total)	Fe^{2+}	Fe^{3+}
Yankee					
07-Y-01	0	limestone	2.78	0.56	2.22
07-Y-02	64	limestone	7.33	nc	nc
07-Y-03	116	limestone	4.62	0	4.62
07-Y-04	153	limestone	0.45	0	0.45
07-Y-05.5	255	limestone	5.41	0	5.41
07-Y-06	299	limestone	4.59	nc	nc
07-Y-07	324	limestone	3.06	0.32	2.74
07-Y-08	349	kimberlite	7.17	0	7.17
07-Y-09	370	kimberlite	10.50	0	10.50
07-Y-10	393	kimberlite	1.99	0.38	1.61
07-Y-11	443	kimberlite	72.62	36.68	35.93
07-Y-12	489	kimberlite	84.70	47.57	37.12
07-Y-13	539	kimberlite	2.13	0.01	2.13
07-Y-14	589	limestone	2.51	0.14	2.37
07-Y-15	639	limestone	2.71	nc	nc
07-Y-16	689	limestone	8.03	nc	nc
07-Y-17	739	limestone	25.59	nc	nc
Zulu					
07-Z-05	0	limestone	27.01	0.22	26.79
07-Z-07	50	limestone	19.91	0.05	19.86
07-Z-09	100	limestone	9.19	nc	nc
07-Z-11	150	kimberlite	11.15	0.02	11.12
07-Z-13	200	kimberlite	4.68	0.02	4.66
07-Z-15	250	kimberlite	2.47	0.01	2.46
07-Z-17	300	kimberlite	9.43	0	9.42
07-Z-19	350	kimberlite	4.21	0.01	4.20
07-Z-21	400	limestone	4.46	0.00	4.46
07-Z-23	450	limestone	18.67	1.19	17.48
07-Z-25	500	limestone	28.84	6.15	22.68
07-Z-27	550	limestone	15.72	nc	nc
07-Z-29	600	limestone	40.05	18.36	21.69
07-Z-31	650	limestone	64.30	46.75	17.55
07-Z-33	700	limestone	49.52	32.35	17.17
07-Z-35	750	limestone	63.64	44.41	19.22
Golf					
06G-01	0	limestone	3.41	0.01	3.40
06G-02	53	limestone	3.05	0.01	3.04
06G-03	102	limestone	4.27	0.01	4.25
06G-04	155	limestone	3.14	0	3.14
06G-05	209	limestone	3.58	0.01	3.57
06G-06	257	limestone	4.15	0.01	4.14
06G-07	309	limestone	3.80	0.01	3.79
06G-08	336	kimberlite	3.09	0	3.09
06G-09	360	kimberlite	2.50	0	2.50
06G-10	411	kimberlite	4.18	0.01	4.17
06G-11	466	kimberlite	3.44	0.01	3.43
06G-12	518	kimberlite	14.39	0.04	14.35
06G-13	569	kimberlite	17.54	0.08	17.46
06G-14	594	limestone	4.92	0	4.91
06G-15	618	limestone	4.52	0	4.52
06G-16	675	limestone	11.94	0.25	11.69
06G-17	722	limestone	5.01	0	5.00

nc = not calculated